

## Analysis of high capacity vehicles for Europe

**Citation for published version (APA):**

Kural, K. (2019). *Analysis of high capacity vehicles for Europe: application of performance based standards and improving manoeuvrability*. [Phd Thesis 1 (Research TU/e / Graduation TU/e), Mechanical Engineering]. Technische Universiteit Eindhoven.

**Document status and date:**

Published: 03/10/2019

**Document Version:**

Publisher's PDF, also known as Version of Record (includes final page, issue and volume numbers)

**Please check the document version of this publication:**

- A submitted manuscript is the version of the article upon submission and before peer-review. There can be important differences between the submitted version and the official published version of record. People interested in the research are advised to contact the author for the final version of the publication, or visit the DOI to the publisher's website.
- The final author version and the galley proof are versions of the publication after peer review.
- The final published version features the final layout of the paper including the volume, issue and page numbers.

[Link to publication](#)

**General rights**

Copyright and moral rights for the publications made accessible in the public portal are retained by the authors and/or other copyright owners and it is a condition of accessing publications that users recognise and abide by the legal requirements associated with these rights.

- Users may download and print one copy of any publication from the public portal for the purpose of private study or research.
- You may not further distribute the material or use it for any profit-making activity or commercial gain
- You may freely distribute the URL identifying the publication in the public portal.

If the publication is distributed under the terms of Article 25fa of the Dutch Copyright Act, indicated by the "Taverne" license above, please follow below link for the End User Agreement:

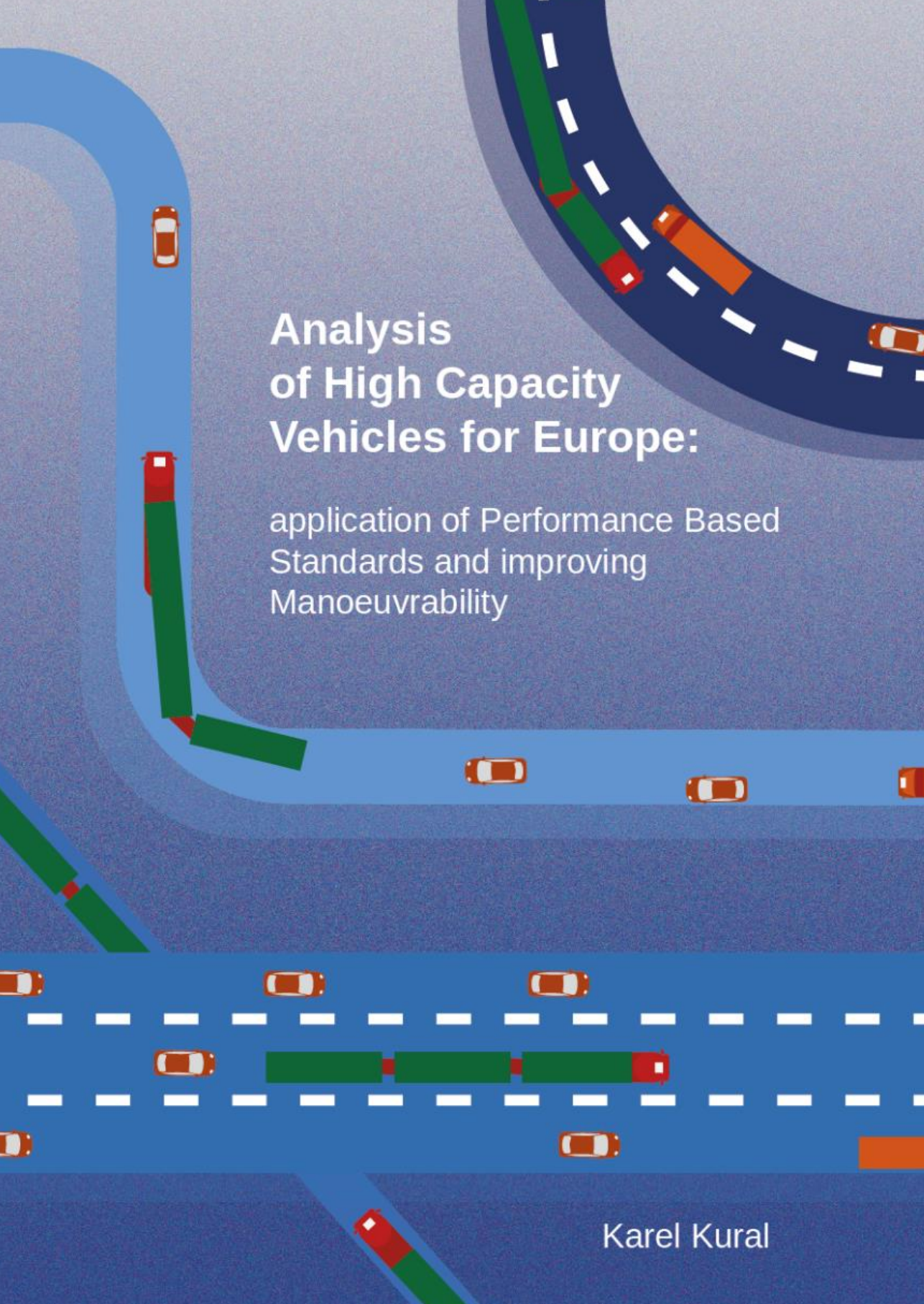
[www.tue.nl/taverne](http://www.tue.nl/taverne)

**Take down policy**

If you believe that this document breaches copyright please contact us at:

[openaccess@tue.nl](mailto:openaccess@tue.nl)

providing details and we will investigate your claim.



# Analysis of High Capacity Vehicles for Europe:

application of Performance Based  
Standards and improving  
Manoeuvrability

Karel Kural

**Analysis of High Capacity  
Vehicles for Europe:  
application of Performance Based  
Standards and improving  
Manoeuvrability**

Karel Kural

2019

Technische Universiteit Eindhoven



Karel Kural (2019). Analysis of High Capacity Vehicles for Europe: application of Performance Based Standards and improving Manoeuvrability.  
PhD Thesis, Eindhoven University of Technology, the Netherlands.

A catalogue record is available from the Eindhoven University of Technology Library.  
ISBN: 978-90-386-4853-8

Cover Design: Remco Wetzels|[www.remcowetzels.nl](http://www.remcowetzels.nl)

Reproduction: Ridderprint|[www.ridderprint.nl](http://www.ridderprint.nl)

©Copyright 2019, Karel Kural, all rights reserved.

All rights reserved. No part of the material protected by this copyright notice may be produced or utilised in any form or by any means, electronic or mechanical, including photocopying, recording or by any information storage and retrieval system, without the prior written permission of the author.

Analysis of High Capacity Vehicles  
for Europe:  
application of Performance Based Standards  
and improving Manoeuvrability

PROEFSCHRIFT

ter verkrijging van de graad van doctor aan de Technische  
Universiteit Eindhoven, op gezag van de rector magnificus  
prof.dr.ir. F.P.T. Baaijens, voor een commissie aangewezen  
door het College voor Promoties, in het openbaar te  
verdedigen op  
donderdag 3 oktober 2019 om 16:00 uur

door

Karel Kural

geboren te Brno, Tsjechië

Dit proefschrift is goedgegeurd door de promotoren an de samenstelling van de promotiecommissie is als volgt:

voorzitter: prof.dr.ir. L.P.H. de Goey  
1<sup>e</sup> promotor: prof.dr.ir. H. Nijmeijer  
2<sup>e</sup> promotor: dr.ir. I.J.M. Besselink  
leden: Prof. B.J.H. Jacobson PhD MSc (Chalmers University of Technology)  
dr.ir. J.P.P. Pauwelussen (HAN University of Applied Sciences)  
prof.dr.ir. P. Zegelaar  
prof.dr.ir. N. van de Wouw

Het onderzoek dat in dit proefschrift wordt beschreven is uitgevoerd in overeenstemming met de TU/e Gedragscode Wetenschapsbeoefening.

*To Alča, Kiki, and Kájík*





# Summary

## **Analysis of High Capacity Vehicles for Europe: application of Performance Based Standards and Improving Manoeuvrability**

The transport sector currently contributes to about a quarter of overall CO<sub>2</sub> emissions in the EU and is the only sector with increasing emissions. One of the major drivers behind this is the growing demand for freight transport resulting from vertical disintegration and globalization. Road freight transport in EU accounts nowadays for about 75% of goods transport on land, and is projected to grow in the forthcoming decade by more than 20% in terms of transported cargo. This represents not only additional environmental burden, but also increasing total load on the existing European infrastructure, which cannot be expanded on short term to accommodate this forthcoming demand. Therefore, severe traffic congestions in the future seems unavoidable, when using current legislative framework that ineffectively prescribes the design of commercial vehicle combinations. These concerns call explicitly for a more efficient road freight transport system.

A promising alternative seems to be the wider implementation of High Capacity Vehicles (HCV's), which are multiple-articulated commercial vehicle combinations, carrying typically standardized loading units. They exceed the weight and length limits prescribed by present European legislation, but are allowed to operate on a national basis. As proved by experiences in a limited number of EU-member states, HCV's are enhancing the productivity and profitability, yet reducing environmental impact and infrastructure load. However, a number of hurdles still exists that obstructs the wider acceptance of HCV's on European scale. Two of them, are used as the main motivation for this study, namely: the restrictive legislative framework, and the poor low-speed manoeuvrability at both forward and reverse driving.

At first, the feasibility to adopt an alternative performance based legislative scheme in Europe is investigated. The biggest advantage of a performance based scheme (PBS) compared to prescriptive policy, is that PBS is more pragmatic and ensures a better fit between the vehicle and the infrastructure through the fulfilment of the performance criteria. This may result in allowing vehicle combinations operating outside of the current EU-directive, which are more suitable for multi-modal logistic operations, and better match to particular segments of the infrastructure network. As a result three types of Future Vehicle Concepts are suggested, that comply with the principles of

proposed legislation, and may significantly contribute to enhancing overall transport efficiency.

The second part of this study addresses the challenges associated with the poor manoeuvrability of HCV's resulting in increased swept path width. A control strategy for active steering of towed vehicle units, such as trailers, is proposed to improve the low-speed manoeuvrability, but also high-speed stability beyond the performance of current vehicle combinations during forward driving. A novelty is the use of a single controller structure for all velocities employing a gain scheduling method for optimal performance at any velocity. To achieve the control objective, the problem is initially formulated as a path following problem and subsequently transformed into a tracking problem using a reference model. To support controller design, a generic non-linear model of a double articulated vehicle, based on a single track model, is employed. The proposed systematic design approach allows to easily adjust the controller for additional trailers or different dimensions, in which only some of the towed vehicles are allowed to steer. The performance of the controller is verified using a high-fidelity multi-body model. Simulation results show substantial reduction of both swept path width and tail swing at low speed, and the rearward amplification at high speed.

Furthermore the manoeuvring in reverse direction is studied. It has been identified in a survey with professional drivers, as the most problematic scenario while operating a HCV's. More importantly, it is required any time the vehicle combination needs to approach a loading dock at the distribution center. In such a situation the towed vehicle units that are originally pulled by the hauling unit will be pushed backwards and become open-loop unstable, because the articulation angles tend to increase without stabilizing control over the steering wheel by the driver. This represents a significant problem for all vehicle combinations having multiple articulation points. A series of full-scale experiments with a number of drivers is accomplished with the objective to understand the major reasons that lead to the mediocre performance of the drivers during the reversing of a multiple-articulated vehicle. The main motives are identified as follows; insufficient driver view, no awareness about the controllability limits, and divergently unstable vehicle behaviour that differs per vehicle combination.

To overcome these issues an innovative framework of the driver support system for docking of multiple articulated vehicles has been developed. The concept employs fiducial markers in combination with computer vision algorithms for the vehicle localization, and the path planner that generates the reference path for the rear most vehicle based on its initial and terminal pose. The path for the docking manoeuvre consists of two moves, that are both viable and short in terms of distance travelled while using the principles of vehicle kinematics and Dubins curves. The core of the support system is the generic bi-directional path following controller, which can be customized to an arbitrary combination of vehicles. The controller adopts the principle of a virtual tractor, and is based on vehicle inverse kinematic behaviour in combination with proportional-integral control actions. The closed-loop stability of the controller has been verified using the linearised system, being consistent with the operational conditions of the docking manoeuvre. Next, the functionality of the bi-directional controller and the path planner is verified on two levels. Firstly with a high-fidelity multi-body model and subsequently on a scaled vehicle combination demonstrator using a camera to localize the vehicle combination. In both cases the

controller proved great potential by satisfying the design criteria with abundant margins. However, there are number of open aspects, which needs to be addressed to bring the concept on the next technology readiness level. Primarily, the interaction between the driver and the support system for semi-autonomous operation and system fail-safe behaviour, are subjects that require further research.



# Contents

<b>Summary</b>	<b>vii</b>
<b>Nomenclature</b>	<b>xv</b>
<b>Acronyms</b>	<b>xix</b>
<b>1 Introduction</b>	<b>1</b>
1.1 History of Road Transport . . . . .	1
1.2 Megatrends Influencing Logistic Sector . . . . .	5
1.3 High Capacity Vehicles . . . . .	10
1.4 Problem Statement and Research Objectives . . . . .	12
1.5 Outline of this dissertation . . . . .	14
1.6 Scientific Contributions and Publications . . . . .	15
<b>2 Performance Based European Legislation</b>	<b>17</b>
2.1 Introduction . . . . .	17
2.2 Current European Legislative Framework . . . . .	18
2.3 Australian PBS Framework . . . . .	22
2.4 Principles for a Future EU-Legislative Framework . . . . .	27
<b>3 Generic Multi-Body Simulation Model</b>	<b>35</b>
3.1 Introduction . . . . .	35
3.2 Model Library . . . . .	36
3.3 Experiments . . . . .	40
3.4 Model Validation . . . . .	42
3.5 Model validation Results and Discussion . . . . .	51
3.6 Summary . . . . .	59

<b>4</b>	<b>Vehicle Performance Analysis</b>	<b>61</b>
4.1	Introduction . . . . .	61
4.2	Representative vehicle combinations . . . . .	61
4.2.1	EU vehicle combinations . . . . .	62
4.2.2	High Capacity Vehicles . . . . .	62
4.2.3	Loading conditions . . . . .	64
4.3	Vehicle modelling and performance assessment . . . . .	64
4.4	Performance analysis results . . . . .	66
4.5	High Capacity Vehicle Combinations after 2020 . . . . .	72
4.6	Summary . . . . .	78
<b>5</b>	<b>Active Trailer Axle Steering Control for High Capacity Vehicle Combinations</b>	<b>79</b>
5.1	Introduction . . . . .	79
5.2	Paper . . . . .	79
<b>6</b>	<b>Reversing of Multiple Articulated Vehicles</b>	<b>99</b>
6.1	Introduction . . . . .	99
6.2	Problem Definition . . . . .	100
6.3	Tests with novice drivers . . . . .	101
6.4	Results form the experiments . . . . .	104
6.5	Improving driver performance . . . . .	109
<b>7</b>	<b>Driver Support for Low-speed Manoeuvring</b>	<b>113</b>
7.1	Introduction . . . . .	113
7.2	Literature Review . . . . .	114
7.3	Path Planning . . . . .	116
7.4	Bi-directional path following controller for an articulated vehicle . . . . .	124
7.5	Conceptual Functionality of the Driver Support System . . . . .	136
7.6	Summary . . . . .	138
<b>8</b>	<b>Implementation and Testing</b>	<b>139</b>
8.1	Introduction . . . . .	139
8.2	Testing with Multi-Body Simulation Model . . . . .	140
8.3	Implementation in a Down Scaled Physical Demonstrator . . . . .	141
8.4	Summary . . . . .	148

<b>9</b>	<b>Conclusions and recommendations</b>	<b>151</b>
9.1	Conclusions . . . . .	152
9.2	Recommendations . . . . .	154
	<b>Appendices</b>	<b>157</b>
<b>A</b>	<b>A Linear Model of a Double Articulated Vehicle</b>	<b>159</b>
A.1	Introduction . . . . .	159
A.2	Modelling assumptions . . . . .	159
A.3	Derivation of equations of motion . . . . .	160
<b>B</b>	<b>Normal and Inverse Kinematic Models</b>	<b>165</b>
B.1	Introduction . . . . .	165
B.2	Kinematic model . . . . .	165
B.3	Inverse Kinematic model . . . . .	169
<b>C</b>	<b>Closed Loop Stability Analysis at Low Speed with Limited Articulation Angles</b>	<b>173</b>
C.1	Introduction . . . . .	173
C.2	Method . . . . .	173
C.3	Linearised Equations . . . . .	175
C.4	Accuracy of the linearised model . . . . .	179
C.5	Driver Model Parameter Sensitivity Study . . . . .	181
C.6	Damping Ratio of the Closed Loop Transfer Function . . . . .	181
<b>D</b>	<b>Vehicle and Controller Parameters</b>	<b>185</b>
D.1	Introduction . . . . .	185
D.2	Vehicle Parameters . . . . .	185
D.3	Controller Gains   Full Scale Multi-body Vehicle model . . . . .	186
D.4	Controller Gains   Scaled Vehicle model . . . . .	186
	<b>Bibliography</b>	<b>187</b>
	<b>Acknowledgements</b>	<b>197</b>
	<b>Curriculum Vitae</b>	<b>199</b>





# Nomenclature

## Constants

$g$  gravitational acceleration [m/s<sup>2</sup>]

## Symbols

$a$  distance between centre of mass and front axle/articulation point [m]  
 $b$  distance between centre of mass and rear axle [m]  
 $\vec{e}$  coordinate system [-]  
 $e_y$  lateral tracking error [m]  
 $e_\theta$  angular tracking error [rad]  
 $g_{vy}$  lateral velocity error scaling coefficient [s<sup>2</sup>/m<sup>2</sup>]  
 $g_r$  yaw rate error scaling coefficient [s<sup>2</sup>/rad<sup>2</sup>]  
 $g_\gamma$  articulation angle error scaling coefficient [rad<sup>-2</sup>]  
 $h$  distance between center of mass and articulation point [m]  
 $\hat{i}$  unit vector [-]  
 $k$  scaling parameter [-]  
 $l$  overall vehicle length [m]  
 $m$  mass [kg]  
 $p$  final path planner curve for forward move [-]  
 $q$  final path planner curve for reverse move [-]  
 $r$  yaw rate [rad/s]  
 $s$  initial path planner curve for reverse move [-]  
 $t$  time [s]  
 $v$  longitudinal velocity component [m/s]  
 $v_y$  lateral velocity component [m/s]  
 $w$  weighting factor [-]  
 $A$  junction point of the docking paths [-]  
 $CM$  vehicle center of the mass [-]

$C_y$	cornering stiffness	[N/rad]
$F_y$	cornering force	[N]
$G_{i j}$	transfer function mapping the i-th input to j-th output	[-]
$H$	corner position of last vehicle unit	[m]
$J$	mass moment of inertia	[kg·m <sup>2</sup> ]
$K_I$	controller integral gain	[Hz]
$K_y$	controller steering sensitivity proportional gain	[-]
$K_\theta$	controller proportional orientation gain	[-]
$L_f$	wheelbase (kinematic model)	[m]
$L_b$	distance of articulation point to the axle (kinematic model)	[m]
$M$	distance from the vehicle combination frontal to the controlled vehicle point (path planner)	[m]
$N$	frontal overhang of the last vehicle unit	[m]
$Q$	rear overhang of the last vehicle unit	[m]
$P$	system pole	[-]
$P_D$	preview distance	[m]
$R$	reference point of nominal path	[-]
$T$	hauling unit frontal overhang	[m]
$U$	controlled vehicle point	[-]
$V$	slip velocity	[m/s]
$X$	global positional coordinate	[m]
$Y$	global positional coordinate	[m]

## Symbols Greek

$\alpha$	axle/tyre slip angle	[rad]
$\beta$	body slip angle	[rad]
$\gamma$	articulation angle between vehicle units	[rad]
$\delta$	steering angle	[rad]
$\delta^*$	virtual steering angle	[rad]
$\zeta$	damping ratio	[-]
$\theta$	yaw angle	[rad]
$\kappa$	path curvature	[1/m]
$\lambda$	pitch angle	[rad]
$\rho$	vector of cornering stiffnesses	[N/rad]
$\varphi$	roll angle	[rad]
$\phi$	path tracking correction angle	[-]
$\Theta$	viable cornering stiffness interval	[N/rad]

**Miscellaneous**

$X^*$	optimal value for $X$
$\hat{X}$	estimate of $X$
$\bar{E}(X)$	expectation value of $X$
$MSE_{(X)}$	mean square error of $X$



# Acronyms

ABS	Anti-lock Brake System
AEBS	Advanced Emergency Braking System
CAN	Controller Area Network
CO <sub>2</sub>	Carbon Dioxide
EU	European Union
E-L	Euler-Lagrange Equations
EC	European Commission
EMS	European Modular System
ESC	Electronic Stability Control
GDP	Gross Domestic Product
GHG	Green House Gasses
GPS	Global Positioning System
GtKm	Gigatonne-kilometre or 10 <sup>9</sup> tonne-kilometre
GUI	Graphical User Interface
GVW	Gross Vehicle Weight
HCV	High Capacity Vehicle
HGV	Heavy Goods Vehicle
ISO	International Organization for Standardization
IRL	Infra Red Light
LDW	Lane Departure Warning
MSE	Mean Squared Error
NO <sub>x</sub>	Nitrogen Oxides
PBS	Performance Based Standards
PWM	Pulse Width Modulation
TCO	Total Cost of Ownership
UNECE	United Nations Economic Committee for Europe
USD	United States dollar
WMS	Warehouse Management System



# Chapter 1

## Introduction

### 1.1 History of Road Transport

Transportation and logistics play a key role in the global economy for the past five thousand years.

Around 2560 B.C., the Egyptians started to build the Great Pyramid of Giza. They used more than two million stone blocks, each typically weighting around 2300 kg, which needed a well organized transport system enabling movement of these blocks by man power and primitive tools over the distance from adjacent mines [82].

In the 3<sup>rd</sup> century B.C., the Romans built a broad network of paved roads across their empire, which covered most of the Europe. The entire network consisted of nearly 80.000 km of paved roads and about four times this number of unpaved roads. These were primarily dedicated to fast movement of Roman legions, but were also used for material and goods transportation. It is remarkable to note, that a minimal width of the road in straight, as well as curved, sections was already established by the Roman Law of Twelve Tables [50], representing one of the first examples of transport infrastructure standardization.

Later in the 12<sup>th</sup> century, an international merchant network, known as Hanseatic League was founded [51], to enhance the cooperation of transport by bundling both inland and sea transport. It stimulated the growth of transport while increasing the trade and travel throughput in Europe and building a competitive environment. In the next centuries a number of foreign markets became accessible to the merchants, which further boosted the economy, especially after the discovery of the "New World", [95].

However, as the most of European inland infrastructure was still the one build by Romans more than thousand years ago, the state of the roads and bridges was desolate [125]. Therefore most of the inland transport in Middle Ages happened on unpaved roads with relatively big wheel-carts being towed by a horse, as seen in Figure 1.1. The roads were mostly uneven and furrowed dirt paths, which were difficult to traverse during bad weather conditions.



Figure 1.1: Wheel-carts towed by horse in the Middle-Ages<sup>[124]</sup>.

Between the end of Middle ages and the start of the Industrial Revolution, the need to make inland transportation and travelling more time efficient became essential, which finally led to renewal of the major roads. It enabled usage of two horse drawn wagons with two axles, as depicted in Figure 1.2, which were not only faster and easier to control, but also capable of transporting more cargo and enabling the option to transport passengers when customized as coaches.



Figure 1.2: Two horse drawn wagon<sup>[45]</sup>.

Although the infrastructure renovation represented notable step forward, it was still a horse, a living animal, moving the wagon forward. Exhausted horses slow down after travelling a longer distances, which is not desirable. It pushed mankind further in researching other possibilities for enhancing transport. The next step appeared to be the steam engine, or in other words the external combustion engine.

The first pioneers started already at the end of 18<sup>th</sup> century, however their vehicles appeared to be far from practical and mostly were seen by public as an odd activity as illustrated by Figure 1.3. It was mainly due to limitations in manufacturing technologies and design methods of the vehicles, which could not fully cope with existing infrastructure [113] available in those days.



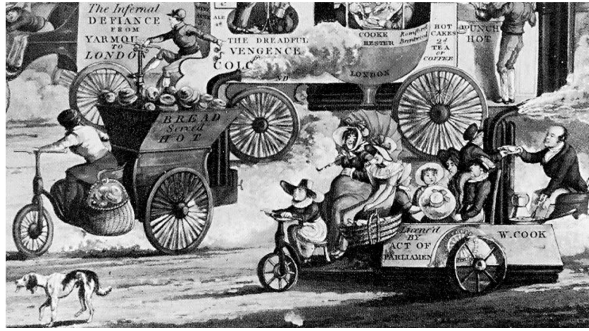


Figure 1.3: Steam cars caricature from 1831<sup>[1]</sup>.

Contrary to road transport, the invention of steam engine led to flourishing of the railway sector. In 1825, the 'Father of the Railways', George Stephenson, built a steam locomotive, named *Locomotion*, for the railway in the north east of England being the first public steam railway in the world. After this success, Stephenson established his company and became the pre-eminent builder of steam locomotives designed for railways in the United Kingdom, United States and much of Europe [53]. This started the steam century era, where the railroads became dominant for inland transportation and over the time penetrated from national and international level up till small local railways between villages with a two foot narrow track.

At the beginning of 20<sup>th</sup> century the first steam propelled vehicles, which could be seriously considered for everyday usage appeared on the roads. Although the steam engine was the most popular form of propulsion, the internal combustion engine took over this lead in the years to come.

In 1908 Henry Ford started mass production of the legendary Model T, as shown in Figure 1.4. Over the next two decades this car significantly influenced the transport of people and goods due to its affordability. Thanks to efficient fabrication on assembly lines the price could be reduced over the years sharply to 260 USD, corresponding to 3510 USD in 2016. More than 16.5 million of these cars have been sold over 19 years of production. The car proved itself in various applications from passenger transport up to commercial transportation of goods. It was used mostly on short, local distances, as the inland long haul transportation was still the domain of the railways.

In the decades after World War II the trucks caught up and slowly surpassed the rail roads in the total transport performance, which is expressed in ton/km. Although the war destroyed and severely damaged most of the European transport infrastructure, it also pushed the development of logistics, vehicle design and technology forward. Trucks could offer more transport flexibility as the length of the paved roads network by far exceeds that of the rail road network, due to lower construction and maintenance costs.

A historical milestone was achieved in year 1955, when Malcom P. McLean bought a steamship company with the rational idea of transporting an entire truck-trailer combination with their cargo still inside, thus avoiding the highly unproductive loading



Figure 1.4: Ford Model T 1926 - commercial vehicle modification<sup>[46]</sup>.

and unloading of goods when switching from one transport mode to the other. In the same year the ship SS Ideal X, formally a World War II oil tanker, was modified to carry trailer vans, later called shipping containers, on the deck and thus became the first container ship in the world. Subsequent developments towards standardized ISO containers and twist lock mechanisms made it possible to ship just the container leaving the tractor and semi-trailer behind, as shown in Figure 1.5.



(a)



(b)

Figure 1.5: a) Beginning of the container era in 1960's<sup>[15]</sup>, b) Swap Body

By using standardised containers for the transport of goods, the transport costs dropped and contributed to creating a global market. Moreover, they stimulated all modes of surface transport, i.e. road, rail, and waterborne, to develop platforms that can accommodate the containers and enabling synchromodal freight transportation which is the optimal, flexible and sustainable allocation of cargo to different transport modes and routes in an infrastructure network. The ISO container is not the only means enabling synchromodality. The swap body, depicted in Figure 1.5b) is another example being extensively used. It is not stack-able, but rather popular in European inland transport due to its lower tare weight, optimized size for the pallets and good interfacing with railway wagons.

In retrospect, one sees that current transport vehicles in general are getting bigger in dimensions and loading capacity, compared to the former generation. This trend can be best illustrated on the container ships, whose capacity since the 60's increased over the decades by more than 1500% to almost 24.000 20ft ISO containers. The 'growth' can be also observed in the railway and road sector where, the length, weight and width of the freight vehicles have increased over the time as well, see e.g. [28], [38], although it was not that dramatic as in case of maritime vessels mainly due to the compatibility with existing infrastructure. Given this trend, the observation can be drawn, that the size is co-related to the economical transport efficiency, which is, and always was, a main driver in logistics.

## 1.2 Megatrends Influencing Logistic Sector

Road freight transport has been continuously evolving over the time, as illustrated in the previous section. However, nowadays it appears to be more dynamic then ever. In [65], a number of Megatrends have been identified which are expected to considerably influence current and future development of logistic sector. The definition of Megatrends given by Schwenker and Raffel [120] is:

*"Megatrends are trends that alter business and society in a profound and lasting fashion, over decades rather than years. They have an impact on every one of us. They fundamentally alter the opportunities and risks for companies. In short, they are those trends that we must always take into account when imaging possible futures."*

Identified megatrends are as follows:

- **Emissions of green house gasses**

The group of Green House Gasses consists of: methane, nitrous oxide, chlorofluorocarbons, water vapour, and carbon dioxide. The last two, i.e. water vapour and carbon dioxide, are primarily linked with fossil fuel combustion in industrial processes, or in thermal power stations to generate the electricity. Fortunately their share is being reduced by using more renewable energy sources such as wind and solar energy. However, the carbon dioxide emission share produced by the transport sector in EU has been progressively growing in past decade, as depicted by Table 1.1, which is problematic.

- **Demand for Transport and Mobility**

Transport performance can be expressed in terms of ton-km, so the mass of the good multiplied with the travelled distance. In Europe, the biggest share of inland transportation is nowadays taken by the road sector with a share of 75.5%, followed by rail with 18.3% and waterways with 6.2% [41]. From 1970 until 1997 European freight has increased by approximately 70% [16]. It is expected that by 2030 the total freight transport volumes in terms of gigaton-km will grow further by approximately 38% with respect to 2011 [17]. The distribution across the transport modes is depicted in Figure 1.6.

This represents a serious problem. The existing European transport infrastructure can not accommodate an additional 38% increase in demand, and expand-

	1990	2014	Difference [%]
Total CO <sub>2</sub> emissions (EU28)	5665.5	4282.1	-24%
Contribution of road transport	724.8	845.3	17%
Share of total emissions (EU28)	13%	20%	7%
Road Transport :			
Cars	459.9	515.9	12%
Heavy duty trucks and buses	188.3	213.9	14%
Light duty trucks	66.3	103.7	56%
Motorcycles	9.1	10.6	16%
Other road transportation	1.1	1.1	2%

Table 1.1: Road transport sector share of CO<sub>2</sub> emissions in EU28 [42].

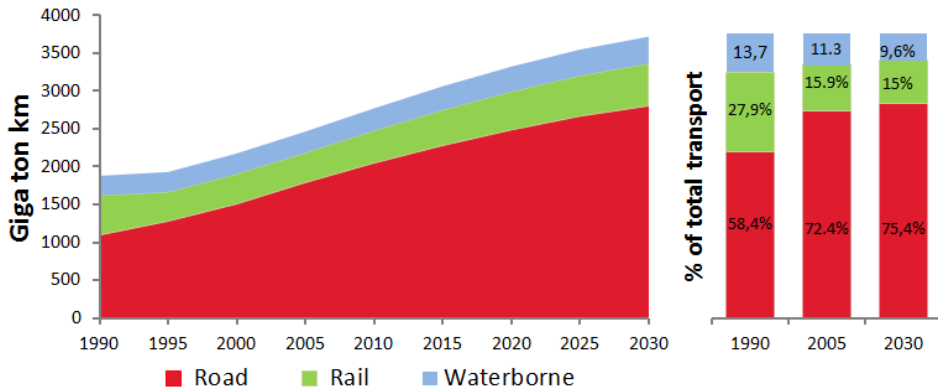


Figure 1.6: Transport Demand Prognosis [17].

ing the capacity of the current infrastructure across Europe by approximately 40% is not viable within the next decades. Even though the increased transport demand can be partially compensated by stimulating the cooperation with other transport modes and frequent employment of synchro-modality, author assumes it is unlikely to resolve the problem entirely given the relatively low flexibility or transport speed of other modes. Therefore the risk of massive traffic congestion in the future seems to be unavoidable, when using the current vehicles and legislative framework. Based on the latest numbers from the European Commission [18], the current costs due to road traffic congestion already correspond to approximately 1% of EU GDP. Hence, both increasing demand for transport and mobility, together with the congestion problem explicitly calls for a more efficient transport system, described in terms of fuel/energy consumption, transport speed, use of existing infrastructure, green house gases emissions, transport costs, synchro-modality.

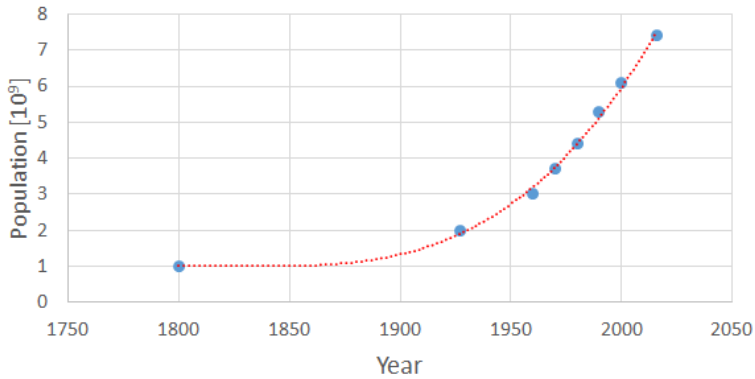


Figure 1.7: Historical development of the world population [13].

- **Urbanization**

World population is growing continuously, as depicted in Figure 1.7. In July 2015 there were more than 7.3 billion people on the planet with the projection of 8.5 billion in 2030 [128]. The population growth is foreseen mainly in urban areas because of natural population growth, rural-urban migration, and administrative changes [127]. These administrative changes may entail the merging of suburban areas or neighbouring towns into a larger city or the foundation of completely new cities. United Nations predict that the urban population will to grow globally by 40% by 2030 with respect to 2010 meaning that two thirds of world population will be living in urban areas.

Due to urbanization an urgent need will develop for more efficient freight transport system. In addition to already described features, this system should not only provide and dispose the goods, but also ideally tackle environmental issues such as noise, air pollution, vibration and visual intrusion [122].

- **Scarcity of natural resources**

It is expected that in the future, the society and business will face the problem of depleting natural resources. The price of oil, which is the main energy carrier for the road transport, were hitting the bottom in beginning of 2016. But a shortage of resources caused by increasing demand, as shown in Figure 1.8, is inevitable. Regardless the question as to when the world will really run out of the oil, the era of very cheap oil and other resources is certainly over.

Novel oil extraction techniques will increase the supply, but they will also lead to an increase of the global oil price. As oil become more scarce, the only solution of bringing oil prices down will be a higher energy efficiency or a reduction of the demand. Nevertheless both approaches will only postpone the discussion about running out of oil [120].

Summarizing these megatrends. It is seems apparent that the road segment will remain dominant transport mode in the future. Moreover it has the highest energy

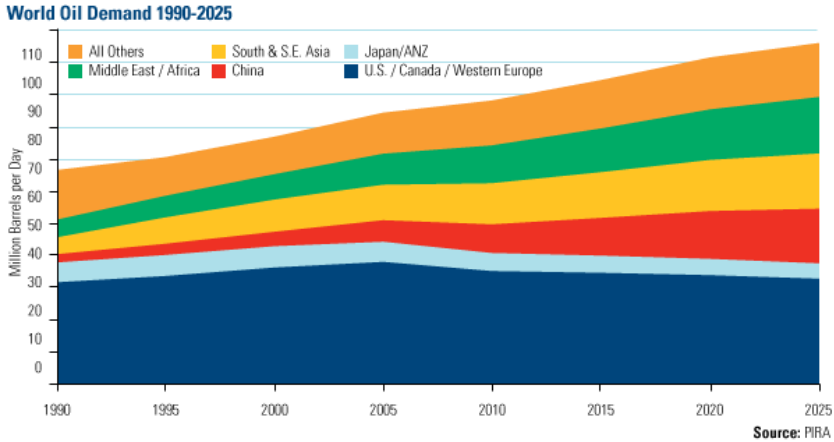


Figure 1.8: World oil demand [100].

consumption from from all freight modes [40], and thus the biggest impact on the environment and society. Hence, requirements can be imposed in order to ensure that future road transport will be smart while using synchromodal approach and systems maximizing the performance of the driver, green and profitable, while complying with market needs and available infrastructure.

Based on results of [65], the requirements on future road freight transport are identified as follows:

- **Synchromodality**

The synchromodal transport is defined as door-to-door movement of goods in standardized loading units by intelligent use of two or more transport modes on their own and in combination to maximise the biggest benefit from each of them so that the sustainability of the overall journey is optimised. This optimising in the use of resources has environmental, societal and economic benefits. Since each transport mode has its strengths and weaknesses, see Figure 1.9, it is important to properly combine the modes based on the application, while employing the strengths of each mode [39]. This may lead to a substantial reduction of road congestion, improved road safety and reduced environmental footprint as the total emission CO<sub>2</sub> will be smaller. These are reasons why synchromodal transport is being promoted by the EC through financial incentives, such as tax reduction or reimbursements, and the development of a so-called TEN-T synchromodal infrastructure network throughout Europe by 2030 [19].

- **Modularity**

Modularity is directly related to choice of a suitable loading unit. It is desirable to transport the cargo with loading units that will interface with majority of modes, have a low tare weight, and enable the highest possible floor utilization for Euro pallets. It is expected that Euro pallets, which have dimensions 80 x

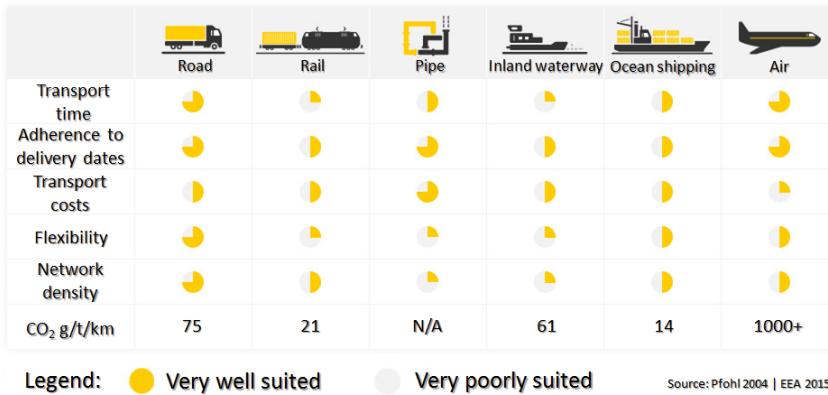


Figure 1.9: Transport mode comparison.

120 cm will dominate the European transport market in the future. Currently three loading units used in EU have intermodal capability; the intermodal 13.6 m long semitrailer, the ISO container, and C-series swap body. Based on the market research [65] and loading unit capabilities, it is expected that 45 foot pallet-wide container and C-745 swap body will dominate intermodal transport in the future. More details regarding their dimensions, floor utilization and tare weight can be found in [65].

- **Efficient usage of transport resources**

The numbers of global deliveries per day is expected to be 500 million in 2025 [48], being minimal of 20% increase compared to current state. To meet this volume, transport companies have to consolidate their delivery strategy and fleets. The most promising logistical concept, resulting from the urbanization megatrend, appears to be the Hub & Spoke (H&S) system [65]. This system uses the hubs that are based outside the city. From these hubs the products are redistributed to the spokes into the city, that are used as a base for the last mile delivery. In an efficient hub system the geographical position of the hub is chosen close to majority of modes and the right techniques and right combination of modes will be used. The usage of H&S system needs to be further developed from the current status; H&S systems are nowadays mainly used by companies individually and not on the co-operative manner.

- **Electrification of powertrain and usage of alternative fuels**

In upcoming decade it is foreseen that the penetration level of fully electric or hybridized powertrains, especially in road transport sector, will increase considerably. This will be primarily driven by the price of batteries which is expected to drop significantly [27] while the capacity will increase using new technologies enabling to expand the energetic storage density. This will enable reduction of emissions if the energy comes from alternative fuels, such as hydrogen, or directly from the renewable electricity sources, as solar or wind energy. Moreover,



Figure 1.10: High Capacity Vehicle<sup>[14]</sup>.

the electrification of powertrain enables better energetic efficiency if the brake energy can be recuperated and the traction forces can be distributed as required to optimize vehicle driving performance.

As mentioned, the majority (75%) of the inland transport in Europe is done via the road. Therefore, it is relevant to project all requirements following from the identified megatrends on this transport mode as the potential environmental, societal and economic gain will be high. Several approaches are identified being:

- Mass use of Zero-emission/hybrid powertrain
- Application of Intelligent Transportation Systems and data sharing
- Vehicular automation at both high- and low-speed
- Improved aerodynamics of vehicle units
- Increased vehicle capacity and better usage of infrastructure

Whereas former three approaches require considerable investments from the side of OEM's, road authorities, and fleet operators, the latter two appear to be 'low hanging fruit' which might be implemented only by re-adjusting legislative boundaries and with minimal technological investments. Hence, the potential of the fifth bullet above, i.e. the implementation of **High Capacity Vehicles (HCV)**, on European level is discussed in next section.

### 1.3 High Capacity Vehicles

A High Capacity Vehicle (HCV) is mechanically connected combination of vehicle units which forms one articulated vehicle combination, an example is shown in Figure 1.10. There are two types of vehicle units that can be distinguished namely the towing vehicle units and trailing vehicle units. Towing vehicle units can provide the tractive forces such as rigid truck or tractor, whereas the trailing vehicle units can be only pulled such as semitrailers, dollies, centre-axle trailers, or link trailers. Hence the



conventional High Capacity Vehicle consists of one towing unit connected to a number of trailing units which may result in various configurations, as shown in Figure 1.11. It implies that the overall vehicle combination length is greater than federal-EU limit of 18.75 m for international long-haul transport. The length range of HCV's may increase to approximately 60 m long vehicle combinations known in Australia as road trains, down to shorter 20 m long combinations.

Based on monitoring the HCV's applications worldwide, or scientific research, a number of benefits have been observed, which are seen as very relevant in view of the identified megatrends. The benefits are listed as follows:

- **Reduction of operational costs**, [7], [105]
- **Less occupied space on the road**, [6], [90]
- **Improved fuel efficiency per ton·km or m<sup>3</sup>·km** [65], [90]
- **Reduced CO<sub>2</sub> emission per ton·km or m<sup>3</sup>·km**, [7], [105], [103], [47], [56].

It is very unlikely that 60 m long HCV combinations, which may be seen in Australia, Canada or South Africa would be directly applicable at the European road infrastructure. However, the so called European Modular System (EMS), as shown in Figure 1.11 has a very high potential. EMS vehicle combinations are using already existing vehicles and loading units and therefore may be globally legalized on national level such as is happening in several of EU-member states. The EMS vehicle combination length is typically limited to 25.25 m and the maximum total loaded weight is 60 t or lower. In this way two EMS vehicles can simply substitute three conventional vehicle combinations (two tractors + semitrailers and one rigid truck + centre axle trailer), with respect to loading and volumetric capacity. In Finland however, the length and weight limits go up to 32 m and 76 t, respectively which allows even higher gains in terms of productivity.

Despite these benefits, it appears to be problematic to implement these HCV's on an European scale for cross border transport. This is primarily due to a missing legal framework on the federal level, as the general acceptance of all 28 jurisdictions in EU is required, which is very difficult to achieve. This can be illustrated for example by the age of the current directive 96/53 EC [29], specifying the dimensions and weights for national and international traffic that was established more than twenty years ago. Even though it was recently amended by directive 2015/719 [38] allowing the application of aerodynamic devices, and thus an increase in the length of vehicle combination, the loading and volumetric capacity, being the key to improved efficiency, remains unchanged.

A feasible model of a legislative framework for commercial vehicles applicable in the EU, including HCV's, may be obtained from Australia, where the most developed legislative framework for operational requirements of HCV's is defined and implemented. The policy is fundamentally different compared to European prescriptive legislation, that restricts the weight and overall length of the vehicle combination to 44 t and 18.75 m respectively. The Australian approach assesses the performance of the vehicle with respect to the safety and infrastructure loading, and this approach is commonly

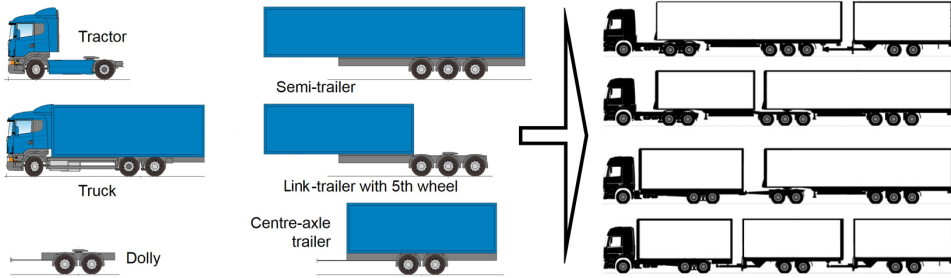


Figure 1.11: Examples of EMS units and their configuration to EMS vehicle combinations up to maximally 25.25 m.<sup>[116]</sup>

known as **Performance Based Standards (PBS)**. The PBS is a practically oriented set of rules enabling to rank the performance of the vehicle combination from different perspectives. Generally speaking it does not matter what the vehicle looks like, but how the vehicle performs in a number of different scenarios.

It is obvious that the Australian PBS are not directly applicable to Europe due to different operational conditions for commercial vehicles such as e.g. infrastructure design criteria or climate. On the other hand, the general principle of PBS framework is sufficiently flexible to be modified and customized for European conditions. Moreover, it can potentially be extended to include criteria related to the societal or sustainability benefits if required.

Furthermore, the PBS legislation can very well represent a platform, which enables the constructive interaction between a number of key stakeholders. Given the practically oriented nature of the PBS framework the safe and sustainable operation for arbitrary vehicle combinations can be guaranteed, while considering its operational condition and the interaction with the infrastructure. The same holds also for other transport modes. Moreover, legislation can be used as a tool for the governments to stimulate vehicle manufacturers (OEM's) in introducing novel technologies, leading to improved vehicle performance defined for example in terms of improved aerodynamic drag, manoeuvrability or dynamical stability. This may be naturally projected to increased transport safety, and productivity while reducing the CO<sub>2</sub> emissions, which will be heartily welcomed by the vehicle operators and society.

Apart from the issues preventing the introduction of HCV's across Europe as discussed in this section, there are a number of other obstacles associated with HCV's. These are explained in the next section and will be used as a motivation to define the research objectives of this dissertation.

## 1.4 Problem Statement and Research Objectives

Future road transport should be *smart*, *green* and *profitable*. The clean and profitable aspects of road transport, i.e. reduction of CO<sub>2</sub> emission and operational costs, appear to be automatically fulfilled when employing HCV combinations, as exten-

sively documented in e.g. [7], [105], [103], [47], [56]. However, the *smart* aspect needs to be elaborated further in order to make the vehicle combinations compliant with future needs. This includes compatibility with available infrastructure in terms of manoeuvrability, and safety, use of inter-modal loading units, which are employable for synchronomodality, and development of systems which ease up the vehicle handling for the driver.

Hence, the definition of a suitable **performance based framework** that will support all above mentioned features, needs to be specified. Subsequently the blueprints of the future vehicle combinations envelopes can be defined that will comply with the requirements on logistics for years 2020+ and fulfil the performance assessment.

The length of HCV's generally is a disadvantage with respect to the low speed manoeuvrability, compared to conventional vehicle combinations. The vehicle spatial envelope, called swept path, is typically dependent on the overall vehicle length. The swept path can be reduced when using active steering of the axles. In this way both low-speed manoeuvrability, but also high-speed stability, can be substantially improved as given in [67].

A very problematic subset of low-speed manoeuvring scenarios, which is common for all vehicle combinations having multiple articulation points is reversing. Reversing occurs typically at distribution centres when the vehicle has to be parked at the loading dock. During the reversing, the towed vehicle that is being normally pulled by the hauling unit will be pushed backwards, which may result in unstable behaviour. The articulation angle tends to increase when it is not being controlled by counter-steering of the hauling unit. As concluded from a query [102], reverse manoeuvring with multiple-articulated vehicles is recognized as one of the most critical tasks by the majority of professional drivers and fleet owners in Netherlands. The associated accidents, although not of a severe (personal) character, are solely caused by driver errors. This is unusual, as in the majority of all accidents involving HCV's [102] the HCV driver is not the originator of the accident. This illustrates the complexity of the reversing task. Although a professional driver does not lack experience for 'normal forward' operation on the highway, not everyone has sufficient skills to reverse an arbitrary vehicle combination with multiple articulations. The driver needs to apply a different control steering strategy for reversing depending on the lay-out of the multiple articulated vehicle combination.

To summarize, the research objectives can be formulated as follows:

- *Propose a suitable vehicle assessment framework that will ensure safe vehicle operation while considering its impact on the infrastructure and environment with a focus on European operational conditions.*
- *Determine the candidate vehicle combinations complying with future logistic requirement, operational safety and reduced impact on the environment.*
- *Investigate the ways in which the high- and low-speed lateral performance of HCV's can be enhanced. Furthermore, the means of the driver support during bi-directional manoeuvring with HCV's at distribution centres will be investigated.*

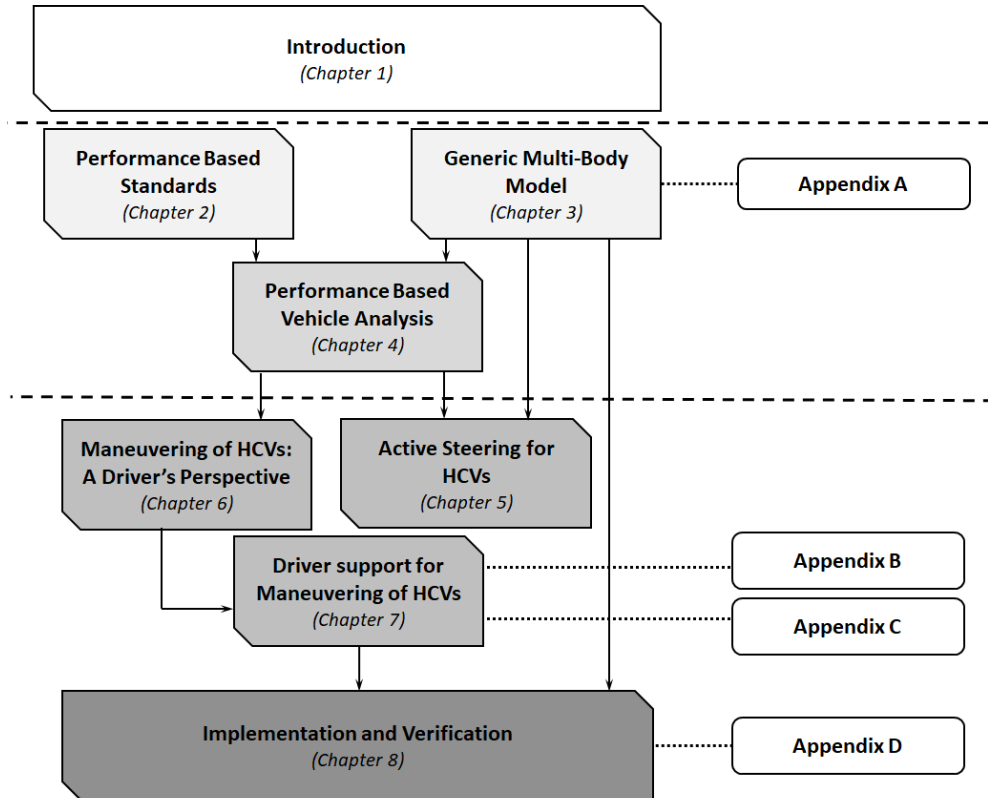


Figure 1.12: Outline of the dissertation.

## 1.5 Outline of this dissertation

The dissertation consists of nine chapters whereas eight is illustrated in Figure 1.12. In Chapter 2 the Performance Based Standards (PBS) framework is introduced, and its adaptations for European conditions. This approach is representing an alternative, flexible legislation that is prescribing the vehicle design less and can contribute to future legislation. Chapter 2 also includes the findings that were published in the study that will be further referred to as the "Book of Requirements". In Chapter 3 a generic and modular multi-body model library for arbitrary commercial vehicle combinations is created and subsequently validated with experimental data. Furthermore, the models will be used in Chapter 4 to simulate the dynamic behaviour of selected HCV's for a number of performance assessments. The performance analysis allows to determine the HCV combinations with the best performance, while considering also profitability and environmental aspects. The result of this chapter will be HCV combinations that will comply with logistical demands for years beyond 2020.

Thereafter the focus is on challenges associated with the bi-directional manoeuvrability of HCV's. Chapter 5 proposes a new control strategy for active steering of HCV

trailing units to improve both low-speed manoeuvrability and high-speed stability. A single controller structure suitable for both low- and high-speed is proposed using a gain scheduling method for optimized performance. In Chapter 6, the driver behaviour during reversing is analysed by experiments, using eye tracking glasses and an instrumented HCV combination. Based on observations from the experiments, a driver support for low-speed manoeuvring with HCV is proposed. In Chapter 7, a path generation algorithm and path following controller for automated docking of multiple-articulated vehicles are proposed, based on the localization input from the camera. The path following control strategy is implemented for verification in Chapter 8, firstly on validated multi-body model introduced in Chapter 3 and in the second phase to a scaled physical model of the HCV combination. Finally, Chapter 9 summarizes the main conclusions and presents a number of recommendations for further research.

## 1.6 Scientific Contributions and Publications

### Contributions

The scientific contributions are as follows:

1. the analysis of current European legislation related to operation of heavy goods vehicles and its subsequent projection into the performance oriented framework using the Australian methodology to outline the foundation for the future legislation enabling more productive road freight transport;
2. design of a novel and generic control strategy for the active steering of trailers of high capacity vehicle combinations improving both low-speed manoeuvrability and high-speed stability through employing a single controller structure for all velocities and gain scheduling method for optimized performance;
3. based on experimental results a novel framework of driver support for docking multiple-articulated vehicles is proposed consisting of: computer vision based localization, a path planner customized for docking scenario, and a generic bi-directional path following controller applicable to arbitrary vehicle combinations.

### Refereed journal publications

- Kural, K., Voskuijl, M., Fengnian, T. & Pauwelussen, J.P., Determination of representative loading conditions for effective semitrailer design, *Transport*, 29(4), pp. 363-375, 2014 (ref. [71])
- Kural, K., Prati, A., Besselink, I.J.M., Pauwelussen, J.P. & Nijmeijer, H., Validation of longer and heavier vehicle combination simulation models, *SAE International Journal of Commercial Vehicles*, 6(2), pp. 340-352, 2013 (ref.[69])

- Kural, K., Hatzidimitris, P., Wouw v.d.,N., Besselink, I.J.M., Nijmeijer, H., Active Trailer Steering Control for High Capacity Vehicle Combinations, *IEEE: Transactions on Intelligent Transportation Systems*, Vol. 2, No. 4, pp. 251-265, 2017 (ref. [75])
- Stensson Trigell, A., Rothamel, M., Pauwelussen, J., Kural, K., Advanced vehicle dynamics of heavy trucks with the perspective of road safety, *Vehicle System Dynamics*, Vol. 55, No. 10, pp. 1572-1617, 2017 (ref. [74])

### Refereed conference contributions

- Kural, K., Besselink, I.J.M., Pauwelussen, J.P. & Nijmeijer, H., Assessment of Dutch longer and heavier vehicles with a performance based approach and its applicability to Europe, *proc. HVTT12*, Stockholm, Sweden, 2012 (ref. [68])
- Kural, K., Prati, A., Besselink, I.J.M., Pauwelussen, J.P. & Nijmeijer, H., Validation of longer and heavier vehicle combination simulation models., *proc. Proceedings SAE ComVeh*, Chicago, USA, 2013 (ref. [70])
- Kural, K., Besselink, I.J.M., Pauwelussen, J.P., Nijmeijer, H. & Patel, K., Analysis of driver behavior during reverse driving of double articulated vehicles, *proc. HVTT 13*, San Luis, Argentina, 2014 (ref. [72])
- Besselink, I.J.M., Kraaijenhagen, B., Pauwelussen, J., Kural, K., et al., Greening and safety assurance of future modular road vehicles, *proc. HVTT 13*, San Luis, Argentina, 2014 (ref. [9])
- Kural, K., Besselink, I.J.M., Xu, Y., Nijmeijer, H. & Tomar, A., Driver support system for improved maneuvering of articulated vehicles using unmanned aerial vehicle, *proc. HVTT14*, Rotorua, New Zealand, 2016 (ref. [73])
- Kraaijenhagen, B., Kural, K., Pauwelussen, J., Weijers, S. & Besselink, I.J.M., A field research on the need of high capacity vehicles to reduce  $CO_2$  and improve profitability, *proc. HVTT14*, Rotorua, New Zealand, 2016 (ref. [66])
- Kural, K., de Saxe, C., Kharrazi, S., Asp, T., Kraaijenhagen, B., Pauwelussen, J., Smart infrastructure access policy: a highway towards more efficient road transport, *Proceedings of 7th Transport Research Arena TRA 2018*, Vienna, Austria, 2018 (ref. [76])
- Kural, K., Schmidt, F., Erlingsson, S., Vierth, I., Cebon, D., Lobig, A., Liedtke, G., FALCON Part IV. Validation of smart infrastructure access policy, *proc. HVTT15*, Rotterdam, Netherlands, 2018 (ref. [77])

## Chapter 2

# Performance Based European Legislation

### 2.1 Introduction

The principle of the European legislative framework as currently in use for the regulation of commercial vehicles is mainly prescriptive. It means that maximum limits for specific vehicle parameters are defined. These are for example vehicle weight and dimensions [29], [38], ensuring a dual objective: vehicle operational safety and predictable interaction with the infrastructure.

An alternative principle for the regulatory framework of commercial vehicle combinations, which do not comply with local prescriptive regulation, can be found in Australia [92], Canada [136], South Africa [94], and New Zealand [23]. Contrary to prescriptive legislation the principle is performance based. It contains several criteria to quantify the level of performance that is requested from the vehicle combination to get the access to a specific segment of the road network. This performance based approach is thus more flexible than prescriptive legislation. In some cases, as e.g. South Africa [76], the performance based scheme is accompanied with a self-regulated accreditation scheme which is mandatory for all participating vehicle operators and which focuses on load optimisation, driver wellness, vehicle maintenance, and productivity. This in total stimulates the implementation of new technology that improves the performance of commercial vehicle for particular criteria and ensures a better fit between the vehicle and the infrastructure, due to differentiation per road class.

In this chapter first, the existing European regulatory framework for commercial vehicles with respect to dimensions, weight, safety, and environment is reviewed. Next, the Australian performance based approach is introduced concisely. Because of the length and weight conflicts with the current prescriptive legislation a new framework is proposed for the usage of HCV's within the EU. The framework is principally based on already existing EU-prescriptive regulations, and combined with selected performance criteria from the Australian regulations, that guarantee operational safety

when the length and weight of the vehicle are not restricted. In addition a number of new performance criteria is proposed, related to the societal benefits that are driven by the megatrends.

## 2.2 Current European Legislative Framework

The current European legislative framework for towing and trailing vehicle units as well as vehicle combinations consists of a number of regulations and directives, as summarized in [64]. It should be noted, that a fundamental difference between a regulation and directive is that the former one must be applied in its entirety across all EU - member states, while a directive sets out the goal that all EU countries must achieve. It is up to individual countries to devise their own laws on how to reach these goals [43].

The legislation related to commercial vehicle limits and requirements can be categorized as follows:

- **Vehicle dimensions** - COUNCIL DIRECTIVE 96/53/EC [29]

Since the vehicle dimensions are prescribed by a directive, it provides to EU-member states a certain degree of freedom, which allows the operation of HCV's on the national level, such as in Nordic countries, Netherlands and Spain. However cross-border transport, that would fully exploit the potential of HCV's, is not permitted without mutual agreement of neighbouring countries. The main vehicle dimension limits as stated in this directive are listed in Table 2.1.

Vehicle Type/Dimension	Max. Limit [m]
Motor Vehicle length	12
Trailer length	12
Semitrailer :	
Coupling point - frontal wall length	2.04
Coupling point - rear wall length	12
Vehicle Combination:	
Tractor - Semitrailer overall length	16.5
Truck - Trailer overall length	18.75
Height	4
Width	2.55

Table 2.1: Maximum Vehicle Dimensions.



Vehicle Weight/Axle Load	Limit [ton]
Motor Vehicle:	
2-axle vehicle	18
3-axle vehicle	26
4-axle vehicle	32
Vehicle Combination:	
Truck - Trailer	40
Tractor - Semitrailer	40
Tractor - Semitrailer with 40-foot ISO container	44
Single Axle:	
Non-driven Axle	10
Driven Axle	11.5
Double Axle Load (Bogie):	
$d < 1$ m	11
$1 \text{ m} \leq d < 1.3$ m	16
$1.3 \text{ m} \leq d < 1.8$ m	19
$d \geq 1.8$ m	20
Triple Axle Load:	
$d < 1.3$ m	21
$d \geq 1.3$ m	24

Table 2.2: Vehicle weight and axle load limits ( $d$ =interaxle distance).

- **Vehicle Weight and Axle Loads** - COUNCIL DIRECTIVE 96/53/EC [29]

The admissible weight is regulated with respect to the gross vehicle weight (GVW) and with respect to an individual axle, or a group of axles. The weight limits ensure that the infrastructure, is protected against over-loaded vehicles. Bridges are of a particular concern. The combination of the axle load and the inter-axle spacing distance  $d$  plays a major role in the loading pattern. Axle load limits, as well as overall vehicle combination weight limits, are listed in Table 2.2.

- **Manoeuvrability** - REGULATION (EU) No 1230/2012 [35]  
- DIRECTIVE 97/27/EC [30]

There are two manoeuvrability criteria that are primarily derived from the design codes of European infrastructure, which limit the maximum curvature of a road according to their classification and maximal allowed speed [110]. The first criterion is the swept path, being the vehicle spatial envelope that is occupied by the vehicle during the manoeuvre. The swept path is depicted by the gray color annulus area depicted in Figure 2.1(a). This area can not be trespassed by the contours of inner and outer most points of the vehicle combination during low-speed steady cornering.

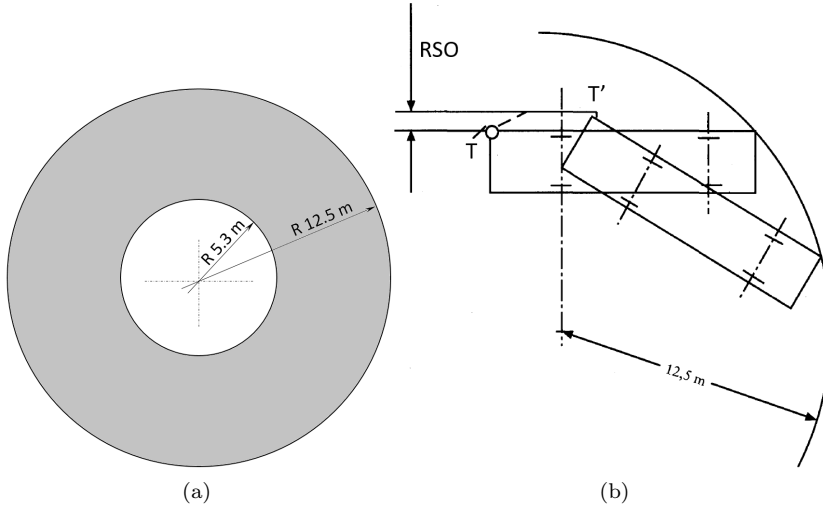


Figure 2.1: (a) Allowed vehicle combination swept area, in gray, (b) Definition of the rear swing out (RSO).<sup>[30]</sup>

The second criterion, called Rear Swing Out (*RSO*), is related to the space, which the vehicle will occupy with its rear most outer corner *T* on an circle with a radius 12.5 m, as depicted on Figure 2.1(b). This criterion is very important for the spatial planing of the infrastructure accessories, such as traffic signs. The maximum allowed limits are listed in Table 2.3.

Rear swing out in turn with a radius of 12.5 m	
Motor Vehicle	0.8 m
Articulated Vehicle	1.2 m

Table 2.3: Rear swing out limits.

- **Traction** - REGULATION (EU) No 1230/2012 [35]

Vehicle traction is regulated to primarily ensure that sufficient torque can be transmitted from the engine to the road through the tyre by prescribing minimal engine power per ton of gross vehicle weight. Next, it prescribes a minimal axle load for the steerable axles to guarantee sufficient cornering force potential in sharp turns to overcome scrubbing of non-steerable axles. Lastly, the minimal slope is specified, that the vehicle is able to climb from the standstill state. The limits associated with the traction are given in Table 2.4.

- **Exhaust Emissions** - REGULATION (EC) No 595/2009 [33]

Since 2013, the exhaust emissions of all new towing vehicle units need to comply with, so called, Euro VI regulation, that limits the emissions of  $NO_x$ ,  $CO$ ,  $HC$ ,

Traction limits	
Driving Axle Load	min. 25 % of GVW
Engine Power	min. 5 kW/t of GVW
Steering Axle Load	min. 20 % of GVW
Slope	min. 12%

Table 2.4: Traction Limits.

and particulates. The exhaust emissions are measured in two different drive cycles:

- World Harmonized Steady-state Cycle,
- World Harmonized Transient Cycle.

Both cycles have been created, to cover representative operational conditions in Europe, but also USA, Japan, and Australia. They might be used in combination with engine map and so called VECTO tool [129] to calculate the fuel consumption and CO<sub>2</sub> emissions of a towing vehicle disregarding however the configuration of all the trailing units. As the complete regulation related to exhaust emissions is rather extensive, we refer to [33] for further details.

- **Brakes and Active Safety Systems** - R (EC) No.661/2009 [32]
  - UNECE Regulation No. 13 [126]

These regulations define mandatory requirements for the braking performance from several perspectives. It indirectly prescribes the usage of an Anti-Lock Brake System (ABS). Besides minimal deceleration on a straight path for a number of scenarios, it also defines braking stability performance for a split surface and parking on a slope, as listed in Table 2.5.

Braking System Criteria	Limit
Minimal Average Deceleration:	
60 km/h to standstill with engaged engine	5 m/s <sup>2</sup>
90 km/h to standstill with disengaged engine	4 m/s <sup>2</sup>
60 km/h to 30 km/h after 20 repetitions	4 m/s <sup>2</sup>
60 km/h to standstill after 6 km of continuous braking	3.3 m/s <sup>2</sup>
Minimal Braking Efficiency:	
50 km/h to standstill on surface with friction 0.8	75%
50 km/h to standstill on surface with friction 0.3	75%
Braking Stability on a straight path:	
90 km/h to standstill with deceleration 4 m/s <sup>2</sup>	Subjective
Braking Stability on split friction surface:	
Max. steering wheel correction from initial speed 50 km/h	240°
Minimal parking ability on a slope with fully laden vehicle:	
Single vehicle	18%
Vehicle combination with unbraked trailer	12%

Table 2.5: Braking system requirement limits

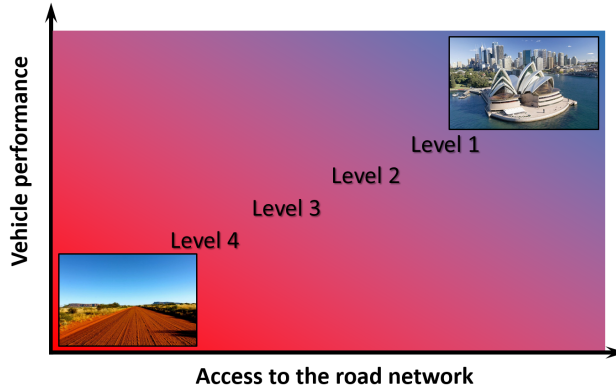


Figure 2.2: Performance of vehicle as a function to the road access.

The regulation also prescribes compulsory active safety systems that needs to be fitted on a vehicle units produced since November 2015. These are Advanced Emergency Braking System (AEBS), Lane Departure Warning (LDW), and Electronic Stability Control (ESC). Conformity requirements on their functionality are defined in the UNECE regulation. However, these are of general character and do not prescribe any detailed requirements related to the vehicle dynamical performance.

## 2.3 Australian PBS Framework

Contrary to the prescriptive legislative framework of the EU, which mainly applies to a single vehicle units, an alternative approach has been successfully implemented in Australia [92], Canada [136], South Africa [94], and New Zealand [23]. This approach is very feasible for vehicle combinations and explicitly defines the performance level required from the vehicle combination with respect to safety, manoeuvrability, and infrastructure loading, rather than mandating limits that should eventually lead to achieve the desired performance, as is the case for prescriptive legislation.

This policy is commonly known as Performance Based Standards (PBS) and is used for vehicle combinations that do not fit in the prescriptive scheme of specific country. Hence, in case of commercial vehicles combinations, one can generally say it does not matter what the vehicle combination looks like, but how it performs in specifically defined scenarios.

The performance of a commercial vehicle is subsequently used to allow access to specific segments of the road network. The road network is categorized into four levels as depicted in Figure 2.2. It ensures a proper match between the vehicle and the infrastructure network in terms of safety, manoeuvrability and bearing capacity of the infrastructure. Moreover, it provides flexibility in the design of vehicles, that is not directly limited by the dimensions, and stimulates the implementation of novel technologies that improve the performance of the vehicle combination.

The Australian performance based scheme [92] can be split into two main parts:

- 16 vehicle safety standards
- 4 infrastructure standards.

First we will concisely, without quantifying the performance levels, summarize the standards related to vehicle safety, which can be categorized into four groups:

- **Low-Speed Longitudinal Performance**

This group is directly related to the traction abilities of the vehicle on a slope, which are linked to the powertrain performance. It aims to assess aspects as commencement of motion, maintaining of motion, or achieving a desirable level of acceleration, such as listed in Table 2.6.

Performance Measure	Explanation
Startability	The maximum uphill gradient, expressed as a percentage, on which the vehicle is capable of commencing forward movement from rest.
Gradeability	The maximum uphill gradient, expressed as a percentage, on which the vehicle can climb at a specified constant speed.
Acceleration Capability	The ability to accelerate the vehicle either from rest or to increase speed.

Table 2.6: Low-speed longitudinal performance measures.

- **High-Speed Longitudinal Performance**

The measures, listed in Table 2.7, can be translated into tracking performance of the vehicle combination. Good tracking performance ensures that the rearmost axle follows the path of the front axle with sufficient fidelity, without endangering other vehicles on the road. Typical behaviour of axle trajectories, while driving high-speed on an uneven banked road, which results in lateral offsets, is depicted on Figure 2.3.

Performance Measure	Explanation
Tracking Ability	Amount of variation in the lateral position of the trailing unit (last trailer) measured relative to the path or track followed by the hauling unit (rigid truck or tractor) on an uneven banked road.
Directional Stability Under Braking	The ability of a vehicle to decelerate while remaining directionally stable, controllable and staying within its lane during heavy braking.
Overtaking Provision	The time taken for another vehicle to safely overtake the vehicle.

Table 2.7: High-speed longitudinal performance measures.

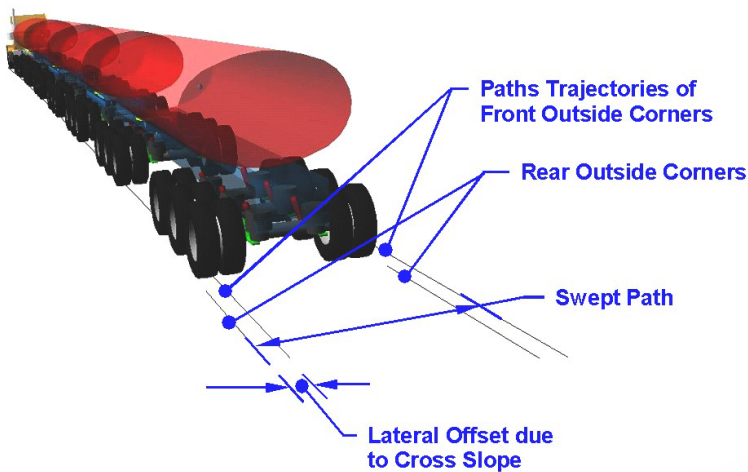


Figure 2.3: A view of axle trajectories while tracking on banked road at high speed<sup>[92]</sup>.

- **Low-Speed Directional Performance**

This group covers the performance regarding low-speed manoeuvrability. This can be translated into the spatial envelope of the vehicle combination that is being swept during a ninety degree turn on a predefined radius, as depicted in Figure 2.4. A big swept path is undesirable, because the vehicle combination will require more road space for turning than may be available. Such a vehicle may intrude into adjacent or opposing lanes, collide with other vehicles, damage roadside furniture, or imperil pedestrians. Performance measures related to the low-speed manoeuvrability are listed in the Table 2.8.

- **High-Speed directional Performance**

The performance measures defined in this group, cover the safety assessment of the vehicle combination behaviour during high-speed evasive manoeuvres, such as for example a lane-change. Typically there are two ways in which the stability

Performance Measure	Explanation
Low-Speed Swept Path Width	The swept path width is the maximum distance, between the outer most and inner most path trajectories of the swept path envelope of the vehicle combination being assessed in the specified low-speed turn. The maximum distance, is the straight line segment intersecting both trajectories perpendicularly to their respective tangents at the intersection points.
Steer Tyre Friction Demand	The maximum friction level demanded of the steer tyres of the hauling unit in a small radius turn at low speed.
Frontal Swing	Frontal swing is the maximum distance between the outermost path of the furthest forward or outside point on the vehicle on the outside of the turn and inner path of the outer most point on the outer tyre sidewall on the forward most outside steered-wheel in the specified low-speed turn. It is measured as the straight-line segment intersecting both trajectories perpendicularly to their respective tangents at the intersection points.
Tail Swing	On the entry side of the turn, the tail swing is the length of the longest line segment perpendicular to the low-speed turn entry tangent intersecting it with the path trajectory of rearward or outside point, on the vehicle unit.

Table 2.8: Low-speed directional performance measures.

of commercial vehicle can be compromised. Firstly, when the lateral acceleration during cornering may generate sufficient overturning moment to lift the tyres at one side of the axle, which may eventually promote a roll-over of entire vehicle combination. Secondly, the risk of so called jack-knifing occurs when the towing vehicle unit becomes oversteered so the gain between the steering angle and articulation angle becomes unstable. It results in rapid growth of the articulation angle between the vehicles that ultimately reaches the mechanical limits of the coupling, which results in an entirely uncontrollable vehicle combination. The performance measures related to high-speed directional performance are listed in Table 2.9.

It should be noted that a performance measure of load transfer ratio is not part of Australian scheme but originates from a Canadian scheme [136]. However as it is seen relevant, it is included in the Table 2.9.

<b>Performance Measure</b>	<b>Explanation</b>
Static Rollover Threshold	The steady-state level of lateral acceleration that a vehicle can sustain during turning without rolling over.
Rearward Amplification	Degree to which the trailing unit(s) amplify or exaggerate lateral acceleration of the hauling unit.
Yaw Damping	The rate at which “sway” or yaw oscillations of the rearmost trailer decay after a short duration steer input at the hauling unit.
Load Transfer Ratio	The proportion of vertical load imposed on the tyres on one side of a vehicle unit that is transferred to the other side of the vehicle unit during a standard lane change maneuver.
Handing Quality (Understeer/Oversteer)	Ratio of the response to steering (change of vehicle direction) to the steering wheel input, and its dependence on vehicle speed and severity of the maneuver.
High-Speed Transient Off-tracking	The lateral distance that the last-axle on the rear trailer tracks outside the path of the steer axle in a sudden evasive maneuver.

Table 2.9: High-speed directional performance measures.

<b>Performance Measure</b>	<b>Explanation</b>
Pavement Vertical Loading*	The axle group loads for a PBS vehicle shall not exceed the maximum permitted on the route network for commercial heavy vehicles. the loads per axle group types are limited to present prescriptive configurations.
Pavement Horizontal Loading*	The degree to which horizontal forces are applied to the pavement surface, primarily in a low-speed turn, during acceleration and on uphill grades.
Tyre Contact Pressure Distribution*	The minimum tyre width that is allowed, the maximum pressure, and pressure variation that is applied to the road surface by a single tyre, or pair of tyres in a dual tyred set.
Bridge Loading (Bridge Formulae)	The maximum load that a bridge can sustain under repeated loading without incurring damage.

Table 2.10: Infrastructure impact measures



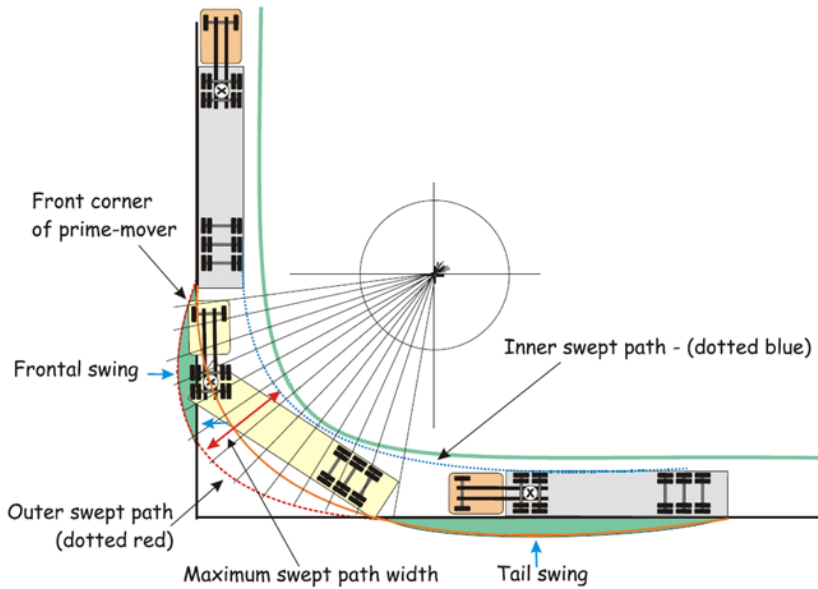


Figure 2.4: Swept path of tractor-semitrailer during low speed ninety-degree turn<sup>[5]</sup>.

- **Infrastructure Impact**

Four infrastructure-related standards, considering the vehicle impact on the pavement and bridges are summarized in Table 2.10. Although these standards are part of the performance scheme some of them (indicated with an asterisk) are prescriptive. The main purpose of this group is to limit the stress on the pavement layers below the surface of the road, to regulate road wear by limiting the impact of the horizontal tyre forces when turning, and tractive tyre forces of the drive axles when a vehicle is accelerating, braking, or climbing an upgrade. Furthermore the standards protect bridges against excessive vertical loading, potentially caused by a vehicle combination, when the weight has to be distributed over a too short vehicle length.

## 2.4 Principles for a Future EU-Legislative Framework

Referring to Section 2.2, it can be concluded that the existing EU regulation does not allow any HCV's, which are longer than 18.75 meters and heavier than 40 tonnes for cross border transport on federal level. In this section, the prescriptive European legislation is compared with the Australian performance based approach to analyse potential similarities. The aim is to maintain the majority of the already established EU-legislation, avoid the redundancies, and implement only the performance measures which are not currently covered. The framework should primarily ensure operational

safety through covering all traffic risks, as defined for instance in [61], which may occur by interconnecting vehicle units into a longer vehicle combination, and yet avoid excessive loading of the infrastructure, if the length and weight limits of the vehicle combination are less restrictive.

The proposed principles of a future legislative scheme have to be compatible with the current infrastructure. Hence, it should be emphasized that several of the prescriptive requirements, such as maximum axle loads or the width and the height of the vehicle combination, have to be preserved as they are determined by infrastructure design criteria.

In order to define the principles, a comparison between the European and Australian approach is given in Table 2.11. It has four columns designating the number of regulation, the Australian PBS measure, current EU-legislation equivalent and proposal for a future EU-legislation. The categorization of the previous section will be used to address the vehicle performance in:

- **Low-Speed Longitudinal Performance** (regulation 1-3)
- **High-Speed Longitudinal Performance** (regulation 4-6)
- **Low-Speed Directional Performance** (regulation 7-10)
- **High-Speed Directional Performance** (regulation 11-16)
- **Infrastructure Impact** (regulation 17-20).

A comparison with all Australian PBS measures, one by one to the current EU-legislation will be made to investigate the possible overlap. Based on the discussion given next, a decision is made, resulting in a proposal for future legislation that is fusing both the performance and prescriptive approach. This proposal is listed in the last column of the Table 2.11.

Regarding the low-speed longitudinal performance, one can observe that the Australian PBS measures are fully covered by current prescriptive EU-legislation. It defines a lower limit for engine power in kW/tonne as well as a minimum slope that the vehicle combination must be able to climb from the standstill. Hence, changes are not really required as the Australian PBS-scheme is fully covered by the existing regulations.

High-speed longitudinal performance is covered by three performance measures. The tracking ability measure in the Australian framework is especially dedicated to assess very long vehicle combinations having three and more articulation points, and length above 35 m. As the deployment of such a vehicle combination on European roads is not anticipated, this measure is not considered to be important for future legislation. Concerning the directional braking stability it can be seen in Table 2.5, that this measure is already extensively covered by current EU legislation. The overtaking provision is not considered relevant for the European condition. It is not planned or expected that HCV's should operate on single lane roads, where they would be overtaken by passenger cars or allowed to overtake other vehicles on the road.

No.	Australian PBS Measure	Current EU-Legislation	Proposed EU legislative principles
1	Startability	R No 1230/2012 - Min. slope	R No 1230/2012 - Min. slope
2	Gradeability	R No 1230/2012 - Min. engine power	R No 1230/2012 - Min. engine power
3	Acceleration capability	R No 1230/2012 - Min. engine power	R No 1230/2012 - Min. engine power
4	Tracking ability	N/A	N/A
5	Directional braking stability	R No 661/2009 - Braking stability	R No 661/2009 - Braking stability
6	Overtaking provision	N/A	N/A
7	Low-speed swept path width	D 97/27 EC - Max. swept area	D 97/27 EC - Max. swept area
8	Steer tyre friction demand	R No 1230/2012 - Min. steer axle load	R No 1230/2012 - Min. steer axle load
9	Frontal swing	N/A	Use Australian definition
10	Tail swing	D 97/27 EC - Tail swing	D 97/27 EC - Max. tail swing
11	Static rollover threshold	N/A	Use Australian definition
12	Rearward amplification	N/A	Use Australian definition
13	Yaw damping	N/A	Use Australian definition
14	Load transfer ratio	N/A	Use New Zealand definition
15	High-speed transient offtracking	N/A	Use Australian definition
16	Handling quality	N/A	N/A
17	Pavement vertical loading	D 96/53/EC - Max. axle load	D 96/53/EC - Max. axle load
18	Pavement horizontal loading	D 96/53/EC - Axle spacing vs. load	D 96/53/EC - Axle spacing vs. load
19	Tyre contact pressure distribution	D 96/53/EC - Air suspension required	D 96/53/EC - Air suspension required
20	Bridge formulae	N/A	N/A

Table 2.11: Comparison of EU legislation with Australian legislation and proposal for future legislative principles.

Manoeuvrability is examined by the directional performance measures at low-speed. As can be seen in Table 2.11, low-speed swept path width and the tail swing are already covered by D 97/27/EC [30], which is proposed to be preserved in the future legislation framework, considering also dimensions and design codes of current infrastructure. However the limits of the maximal swept path width should be reviewed and projected into number of access levels, which will be consistent with infrastructure segments where the vehicle combinations should operate, considering the fact that HCV's do not need to have general access to the entire infrastructure. The steer tyre friction demand is regulated through the prescriptive limit of minimal vertical load on the steerable axle. Furthermore this regulation prescribes minimal vertical load on the driven axle ensuring sufficient traction in the slopes and in sharp corners where a high level of wheel slip on non driven and non-steered tyres is anticipated. Hence, it is recommended to employ the current regulation also in the future. A missing measure is the frontal swing, that is not addressed in current EU-legislation. The performance of the vehicle combination for this standard is strongly correlated to the distance between the center of the front steerable axle, and frontal outside corner of the hauling unit. This distance is very likely to increase in the near future.

This is due to expected innovations of the front end design, which will enhance the vehicle aerodynamics. Therefore is proposed to incorporate this measure as defined by Australian PBS scheme in future legislation. It will ensure that new cabin designs, or other vehicles in the combination, such as e.g. steered dollies, will not have an impact on the roadside furniture or imperil the pedestrians.

Directional performance at high-speed is crucial. It primarily assesses the vehicle stability during evasive manoeuvres, which might occur on the highway at velocities above 80 km/h when trying to avoid e.g. a sudden obstacle. Current EU-regulation simply limits the length, weight, and since 2015 prescribes obligatory active safety systems on board (AEBS, LDW, and ESC), which combined together should guarantee stability. However, the regulation does not contain any specific performance requirements, which are mandatory for the conformity of vehicle safety and stability. To cover these aspects more profoundly, it is proposed to incorporate the Australian performance-based principles in the future legislation. It contains explicit definitions of vehicle dynamic performance that is required to guarantee lateral stability at high speed. This approach will ensure that HCV's, which are longer than 18.75 meters, and heavier than 40 tonnes, perform on comparable level as already existing vehicle combinations, which operate within D 96/53/EC [29], and thus do not represent a potential risk when executing dynamic manoeuvres at high speed. The measure of handling quality, in line 16, will not be incorporated as the definition in the Australian scheme is not finalized and not in use as well.

The last category, as listed in Table 2.11, are infrastructure requirements. The PBS measures number 17-19, related to the pavement loading are well covered by current principles of European legislation, which is proposed to be preserved. However, the performance standard that accounts for the impact of a vehicle combination on a bridge is not defined in Europe. The fundamental reason is probably the different design criteria for bridges in all 28 European jurisdictions, which would be very difficult to harmonize, considering the existing infrastructure. Nevertheless, bridge formulae that would be able to assess the impact of vehicle combinations, considering

its dimensions and loading conditions, on bridges, is seen as very beneficial. Therefore extensive research should be done to investigate, whether the concept of generic bridge formulae can be applicable to European conditions, which incorporates the various bridge design criteria. Subsequently it can be used the design or evaluation of new bridges. For now however, the Australian bridge formula is not included in the principles of future legislation, as it is not considered to be representative for European conditions.

As described earlier, the Australian scheme specifies four performance levels for each standard, which are used as access criteria for dedicated segments of the infrastructure network. In the proposal of principles for the future EU-legislation concept, no performance levels are included because of two reasons. Firstly, the existing levels are based on Australian operational conditions, frictional levels, or infrastructure design criteria and dimensions, which are not identical to Europe. Secondly, the intention of the proposal is not to copy the Australian approach and having four different road levels. In Europe, except for Scandinavia, one can not observe large-space remote areas, such as the Northern territory in Australia. Therefore, it is logical to primarily specify one level of performance that will fit to the main European road network, such as for example the TEN-T corridors, because the HCV's should primarily operate here and bypass the city-centers or residential areas while emphasizing synchronomodality. A feasible example can be found in the Netherlands, where the national heavy vehicle regulator (RDW) provides open-access digital map [26] of the roads, which are granted by the exception to allow HCV's operation as shown in Figure 2.5. In practice, if the vehicle operator wants to drive a HCV on certain infrastructure segment, he officially requests RDW to assess required infrastructure section. RDW will use well defined assessment procedure [84], which reflects on the infrastructure and vehicle dimensions, including also the manoeuvrability. If the infrastructure segment satisfy the criteria, the road 'opens' for HCV's, becomes a green in the digital map, and can be used by all other operators as well. In case of assessment failure, the segment becomes definitely red, and no HCV's are granted with the access.

Given the fact that part of the society is opposing nowadays to deployment of HCV [96], it is seen as desirable to incorporate in the future regulation also measures that can quantify the performance of the HCV's versus classical HGV in terms of societal benefits. Presenting the added value in terms of societal benefits, might build a bridge between the road transport sector and the policy makers. A generic proposal of areas with societal impact, that might be applicable for this purpose, may be found in [135]. It includes:

- Safety (Road crash casualties, or number of accidents)
- Public health
- Mobility & congestion
- Sustainability
- Infrastructure utilization
- Economic impact

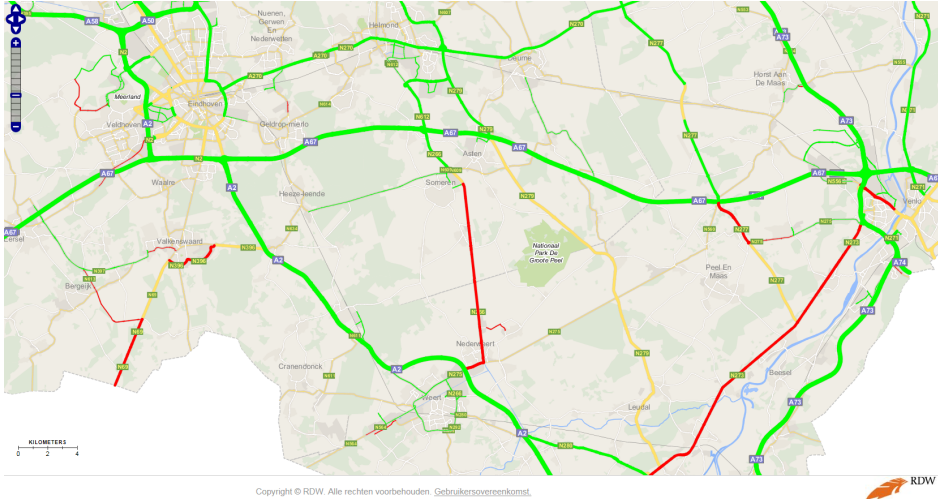


Figure 2.5: Digital open-access map in Netherlands [26] designating infrastructure segments which may be accessed by HCV's where green color designates accessible roads, red coloured segments are forbidden for HCV's operation, and uncoloured segments are to be assessed but HCV's can not operate there either.

- Decarbonisation and environmental impact

Obviously, the translation of all societal impact areas into explicit benefit-related measures may be complex and goes beyond the scope of this research. In accordance with previous research [65], it is proposed to begin with Economic impact and de-carbonisation. Both can be established using already existing methodology and measures for certain model scenarios that can be standardized. The proposed societal benefits performance measures are listed in Table 2.12.

No.	Societal Benefit Measure	Units
1	Carbon dioxide pollution - load-wise	CO <sub>2</sub> /ton.km
2	Carbon dioxide pollution - volume-wise	CO <sub>2</sub> /m <sup>3</sup> .km
3	Fuel consumption - Load-wise	l/ton.km
4	Fuel consumption - Volume-wise	l/m <sup>3</sup> .km
5	Transport costs - Load-wise	€/ton.km
6	Transport costs - Volume-wise	€/m <sup>3</sup> .km

Table 2.12: Proposed societal benefit measures for future regulations

Considering the comparison of European and Australian the legislative principles, in Table 2.4 two main conclusions may be drawn. At first, it may be observed that current EU-legislation already has performance based elements, and by simply increasing the maximal vehicle combination length the HCV's can be implemented, when complying with the rest of already existing regulations and directives. Secondly, no

performance or prescriptive measures are established in current EU-legislation regarding the high speed directional performance which is of particular importance. The measures included in this group are related more than any other to the traffic safety, and lateral stability of a vehicle combination at high speeds. Therefore it should be emphasized to include these measures in the principles of the future legislation.

The proposal of principles for future EU legislation framework, in Table 2.4 and Table 2.12 will be used in Chapter 4 to evaluate the concepts of HCV's that will comply with logistic needs for years beyond 2020, regarding, safety, environmental, and profitability aspects.





## Chapter 3

# Generic Multi-Body Simulation Model

### 3.1 Introduction

To assess the performance of arbitrary vehicle combinations a modular model library needs to be created. This multi-body model library has to be flexible and generic, thus the modification of parameters or vehicle configuration has to be possible with minimal effort. To avoid complexity, the model should include only the vehicle components, which significantly influence the vehicle dynamic behaviour for the performance assessment manoeuvres described in Chapter 2.

For these reasons, the model is built using a multi-body formalism. The equations of motion are generated automatically by the software package. In this case SimMechanics, the multi-body toolbox of MATLAB/Simulink, is used.

The chapter is structured as follows. Firstly, the development and the topology of vehicle models are described. Next, testing and validation with three different vehicle combinations are done to increase the fidelity of the model. Finally, a systematic step-wise approach is defined, and the models are validated against the experimental data covering both low- and high-speed scenarios. The scenarios for the validation are selected to be representative for test manoeuvres defined in the future regulations as proposed in previous chapter.

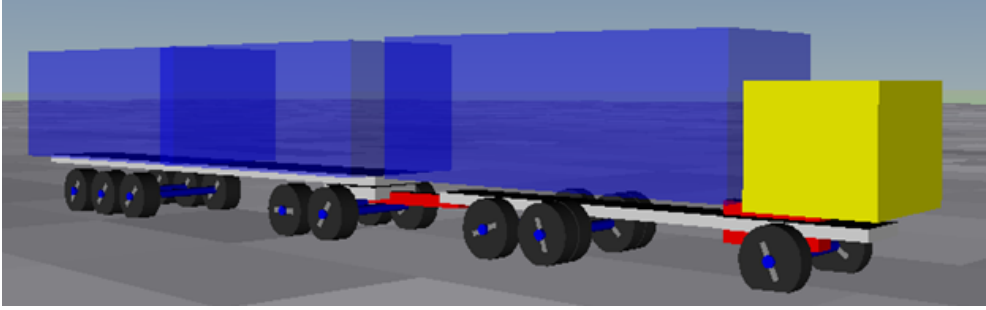


Figure 3.1: Model visualization of a HCV by the Virtual Reality Toolbox.

## 3.2 Model Library

Considering a high number of permutations of standardized vehicle components which are needed to build various types of HCV's a library-based modelling approach is preferable. The performance criteria, identified in Chapter 2 and given in Table 2.11, can be used to motivate the modelling approach. The criteria can be translated into driving scenarios which the vehicle models have to be able to reproduce with high level of fidelity. These are: the high speed handling behaviour which includes the roll dynamics of each vehicle unit, the low speed manoeuvring, the longitudinal dynamics covering both braking and acceleration on flat roads but also on the slopes.

Given that, it has been decided to build up the model library using a multi-body formalism as it handles complex non-linear mechanical system dynamics without the need to manually derive the dynamic equations of motion or constraint equations, which is seen beneficial given the scope of this study. Multi-body modelling approach is successfully employed in virtual prototyping for more than 30 years. Nowadays, a number of commercially available multi-body oriented packages are on the market. In principle, they can be clustered in two groups:

- Dedicated Multi-body packages (TruckSim, IPG Truckmaker, or DYNA4)
- Generic Multi-body packages (ADAMS, SimPack, LMS Virtual Lab, Modelica or MATLAB/SimScape).

Dedicated multi-body packages are easy to operate due to built-in graphical interface and user friendly visualization tools. However the flexibility and the modularity for applied research and development may prove to be a limitation, which is in contrast very good in case of generic multi-body packages.

The model library is created in SimMechanics, the multi-body modelling toolbox of MATLAB/Simulink. Although SimMechanics is not especially designed for simulating vehicle dynamics, due to its flexibility one can customize it for this application while maintaining good interfacing with other MATLAB Toolboxes. An essential part of the vehicle model is undoubtedly the tyre, which is represented by the TASS Delft-Tyre model. The visualization and animation of a vehicle is done using the MATLAB Virtual Reality Toolbox, as depicted in Figure 3.1.

The model library consists of generic, modular and self-contained systems and sub-subsystems that represent types of commercial vehicles and their main components. The initial version was developed at the Eindhoven University of Technology, by Dr.Ir. I.J.M. Besselink [8], which was further expanded by a graphical user interface, enabling to rapidly build arbitrary vehicle combination, active safety systems such as ABS, and PBS-test routines including the post-processing scripts.

The commercial vehicle library is divided in five main sections:

- Towing vehicle units (tractors, rigid trucks)
- Trailing vehicle units (semitrailers, dollies, link-trailers, etc.)
- Assemblies (cabins, loading units, axles, etc.)
- Components (tyre, brake system, powertrain)
- Utilities (filters, sensors, active safety systems, etc.)

The library structure is highly modular in order to give the user freedom to create many different combinations of vehicle units. At the same time, the user has the flexibility to customize all the components of each sub-model which are then automatically propagated to the top-level model. The main objective of the library is to represent a general vehicle and avoid details that may differ between manufacturers as for example non-linearities in chassis suspension, roll steer or cabin-chassis suspension layout. These can be introduced when needed.

Every sub-model has its own local coordinate system, with respect to which the position and the dimension of the components within this model are specified. For the towing vehicles, the origin of its own coordinate system is placed at the front tyre contact point. For towed units, the origin is the point where a vertical line passing through the kingpin or coupling is crossing the ground. When creating a vehicle combination, the local coordinate system of the towing vehicle is considered the global coordinate system with respect to which the local systems of all the units are positioned. The coordinate systems are right handed i.e. the positive X-axis points forward, the positive Y is towards left and Z-positive is directed upward, as depicted in Figure 3.2.

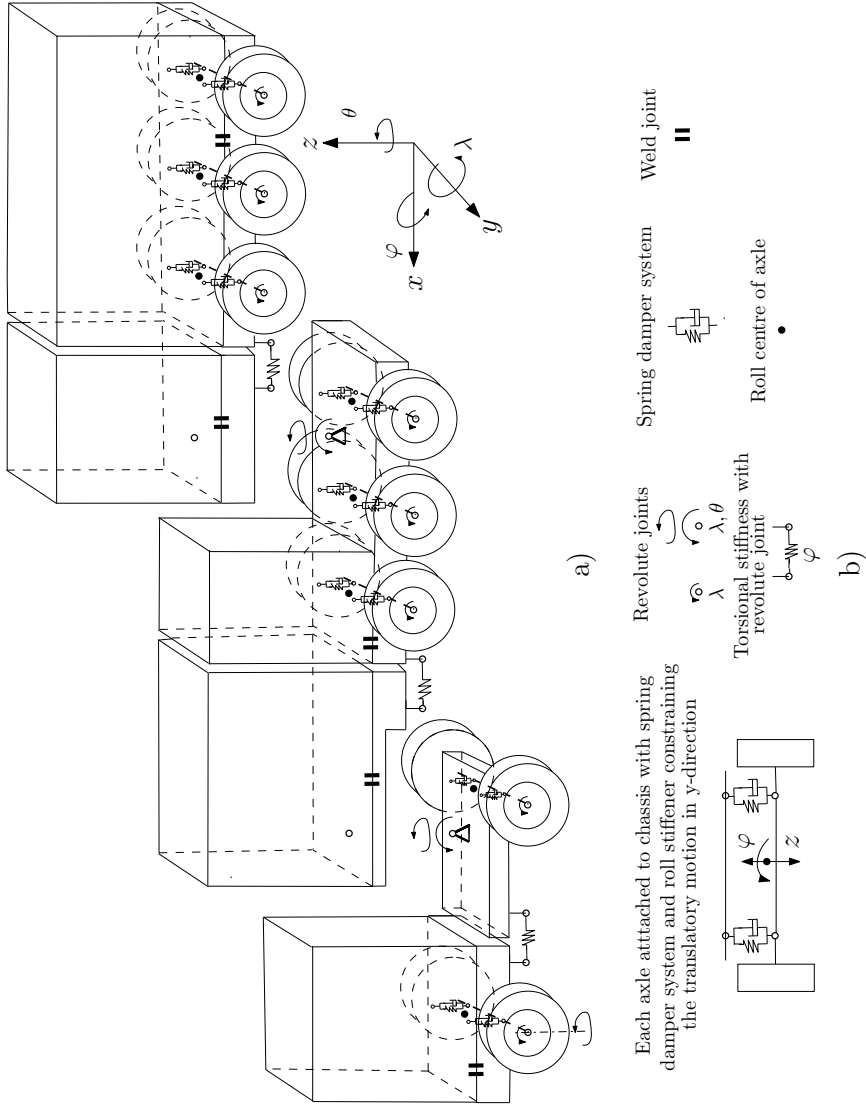


Figure 3.2: Multi-body vehicle model a) Visualization of multi-body model degrees of freedom b) Legend.

As an example we will demonstrate the topology of the multi-body model, which consists of 2-axle Tractor, link-trailer, and a semitrailer, which is also known as a B-Double HCV. Both trailers are equipped with 3 axles, as shown in Figure 3.2. The tractor module is composed of a chassis divided into two parts, front and rear, connected to each other with a revolute joint and a torsional spring to include the torsional stiffness of the vehicle frame. Cabin and engine are rigidly connected to the chassis and the steer and drive axle are linked to the chassis by means of suspension system. The axle module has only two degrees of freedom with respect to the chassis module: the z-axis translation and the x-axis rotation, see Figure 3.2. Two linear springs and two linear dampers are included, one on the left and one on the right side of the axle. A torsional spring is located at the roll center, representing the anti-roll bar that in combination with a already mentioned revolute joint between the front and rear part of the chassis allows to model the roll dynamics which is essential for heavy goods vehicles as described in [58]. On both ends of the steering axle is a revolute joint with rotational degree of freedom around the z-axis which connects the axle with the wheel hub. The angles at these joints are determined by the steering system.

For validation purposes, this steering angle has been directly measured on the wheel hubs. These wheel hubs are then connected to the Delft Tyre module, using a revolute joint, which represents the wheel bearing. On both ends of the driven axle, these joints receive a moment generated by the driveline model. Similarly the brake moment may be applied to all axles.

The link-trailer and semitrailer are composed in a similar way: the chassis is divided in a front and rear part connected by a torsional spring in between. The loads are connected rigidly to each chassis element, and the three axles are linked through a suspension system similar to the tractor module. As none of the axles is steerable, all the wheels are directly connected to the axle by a revolute joint. Furthermore, the kingpin is rigidly connected to the chassis, for the coupling with other towing units through the 5<sup>th</sup> wheel. The coupling joint between kingpin and the 5<sup>th</sup> wheel has yaw and pitch degree of freedom, but no flexibility in the roll direction, or play is assumed. The center of gravity of the trailer depends on the masses of the vehicle components and on the cargo, which is modelled using a mass density.

The Delft-Tyre Model governs the vertical, lateral and longitudinal forces of the tyres, employing the Magic Formula tyre model of Pacejka [99]. The library includes three types of tyre parameter sets, one for the steered axle, one for the driven axle and another one for the trailer axle. In the validation process, also the tyre model parameters have been slightly adapted to adjust the cornering stiffness so the model matches the measurement output better.



Figure 3.3: Three types of HCV combinations used in the experiments.

### 3.3 Experiments

To increase the fidelity and validate the multi-body models several full scale experiments have been done with three different HCV combinations:

1. 6x2 Rigid truck, 2-axle dolly, and 3-axle container semitrailer (TK6x2-DY2-ST3)
2. 4x2 Tractor, 3-axle link trailer, and 3-axle double-decker semitrailer(TR4x2-LK3-ST3)
3. 6x2 Tractor, 2-axle semitrailer, and 2-axle central axle trailer(TR6x2-ST3-CT2).

As shown in Figure 3.3, all HCVs have two articulation points and a length of 25.25 m. The vehicle combinations are chosen differently on purpose, in order to validate different vehicle configurations from the library. Furthermore each vehicle combination is tested in two different loading conditions to evaluate dynamic behaviour for different axle loads and moments of inertia. The overall maximal vehicle weight for all three combinations is limited to 60 tonnes, which is also the maximum allowed for HCVs in The Netherlands.

The instrumentation involves more than 100 measurement channels enabling to collect sufficient data required for the validation of multi-body model behaviour in longitudinal, lateral and vertical direction. Considering the nature of the performance based framework as described in previous chapter, the emphasis is on validating the vehicle models for high-speed handling and low-speed manoeuvring.

A schematic overview of the sensors on the second HCV combination is given in Figure 3.4. As can be seen, the position, velocity and acceleration are measured for

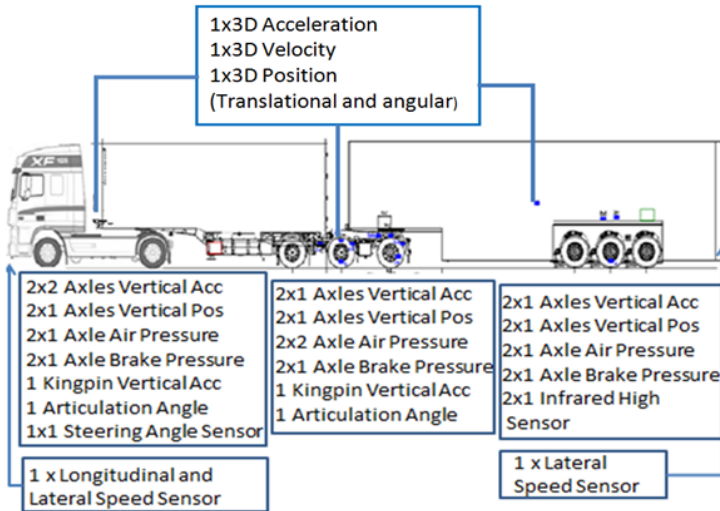


Figure 3.4: Sensors instrumentation used in experimental testing.

each vehicle body in translational and rotational direction. Additional potentiometer sensors measuring the displacement between chassis and axles, as well as vehicle bodies with respect to each other, are incorporated. Potentiometers are used for measurement of the steering angle of the front axle for both the left and right wheel. Furthermore, signals from the CAN-bus of the towed vehicle are recorded, such as the angular velocity of wheels, the engine torque, and the brake pressure. The sampling frequency is in most of cases 100 Hz, only the signals coming from the CAN-bus are limited to 10 Hz. The instrumentation for the two other vehicle combinations is done in the same way.

The tests are executed on proving grounds at Lelystad in Netherlands and Jeversen in Germany. The vehicles are tested for both high and low-speed scenarios, but also on different road frictional surfaces. Each vehicle combination is weighted per axle for both loading conditions and in an empty state. Test scenarios are performed in accordance with ISO 14791:2000 E [59] and the Australian PBS scheme [92].

The test plan manoeuvres are:

High-speed:

- Single Sinusoidal steer input at 0.4 Hz
- Pulse steer (half sine)
- Single lane change
- Steady state cornering
- Braking on different surfaces with different deceleration and road curvature
- J-turn
- Maximum longitudinal acceleration.

Low speed:

- 90 and 180 degree circle with an external radius of 12.5 meters
- Passing over a vertical obstacle
- Rearward parking manoeuvre

Each test session commenced with calibration measurements, which aimed to obtain all sensor readings at static conditions when the vehicle combination is straightened, i.e. the articulation angles, and longitudinal speed equate nil.

### 3.4 Model Validation

A quantitative validation of the dynamic multi-body model is necessary and important step to gain the confidence in the simulation results, which presumes the availability of the experimental data. Thus, the model can be used for credible research. It is targeted to the model applications mentioned earlier, i.e. low speed manoeuvrability and high speed handling. The process of validation can be seen as a step-wise procedure depicted in the Figure 3.5, which should primary lead to achieve the consistency between the multi-body model results and the measurement data given the same input.

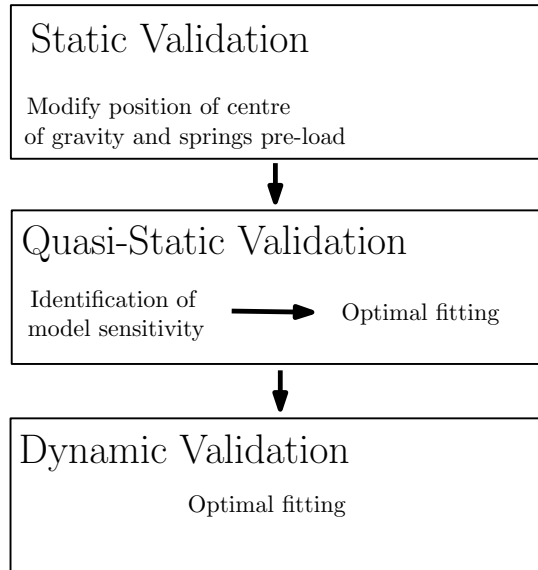


Figure 3.5: Stepwise model validation process diagram.



The steps given in Figure 3.5 can be described as follows:

- **Static Validation**

The validation process of an articulated vehicle model starts with the static validation, i.e. the vehicle combination is standing still, and serves mainly as a verification of the static vertical tyre forces. The load distribution between the axles is not only dependent on the position of the centre of gravity of particular vehicles but also, due to the air spring utilization, on the load levelling of individual axles. This levelling is normally mastered by a fully automated controller, however the level of precision is sometimes limited, which could result in parasitic forces. The vertical tyre forces can primarily be tuned in two ways, which are linked to each other assuming the geometry is exactly known. The position of the centre of gravity should be adopted and should correspond to the vehicle known mass properties. Next suspension levelling can be done through setting appropriate pre-load to the vertical springs for each axle group. As the vehicle model is statically indeterminate, the second step is used for fine tuning. Due to large influence of the static tyre forces on the overall vehicle behaviour, correct results are a prerequisite for consecutive validation steps.

- **Quasi-static Validation**

Next the quasi-static conditions will be examined on two levels, firstly the steady state vehicle handling properties will be analysed at high speed, and secondly low speed manoeuvrability will be evaluated.

As for steady state cornering the model is validated, with a constant longitudinal velocity and steering angle as inputs. The key signals are:

- yaw rate
- lateral velocity
- articulation angles
- roll angle

To get a better understanding of the influence of particular model components such as tyres, suspension and vehicle body stiffness, a sensitivity analysis was executed. The multi-body model of the vehicle combination has been set to drive with a constant forward velocity of 45 km/h and fixed steering angle, to perform steady state cornering on circle with a radius of 50 m, resulting in a lateral acceleration of  $3.125 \text{ m/s}^2$ , which was maintained for all the parameter variations. Subsequently, an identification of the most responsive vehicle parameters, is done.

The following parameters of vehicle model are modified in a range of  $\pm 15\%$  for the Tractor, Link-Trailer, and Semitrailer:

- Cornering stiffness of the tyre (through a scaling coefficient)
- Tyre road friction coefficient (through a scaling coefficients)
- Axle roll stiffness

- Body torsional stiffness
- Suspension vertical spring stiffness.

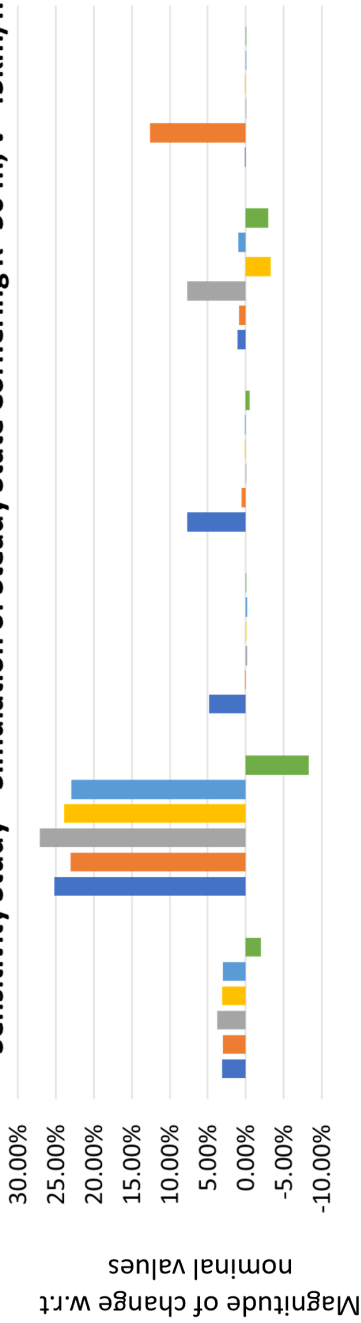
The outcome of this sensitivity analysis [69] is shown in Figure 3.6. It can be observed that the tyre cornering stiffness is by far the most influential parameter for vehicle steady state handling behaviour. Its influence on yaw rate, lateral velocity and articulation angles reaches values of 20% with respect to the base-line configuration, whereas in case of other parameters we obtain significantly lower values.

Given the tyre cornering stiffness as the most influential vehicle parameter for the handling behaviour, it is meaningful to proceed with model validation through the identification of tyre cornering stiffness values. Contrary to e.g. a vehicle wheel base, the tyre cornering stiffness is not easy to directly measure or acquire from the tyre manufacturer. Moreover, it depends on the level of tyre wear, inflation pressure, or vertical tyre load. Hence, the cornering stiffness of the axle groups is identified based on the measurement data. The identification by only a random parameter variation would be rather difficult because the cornering stiffnesses of all four axle groups are influencing the overall vehicle combination behaviour. Therefore, hereafter we apply an error minimization technique in combination with the measurement data, and simplified vehicle model in order to identify the tyre cornering stiffnesses.

The measurement data which are used to identify the cornering stiffnesses were obtained at steady state cornering conditions on circle with sufficiently large radius ( $R=100$  m) that avoids tyre scrubbing and constant forward velocity of 55 km/h.

Considering the lateral acceleration level of the commercial vehicle during steady state cornering the side slip angles will be limited and one can assume the tyre behaviour to be linear. It is primarily due to the rollover instability of the vehicle which would precede the non-linear tyre behaviour occurring at bigger tyre slip angles. Hence, the simplified model is based on a single track (bicycle) model of a double articulated vehicle with linear tyres, see Figure 3.7. All angles are assumed to be small and can therefore be linearized. Each vehicle body (truck, trailer 1, and trailer 2) is characterized by the dimensions  $a_i, b_i, l_i, h_i, T_1$ , its mass  $m_i$  and moment of inertia  $J_i$ , which are known time invariant constants. Furthermore, the bodies are assumed to be rigid and the tyres of each axle group are lumped together into single tyre with corresponding multiple stiffness. The tyre forces  $F_{y1-4}$  are modelled by a linear tyre model, i.e. a product of tyre slip angle  $\alpha_{1-4}$ , and cornering stiffness  $C_{1-4}$ . No friction or play is assumed to be present in the articulation joints. The vertical motion is neglected since the model is planar, the rotations, which involve movement outwards of the x-y plane such as roll and pitch are not considered. The model variables as well as the global, earth-fixed, co-ordinate system  $\vec{e}^0$  are shown also Figure 3.7.

**Sensitivity Study – Simulation of Steady State Cornering R=50 m, v=45km/h**



Roll Angle Tractor	3.11%	25.27%	4.83%	7.68%	1.13%	0.17%
Roll Angle Trailer 2	2.99%	23.08%	0.16%	0.55%	0.85%	12.62%
Articulation Angle 1	3.80%	27.17%	-0.23%	-0.03%	7.74%	-0.08%
Articulation Angle 2	3.11%	23.90%	-0.11%	0.14%	-3.24%	0.05%
Yaw Rate Tractor	2.98%	22.96%	-0.14%	0.02%	1%	-0.01%
Lateral velocity Tractor	-2.03%	-8.31%	-0.02%	-0.51%	-2.99%	-0.02%

Figure 3.6: Sensitivity analysis outcome.

Equations of motion are derived using a Lagrangian approach. Herewith, we employ coordinates defined in the local co-ordinate system  $\bar{e}^1$  being attached to the first vehicle center of gravity. Hence resulting equations will not depend on the orientation of the truck  $\theta_1$ .

Variables  $\dot{X}_1$  and  $\dot{Y}_1$  are the time-derivatives of the global position co-ordinates  $X_1$  and  $Y_1$  of the first vehicle center of mass  $CM_1$ .  $\gamma_1$  and  $\gamma_2$  are the articulation angles between the bodies as shown in Figure 3.7. The yaw rate  $r_1 = \dot{\theta}_1$  of the truck is defined as time-derivative of the yaw angle  $\theta_1$ . Yaw angles of trailer 1 and trailer 2 are defined by means of articulation angles as:

$$\begin{aligned}\theta_2 &= \theta_1 - \gamma_1 \\ \theta_3 &= \theta_1 - \gamma_1 - \gamma_2.\end{aligned}\tag{3.1}$$

From these yaw angles, the related yaw rates follow:

$$\begin{aligned}r_2 &= \dot{\theta}_2 = r_1 - \dot{\gamma}_1 \\ r_3 &= \dot{\theta}_3 = r_1 - \dot{\gamma}_1 - \dot{\gamma}_2.\end{aligned}\tag{3.2}$$

The longitudinal velocity  $v$  and lateral velocity  $v_y$  of the truck in the frame  $\bar{e}^1$  are given by:

$$\begin{aligned}v &= \dot{X}_1 + v_y \theta_1 \\ v_y &= \dot{Y}_1 - v \theta_1.\end{aligned}\tag{3.3}$$

The derivation of the equations of motion for a double articulated vehicle combination can be found in Appendix A. Here we present the reduced form of the equations for a steady state situation, assuming constant longitudinal speed  $v$  and all state derivatives equal to zero, which corresponds to the steady state.

The reduced equations of motion for  $\dot{v}_y, \dot{r}_1, \dot{\gamma}_1, \dot{\gamma}_2 = 0$  read:

$$\begin{aligned}\sum_{i=1}^3 m_i v r_1 &= -\frac{1}{v} [(C + C_t) v_y + (C_s - (h_1 + b_2) C_3 - (h_1 + l_2 + b_3) C_4) r_1] \\ &+ C_1 \delta_1 + C_t \gamma_1 + C_4 \gamma_2\end{aligned}\tag{3.4}$$

$$\begin{aligned}-(m_2 + m_3) h_1 v r_1 &= a_1 C_1 \delta_1 - (b_3 + l_2 + h_1) C_4 \gamma_2 \\ &- \frac{1}{v} [(C_s - (b_2 + h_1) C_3 - (b_3 + l_2 + h_1) C_4) v_y] \\ &- \frac{1}{v} [(C_q + (b_2 + h_1)^2 C_3 + (b_3 + l_2 + h_1)^2 C_4) r_1] \\ &- [(b_2 + h_1) C_3 + (b_3 + l_2 + h_1) C_4] \gamma_1\end{aligned}\tag{3.5}$$

$$\begin{aligned}-(m_2 a_2 + m_3 l_2) v r_1 &= \frac{1}{v} [((h_1 (b_3 + l_2) (b_3 + l_2)^2) C_4) r_1] \\ &- \frac{1}{v} [(b_2 C_3 + (b_3 + l_2) C_4) v_y - (b_2^2 + b_2 h_1) C_3] \\ &+ (b_2 C_3 + (b_3 + l_2) C_4) \gamma_1 + (b_3 + l_2) C_4 \gamma_2\end{aligned}\tag{3.6}$$

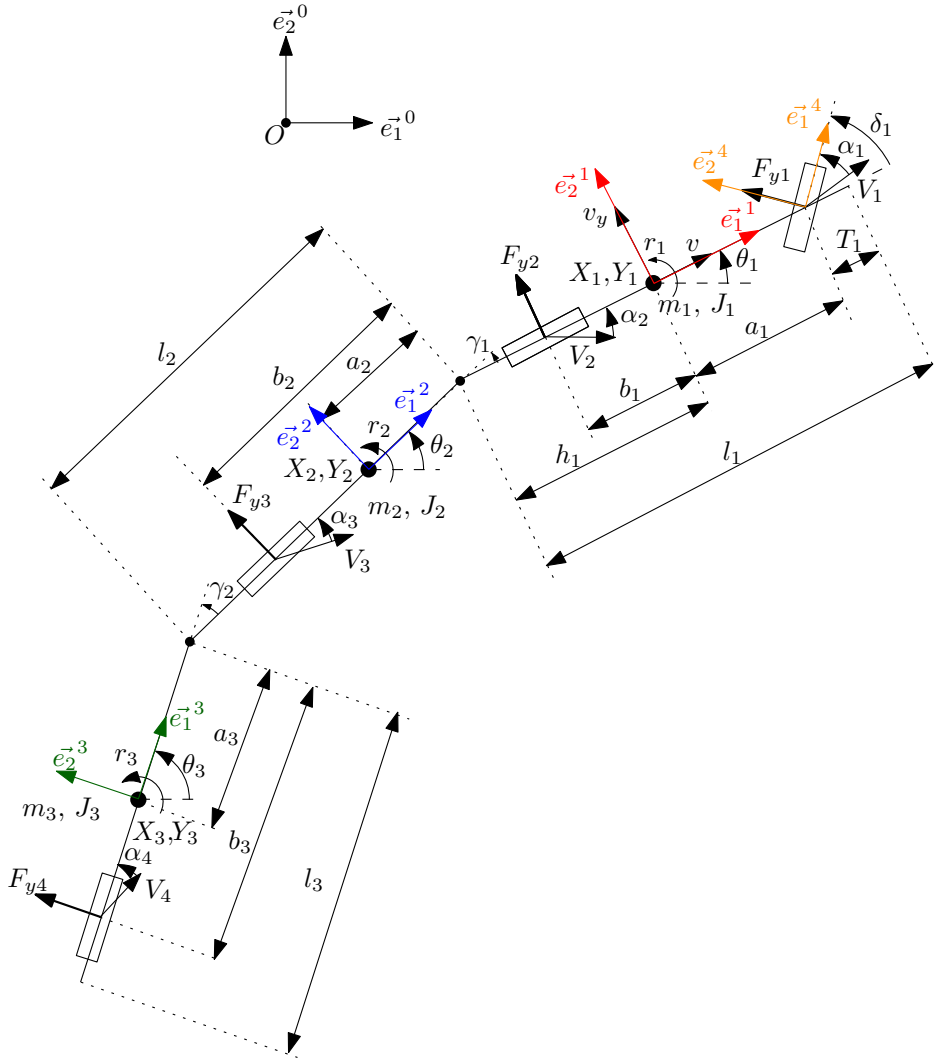


Figure 3.7: Linear single track model with two articulations.

$$\begin{aligned}
-m_3 a_3 v r_1 &= -\frac{1}{v} b_3 C_4 (v_y - h_1 r_1 - l_2 r_1 - b_3 r_1) \\
&+ b_3 C_4 (\gamma_1 + \gamma_2),
\end{aligned} \tag{3.7}$$

where,  $C = C_1 + C_2$ ,  $C_t = C_3 + C_4$ ,  $C_s = a_1 C_1 - b_1 C_2$ , and  $C_q = a_1^2 C_1 + b_1^2 C_2$ . Subsequently, the derived equations of motion (3.4)-(3.7) are rewritten in the form suitable for the cornering stiffness identification:

$$v_{yc}(t) = f(r_{1M}(t), \gamma_{1M}(t), \gamma_{2M}(t))[\rho] \tag{3.8}$$

$$r_{1c}(t) = f(\gamma_{1M}(t), \gamma_{2M}(t), v_{yM}(t))[\rho] \tag{3.9}$$

$$\gamma_{1c}(t) = f(\gamma_{2M}(t), v_{yM}(t), r_{1M}(t))[\rho] \tag{3.10}$$

$$\gamma_{2c}(t) = f(v_{yM}(t), r_{1M}(t), \gamma_{1M}(t))[\rho], \tag{3.11}$$

where,  $v_{yM}(t), r_{1M}(t), \gamma_{1M}(t), \gamma_{2M}(t)$  are the time series of the vehicle states measured at steady state cornering,  $\rho = [C_1, C_2, C_3, C_4]^T$  is a vector of cornering stiffnesses, and  $v_{yc}(t), r_{1c}(t), \gamma_{1c}(t), \gamma_{2c}(t)$  are time series of vehicle states which are calculated on the basis of measurement data and the vector of cornering stiffnesses.

Given the measured time series of vehicle states to be fixed and the fact the measurement is done at steady-state cornering, thus considering both the steering angle  $\delta$  and forward velocity  $v$  as constants, along with known vehicle dimensions and mass properties, the only degree of freedom to shape the  $v_{yc}(t), r_{1c}(t), \gamma_{1c}(t), \gamma_{2c}(t)$  is the vector of cornering stiffnesses  $\rho$ .

Hence, the cornering stiffness identification is based on minimization of the mean square error between measured and calculated vehicle state, over fixed time interval  $t = [0, t_{max}]$ . It should be emphasised that measurement data should be chosen only for the conditions which are quasi-static, i.e. the variation of cornering forces in time is minimal, and over sufficiently long time interval so the results will be less sensitive for the measurement noise. The total error over the time used for the minimization is defined by:

$$\begin{aligned}
\varepsilon(t_{max}, \rho) &= \frac{1}{t_{max}} \sum_{t=0}^{t_{max}} \left[ g_{v_y} (v_{yM}(t) - v_{yc}(t, \rho))^2 + g_r (r_{1M}(t) - r_{1c}(t, \rho))^2 \right. \\
&\quad \left. + g_{\gamma_1} (\gamma_{1M}(t) - \gamma_{1c}(t, \rho))^2 + g_{\gamma_2} (\gamma_{2M}(t) - \gamma_{2c}(t, \rho))^2 \right],
\end{aligned} \tag{3.12}$$

where  $g_{v_y}, g_r, g_{\gamma_1}, g_{\gamma_2}$  are scaling coefficients allowing to weight, if necessary, the corresponding error and mainly ensuring the squared errors are unit-less and thus summable. The total squared error  $\varepsilon(t_{max}, \rho)$  can be subsequently used to define a cost function defined as:

$$W(\rho) = \bar{E}\varepsilon(t_{max}, \rho), \tag{3.13}$$

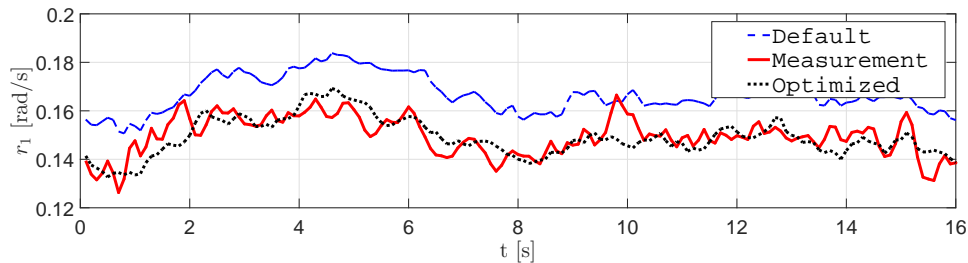
which is based on expected value of total error enabling to maximize the posterior probability of the vector function. Through the subsequent minimization of the cost function over the range of viable cornering stiffnesses interval  $\Theta$ , the matrix of identified cornering stiffnesses is obtained:

$$\rho^* = \underset{\rho \in \Theta}{\operatorname{argmin}} W(\rho). \quad (3.14)$$

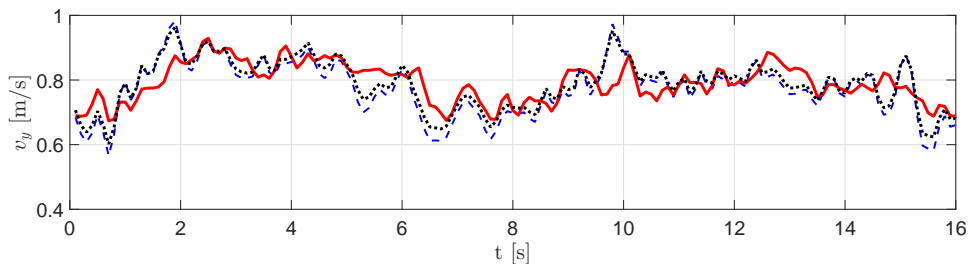
The identified cornering stiffnesses  $\rho^*$  is obtained by means of an Interior-Point Algorithm, which is a minimization algorithm suitable for constrained nonlinear multivariable functions defined in [11], [12], and [134]. As the convexity of (3.12) with respect to parameters is not guaranteed only the local minimum is found. To obtain the results which are quantitatively realistic the constraints have to be set properly. The constraints are represented by lower and upper bound of  $\Theta$ , which are set to be  $\pm 20\%$  from the default values of  $C_{1-4}$  available in the model library. The scaling coefficients equate  $g_{v_y} = g_r = g_{\gamma 1} = g_{\gamma 2} = 1$ . Achieved results of the optimization are illustrated in Figure 3.8 for steady state cornering at constant velocity 55 km/h with a radius 100 meters and measurement interval of 16 seconds with measurement sampling frequency 100 Hz. The red solid line in Figure 3.8 represents the experimentally obtained data, the dashed blue line depicts the output of the model with default values of cornering stiffness and black dotted one shows the output of the model with cornering stiffnesses obtained after the identification.

As can be seen from Figure 3.8, after the identification the model is better in agreement with the measurement. Some differences between the measured data and the simulation can however be still observed. They probably originate from the measurements and the processing noise of the sensors.

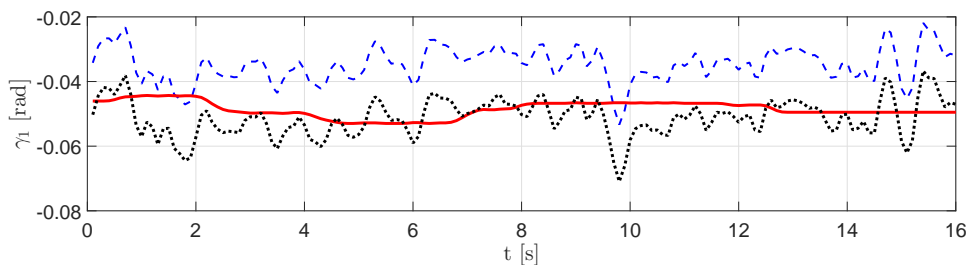
The identified cornering stiffnesses  $\rho^*$  represent a very good starting point for fine tuning of the tyre cornering stiffness by means of scaling coefficients in the Delft-Tyre module of the full multi-body model. The steady state roll response of the vehicle model is adjusted in accordance with the sensitivity analysis. To conclude the quasi-static part it is feasible to check the validity of the model during a similar operational condition, for example with a different velocity and radius as given hereafter.



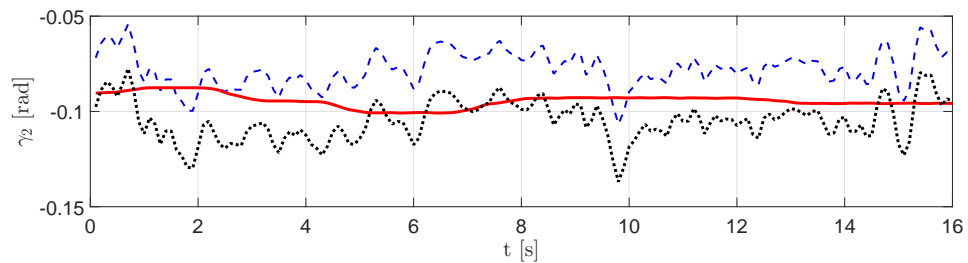
(a) Yaw rate of the Tractor



(b) Lateral velocity of the Tractor



(c) Articulation angle between Tractor - Trailer 1



(d) Articulation angle between Trailer 1 - Trailer 2

Figure 3.8: Optimization results for steady state cornering at lateral acceleration  $2.33 \text{ m/s}^2$  illustrating the benchmark of experimental measurements (red solid line) with results delivered by the model with default and optimized cornering stiffnesses by blue dashed and black dotted lines, respectively.



- **Dynamic Validation**

The last level of the validation deals with the dynamic conditions such as sine-steer input or a lane change manoeuvre at high speed. Since the majority of the vehicle parameters have already been identified during the previous two steps, the remaining parameters to modify the simulation model behaviour are the damping of the suspension and the moment of inertia of vehicles.

The characteristics of the dampers are obtained from the manufacturer and do not vary significantly between different vehicles. In contrast, the moment of inertia differs considerably for every vehicle and depends on the bodywork and the location of the cargo. It can be obtained either through a calculation using the parallel axis theorem or again by an optimization proposed earlier for estimation of tyre cornering stiffness.

### 3.5 Model validation Results and Discussion

The results of three-step model validation, which is shown in Figure 3.5, will be presented here. For the sake of conciseness only one representative manoeuvre per step is given and discussed.

As input for simulation only the steering angle of the towing vehicle and its driven angular wheel velocity are used. The solid black line is always used for measured data and the red dashed one for simulation output. There exists a number of approaches to judge the accuracy of the dynamic model against the measurement data, such as evaluation of the root mean square error over the time interval [60], Pearson correlation coefficient [83], or visual inspection of the vehicle states [44] or [79]. Considering the fact we want to validate the model library on a general level, the last approach is chosen for all graphs given hereafter.

- **Static Validation**

The validation is presented for two loading conditions when different loading patterns have been applied to test combination # 2 (4x2 Tractor, 3-axle link trailer, and 3-axle double-decker semitrailer). The first loading condition in Figure 3.9, corresponds to a normal load distribution. In the second one, which can be described as extreme loading, most of the load of the first trailer has been shifted towards the front, hence the majority of the load is carried by the tractor rear axle. In Figure 3.9 the comparison between measured and simulated vertical load for each tyre is depicted. One can see that a good agreement is obtained.

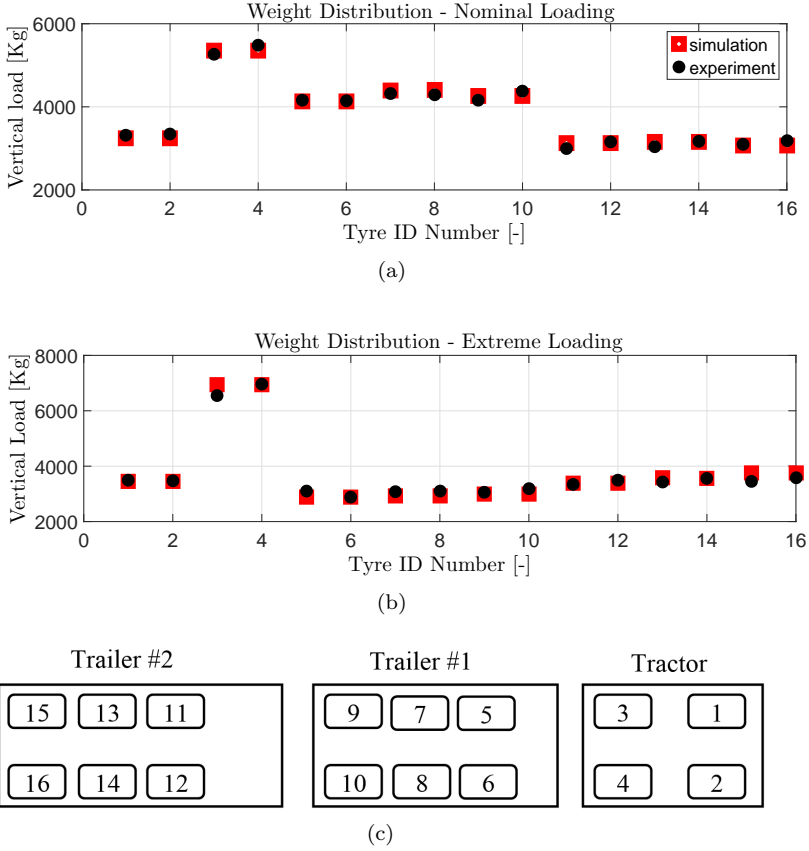


Figure 3.9: Static model validation results of vehicle #2; (a) Nominal loading, (b) Extreme loading, (c) Legend of tyre identification number.

- Quasi-Static Validation

Quasi-static handling manoeuvres are understood as manoeuvres, which do not include dynamic variation of the tyre slip angles and vehicle velocity states. It can be achieved either by driving with very low velocities, or by a minimal variation of the steering angle and longitudinal velocity over time.

For the validation we present one for each case for the combination Tractor-Link Trailer-Semitrailer, which are:

- High-speed steady state cornering with radius  $R = 100$  m at 45 km/h
- Low-speed 90 degrees corner with radius  $R = 12.5$  m at 10 km/h.

The statically validated model will be used in combination with the identified cornering stiffnesses as described in section 3.4.

Concerning the results of high-speed cornering, depicted in Figures 3.11, and 3.10, a good match of all important vehicle states can be seen. A discrepancy

can be observed in case of the roll angle of the tractor, which is most likely caused by a measurement error of the sensor, a gyroscope, which measures the roll rate and the roll angle is subsequently obtained by integration. To compensate for the integration drift, typically the accelerometers and GPS signal are used. In contrast the roll angle of semitrailer is more consistent because this angle has been obtained by a laser sensor measuring the absolute vertical distance of the vehicle body to the ground. The simulation output for low-speed manoeuvring, depicted in Figure 3.12, is also in agreement with experimental data. The only major mismatch can be observed at the peak of the articulation angle  $\gamma_1$  between the tractor and the link-trailer. Similar behaviour is already observed in high-speed cornering, see Figure 3.11b, and here the trend is magnified. It may be explained by the simplified suspension model, which does not include elastic compliance in some suspension parts contributing to roll steer in combination with compliance in the fifth wheel of the link-trailer. Furthermore, some influence can be also accounted for the non-linear tyre behaviour and tyre scrubbing occurring during sharp low-speed cornering.

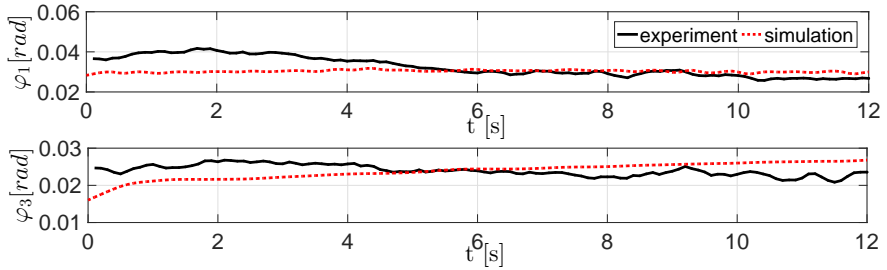
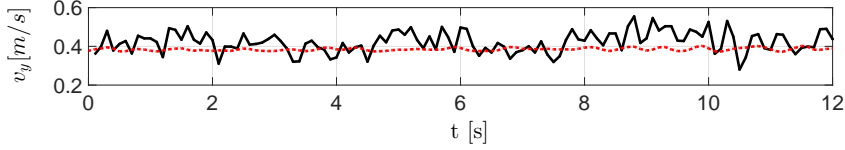
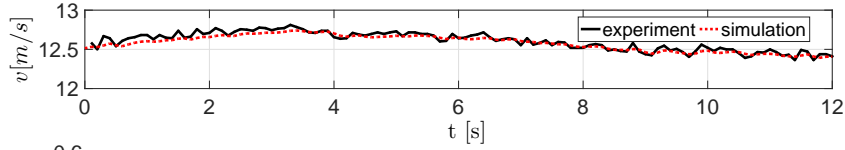
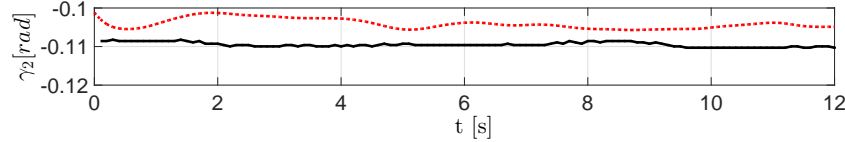
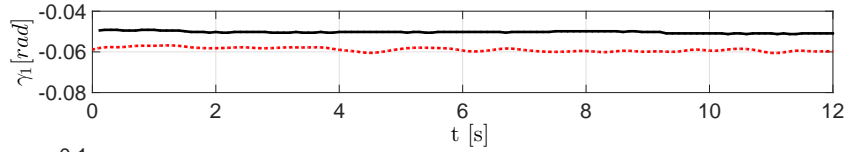


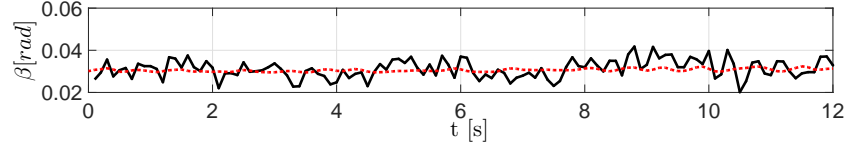
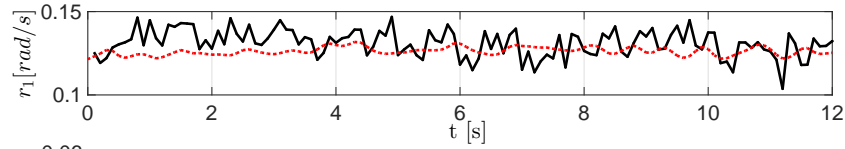
Figure 3.10: Model validation results for roll angles of Tractor and Semitrailer.



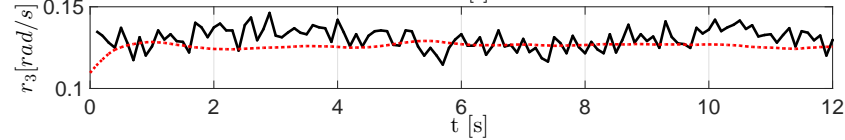
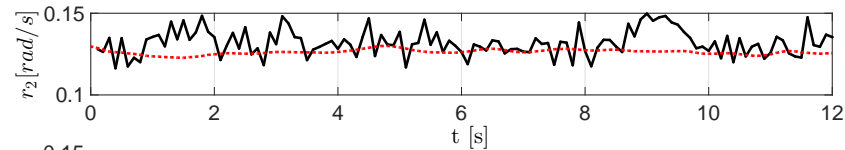
(a) Longitudinal and lateral velocity of the Tractor



(b) Articulation angles

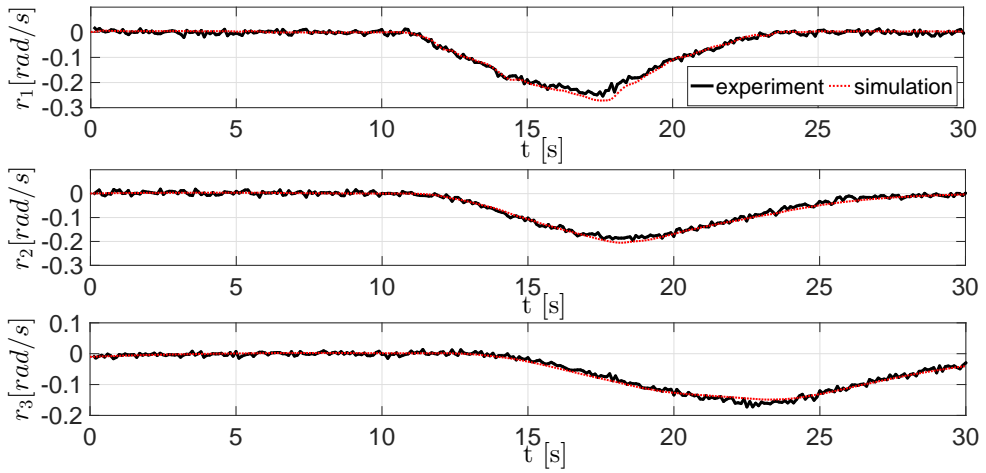


(c) Yaw rate and body slip angle of the Tractor

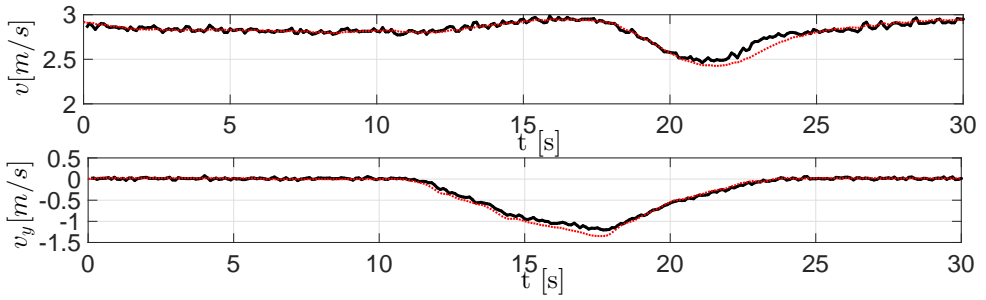


(d) Yaw rate of Link-trailer and Semitrailer

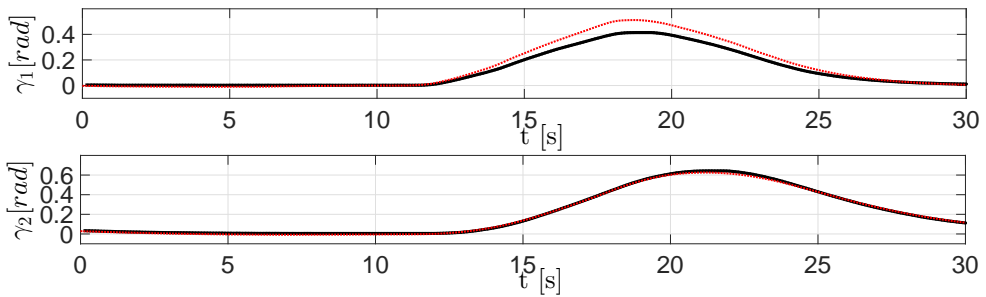
Figure 3.11: Quasi-static high-speed model validation results at the lateral acceleration  $1.56 \text{ m/s}^2$ .



(a) Yaw rate of Tractor, Link-Trailer, and Semitrailer respectively



(b) Longitudinal and lateral velocity of the Tractor

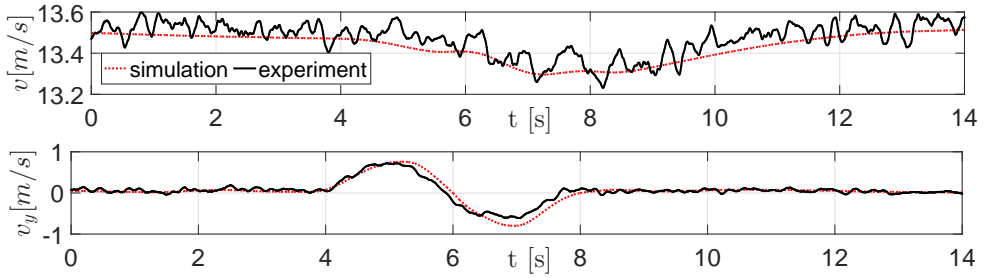


(c) Articulation angles

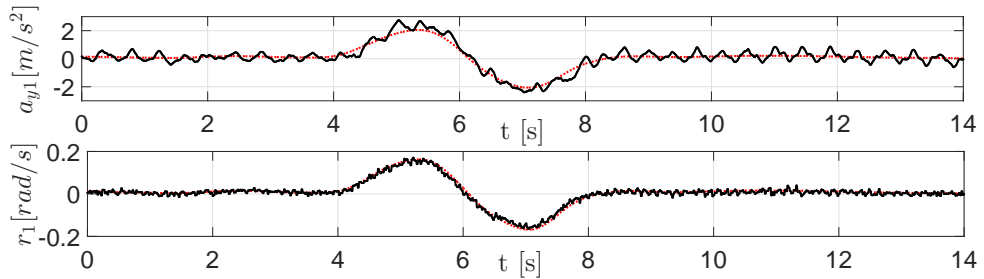
Figure 3.12: Quasi-static model validation results at low-speed cornering at the lateral acceleration  $0.63 \text{ m/s}^2$ .

- Dynamic Validation

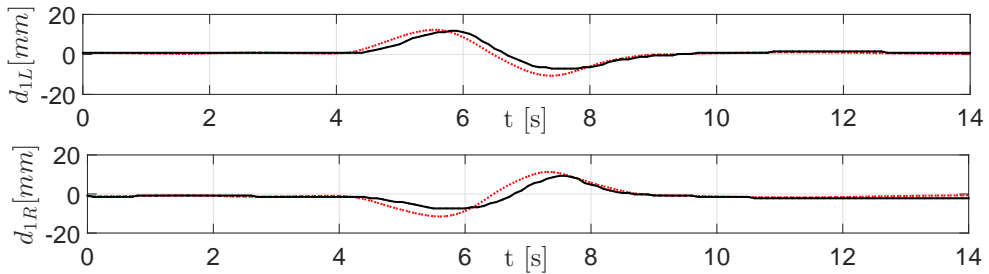
For validation of dynamic vehicle behaviour a lane change manoeuvre at 50 km/h will be shown. The validation is performed on combination Rigid truck-Dolly-Semitrailer, which is also already statically and quasi-statically validated. The graphs are presented for each vehicle combination unit separately. The truck behaviour can be seen in Figure 3.13, followed by the dolly in Figure 3.14, and the semitrailer in Figure 3.15.



(a) Longitudinal and lateral velocity of the Truck



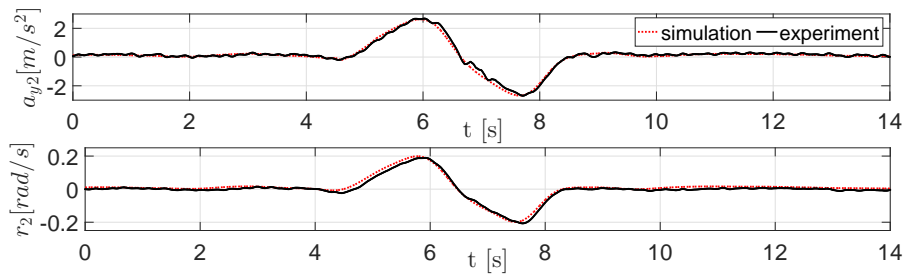
(b) Lateral acceleration and yaw rate of the Truck



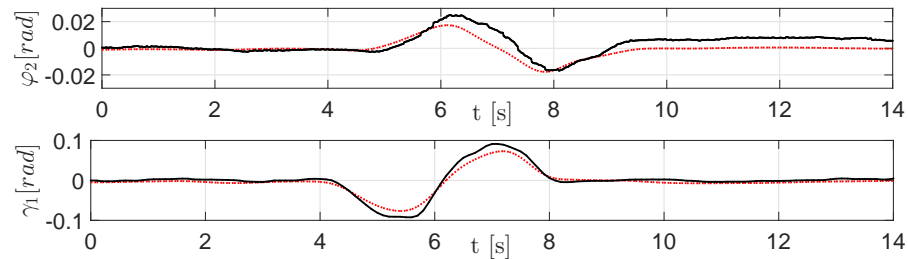
(c) Axle chassis distances of the Truck

Figure 3.13: Dynamic model validation results at high-speed lane change, Truck.

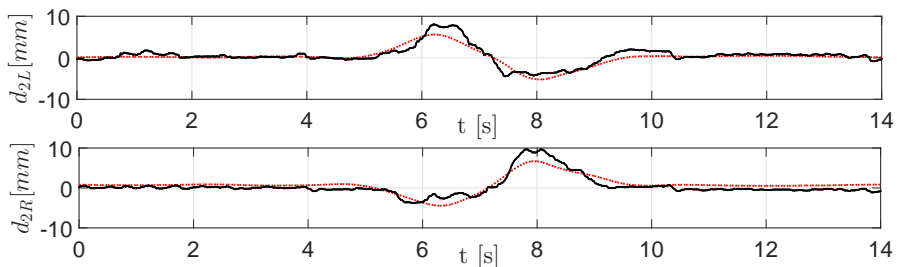
In Figure 3.13, one can observe a small difference in the axle chassis distance amplitudes in the negative and positive region which is not noticeable in the model. It is most likely caused by the linearisation of the springs and dampers in the suspension model. The dampers have in reality a different damping ratio for extension and compression and the springs have a progressive stiffness characteristics which both are not modelled. Additional limitation is the simplified model of the vehicle frame which allows only one degree of freedom in torsion and the degrees of freedom between the cabin and the chassis, which were not modelled. All effects however have minor impact on the overall combination behaviour as the difference is in the order of millimetres. The remaining vehicle states are in good agreement.



(a) Lateral acceleration and yaw rate of the Dolly



(b) Roll and articulation angle of the Dolly

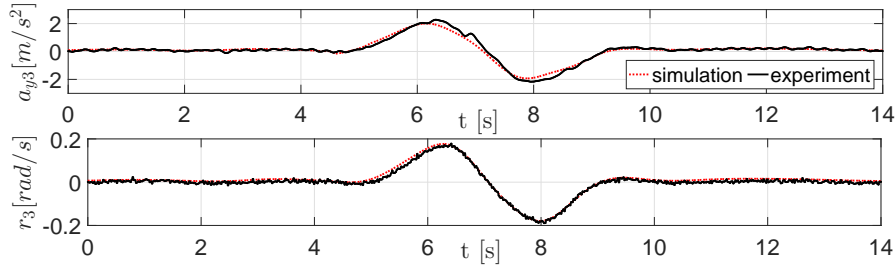


(c) Axle-chassis distance of the Dolly

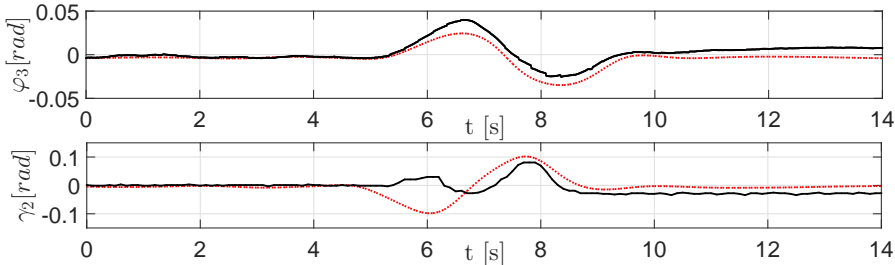
Figure 3.14: Dynamic model validation results at high-speed lane change, Dolly

Besides the lag in roll angle and the reduced amplitude, no special behaviour or deviations in Figure 3.14 are observed. Since the roll angle seems to be consistent with the chassis-axle position, it may be concluded that the sensor output is influenced by numerical integration drift that may cause relative big error at very small angles.

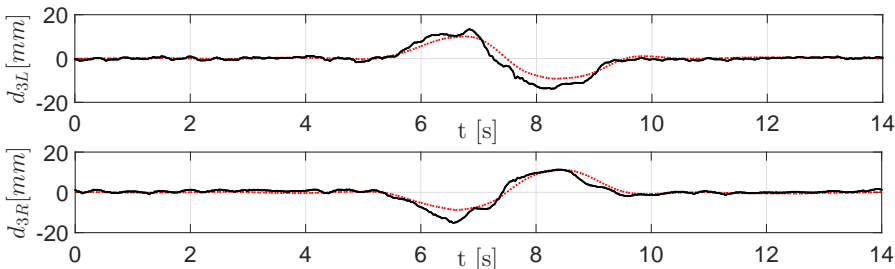
Figure 3.15 depicts all effects described in the two previous paragraphs. Furthermore it shows an illustrative case of the sensor malfunctioning as can be seen in the dolly-trailer articulation angle. The readings of the sensor between 5 and 7 seconds are apparently wrong, since they are not consistent with other measurements and the vehicle is unlikely to make this motion.



(a) Lateral acceleration and yaw rate of the Semitrailer



(b) Roll and articulation angle of the Semitrailer



(c) Axle-chassis distance of the Semitrailer

Figure 3.15: Dynamic model validation results at high-speed lane change, Semitrailer.



### 3.6 Summary

This chapter deals with the validation of multi-body vehicle models with by the data obtained from testing. Full-scale experiments were done for multiple vehicle combinations at different velocities and loading conditions to ensure that the captured data covers sufficiently the operational range required for the performance assessment. Furthermore, a systematic approach is proposed to validate the vehicle combination model. The approach is composed of three steps: static, quasi-static and dynamic. As appears from a sensitivity analysis, the quasi-static validation part has an important role because the tyre cornering stiffnesses, which influence mostly the vehicle handling behaviour, needs to be identified properly in this step. To identify the tyre cornering stiffnesses, we propose a multi-variable constrained minimization of the cost function that sums the errors between the measured and the calculated vehicle states, employing a simplified linear single track model. The results of the identified cornering stiffnesses differ in a range of approximately 10% from the default values of the model library. Subsequently, the identified cornering stiffnesses are applied to multi-body models. Even though the multi-body models are simplified, the validation results show a good match between the simulation model output and the measurement data. Therefore, the library is considered to be representative for the dynamic behaviour of real vehicle combinations and thus suitable for performance assessment of various vehicle combinations, which will be discussed in the next chapter.



# Chapter 4

## Vehicle Performance Analysis

### 4.1 Introduction

In this chapter a number of Heavy Good Vehicle types is defined at first. Selected vehicle combinations will include current ones that comply with directive 96/53/EC, but also a number of HCV's that are legalized on national level in a number of European states. Subsequently, all vehicles are modelled using the multi-body library described in Chapter 3. Then they are virtually assessed against selected performance criteria as defined in the previous Chapter 2. Based on the assessment results, three new vehicle combination concepts will be defined that comply with criteria, which are seen as obligatory for vehicle combinations beyond years 2020+.

### 4.2 Representative vehicle combinations

It is anticipated that new vehicle combinations for long-haul transport, which satisfy the future requirements, will continuously evolve from the ones operating currently around the world. A step introduction of fundamentally new vehicle combinations is unlikely considering required investments into new production facilities from OEMs which would be significant, and the fact that the logistic industry is mainly driven by the size of loading units and pallets which are fixed and not likely to change either. Hence, a selection of representative vehicles will be made; vehicles complying with 96/53/EC and vehicles that operate outside this regulatory framework based on national legislations as for example High Capacity Vehicles (HCV) used widely in Scandinavia or the Netherlands. While selecting the vehicles, the choice of the loading unit is also taken into account. Hence, only vehicles which combine multiples of ISO-containers (20 ft, 40 ft, and 45 ft) or swap bodies (C 782) and semi-trailers (13.6 m) are considered because of the good inter-modal transport potential. Each vehicle combination is specified with sufficient level of detail allowing an assessment of vehicle performance as described in Chapter 2. Those details however, are not presented in this work, and reference is made to [65].

Table 4.1 and Table 4.2 show the selected vehicles to be evaluated. Following the internationally agreed abbreviations defined in [112] for hauling units will be used: TK-Rigid Truck and TR-Tractor in combination with the conventional designation regarding the total number of wheels and driven wheels only. For the towing vehicles the abbreviations read: ST-Semitrailer, CT-Central axle trailer, FT-Full trailer, LT-Link Trailer, DY-Dolly complemented with the number which is designating the number of undriven axles. In case that some axles would be driven the convention from the hauling units should be used. At the end of the abbreviation in brackets the loading units are specified.

#### 4.2.1 EU vehicle combinations

Selected vehicle combinations in Table 4.1 are common combinations, which can currently be seen on European roads. These vehicles operate within the Directive 96/53/EC for international transport and thus are legal in all EU-member states and can be used for cross border transport.

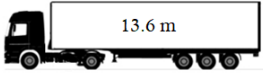




Standard vehicles				
Name	Picture	Origin	GVW	Length
TR4x2-ST3 (13.6m)		EU	40 t	16.4 m
TK6x2-CT2 (2x7.8m)		EU	40 t	18.7 m
TK6x2-FT1+1 (2x7.8m)		EU	40 t	18.7 m
TR6x2-ST3 (45 ft)		EU	44 t	17.1 m
TK6x2 (7.8 m)		EU	26 t	10.2 m

Table 4.1: Representative European vehicle combinations to be assessed.

#### 4.2.2 High Capacity Vehicles

High Capacity Vehicle (HCV) combinations in Europe are typically limited by a gross vehicle weight of 60 tonnes and length of 25.25 meters. However, in recent years there is a trend, especially in Sweden and Finland, to employ even longer and in some cases also heavier vehicle combinations, where GCW goes up to 74 tonnes. Such vehicles are mainly used for the mining industry. As can be seen in Table 4.2, we will select some of those vehicle combinations because of their good multi-modal potential, but the GVW will be limited to 60 tonnes.

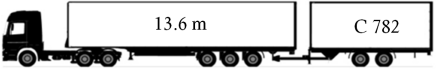





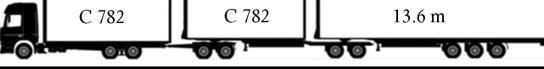
High-capacity vehicles				
Name	Picture	Origin	GVW	Length
TR6x4-ST3-CT2 (13.6m+7.8m)		NL	60 t	25.2 m
TK6x4-DY2-ST3 (7.8m+13.6m)		NL	60 t	24.6 m
TR6x4-LT3-ST3 (20ft+40ft)		NL	60 t	23.5 m
TR6x4-LT2-ST3 (7.8m+13.6m)		DK	60 t	25.2 m
TK 6x4-CT2-CT2 (3x7.8 m)		SE	60 t	27.4 m
TR 6x4-ST3-DY2-ST3 (2x45 ft)		SE	60 t	32 m
TK 6x4-DY2-LT2-ST3 (2x7.8 m+ 13.6 m)		SE	60 t	33.3 m

Table 4.2: Representative high capacity vehicle combinations.

### 4.2.3 Loading conditions

The European Directive 96/53/EC prescribes the maxima for axle loads as explained in Table 2.2. It is accounted that these limits should be considered, while selecting representative loading because of existing infrastructure design criteria, that have been used to design the current roads. Furthermore, the loading condition has to be generic and based on real data in order to obtain representative results.

In Europe the potential weight and volumetric loading capacity of the commercial vehicles is not fully exploited. According to [2] and [21] the volumetric and spatial loading utilization of loading units is on average 82%, and 92%, respectively. As for the weight loading capacity, the numbers are even lower. As depicted in Figure 4.1, the average load factor for a tractor semitrailer, being the most frequently used international long-haul commercial vehicle in EU, yields 15.2 tonnes [107]. Considering the potential loading capacity of a 13.6 m semitrailer, which is approximately 26 tonnes, the average load factor reaches 58% only. Combining the volumetric and weight utilization percentages one obtains a load density of  $213 \text{ kg.m}^{-3}$ , which is considered as a representative loading condition and will be applied to all vehicle combinations for the dynamical analysis hereafter.

This illustrates that volume is more important for the long haul transport sector in comparison to the weight. The volumetric utilization will be used to determine the height of the cargo center of gravity above the loading floor, assuming that the load is uniformly distributed. The height of the centre of gravity is a decisive parameter that significantly influences vehicle combination dynamic behaviour.

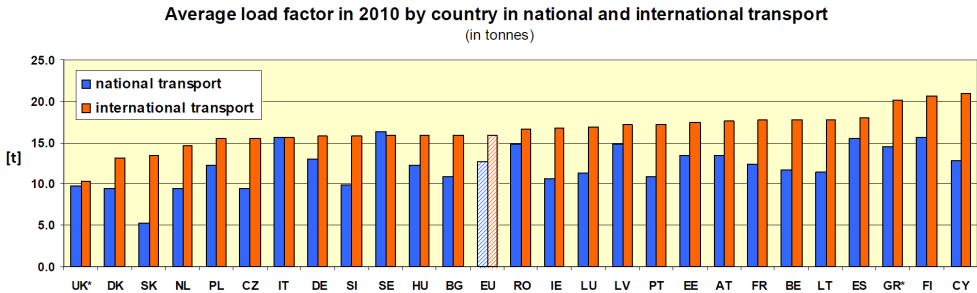


Figure 4.1: Average loading conditions in Europe for Tractor Semitrailer<sup>[107]</sup>

## 4.3 Vehicle modelling and performance assessment

The vehicle combinations listed in Tables 4.1 and 4.2 and have been created using the multi-body model library described in the previous chapter. Active safety systems, such as ABS, ESP or active steering of trailer axles are not modelled. Their modelling would add considerable complexity, and complicate the executability of some manoeuvres because of the safety system interventions. Above all it would not provide additional insight, which combinations are passively more save than other,

due to the design or configuration of vehicle units, which is the primary scope of the analysis.

The assessment of all vehicle combinations requires extensive modelling and simulation effort. Hence, it was decided to compile a set of scripts that will automate and speed-up the assessment process. On the top layer a graphical user interface (GUI) was added, to aid the user friendliness. The resulting tool consists of three parts:

- The multi-body model generator

The vehicle combination model is created using the GUI, which is generating the MATLAB/Simulink model by selecting the appropriate particular components from the library. The model is at the same time parametrized by selecting a set of vehicle parameters, such as dimensions, weight or suspension properties, which are relevant for the performance assessment of the vehicle in the context defined in Chapter 2.

- Simulation

Predefined simulation inputs are used to simulate various predefined manoeuvres, while storing all relevant simulation outputs.

- Post-processor

Simulation outputs are post-processed in order to obtain results, in a form which is consistent with the performance criteria as defined by the legislation. An example can be seen in Figure 4.2, where the low speed swept path width is analysed by the post-processor using the simulation output.

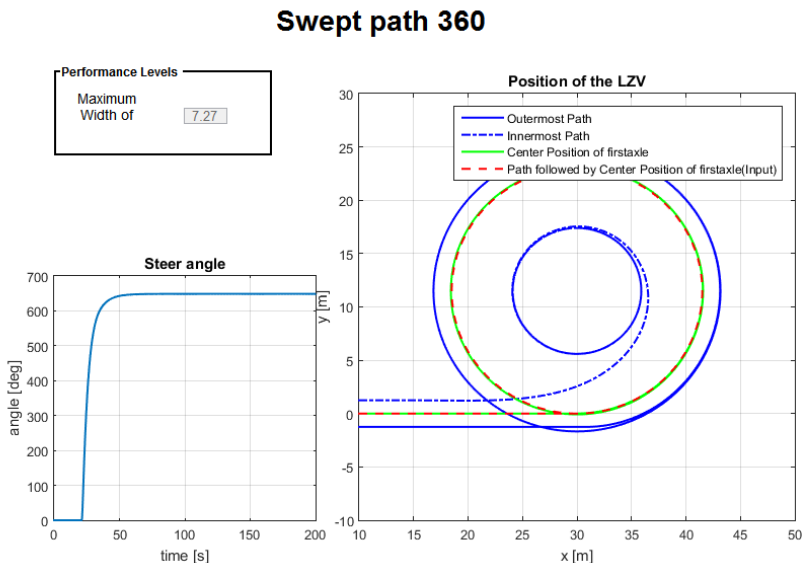


Figure 4.2: Post-processed swept path width for TK 6x4-CT2-CT2(3x7.8 m) given by the width of the annulus between the inner and outermost path.

## 4.4 Performance analysis results

In this section we will present the results of the performance analysis for the selected vehicle combinations, represented by EU vehicle combinations and HCV's, which are both introduced in section 4.2. A red line in each of following figures marks to the performance benchmark of vehicle combinations and indicates the worst performing standard vehicle combination, which complies with current directive 96/53/EC.

- Low-Speed Longitudinal Performance

Hereby the startability is simulated to evaluate the safety risk associated with starting the vehicle combination on an uphill grade. The results in Figure 4.3 represent the maximal grade of the slope in percent, where the vehicle combination is able to start and maintain forward motion. Percentage grade is defined to mean 100 times the change-in-height divided by the horizontal distance over which the height change occurs. Meaning a grade of 100% corresponds to a grade line of 1:1 or 45° incline. Hence, the higher the grade, the better the performance.

In terms of startability HCV's having a 6x4 rigid truck as a hauling unit are able to drive up a steeper slope than the standard vehicle combinations, as shown in Figure 4.3. Rigid trucks in general obtain better results due to rise of vertical force on the driven wheels at the slope in comparison to tractors. More importantly, the other combinations have a worse performance due to a lower proportion of the GVW, which is carried over the driven axles, and which does not satisfy the current limit that prescribes a minimum of 25% of the GVW supported by the driven axles. Nevertheless, it can be observed that all vehicle combinations comply with a minimal slope of 12%, where the vehicle has to start and maintain the motion, such as prescribed by European regulation R. No. 1320/2012 [35].

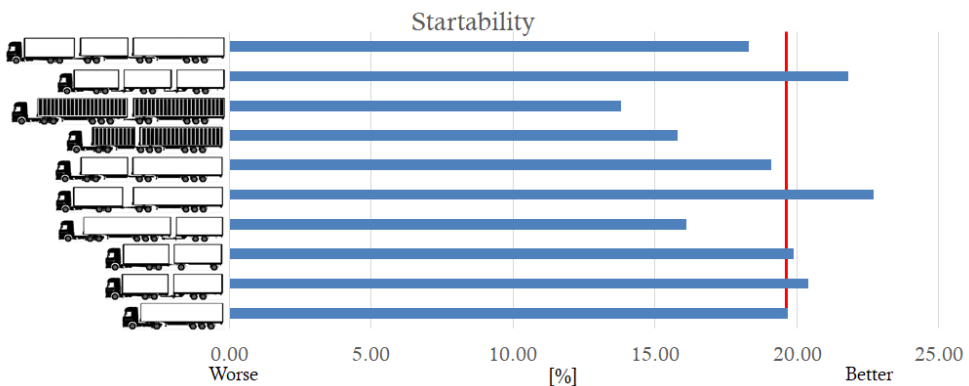


Figure 4.3: Performance results for startability.



- High-Speed Longitudinal Performance

Within this category tracking ability is selected. This assessment is aiming to evaluate the safety risk associated with sufficient lateral clearance ensuring that all units of the vehicle combination remain within the width of lane while cruising over a straight segment of the road at high-speed. The test is executed during a speed of 90 km/h. The road surface must have an overall unevenness level in each wheel path of not less than 3.8 *m/km* IRI (International Roughness Index). Moreover, the test section must have an average cross-fall, falling to the left when viewed in the direction of travel, of not less than 3.0% with standard deviation of not less than 1.0%. The vehicle combination is controlled by a driver model ensuring the tracking of the reference path by the hauling unit on the road segment having the given specification and the length of at least 1000 *m*. The swept path of the vehicle is measured according to the definition in [92]. The higher the value, the worse the result.

The results are shown in Figure 4.4. The width of all examined vehicle combinations is the same and equal to 2.55 *m* , but the tracking ability performance differs considerably. Although the absolute difference between the best and the worst performing vehicle combination is approximately 30 *cm*, we can observe that tracking ability is mainly dependent by the number and type of the coupling, number of axles, and the effective wheelbase of the vehicle units. Therefore HCV combination TR6x2-LT3-ST3 has a better performance than all existing vehicle combinations. In contrast, the worst performing vehicle combinations are TK6x4-CT2-CT2 and TR6x4-ST3-CT2. Yet, considering a typical width of European highway lane equal to 3.5 *m*, the swept path of all investigated vehicles is within the limits.

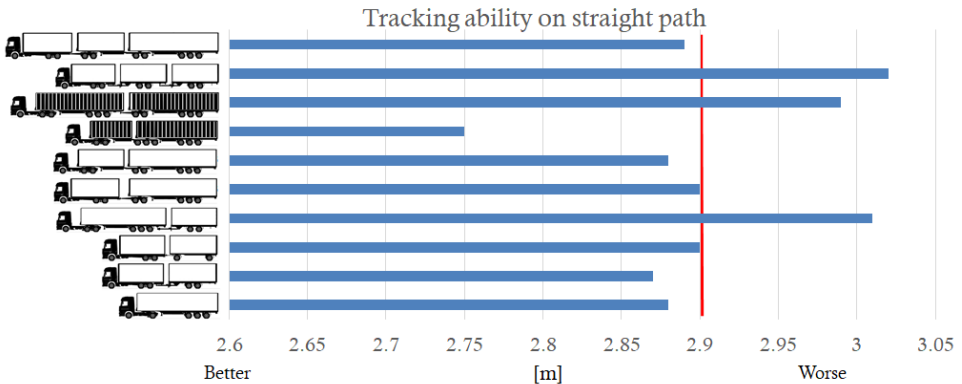


Figure 4.4: Performance results for tracking ability.

- Low-Speed Directional Performance

The low-speed swept path width is used to determine the safety risk associated with turns at intersections. The swept path is a measure to identify the road space required by a vehicle when making low-speed turns. The vehicle negotiates a prescribed 90 degree turn with 12.5 m radius at a speed of 5 km/h. The swept path is determined and maximal width is subsequently measured in accordance with [92]. The higher the value of the swept path width, the more road space is needed and the worse manoeuvrability of the vehicle combination.

Figure 4.5 shows that none of the HCV's combinations has a performance similar to that of the standard vehicle combinations. This is due to the increased overall length of the HCV combinations, and the fact that only unsteered trailer axles are considered. The low-speed swept path performance can be substantially improved by active or passive axle steering systems, increasing the number of articulation points or by decreasing the distance between axles.

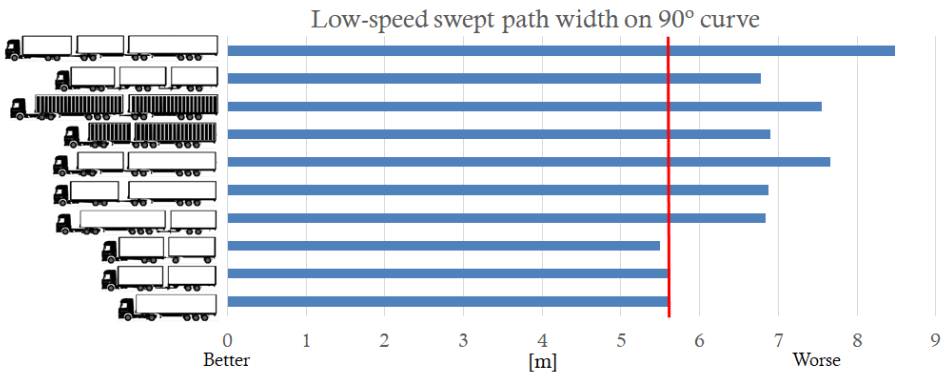


Figure 4.5: Performance results for swept path width.

- High-Speed Directional Performance

Herewith, the yaw damping is considered, which is a measure for attenuation of sway oscillations of rigid vehicles or between trailers of multi-articulated vehicles. Yaw damping is determined by measuring the decay of the yaw rate oscillation after a short-duration steer input defined in ISO 14791:2000(E). The forward speed is 88 km/h. The calculation of the yaw damping coefficient is done according to [92]. The lower the value of the yaw damping the worse the vehicle combination performance.

Figure 4.6 shows that combinations TR6x4-ST3-CT2 and TK6x4-CT2-CT2 are not in the range of the standard vehicle combinations. All combinations having the link trailer (TR6x4-LT2-ST3, TR6x4-LT3-ST3, and TK6x4-DY2-LT2-ST3) yield a better performance than the other combinations. This is mainly due to the wheels close to the vehicle unit corners and the roll coupling between the units which is provided by the fifth wheel. The number of articulations and the distance between the kingpin and the axle groups play also an important role.

A higher number of articulations and a smaller distance between the kingpin and axle group are not favourable for the yaw damping, as illustrated by vehicle combinations TR6x4-ST3-CT2 and TK6x4-CT2-CT2 in Figure 4.6.

The yaw damping coefficient can be increased by different technological improvements such as air suspension, roll-coupled modules, increasing the number of the axles or the height of the roll-centre.

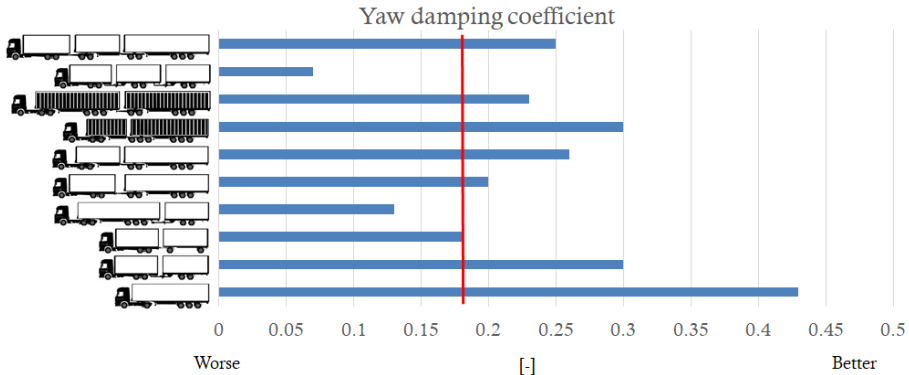


Figure 4.6: Performance results for yaw damping coefficient.

- Infrastructure Impact

For the impact on the infrastructure the pavement vertical loading was selected. This standard is introduced to limit the stress on the pavement layers below the surface of the road. It is primarily governed by the vertical axle forces on the pavement, which are used in combination with Equivalent Standard Axle Load (ESAL) to calculate the road damage [57]. The higher the force, the worse the performance. The GVW of vehicle combinations that comply with directive 96/53/EC is limited to 40 tonnes, whereas all HCV's are loaded up to 60 tonnes.

In Figure 4.7 the highest axle load per vehicle combination is depicted. It can be seen that maximal load is exerted by TR4x2-ST3, which is the most common commercial vehicle combination operating in Europe today. Furthermore it can be noticed that a number of HCV's performs substantially better than standard vehicle combinations, even though the GVW is larger. It is due to fact the GVW is distributed across multiple axles.

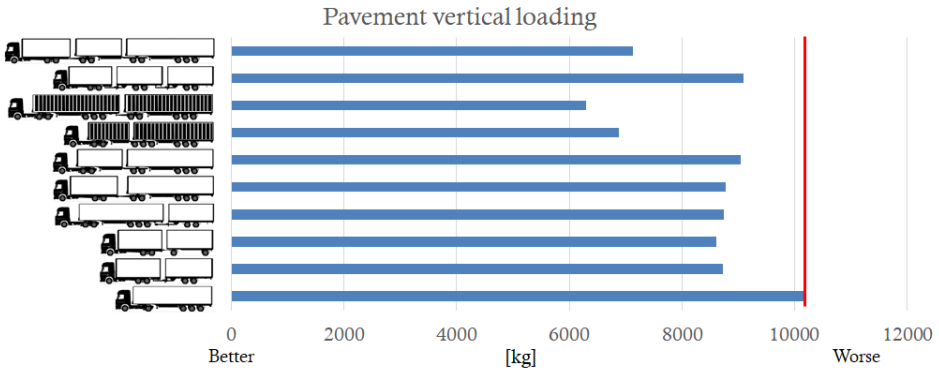


Figure 4.7: Performance results for maximal vertical axle load.

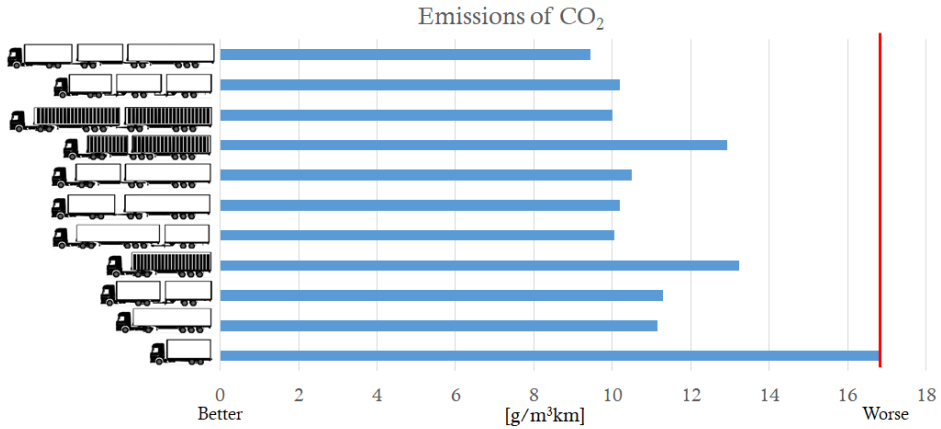
- Societal Benefits Standards

The majority of international long haul transport in Europe is prioritizing volume instead of weight, as described on page 64. Hence, two selected standards from an environmental and economic perspective in this category are related to the volume. They are quantified in terms of CO<sub>2</sub> emissions and total cost of ownership. Models were provided through the courtesy of MAN A.G. and the calculation averages the results obtained on a route from Munich to Leipheim, an ACEA drive-cycle.

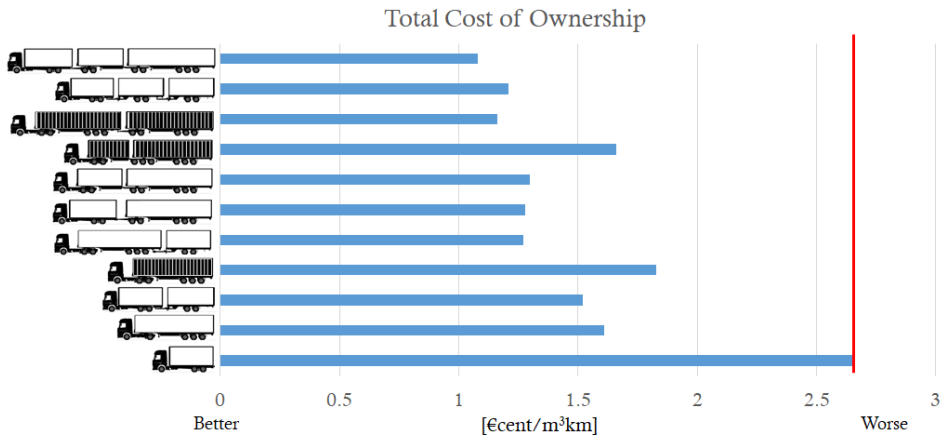
In this analysis also two additional standard vehicle combinations are included being: TR6x2-ST3 bearing 45ft container and TK6x2 bearing C782 swap-body. The vehicles are chosen because of their good inter-modal potential and frequent usage in Europe.

The first results are related to the environment and quantify the amount of CO<sub>2</sub> emitted while transporting one cubic meter over a distance of one kilometre as long-haul transport in Europe is mainly volume oriented. It can be observed that all HCV's emit less carbon dioxide m<sup>3</sup>.km compared to standard combinations of vehicles. From the HCV's the vehicle combination TR6x4-LT3-ST3 (20 ft +40 ft) has the highest emissions due to the lower available internal volume of the container loading units and their increased tare weight compared to swap bodies or semitrailer bodywork, which can be seen in the vehicle combination TR6x4-LT2-ST3 (7.8 m + 13.6 m) that performs better.

The second societal benefit standard, related to profitability, evaluates the Total Cost of Ownership (TCO) per one cubic meter transported over a distance of one kilometre. TCO aggregates the costs related to fuel consumption, driver salary, vehicle depreciation, maintenance, toll fees, and other costs associated with the daily operation. A more elaborate distribution of costs to determine TCO, along with other results related to the societal benefits can be found in [65].



(a)



(b)

Figure 4.8: Societal benefits performance (a) Carbon dioxide emissions per volume-distance, (b) Total cost of ownership.

A comparison of the standard vehicle combinations with the HCV's in Figure 4.8b shows that all HCV combinations are as profitable as the standard combinations or even more. Although for combination TR6x4-LT3-ST3 a higher tare weight of the containers combined with a lower volume leads to an increase in the TCO the rest of HCV's performs substantially better than standard vehicle combinations. The difference between the mostly used vehicle combination in Europe, TR4x2-ST3, and combination TR6x4-ST3-DY2-ST3 is more than 30%.

## 4.5 High Capacity Vehicle Combinations after 2020

In the previous subsection the performance of vehicle combinations is discussed that are defined in Figure 4.1 and 4.2. The results show that the performance of the HCV's is usually in the range of the standard vehicle combinations allowed for cross-border transport in EU. However, this is not true for low-speed manoeuvring where the clear distinction between the standard and HCV combinations is obvious and current infrastructure may not be able to accommodate these vehicles on an European scale.

Moreover, as can be seen in Figure 4.9, there exists certain interaction between high-speed stability, represented by yaw damping, and low-speed manoeuvrability, represented by swept path width. It appears that HCV combinations that are stable at high-speeds have a reduced performance on manoeuvrability and vice versa.

Additional technological improvements or changes in technical characteristics are necessary to bring the performance of HCV's closer to the range of the standard vehicle combinations. A feasible solution could be an active steering system of certain axles, which may considerably reduce the swept envelope during low-speed manoeuvring, in combination with infrastructure access policy ensuring the match between the vehicle performance and the infrastructure specifications. Moreover, electric powertrain distributed over the selected axles of the vehicle combination may improve the longitudinal performance and decrease the energetic consumption by harvesting the energy from the braking.

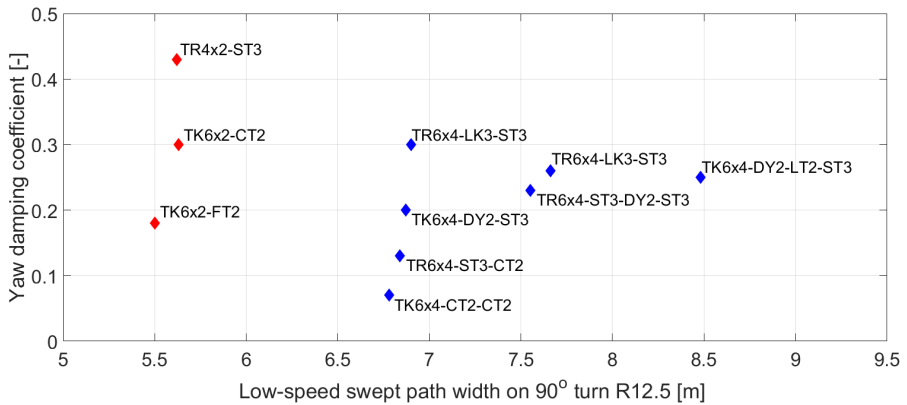


Figure 4.9: Lateral stability versus low speed manoeuvrability of vehicle combinations

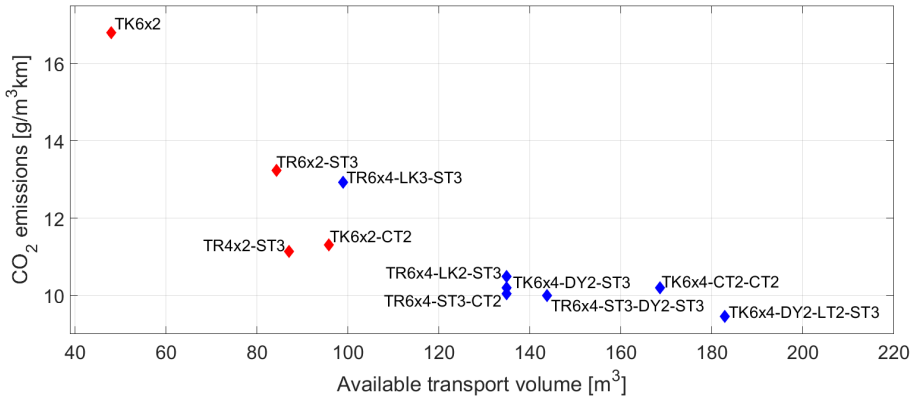


Figure 4.10: Carbon dioxide emissions versus available transport volume of vehicle combinations.

Considering the assessment results related to the environmental performance one can conclude that increasing the available transport volume per vehicle combination generally contributes to the reduction of CO<sub>2</sub> emissions, as depicted in Figure 4.10. A similar trend can be also observed in profitability where the increasing of transport volume capacity per vehicle leads to cost reduction for both *ton.km* and *m<sup>3</sup>.km*.

Therefore future vehicle concepts should be based on using multiples of standard multi-modal loading units and increase the volumetric capacity compared to the standard vehicle combinations. According to [65] the primary loading units to be used in the future are 45-foot container and C745 swap body.

Considering the box-like shape of current vehicle combinations, it is envisaged that in the future a substantial effort should be given to the aerodynamics in order to reduce the aerodynamic drag. Hence a recent EU directive 2015/719 [38] provides a provision for elongation of the truck cabin and the trailer tail to optimize the aerodynamic performance. Moreover, the aerodynamic features should be actively controlled and may not be invasive in low speed manoeuvring, but provide reasonable reduction of air drag during long-haul high-speed operation.

Examples of aerodynamic devices, are depicted in Figure 4.11:

- Prolonged cabin - enabling the reduction of frontal air drag, enlargement of the crash zones of the vehicle and more space devoted to the driver comfort as well as packaging of necessary components (e.g. systems for emission reduction).
- Foldable boat tail - reducing the overall vehicle aerodynamic drag
- Side skirts - reducing aerodynamic drag, increasing under-run protection and reducing water spray effects.



Figure 4.11: Aerodynamic drag reducing components (from left to right): Aerodynamic and prolonged cabin [132], Foldable boat tail [118], Side skirts [131].

Three concepts of future vehicle combinations will be defined. The vehicle combinations will be safe to operate on current infrastructure, moreover they will be environmentally and economically more efficient than current standard vehicle combinations from Figure 4.1. Hence they will satisfy the requirements for the smart green and profitable transport, which are essential for sustainable road transportation in the years 2020+.

#### **Future Concept I.- Swap-body Combo**

The usage of the C-series swap-body is predicted to increase considerably in the future Europe due to the high floor utilization percentage and similar dimensions with a 20 foot ISO-container. Therefore a first future concept, shown in Figure 4.12(a), has been designed to carry these loading units. A short survey among the transport companies has revealed that the C745 and C782 swap-body have the greatest potential. This vehicle concept has been envisaged as a standard size truck towing a actively steerable dolly and an extended semi-trailer allowing to carry two C745 or C782 swap-bodies. The last axle of the semi-trailer is self-steerable, which improves the manoeuvrability. The dolly can be equipped with an independent powertrain unit that may supply the traction force during uphill gradients, harvest the energy while braking or autonomously park the semitrailer unit at the distribution center towards a docking gate.

The concept I. can be easily integrated in a hub & spoke system; the truck can reach the inner city, while the longer semi-trailer can be towed by a conventional tractor to another destination or unhitched and split if needed for further manipulation. As can be seen in Figure 4.12(a) an aerodynamic and prolonged cabin as well as boat tail and active inter-unit flaps are foreseen.

#### **Future Concept II. - Double Container semitrailer**

The second future concept, depicted in Figure 4.12(b), is a combination of a 6x4 tractor and two semi-trailers with a self-steerable rear axle, which are both able to carry 45 foot containers. 45 foot containers are selected due to their very high floor utilization ratio, which reaches up to 96% when using Euro-pallets.

The semi-trailers are interconnected by means of a steerable dolly. The dolly axles as well as the articulation point can be locked at high speed; this substantially improves the high-speed stability performance compared to the combination TR6x4-ST3-DY2-ST3, which has always an additional articulation point. At low speed the lock is



released, and so the manoeuvrability performances are guaranteed thanks to the steerable dolly axle and released articulation point. This dolly thus makes it possible to achieve the best performance for both low-speed and high-speed. The dolly can be locked for example via wedges, which will lock a four-bar mechanism connecting the semi-trailer with the body of the dolly. In addition the dolly is accounted to be also equipped with an independent powertrain unit that can supply/harvest the energy or park the semitrailer if needed similar to Concept I.

### **Future Concept III - Transport Bus**

The third concept can be seen as a transport bus, which is able to accommodate a 45 foot container and is connected via a dolly with a semi-trailer, which can also accommodate a 45 foot container. The bus has five axles, where three axles are steerable and two are driven, such that an aggregate load distribution is ensured as well as traction on the driven axles. The dolly has similar features as described for previous concepts, so the combination is very stable during high speed and provides sufficient traction force for startability and gradeability. Good low-speed manoeuvrability is ensured through the steerable dolly, and the last axle of the semi-trailer is self-steerable, as in all previous concepts. The concept is depicted in Figure 4.12(c).

All three future vehicle concepts have been subjected to the performance assessment including stability, manoeuvrability and pavement loading. A comparison of the new concepts with the worst performing legal vehicle combination (complying EC 96/53) and the worst performing current HCV combination generally results in better or comparable performance. The important result of this analysis underlines the realistic and even immediate feasibility of the usage of these three future concepts on European roads. For a detailed overview of the assessment results we refer to [65], where all the results are fully documented.

It should be emphasized that to achieve this a performance special support systems needs to be implemented with mandatory features, such as Anti-lock braking system, Anti-Roll Over and Active steering systems. Although installation of such systems requires certain initial investment for the fleet owners, it pays very quickly back due to the increased vehicle capacity as shown hereafter.

For a proper comparison in terms of economic and environmental performance it is relevant to compare use cases where the fleet of vehicles is transporting an identical volume and not vehicles one to one because the transport volume differs considerably.

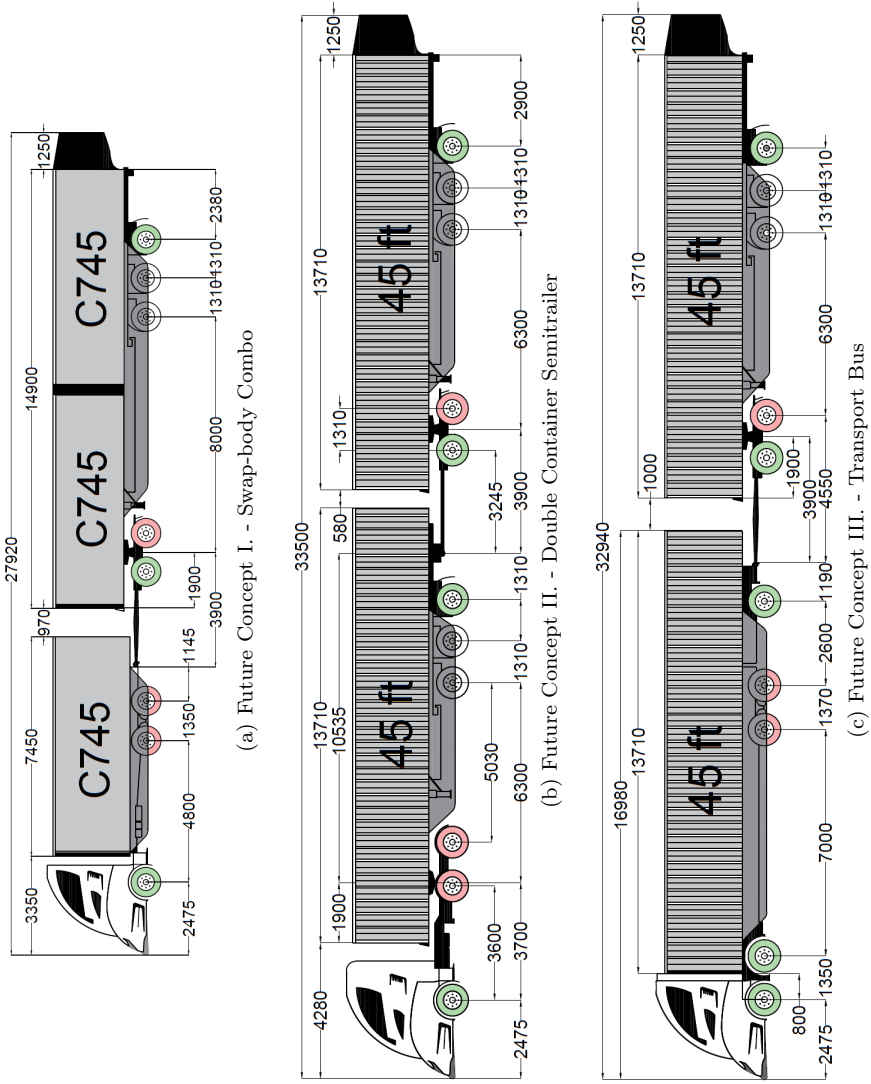


Figure 4.12: High capacity vehicle combinations for years 2020+, red axle = driven, green axle = steerable.

For Future Concept I. (TK6x4-DY4x2-ST3) two different use cases are possible:

- a replacement of three articulated vehicles (TK6x2-CT2) by two (TK6x4-DY4x2-ST3).
- a replacement of three rigid trucks (TK6x2) with only one loading unit per truck by one (TK6x4-DY4x2-ST3).

For Future Concept II. (TR6x4-ST3-DY4x2-ST3) and Future Concept III. (TK10x4-DY4x2-ST3) a replacement of two road trains (TR6x2-ST3) is possible. All use cases are listed in Table 4.3.

Use Case	Standard Veh. Comb.	Future Concept
1	3 x TK6x2-CT2(2xC782)	2xTK6x4-DY4x2-ST3(3xC745)
2	3 x TK6x2(C745)	TK6x4-DY4x2-ST3(3xC745)
3	2 x TR6x2-ST3(45ft)	TR6x4-ST3-DY4x2-ST3(2x45ft)
4	2 x TR6x2-ST3(45ft)	TK10x4-DY4x2-ST3(2x45ft)

Table 4.3: Use cases of replacement of standard vehicles by Future Concepts.

Use Case	Vehicle Combination	Fuel consumption	CO <sub>2</sub> Emission	Effectively transported volume of freight	CO <sub>2</sub> emission per m <sup>3</sup> of freight per km travelled	Potential gain
		[l/100km]	[g/km]	[m <sup>3</sup> ]	[g/m <sup>3</sup> km]	[%]
1	3 x TK6x2-CT2 (2xC782)	102.2	2727.9	241.4	11.3	
	2 x FC-I	89.1	2379.4	229.8	10.4	<b>8.4</b>
2	3 x TK6x2(C745)	74.2	1981.2	117.9	16.8	
	1 x FC-I	44.6	1189.7	114.9	10.4	<b>38.4</b>
3	2 x TR6x2-ST3(45ft)	68.6	1831.7	138.3	13.2	
	1x FC-II	51.6	1377.8	138.3	10.0	<b>24.8</b>
4	2 x TR6x2-ST3(45ft)	68.6	1831.7	138.3	13.2	
	1x FC-III	51.3	1369.4	138.3	9.9	<b>25.2</b>

Table 4.4: Emission related benchmarking of standard vehicles by Future Concepts.

Based on a comparison of defined use cases, the CO<sub>2</sub> emissions related to the volume-related transport are listed in Table 4.4. As already seen with the existing HCV's, for the future concepts too, there is a substantial CO<sub>2</sub> reduction saving potential of about one quarter. As can be seen, in some use cases even a reduction of about 35% is possible if the three standard vehicles are replaced by one future concept. For this use case, however, one must keep in mind that a higher mileage per hauling unit will be required to distribute the loading units if the fleet owner has only one vehicle combination instead of three trucks available. Thus the mileage per hauling unit will rise in conjunction with a decrease in the total fuel savings. Moreover, the

Use Case	Vehicle Combination	Effectively transported volume of freight	TCO per m3 freight per km travelled	Potential gain
		[m <sup>3</sup> ]	[€Ct/m <sup>3</sup> km]	[%]
1	3 x TK6x2-CT2 (2xC782)	241.4	1.52	
	2 x FC-I	229.8	1.28	<b>15.5</b>
2	3 x TK6x2(C745)	117.9	2.65	
	1 x FC-I	114.9	1.28	<b>51.6</b>
3	2 x TR6x2-ST3(45ft)	138.3	1.83	
	1x FC-II	138.3	1.17	<b>36.0</b>
4	2 x TR6x2-ST3(45ft)	138.3	1.83	
	1x FC-III	138.3	1.18	<b>35.7</b>

Table 4.5: TCO related benchmarking of standard vehicles by Future Concepts.

substitution of three rigid trucks by one HCV may decrease the flexibility in delivery planning.

Lastly the Total Cost of Ownership is analysed being one of the most relevant factors for the fleet owners. The TCO has been calculated on the same assumptions as for the standard and HCV's. In Table 4.5 the results are listed. It can be seen that TCO costs per unit of volume for all three future concepts are considerably lower compared to standard vehicles.

The comparison shows potential savings of 15% for replacement of three standard articulated vehicles by two future concepts or even about 50% for replacement of three single trucks. For future concepts II. and III. savings of about 36% compared to the existing vehicles are possible. There are no great differences in the TCO between future concepts II. and III., as the only difference is in the layout of the combination with tractor unit or rigid truck with nearly the same tare weights and payloads.

## 4.6 Summary

Although the future concepts may offer substantial improvements in terms productivity and transport efficiency, there are still issues which need to be resolved before the concepts can be introduced in real-life operation. Clearly one of these issues is supporting the driver during reversing, which might be beyond his/her capabilities if the vehicle combination has two or three articulation points. Another challenge is linked with combining sufficient high-speed stability and good low-speed manoeuvrability, which may be realized through active steering. Both of these challenges are investigated in Chapters 5 and 6, respectively.

## Chapter 5

# Active Trailer Axle Steering Control for High Capacity Vehicle Combinations

### 5.1 Introduction

The poor low-speed manoeuvrability performance of HCV's in comparison to traditional vehicle combinations, is a result of the vehicle combination length and the limited number of articulation points. In general, the manoeuvrability depends on the distance between the articulation joint and the center of the axle group. This increases with every additional unsteered unit in the vehicle combination and results in a wider swept path. However, the manoeuvring performance can be improved by active axle steering through control of axle steering angle. Active steering can be also employed to improve the high-speed stability defined by established performance measures, as listed in Table 2.9.

This chapter, contains the journal article [75], that proposes a novel control strategy for active axle steering of trailing units of a HCV to improve both low-speed manoeuvrability and high-speed stability. A single controller structure for all velocities is proposed using a gain scheduling method for optimal performance at any velocity. The controller is finally implemented to a high-fidelity multi-body model of Future Concept I., introduced in Chapter 4, and results are provided for both the controlled and uncontrolled case.

### 5.2 Paper

The journal article is presented at the next pages.

# Active Trailer Steering Control for High Capacity Vehicle Combinations

Karel Kural, Pavlos Hatzidimitris, Nathan van de Wouw, Igo Besselink, and Henk Nijmeijer,  
*Fellow IEEE*

**Abstract**—In this paper, a new control strategy for the active steering of a trailers of longer and heavier vehicle combinations is proposed to improve both low speed maneuverability and high speed stability. A novelty of the approach is in the use of a single controller structure for all velocities using a gain scheduling method for optimal performance at any velocity. To achieve such a control objective, the problem is initially formulated as a path following problem and subsequently transformed into a tracking problem using a reference model. To support controller design, a generic nonlinear model of a double articulated vehicle, based on a single track model, is employed. The proposed systematic design approach allows to easily adjust the controller for additional trailers or different dimensions, in which only some of the towed vehicles are allowed to steer. The performance of the controller is verified on a high-fidelity multi-body model for evidencing the practical applicability of the approach. Simulation results show substantial reduction of both, the swept path width and tail swing for low speed, and the rearward amplification for high speed.

**Index Terms**—Active steering, Intelligent Vehicles, Land Transportation, Vehicle safety and maneuverability.

## I. INTRODUCTION

**R**OAD freight transport plays a key role in the European economy. In Europe, about 75% of total inland transport is performed by trucks versus just 18.5% by rail and 6.5% by waterway [1]. Besides that, the quantity of transported goods is continuously increasing, which is related to the development level

K. Kural is with the Department Mechanical Engineering, Eindhoven University of Technology, Eindhoven Netherlands (e-mail: karel.kural@han.nl), and with HAN Automotive Research, HAN University of Applied Sciences, Arnhem, Netherlands.

P. Hatzidimitris performed this work while affiliated with the Department Mechanical Engineering, Eindhoven University of Technology, Eindhoven Netherlands

N. van de Wouw is with the Department Mechanical engineering, Eindhoven University of Technology, Eindhoven, Netherlands (e-mail: N.v.d.Wouw@tue.nl), with the Department of Civil, Environmental & Geo- Engineering, University of Minnesota, Minneapolis, U.S.A., and with the Delft Center for Systems and Control, Delft University of Technology, Delft, Netherlands

of national economies. However, this has a substantial impact on the wear and tear of roads as well as on the amount of traffic jams caused by commercial vehicles. Even though OEM's (Original Equipment Manufacturers) are stimulated by the national governments to produce cleaner and more efficient vehicles, e.g., through the EURO 6 standard, road transport still consumes more than 26% of the total energy in Europe [2]. Besides this being an economical argument, it is also an ecological argument: 19% of the greenhouse gases emission is caused by road transport [2].

Although lately fuel prices have decreased significantly, in the future it is expected that prices will eventually start rising again resulting in higher operational costs for transportation companies and fleet owners. Hence, it is clear that reducing the fuel consumption of road transport is desirable from several perspectives. As the intensity of road transport usage is unlikely to diminish in the future, significant improvements in fuel efficiency are needed.

Besides improving the efficiency of combustion engines, a promising alternative are High Capacity Vehicles (HCV). HCV's are trucks, which typically tow multiple of trailers having also multiple articulation points. An overview of several types of HCV's is given in Figure 1.

With their increased capacity, originating in length up to 25 meters and weight up to 60 tonnes, HCV's achieve an improved emission efficiency reducing more than 25% of emitted grams Carbon Dioxide/ton/km. [3] compared to the most frequently used conventional combination of tractor with semitrailer. Besides this positive environmental effect, HCV's have also a positive economic effect. More cargo transported and a reduced truck/cargo ratio results in less drivers needed to transport same amount of cargo. These positive effects contribute currently to a rising number of HCV's on European roads.

Unfortunately, the length of HCV's also represents a challenge with respect to the low-speed maneuverability and sometimes also high-speed stability, compared to most conventional configurations of

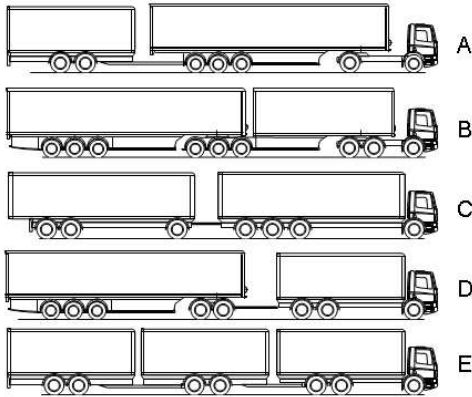


Fig. 1. Examples of HCV configurations.

commercial vehicles. In this scope, several measures exist to quantify the performance of these vehicles ensuring their safe operation given existing infrastructure [4]. In this paper, the measures we will focus on are the swept path width, and tail swing for low-speed maneuverability. The swept path width is the maximum distance that the rear axle of a vehicle combination tracks inside the path taken by the steering axle in a low speed turn, whereas the tail swing refers to the maximum lateral distance that the outer rearmost point on a vehicle moves outwards, perpendicular to its initial orientation, when the vehicle commences a small-radius turn at low speed. For high-speed stability, which is related to yaw and/or roll instability, a rearward amplification measure is used, being the degree to which the trailing unit(s) amplify or exaggerate lateral acceleration of the hauling unit.

Both low-speed maneuverability and high-speed stability can be significantly improved by active steering of trailers. The actively steered trailer is not a new idea as the first patents [5], [6] were registered already in the early 1930's. Since then, this approach has evolved and was subject of extensive research in the automotive field as well as in robotics. However, the control problem considered in these two fields are essentially different. Namely, in mobile robotics research, the steer angle of the first axle is generally seen as a control input, whereas in automotive field it is the driver who controls the first axle and the control input is associated with the steering of particular trailer axles to satisfy given criteria.

Generally speaking, three different types of controllers exist; firstly, controllers improving only low-speed maneuverability, secondly, controllers only

for high-speed instability or, thirdly, combined controllers that can deal with both situations. Each type has its advantages and disadvantages either in performance or implementation demands.

Low-speed controllers are typically associated with the robotic vehicles, employing very often a kinematic model to support the design of the controller [7], [8], [9], [10] and [11]. Although the kinematic model does not include tyre forces, body slip and inertial effects and is substantially simpler than a dynamical one, it provides sufficiently accurate results for the robots that typically drive at low speed. The wheeled robots in these papers also do not have multiple axles per body, which results in significant sideslip of the tyres in case of real HCV's; therefore making kinematic models less suitable for real HCV's even in low-speed. The kinematic models used in the reference above are mostly affine in the control input meaning that classical nonlinear control design methods can be employed.

High-speed controllers are often based on linearized dynamical models by assuming small articulation angles. This is a valid assumption, since in typical operational scenarios, such as a lane change, the articulation angles do not exceed ten degrees. This assumption clearly does not hold for low-speed maneuvering. In [12], [13], and [14], linear quadratic regulator (LQR) methods are used to reduce rearward amplification at high speeds. In [15], a sliding mode controller is proposed based on a simplified three degrees of freedom nonlinear model. Assuming small steering angles and using the lateral tyre forces as a control input, the system becomes affine in the control input. The desired tyre forces that are generated by the controller are then translated into steering angles using an inverse tyre model.

Based on the heading angle method in [16], a new combined controller design is proposed in [17] and [18] for tractor semi-trailer combination. This controller design consists of a feed-forward part based on a kinematic model that operates at low speed only, and PID feedback controller based on a simplified dynamical model, which is applied exclusively at high speeds. The controller aims to reduce the swept path as well as rearward amplification. An alternative combined approach with comparable results, called Virtual Rigid Axle Command Steering (VRACS), is documented in [19]. The controller uses the velocity of articulation angles to steer the towed bodies with the same steer velocity. The steering is delayed with respect to articulation angle velocity and the delays are optimized empirically using simulations.

The contribution of this paper is to solve the

combined problem of low-speed maneuverability and high-speed stability of HCV's by proposing a novel and systematic approach on the basis of a sufficiently generic and accurate vehicle model. The uniqueness of the method is based on the employment of a single controller structure for velocities in the range [1 – 90] km/h using a gain-scheduled feedback and feedforward controller. Optimal performance at any velocity within mentioned range can be achieved for arbitrary vehicle configurations. As a representative case study, we consider a rigid truck, dolly, and semitrailer vehicle combination, as recent research [3] identified this vehicle combination as one of the potential candidates for most efficient means of road transport for years 2020+. The combination, with total length of nearly 28 meters, is capable of carrying 3 x 782 swap bodies, which are the loading units having high inter-modal potential.

The paper is organized as follows. Section II covers the derivation of a nonlinear dynamical model of double articulated vehicle using the Lagrangian method and the description of the high-fidelity multi-body model that will be used for verification. In Section III, the control problem is formulated and the reference model is derived. In Section IV, a gain-scheduling controller design method is developed based on a linearization of the dynamical model. Controller verification in a number of operational scenarios is documented in Section V. Finally, the discussion and conclusions are presented in Section VI.

## II. VEHICLE DYNAMICS MODELING

As described earlier, most of the existing controller designs are based on kinematic models. Although kinematic models are typically much simpler than dynamic models, the former do not take tyre forces into account, and are only valid at low speed and limited tyre slip. Since the goal is to design the controller structure for active steering that is valid for any realistic speed, a dynamic model that includes also tyre forces is constructed next.

### A. State-Space Model

The model is based on a simplified single track (bicycle) model of a double articulated vehicle, see Figure 2. Each vehicle body (truck, dolly, and semitrailer) is characterized by the dimensions  $a_i, b_i, l_i, h_i$ , its mass  $m_i$  and moment of inertia  $J_i$ . Furthermore, the bodies are assumed to be perfectly rigid and the tyres of each axle were lumped together into single tyre with double stiffness. Horizontal tyre

forces are characterized by a linear tyre model, and the cornering stiffness is based on Pacejka's Tyre Magic Formula [20] from available tyre property data. No friction or play is assumed in the articulation joints. The vertical motion is neglected since the model is planar. Therefore, the rotations, which involve movement outwards of x-y plane such as roll and pitch are not considered. The model variables as well as the global, earth-fixed, co-ordinate system  $\bar{e}^0$  are shown in Figure 3. Note that for clarity reasons only the tyre forces on first and last axle are illustrated, although these act on all axles.

Equations of motion are derived using a Lagrangian approach. Herewith, we employ coordinates defined in the local co-ordinate system  $\bar{e}^1$  being attached to the truck center of gravity, such as depicted in Figure 2. The resulting equations will not depend on the orientation  $\psi_1$  of the truck.

Furthermore, note that  $\dot{X}_1$  and  $\dot{Y}_1$  are the time-derivatives of global position co-ordinates  $X_1$  and  $Y_1$  of the truck center of mass  $CM_1$ .  $\theta_1$ , and  $\theta_2$  are the articulation angles between the bodies as defined in Figure 3. The yaw rate  $r_1 = \dot{\psi}_1$  of the truck is defined as time-derivative of the yaw angle  $\psi_1$ . Yaw angles of the dolly and semitrailer are defined by means of articulation angles as  $\psi_2 = \psi_1 - \theta_1$  and  $\psi_3 = \psi_1 - \theta_1 - \theta_2$ , respectively. From these yaw angles, the related yaw rates follow:  $r_2 = \dot{\psi}_2 = r_1 - \dot{\theta}_1$  and  $r_3 = \dot{\psi}_3 = r_1 - \dot{\theta}_1 - \dot{\theta}_2$ .

The following set of generalized velocities will be used for the model:

$$\underline{v} = [u_1, v_1, r_1, \dot{\theta}_1, \dot{\theta}_2]^T \quad (1)$$

where longitudinal velocity  $u_1$  and lateral velocity  $v_1$  in the frame  $\bar{e}^1$  are given by:

$$\begin{aligned} u_1 &= \dot{X}_1 \cos \psi_1 + \dot{Y}_1 \sin \psi_1, \\ v_1 &= -\dot{X}_1 \sin \psi_1 + \dot{Y}_1 \cos \psi_1. \end{aligned} \quad (2)$$

and can be seen as local quasi coordinates.

A detailed derivation of the equations of motion for the vehicle combination can be found in [21]. The resulting model can be written in the form:

$$M(\theta_1, \theta_2)\dot{\underline{v}} + H(\theta_1, \theta_2, \underline{v}) = \underline{Q}_v. \quad (3)$$

Matrices  $M$ ,  $H$ , and  $\underline{Q}_v$  are listed in Appendix A. Next, the equation of motion in (3) are transformed into state-space form, such that the system can be described by a first-order nonlinear differential equation as follows:

$$\dot{x} = f(x) + g(x, u, w(t)), \quad (4)$$



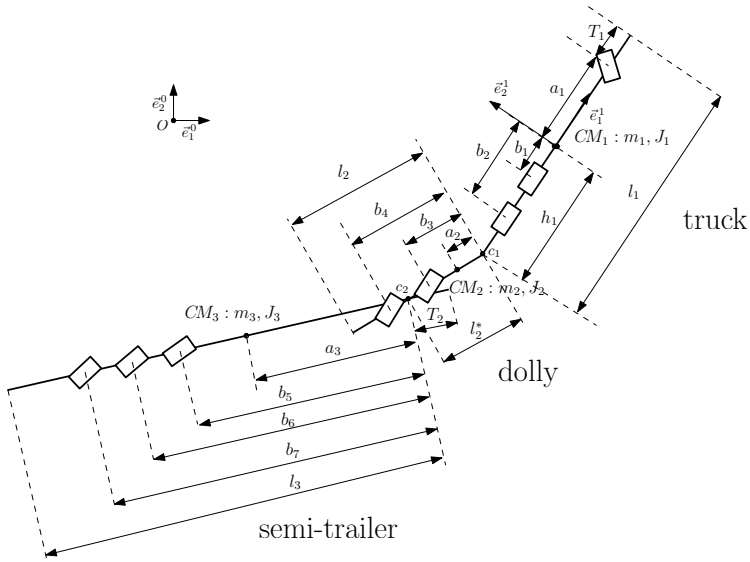


Fig. 2. Double articulated single track model with dimensions and coordinate systems.

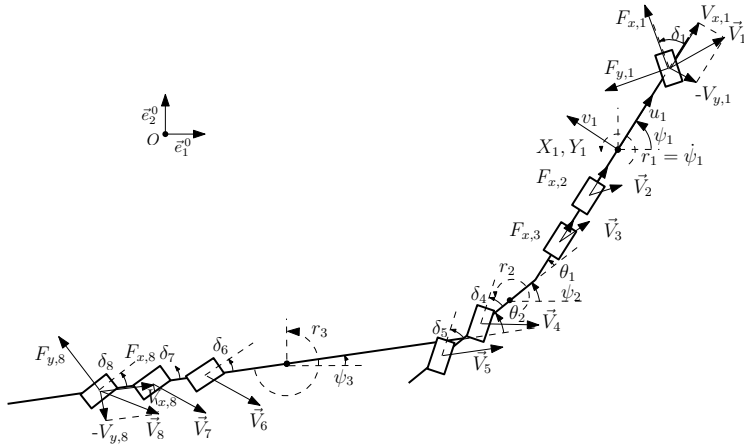


Fig. 3. HCV single track model variables.

where

$$f(x) = \begin{bmatrix} \dot{\theta}_1 \\ \dot{\theta}_2 \\ -M^{-1}H \end{bmatrix}, g(x, u, w(t)) = \begin{bmatrix} 0 \\ 0 \\ M^{-1}Qv \end{bmatrix} \quad (5)$$

and  $x = [\theta_1, \theta_2, \underline{v}^T]^T = [\theta_1, \theta_2, u_1, v_1, r_1, \dot{\theta}_1, \dot{\theta}_2]^T$  are the system states,  $u = [\delta_4, \delta_5, \delta_6, \delta_7, \delta_8]^T$  are the control inputs (dolly and semi-trailer steering angles), see Figure 3, and  $w = [\delta_1, F_{x,2}, F_{x,3}]^T$  are the external inputs controlled by the driver being the steering angle of the first axle, and traction forces on

the driven axles, respectively. The traction forces are employed directly for controlling longitudinal velocity of the truck  $u_1$ , without considering longitudinal tyre slip, required to cover true braking situations. This state-space system can be used for simulation purposes and as a basis for the controller design.

### B. High-Fidelity Model

Next, the high-fidelity multi-body model will be described that has been validated against experimental test data in [22]. This model will be used for the

verification of the controller design, proposed in Section IV., and is primarily intended for the simulation based analysis of performance measures described earlier (such as the swept path width, tail swing and rearward amplification).

The model is built by means of the Commercial Vehicle Library (CVL) [23], which is a highly generic library consisting vehicle assemblies (e.g., truck, trailers, semitrailers, etc.) and additional vehicle components (brake system, driveline, etc.) developed in Matlab/SimMechanics by the Eindhoven University of Technology. The purpose of the library is to provide a base for building representative and generic vehicle models while avoiding low-level details (such as, e.g., non-linearities in chassis suspension, roll steer or cabin-chassis suspension) that do not substantially impact overall dynamical behavior. Furthermore, the model can be visualized, using Matlab Virtual Reality Toolbox see Figure 4.

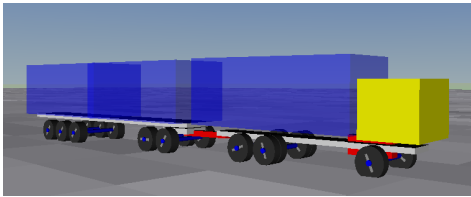


Fig. 4. Multi-body model of rigid truck with dolly and semitrailer created by CVL.

The chassis of each vehicle is divided in two parts, a frontal and rear segment. They are connected to each other with a rotational degree of freedom enabling to model torsion of the chassis during cornering. Cabin, engine and cargo loading units, which are represented as bodies possessing mass and inertia, are rigidly welded to a neighboring chassis segment hereby not introducing additional degrees of freedom with respect to the chassis. Both axle types, i.e. steerable or driven, are attached to the particular chassis segment by means of rotational and translational degrees of freedom. It enables to model vertical deflection of the suspension, as well as roll and pitch movement of the vehicle body, which is not considered in the state-space model derived in Section II-A. This represents one of the essential differences between the two models contributing to distinctive vehicle behavior especially during highly dynamic maneuvers. Another additional component of the high-fidelity model, which is substantially different to the state space model, is the nonlinear tyre model with relaxation behavior based on the

Delft-Tyre library [24]. Since the tyre is the interface between the road and the vehicle responsible for generating reaction forces in all three directions it has dominant impact on the overall vehicle dynamics.

### III. CONTROL PROBLEM FORMULATION

The controller, to be designed in this paper, aims to minimize the swept path width, while ensuring zero tail swing during low-speed maneuvers and aims to suppress rearward amplification during high-speed maneuvers.

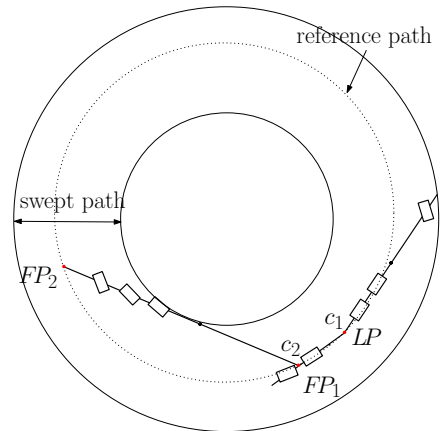


Fig. 5. First combination of  $LP$ ,  $FP_1$ , and  $FP_2$ .

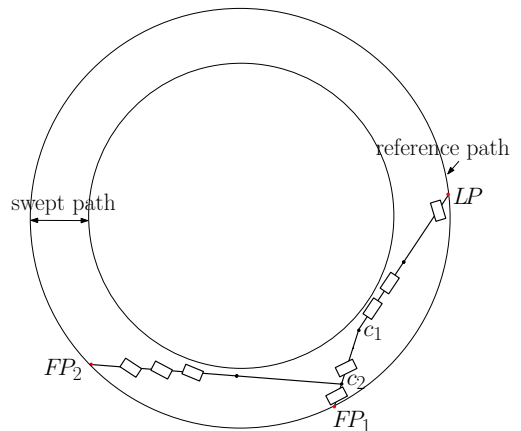


Fig. 6. Second combination of  $LP$ ,  $FP_1$ , and  $FP_2$ .

To achieve this dual objective, the control problem is initially formulated as a path following problem and subsequently transformed into a tracking

problem using a reference model for the dolly and semitrailer. The general idea of the path following strategy is that particular points located on the dolly and semitrailer converge to and follow a path traveled by a particular point on the truck. The follow points on the dolly and semitrailer are referred as  $FP_1$  and  $FP_2$ , respectively, whereas the lead point on the truck is referred as  $LP$ . Different choices for these points can be made and these choices have distinct advantages and disadvantages. Two combinations of lead and following points are provided in Figures 5 and 6.

In Figure 5, the lead point  $LP$  is the first coupling point ( $c_1$ ) and the following points are the second coupling point ( $c_2$ ) and the rear end of the semitrailer. In Figure 6, the lead point is at the front of the truck, whereas the follow points are at the rear of both dolly and semitrailer. As can be observed by comparing Figures 5 and 6, the second combination of lead and follow point not only eliminates the tail swing of the dolly, but also significantly reduces the swept path of the combination. These advantages make the second combination of lead and following points the most favorable choice, which is also advocated in [21].

**Remark 1** *In case of a high-speed dynamic maneuver, it is proposed to move the lead point closer to the truck center of mass  $CM_1$ . The path governed by such selected lead point is generally smoother and thus reference articulation angles (that will be described below) evolve slower. This, in turn, results in smaller lateral accelerations of the dolly and semitrailer, which are more important at high speeds than swept path width. Hence, all results below presented for high-speed maneuver assume the lead point to be at  $CM_1$ .*

The path following problem can be transformed into a tracking problem using a reference model for the dolly and semitrailer as shown in Figure 7. In the reference model the location and the orientation of the truck coincides with that of the actual truck and the follow points, which are located on reference path defined by the past evolution of the absolute Cartesian coordinates  $X_{LP}$  and  $Y_{LP}$  of the lead point, see Figure 7. and 6. The associated articulation angles of the reference model can then be used as the desired angles for actual vehicle combination. This method is an extension of the concept proposed in [10] and [25] for mobile robots.

In order to find the feasible position for the first follow point ( $FP_1$ ) that will coincide with the path of the lead point ( $LP$ ), the distance between the point

on the reference path and the first coupling point ( $X_{C_1}, Y_{C_1}$ ) is calculated. The objective is to find a point on the path for which the distance between that point and the fifth wheel position ( $X_{C_1}, Y_{C_1}$ ) is equal to the distance  $l_2$ , representing the total length of the dolly. To achieve this objective, the time variable  $\hat{\tau}_1$  is introduced. This time variable is used to characterize the time instant ( $t - \hat{\tau}_1$ ) for which the distance between the position of the lead point ( $X_{LP}(t - \hat{\tau}_1), Y_{LP}(t - \hat{\tau}_1)$ ) is feasible for the current position of the first follow point  $FP_1$  (at time  $t$ ). This time instant is determined by solving the following minimization problem:

$$\hat{\tau}_1(t) := \min_{\tau_1} \{ \tau_1 \geq 0 \mid f_{\tau_1}(t) = 0 \}, \quad (6)$$

subject to  $|\theta_{1d}(t)| < \pi/2$ ,

where  $f_{\tau_1}(t)$  is defined as:

$$f_{\tau_1}(t) := (X_{c_1}(t) - X_{LP}(t - \tau_1))^2 + (Y_{c_1}(t) - Y_{LP}(t - \tau_1))^2 - l_2^2, \quad (7)$$

where  $X_{c_1}(t)$  and  $Y_{c_1}(t)$  describe the position of the first coupling point at time  $t$ ,  $X_{LP}(t - \tau_1)$  and  $Y_{LP}(t - \tau_1)$  describe the position of the front wheel at time  $(t - \tau_1)$ , and  $\theta_{1d}(t)$  in (6) is the desired articulation angle between the truck and the dolly and is a result of  $\hat{\tau}_1$  (see (9), (10), and (12) below). The position coordinates  $X_{c_1}(t)$ ,  $Y_{c_1}(t)$  in (7) can be derived from the lead point position  $X_{LP}(t)$  and  $Y_{LP}(t)$ , which is assumed to be known from the knowledge of yaw rate, longitudinal, and lateral velocity of the truck:

$$\begin{aligned} X_{c_1}(t) &= X_{LP}(t) - l_1 \cos(\psi_1(t)), \\ Y_{c_1}(t) &= Y_{LP}(t) - l_1 \sin(\psi_1(t)). \end{aligned} \quad (8)$$

Solving the equation  $f_{\tau_1} = 0$ , in the objective function in (6), may generally result in multiple crossings between the circle with radius  $l_2$  and the lead point path. The minimization part of the problem in (6) describes the search for the minimum value of  $\tau_1$ , which still satisfies the condition  $|\theta_{1d}(t)| < \pi/2$ , being typically the mechanical limit of the coupling. This condition ensures that solution does not result in the first (i.e., closest to the  $LP$ ) erroneous minimizer as is shown in Figure 8, but does result in the correct minimizer, which is the next smallest  $\tau_1$  as can be seen in the same figure. In practice, the curvature of the path of the lead point, being defined as inverse to the curve radius, is typically smaller than depicted in Figure 8, which also avoids the occurrence of the erroneous minimizers.

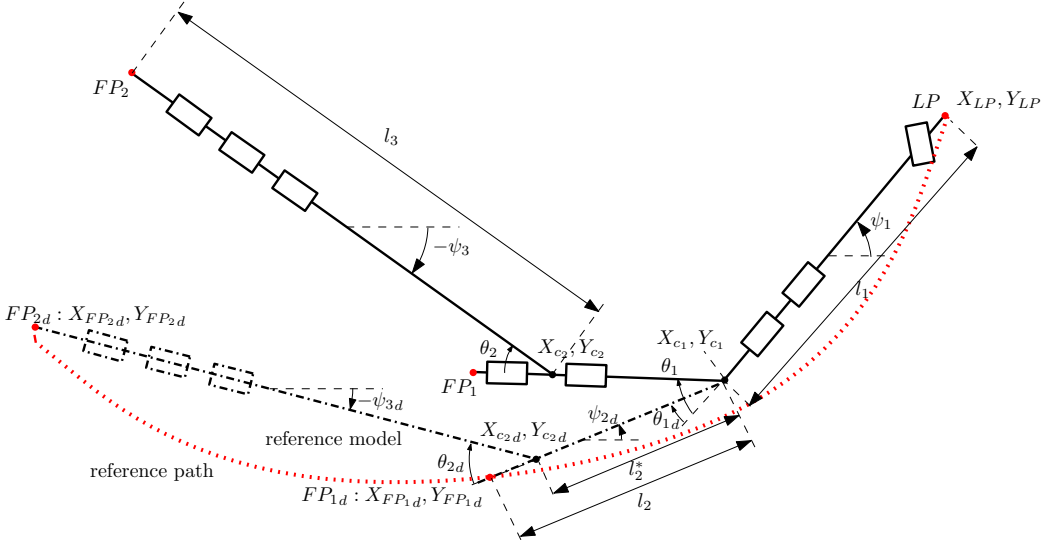


Fig. 7. Reference Model (actual truck, dolly and semitrailer combination in solid, reference configuration in dot dashed line, reference path in red dotted).

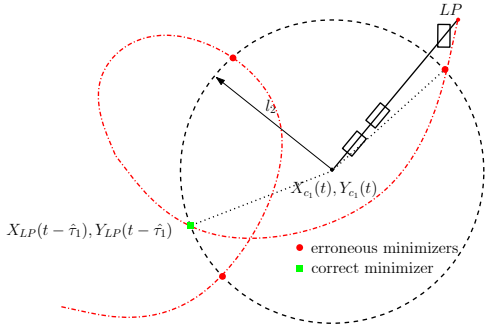


Fig. 8. Minimization process to find  $\hat{\tau}_1$ .

Then, the desired coordinates of the first follow point can be determined using  $\hat{\tau}_1$  from (6):

$$\begin{aligned} X_{FP1_d}(t) &= X_{LP}(t - \hat{\tau}_1), \\ Y_{FP1_d}(t) &= Y_{LP}(t - \hat{\tau}_1). \end{aligned} \quad (9)$$

Subsequently, the desired yaw angle of the dolly is derived:

$$\psi_{2_d}(t) = \text{atan2}(Y_c(t), X_c(t)), \quad (10)$$

where  $Y_c(t) = Y_{c1}(t) - Y_{FP1_d}(t)$ , and  $X_c(t) = X_{c1}(t) - X_{FP1_d}(t)$ . The usage of  $\text{atan2}$  function ensures an appropriate range of  $[-\pi, \pi]$  for  $\psi_{2_d}(t)$ . Analogously, the desired position

coordinates of the second follow point ( $FP_{2_d}$ ) can be derived, which in turn leads to a desired yaw angle  $\psi_{3_d}(t)$  for the semitrailer.

Finally, the desired articulation angles are derived from the desired yaw angles as follows:

$$\theta_{1_d}(t) = ((\psi_1(t) - \psi_{2_d}(t) + \pi) \bmod 2\pi) - \pi, \quad (11)$$

$$\theta_{2_d}(t) = ((\psi_{2_d}(t) - \psi_{3_d}(t) + \pi) \bmod 2\pi) - \pi. \quad (12)$$

**Remark 2** The modulo operator is needed in (11), since  $\psi_1(t)$  is calculated by integration of  $r_1(t)$ , whereas  $\psi_{2_d}(t)$  follows from an  $\text{atan2}$  function. Therefore,  $r_1(t)$  does not have a constrained range, while  $\psi_{2_d}(t)$  is constrained to a range  $[-\pi, \pi]$ . In (12), the modulo operator is needed in the case where  $\psi_{2_d}(t) = \pi - \epsilon$  and  $\psi_{3_d}(t) = -\pi + \epsilon$ , where  $\epsilon$  and  $\epsilon$  are some arbitrary small positive angles. This would result in  $\theta_{2_d}(t) = 2\pi + \epsilon + \epsilon$ , which is reduced to  $\theta_{2_d}(t) = \epsilon + \epsilon$  by the modulo operator. In both equations,  $\pi$  is added inside the operation and subtracted afterwards, such that  $\theta_{1_d}$  and  $\theta_{2_d}$  are constrained to the interval  $[-\pi, \pi]$  instead of the interval  $[0, 2\pi]$ .

The tracking problem can be stated using the dynamic model (4), (5) derived in Section II-A. The

dynamic model, can be now summarized as follows:

$$\begin{aligned} \dot{x} &= f(x) + g(x, u, w(t)), \\ y &= \begin{bmatrix} \theta_1 \\ \theta_2 \end{bmatrix}, \end{aligned} \quad (13)$$

where  $y$  is the measured output, consisting of the articulation angles. The goal of the control problem is to design a controller for  $u = [\delta_4, \delta_5, \delta_6, \delta_7, \delta_8]^T$  such that the output  $y$  tracks the reference signal  $y_d(t) = \begin{bmatrix} \theta_{1d}(t) \\ \theta_{2d}(t) \end{bmatrix}$ ; that is:

$$e(t) := y_d(t) - y(t) \rightarrow 0, \quad \text{for } t \rightarrow \infty, \quad (14)$$

where  $\theta_{1d}(t)$ ,  $\theta_{2d}(t)$  are given by (11) and (12). Since the reference signals are based on the reference model, this ensures the accomplishment of the original (path-following) goal of the follow points coinciding with the lead point path. In addition, the closed-loop system should exhibit stable dynamics satisfying the generalized Nyquist criterion.

#### IV. CONTROLLER DESIGN

As mentioned earlier, the control objective is, besides the stable error dynamics, to ensure the convergence of the tracking errors  $e_1 = \theta_{1d}(t) - \theta_1(t)$  and  $e_2 = \theta_{2d}(t) - \theta_2(t)$  to zero, such that the follow points track the reference path governed by the lead point by means of steering angles on the dolly  $[\delta_4, \delta_5]$  and the semitrailer  $[\delta_6, \delta_7, \delta_8]$ . Using these five steering angles as independent control inputs would result in an over-actuated system, which would result in an unnecessarily complex controller design. Therefore we opt to control the individual dolly axles as well as individual semitrailer axles with equal angles, i.e.,  $\delta_4 = \delta_5$ , and  $\delta_6 = \delta_7 = \delta_8$ . Furthermore, the controller design combines both feedback and feedforward controllers. Both parts of the controller are being gain scheduled with the longitudinal velocity  $u_1$  as a scheduling variable. This results in the controller structure introduced in Section IV-A. The design of the feedback part of the controller, based on a velocity-dependent linearized vehicle model, is treated in Section IV-B, followed by a closed-loop stability analysis in Section IV-C. Finally, the feedforward design is discussed in Section IV-D.

##### A. Controller structure

In Figure 9, the proposed controller structure is depicted. It includes the reference model, see Section III, a feedback controller, and a feedforward controller (in red), which together generate the control input  $\tau = [\tau_1, \tau_2]^T := [\delta_4, \delta_6]^T$  for the nonlinear

system representing the vehicle combination. The input  $w = [\delta_1, F_{x,2}, F_{x,3}]^T$  is provided by the driver under the assumption that  $F_{x,2} = F_{x,3}$ .

The reference model employs information of vehicle states  $u_1, v_1$ , and  $r_1$  that are being primarily determined by the driver inputs. In practice, they are either measured or estimated from available measurements in order to derive reference articulation angles  $y_d = [\theta_{1d}, \theta_{2d}]^T$ . The tracking error  $e(t) := y_d(t) - y(t)$  is used as an input to the feedback controller. The gain-scheduled feedback controller incorporates a dynamic decoupler and a multiple input multiple output (MIMO) PID controller. As a scheduling variable the longitudinal velocity  $u_1$  of the first vehicle is being used, which also holds for the feedforward part of the controller. Figure 9 shows that feedforward controller consist of two branches. The left branch in Figure 9 includes a low-pass filter  $L_d$ , with velocity dependent ( $u_1$ ) cut-off frequency that prevents high-frequency content of the reference signal in the control loop. The right branch includes a linearized vehicle model  $G_{y/\delta_1}$ , described in [21], that is using longitudinal velocity as scheduling parameter and denotes the transfer function from the input of the driver steering angle  $\delta_1$  to articulation angles  $\hat{y}^w = [\hat{\theta}_1^w \ \hat{\theta}_2^w]^T$ . Subsequently, the difference  $y^f$  between the filtered desired articulation angle and the articulation angle introduced by the driver is used as an input for the feedforward controller, which is based on a linearized plant model inversion.

##### B. Feedback Controller Design

The plant dynamics in (13) is described by a MIMO system with two inputs ( $\tau_1, \tau_2$ ) and two outputs ( $\theta_1, \theta_2$ ). The intention is to use additional PID controller with  $e$  as an input.

The feedback controller design is based on linearized plant models derived from the nonlinear model in (13), that are obtained by linearization around equilibria of steady states characterized by,  $\dot{x} = [\dot{\theta}_1, \dot{\theta}_2, \dot{u}_1, \dot{v}_1, \dot{r}_1, \dot{\theta}_1, \dot{\theta}_2]^T = \underline{0}$ . Hereto, Equation (3) needs to be solved for  $\dot{x} = 0$  resulting in:

$$H(\theta_1, \theta_2, u_1, v_1, r_1) = \underline{Q}_v(\theta_1, \theta_2, u_1, v_1, r_1, \delta_1, \delta_4, \delta_6). \quad (15)$$

Equilibria satisfying (15) are calculated numerically. For this purpose, four variables  $\theta_1, \theta_2, u_1$ , and  $r_1$ , were fixed and subsequently the other variables can be obtained by solving (15). These fixed states were chosen because these are most representative to characterize the vehicle combination in terms of the desired nominal steady-state configuration. This

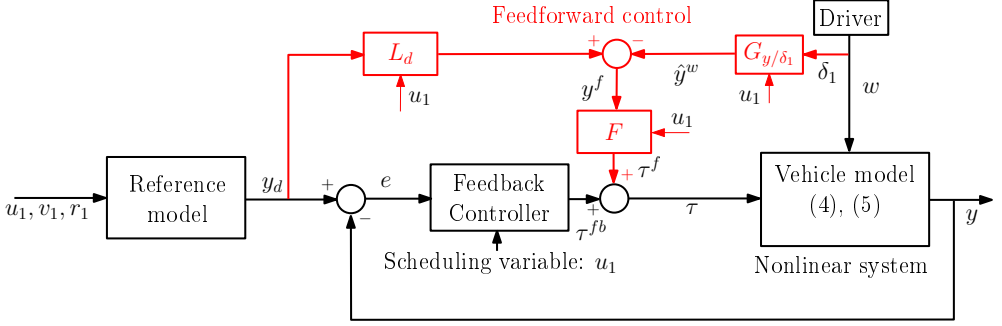


Fig. 9. Controller structure.

yields the equilibrium state  $x_{eq}$ , and input vectors  $\tau_{eq}$  and  $w_{eq}$ . Around equilibria, linearized models can be derived, which describe the system behavior close to these points. Since there exist infinitely many equilibria (depending on, e.g., the forward speed or curvature of the path considered), only a relevant subset of equilibria is used as basis for deriving a representative set of linearized models to be used as a basis for controller design.

This subset contains equilibria for driving on a straight path with  $u_{1eq} = [1, 90]$  km/h with zero articulation angles, and equilibria for steady-state cornering at  $u_1 = 10$  km/h with different curvatures. Using these equilibria, linearized time-invariant systems can be derived of the following form:

$$\begin{aligned} \dot{\hat{x}} &= A(u_1)\hat{x} + B(u_1)\hat{\tau} + B_w(u_1)\hat{w} \\ \hat{y} &= C\hat{x}, \end{aligned} \quad (16)$$

where  $\hat{x} = (x - x_{eq})$ ,  $\hat{\tau} = (\tau - \tau_{eq})$ ,  $\hat{w} = (w - w_{eq})$ , and system matrices  $A(u_1), B(u_1), B_w(u_1)$  are parametrized by the (constant equilibrium) longitudinal velocity  $u_1$ . The output matrix  $C$  follows from the fact that the two articulation angles compose the measured output:

$$C = \begin{bmatrix} 1 & 0 & 0 & 0 & 0 & 0 & 0 \\ 0 & 1 & 0 & 0 & 0 & 0 & 0 \end{bmatrix}. \quad (17)$$

For the purpose of controller design, we use a transfer function model, corresponding to (16), describing the relation between the inputs  $\tau$  and  $w$  and the outputs  $y$  as follows:

$$\hat{y}(s) = G_{y/\tau}(s, u_1)\hat{\tau}(s) + G_{y/w}(s, u_1)\hat{w}(s), s \in \mathbb{C}. \quad (18)$$

These transfer functions are given by:

$$\begin{aligned} G_{y/\tau}(s, u_1) &= C(sI - A(u_1))^{-1}B(u_1) \\ G_{y/w}(s, u_1) &= C(sI - A(u_1))^{-1}B_w(u_1). \end{aligned} \quad (19)$$

The linearized models obtained from the straight driving subset will be employed in this work to derive the feed-forward controller and analyze the local stability, whereas the steady-state-cornering based linear models can be used for the cross-verification of the local stability of the feedback controlled system. The transfer function  $G_{y/\tau}(s, u_1)$ , for straight driving scenarios, can be used to produce Bode plots that give an insight in the dependency of the plant dynamics on the longitudinal velocity  $u_1$  as depicted in Figure 10. Regarding the Bode plots for steady-state cornering we refer to [21].

In Figure 10, we care to stress two important aspects. Firstly, the largest differences in dynamic behavior can be seen in the frequency range of 0.4-0.5 Hz, where the system with increasing longitudinal velocity shows decreased damping of the resonance, which in higher velocities eventually evolves in the gain amplification for  $G_{\theta_1/\tau_1}(s, u_1)$  and  $G_{\theta_2/\tau_1}(s, u_1)$ . Secondly, it can be observed that the MIMO system in Figure 10 is strongly coupled. Namely the influence of  $\tau_1$  on  $\theta_2$  is substantial and as can be observed in lower left Bode plot of Figure 10. This coupling has a negative effect on the performance of diagonal feedback controllers, as such coupling can be regarded as an internal disturbance. Hence, dynamical decoupling will be used to partly decouple the input-output dynamics resulting in diagonally dominant dynamics. This is achieved by ensuring that the off-diagonal terms in  $G_{y/\tau}(s, u_1)$  are zero by dynamic decoupler design in Figure 11.

To fully decouple the linearized plant  $G_{y/\tau}(s, u_1)$ , we define the decoupling matrix  $D(s, u_1) = \begin{bmatrix} D_{11} & D_{12} \\ D_{21}(s, u_1) & D_{22} \end{bmatrix}$ . In order to maintain the diagonal dynamics, the gains  $D_{11} = D_{22} = 1$ . Since the influence of  $\tau_2$  on  $\theta_1$  is already insignificant

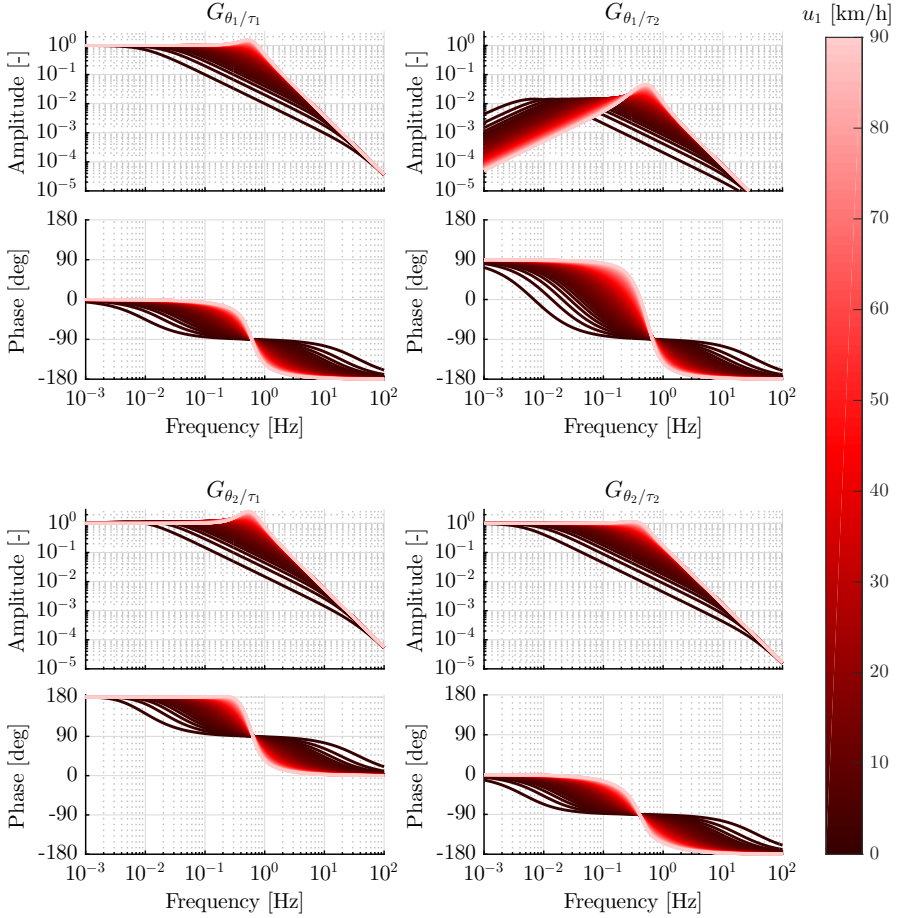


Fig. 10. Bode diagrams of  $G_{y/\tau}(j\omega, u_1)$  for straight driving with  $u_1^{eq} \in [1, 90]$  km/h and  $\theta_1^{eq} = 0$ ,  $\theta_2^{eq} = 0$ ,  $r_1^{eq} = 0$ .

( $G_{\theta_1/\tau_2}(s, u_1)$  is small compared to the other elements in  $G_{y/\tau}(s, u_1)$ ) we take  $D_{12} = 0$ . Hence, the only remaining gain to design is  $D_{21}(s, u_1)$ , which is done by solving the equation:

$$G_{\theta_2/\tau_1}(s, u_1)D_{11} + G_{\theta_2/\tau_2}(s, u_1)D_{21}(s, u_1) = 0. \quad (20)$$

This results in  $D_{21}(s, u_1) = -G_{\theta_2/\tau_1}(s, u_1)G_{\theta_2/\tau_2}^{-1}(s, u_1)$  (while using  $D_{11}=1$ ), being the only frequency dependent gain in the decoupling matrix. Furthermore, as both  $G_{\theta_2/\tau_1}(s, u_1)$  and  $G_{\theta_2/\tau_2}(s, u_1)$  are derived from the plant model that was linearized for particular longitudinal velocity the gain  $D_{21}(s, u_1)$  also needs to be scheduled in dependency of truck forward velocity  $u_1$ .

The gain scheduling method will be also used

to adjust the gains of PID controller  $H_{11}(s)$  and  $H_{22}(s)$ , see Figure 12, based on gain-scheduling variable  $u_1$ . The diagonal PID-type controller is given by  $H(s, u_1) = \begin{bmatrix} H_{11}(s, u_1) & 0 \\ 0 & H_{22}(s, u_1) \end{bmatrix}$ , where  $H_{11}(s, u_1)$  and  $H_{22}(s, u_1)$  are two single input single output PID controllers. The input of  $H(s, u_1)$  is the column with tracking errors  $e = [e_1 \ e_2]^T$ . The PID-type controllers are defined as follows:

$$H_{11}(s, u_1) = K_{P_1}(u_1) + K_{I_1}(u_1) \frac{1}{s} + \frac{K_{D_1}(u_1)s}{N_1s + 1},$$

$$H_{22}(s, u_1) = K_{P_2}(u_1) + K_{I_2}(u_1) \frac{1}{s} + \frac{K_{D_2}(u_1)s}{N_2s + 1}, \quad (21)$$

where  $K_{P_1}(u_1)$ ,  $K_{I_1}(u_1)$ ,  $K_{D_1}(u_1)$  are, respectively, the proportional, integral and derivative gains

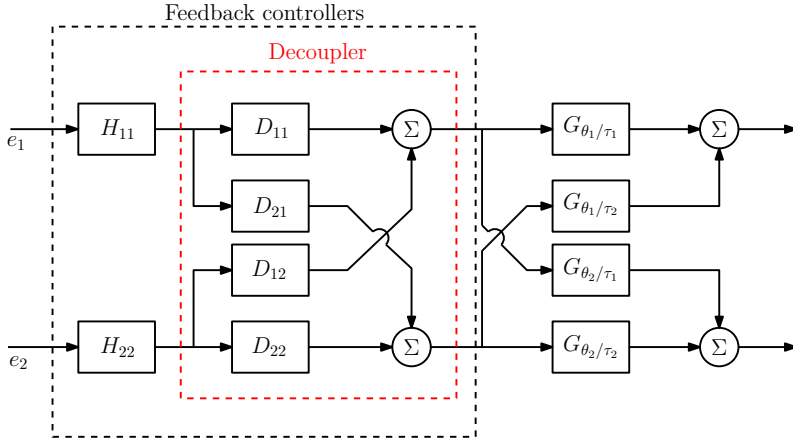
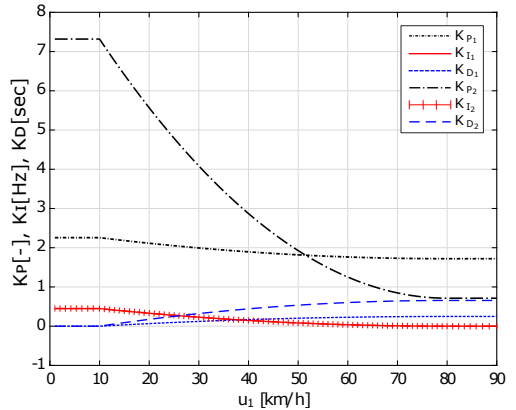


Fig. 11. Feedback controllers with decoupler.

of  $H_{11}(s, u_1)$  and  $K_{P_2}(u_1)$ ,  $K_{I_2}(u_1)$  and  $K_{D_2}(u_1)$  are the corresponding gains of  $H_{22}(s, u_1)$ .  $N_1 = 10\pi$  and  $N_2 = 10\pi$  are the first-order low-pass filter constants, which are needed to make the derivative terms proper. The values correspond to a cut-off frequency of 5 Hz which is appropriate for the governing system dynamics. To ensure a continuous dependency on  $u_1$ , the gains will be defined by the quadratic function of longitudinal velocity  $u_1$ :

$$\begin{aligned}
 K_{P_1}(u_1) &= k_{P_1}^0 + k_{P_1}^1 u_1 + k_{P_1}^2 u_1^2, \\
 K_{I_1}(u_1) &= k_{I_1}^0 + k_{I_1}^1 u_1 + k_{I_1}^2 u_1^2, \\
 K_{D_1}(u_1) &= k_{D_1}^0 + k_{D_1}^1 u_1 + k_{D_1}^2 u_1^2, \\
 K_{P_2}(u_1) &= k_{P_2}^0 + k_{P_2}^1 u_1 + k_{P_2}^2 u_1^2, \\
 K_{I_2}(u_1) &= k_{I_2}^0 + k_{I_2}^1 u_1 + k_{I_2}^2 u_1^2, \\
 K_{D_2}(u_1) &= k_{D_2}^0 + k_{D_2}^1 u_1 + k_{D_2}^2 u_1^2.
 \end{aligned} \tag{22}$$

The tuning of the PID controller parameters is based on several low- and high- speed simulations, i.e., for  $u_1 = 10$  km/h, and 80 km/h, while aiming to minimize both the tracking errors  $e$  and the control inputs  $\tau$ . As can be seen in Figure 10, the linearized system is supercritically damped at low speeds ( $u_1 < 15$  km/h). This means that at low speeds no overshoot for both articulation angles  $\theta_1$ ,  $\theta_2$  based on steering input  $\tau_1$ ,  $\tau_2$  occurs, which would eventually result in the increased swept path. Hence the derivative action of a PID controller, that is typically used to provide damping to the closed-loop system, is not needed in this scenario to avoid overshoot. Namely, the proportional and integral constants at  $u_1 = 10$  km/h are chosen such that the closed-loop system is still supercritically damped.


 Fig. 12. Gain-scheduling of PID gains. The integral parameters are equal ( $K_{I_1} = K_{I_2}$ ).

At high speeds, where a lane change is considered as a key maneuver, no steady-state cornering takes place. Therefore, no steady-state tracking errors occur; thus, no integral term in the PID controllers is needed to regulate the errors to zero. However, the derivative component of PID controller is essential, as can be seen in Figure 12, to provide sufficient damping and avoid the rearward amplification, which might eventually result in roll-over accident.

These two assumptions substantially simplify the gain tuning process. Due to the fact that the polynomials are defined by three parameters, three boundary conditions need to be formulated. A requirement is imposed such that  $\frac{dK(80)}{du_1} = 0$  for all parameters. Doing this, we force the extremum (minimum for



the proportional and integral terms, maximum for the derivative terms) of the polynomial functions to occur at 80 km/h. This forces a monotonic trend of the gains between  $u_1 = 10$  and  $u_1 = 80$  km/h, since the functions (22) are quadratic ; namely, such functions show a monotonic trend before (and after) the extremum.

The tuning of the gains has been done manually as follows. At first, the gains were optimized for the single track model and, thereafter, the gains corresponding to each PID controller are scaled, with a factor smaller than 1, based on simulations of the high-fidelity model. The latter step is performed to avoid excessive oscillatory behavior in the control inputs  $\tau$  of the high fidelity model. This behavior is caused by unmodeled dynamics in single-track model compared to the high-fidelity model, such as the nonlinear tyre dynamics. In Figure 12, the resulting dependency of the PID gains on the longitudinal velocity  $u_1$  is depicted.

### C. Closed-loop Stability Analysis

The tuning of feedback controllers should result in stable closed-loop system with sufficient stability margin for all linearized plants ( $u_1 \in [1, 90]$  km/h).

To investigate the closed-loop stability of the MIMO system, depicted in Figure 11, the generalized Nyquist stability criterion [26] is used. The MIMO closed-loop transfer function matrix is given by  $G_{CL}(s, u_1) = G_{OL}(s, u_1) (I + G_{OL}(s, u_1))^{-1}$ , where  $G_{OL}(s, u_1) = G_{y/\tau}(s, u_1)D(s, u_1)H(s, u_1)$  is the open-loop transfer function matrix, which is combining the previously defined linearized plants, the decoupler, and the controller, respectively.

The generalized Nyquist criterion states that the number of unstable closed-loop poles equals the (net) number of times the locus of  $\det(I + G_{OL}(s, u_1))$  encircles the origin in clockwise direction plus the number of unstable open-loop poles. Using the state-space linearized plant models in (16), it has been verified within the scope of [21] that number of open-loop unstable poles is zero. Therefore, to obtain a stable closed-loop system no encirclements of the origin in clockwise direction should occur in the Nyquist plot of  $\det(I + G_{OL}(s, u_1))$ .

The disadvantage of using a locus of the determinant is that the resulting Nyquist plot combines the effects of the controllers  $H_{11}(s, u_1)$  and  $H_{22}(s, u_1)$  into one graph. This is not desirable, as the controllers can not be tuned independently in this way. Hence, instead of the determinant locus we will use the eigenvalue loci of  $G_{OL}(s, u_1)$ .

In order to do that, we rewrite  $\det(I + G_{OL}(s, u_1))$  as a function of  $\lambda_i(s)$ , which are the eigenvalues of  $G_{OL}(s, u_1)$  that are parametrized by  $s$ :

$$\det(I + G_{OL}(s, u_1)) = \prod_{i=1}^2 (1 + \lambda_i(s)). \quad (23)$$

It should be emphasized that eigenvalues  $\lambda_1(s)$  and  $\lambda_2(s)$  do not refer to the poles of the system, but to the eigenvalues of the open-loop transfer function matrix  $G_{OL}(s, u_1)$  (for  $s = j\omega$ ) that has size of  $2 \times 2$ .

Because, for  $s = j\omega$ ,

$$\arg(\det(I + G_{OL}(j\omega))) = \sum_{i=1}^2 \arg(1 + \lambda_i(j\omega)), \quad (24)$$

we have that, any change in the angle of  $\det(I + G_{OL}(s, u_1))$  results from the sum of phase changes in the terms  $(1 + \lambda_i(s))$  (for  $i = 1, 2$ ). Hence, encirclement of the origin in the complex plane by  $\det(I + G_{OL}(s, u_1))$  can be computed from the encirclements of  $(-1, 0j)$  by the combination of the eigenloci of  $\lambda_1(s)$  and  $\lambda_2(s)$  [27].

As shown in Figure 10, the gain of  $G_{\theta_1/\tau_2}(s, u_1) \approx 0$ . Considering this fact, and the effect of gain-scheduled dynamical decoupler, the linearized open loop transfer function matrix  $G_{OL}(s, u_1)$  can be considered as diagonal, i.e.  $G_{OL,12}(s) \approx G_{OL,21}(s) \approx 0$ . Thus, the eigenvalues of  $G_{OL}(s, u_1)$  are the systems in the diagonal, i.e.  $\lambda_1(s) \approx G_{OL,11}(s, u_1)$ , and  $\lambda_2(s) \approx G_{OL,22}(s, u_1)$ .

This is equivalent to considering the diagonal system as a multiple Single Input Single Output (SISO) system and assessing the stability of the two systems  $G_{OL,11}(s, u_1)$ , and  $G_{OL,22}(s, u_1)$  using normal Nyquist criterion. This enables separate tuning of the controllers  $H_{11}(s, u_1)$  and  $H_{22}(s, u_1)$  for robust stability. Nyquist plots of  $\lambda_1(s)$  and  $\lambda_2(s)$  for straight driving and  $r_1^{eq}, \theta_1^{eq}, \theta_2^{eq} = 0$  are shown in Figure 13, where it is made clear that stability margins of all closed-loop systems (i.e., for  $u_1 \in [1, 90]$  km/h) are sufficiently large. Given the asymptotic stability of the linearized dynamics (through satisfaction of the generalized Nyquist criterion), we can now conclude that the equilibria (used as a basis for linearization) are locally asymptotically stable equilibria of the nonlinear plant dynamics in (13) in closed loop with the proposed controller.

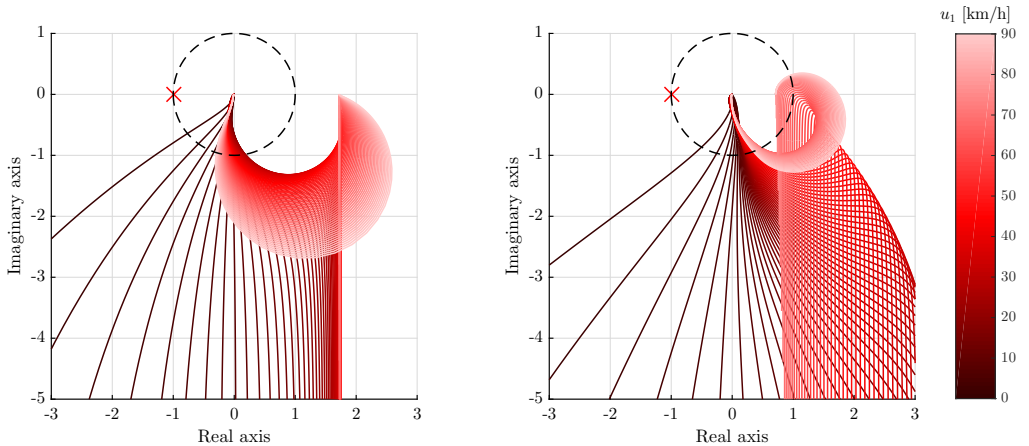


Fig. 13. Nyquist eigenloci of a)  $\lambda_1(s)$  and b)  $\lambda_2(s)$  corresponding to the open-loop systems  $G_{OL,11}(s, u_1)$  and  $G_{OL,22}(s, u_1)$ , respectively, for to gain-scheduled controllers of the dolly (left), and the semitrailer (right).

#### D. Feedforward design

Besides the feedback controller, also the feedforward controller is gain-scheduled on the basis of  $u_1$ . In particular, the coefficients of the transfer functions corresponding to a  $2 \times 2$  feedforward controller are being scheduled with  $u_1$ . For the controller  $F(s)$ , shown in Figure 9, the plant inversion method was applied in a sense described in [26]. In order to make the controller causal a second-order Butterworth low-pass filter  $L(s)$  was included. The order of the filter was chosen such that  $F(s)$  is proper, whereas the choice of cut-off frequency of 50 Hz aimed to primarily remove high-frequency content from the reference signals. Therefore  $F(s) = G_{y/\tau}(s)^{-1}L(s)$ .

Because the reference signal  $y_d$  may also contain high-frequency noise (e.g. due to a sampled data implementation that is needed for practical applications), an extra 4<sup>th</sup>-order Butterworth low-pass filter  $L_d(s)$  is added, see Figure 9, with a  $u_1$ -dependent cut-off frequency.

The last component of the feedforward controller design involves extra path that takes care of the effect of the driver input on the output represented by articulation angles via transfer function  $G_{y/\delta_1}(s)$ , see Figure 9. From a control point of view, the input from the driver can be considered as a disturbance. Physically, this means that when the driver steers, the vehicle starts to corner, which induces articulation between the bodies. The effect of this exogenous driver input is relatively large, and if not taken into account, a feedforward controller based on  $y_d$  only may actually degrade instead of improve the performance of the system. Hence  $\hat{y}^w = G_{y/\delta_1}(s)$

is subtracted from the (filtered) reference signal  $y_d$ . The resulting signal  $y^f = y_d - \hat{y}^w$  is the input of the feedforward controller  $F(s)$ . The interpretation of  $y^f$  can be seen as the difference between the desired articulation angles and the articulation angles that would be induced only by driver action  $\delta_1$ . If the feedforward controller would be an exact representation of the (nonlinear) plant, then the tracking error would converge to zero. In practice, this means that the feedforward is only exact for small perturbations when the vehicle is driving straight (since we only use  $u_1$  as scheduling variable). However, the resulting errors are still small for large articulation angles, which the feedback controller can regulate the errors towards zero, as is shown in next section.

## V. CONTROLLER SIMULATIONS

In this section, a number of simulation studies are presented in order to verify the functionality of the controller that is based on the nonlinear single track model. The aim is to benchmark the controller performance for both high- and low-speed scenarios compared to the baseline uncontrolled vehicle combination. As an objective assessment measure, the metrics such as defined by the PBS framework [4] will be used. Namely, the rearward amplification will be used for high-speed performance assessment and the vehicle swept path width for low-speed maneuverability. For these simulation studies, the high fidelity multi-body model described in Section II-B will be used in order to also assess the robustness of proposed control strategy in the presence of dynamics

aspects ignored in the single track model used for controller synthesis.

### A. Low-speed Maneuvering

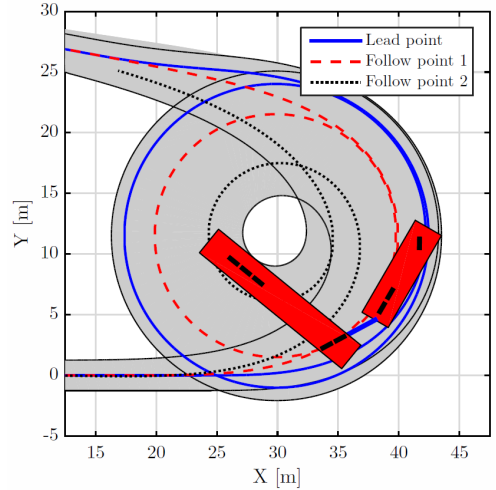
The low-speed maneuverability is tested for a roundabout maneuver (with a radius of 12.5 m) with constant longitudinal velocity  $u_1=10$  km/h. The maneuver consists of the entry into the roundabout, followed with the approximately one and half turn and finished by exiting the roundabout. The resulting swept path for both the uncontrolled and controlled vehicle combination is shown on Figure 14 as well as the path of lead and follow points.

The swept path is defined by the outer path of the front right corner of the truck and the path of the left side of the semitrailer. The decisive performance factor is the swept path width, which is for the uncontrolled case 11.2 m (current EU legislation allows only for 7.2 m), whereas with the proposed path-following controller it can be reduced to 5.1 m, representing an improvement of approximately 55%. The driver and control inputs are shown in Figure 15(a). As can be seen, the feedforward part of the controller,  $\tau_i^f$ , provides main contributions to the steering signals. Hence, it can be deduced that feedforward controller performs well even for large articulation and steering angles, although it is based on a linearization around straight path driving. The imperfections of the feedforward are mostly corrected by feedback controller,  $\tau_i^{fb}$ , which is leads to close tracking of the reference articulation angles such as depicted in Figure 15 (b) and (c).

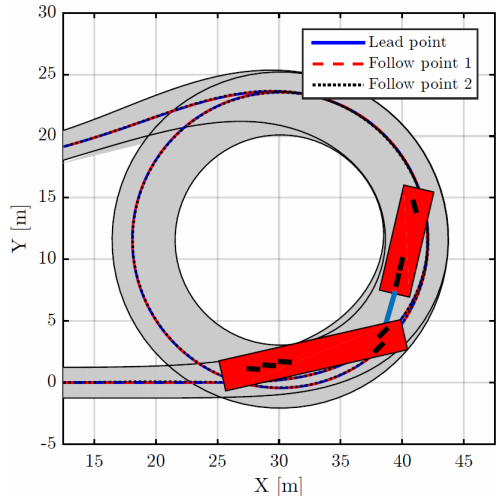
### B. High-speed Stability

For the high-speed stability assessment, we perform a lane change maneuver at 80 km/h, where the yaw and roll stability can become an issue for HCV. The maneuver is performed using a predefined profile of the steering angle  $\delta_1$ ; that is single period sinusoid with frequency of 0.4 Hz. The frequency is chosen according to [4] due to its maximal gain for commercial vehicles handling response resulting typically in higher rearward amplification, that will be used as assessment criterion. The rearward amplification describes the ratio of the maximal achieved lateral acceleration of the dolly ( $RA_{21}$ ) and the semitrailer ( $RA_{31}$ ) compared to the maximal achieved lateral acceleration of the truck; namely, on the second and third axle of the dolly and semitrailer, respectively, and the first axle of the truck.

A benchmark comparison of the lane change scenario for controlled and noncontrolled case is



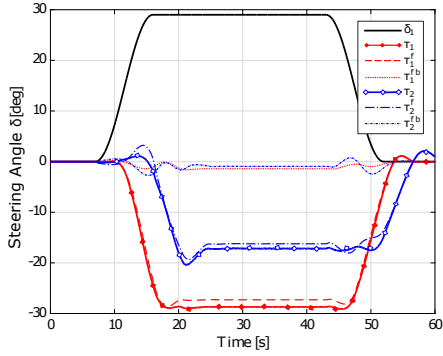
(a) Noncontrolled Situation.



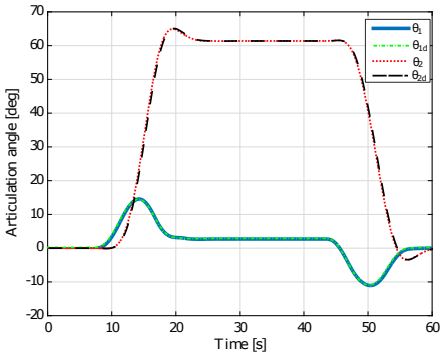
(b) Path Following Control.

Fig. 14. Vehicle swept path during low-speed maneuvering.

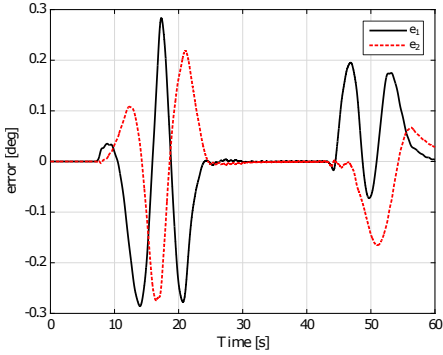
again provided. The path comparison is shown in Figure 16, followed by lateral acceleration  $a_{yi}$  for all vehicles in the combination in Figure 17. For the noncontrolled case, both dolly and semitrailer paths exhibit lateral acceleration overshoot compared to the lead path of the truck. This is projected to the vehicle swept path that is designated by the gray region in Figure 16(a). Furthermore, one can observe lateral acceleration amplification along the vehicle combination resulting in rather high values of  $RA_{21} = 1.68$  and  $RA_{31} = 2.05$ . When the path



(a) Driver and controller inputs.



(b) Reference and actual articulation angles.

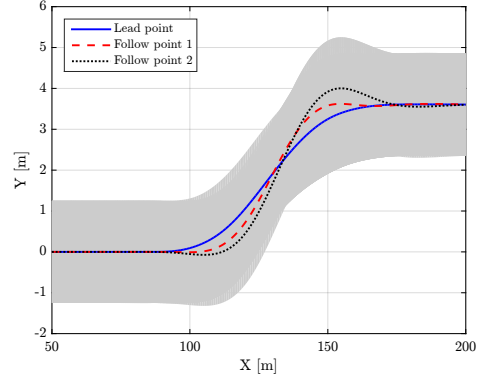


(c) Tracking errors  $e_1 = \theta_{1d} - \theta_1$  and  $e_2 = \theta_{2d} - \theta_2$ .

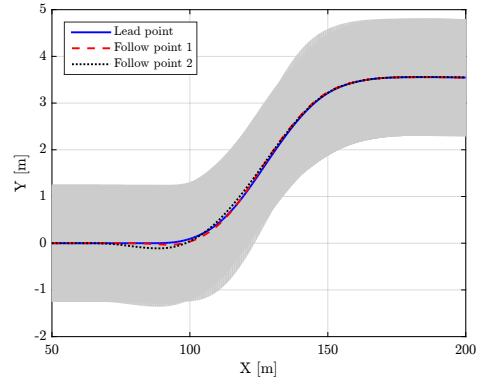
Fig. 15. Low-speed maneuvering performance.

following controller is engaged, the path of the dolly and semitrailer is much smoother and without overshoots. The amplification of the lateral acceleration is suppressed resulting in  $RA_{21} = 1.12$  and  $RA_{31} = 0.81$ , representing a reduction of 30% and

60%, respectively, and it physically means that the lateral acceleration of all vehicles in the combination is quite uniform, which generally reduces the risk of rollover accident.



(a) Noncontrolled Situation



(b) Path Following Control

Fig. 16. Vehicle swept path during high speed maneuver.

Although the path following control substantially improves the performance of the vehicle combination, one can observe that the control is slightly suboptimal particularly in the beginning of the maneuver due to feed forward contributions depicted on Figure 19. Namely, the dolly and semi-trailer axles start to steer in the opposite direction of  $\delta_1$ . This causes an additional tail-swing and small tracking errors in transients as can be seen in Figure 16 (b) and Figure 18, respectively. This problem is caused by the difference between the high fidelity multi-body model and the single-track model. Since the feedforward controller is based on the single-track model, it is not exact for the multi-body model. This

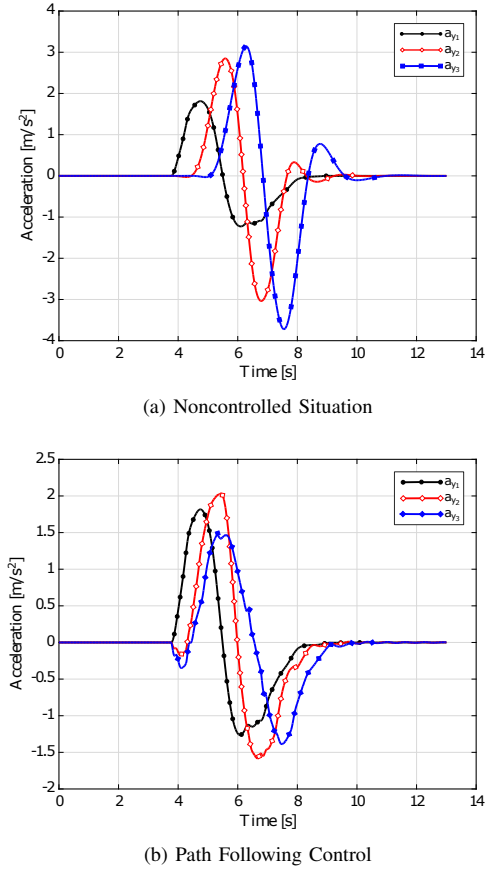


Fig. 17. Lateral accelerations of the vehicles during high speed maneuver.

becomes in particular apparent at high-speeds, where unmodeled dynamics in the single-track model, such as for example roll motion, affects the vehicle combination behavior. This effect can be explained in more detail as follows. The reference model uses the actual states  $(u_1, v_1, r_1)$  to derive the reference signals  $y_d$ , which are then subtracted from  $\hat{y}^w$  (see Figure 9). The  $\hat{y}^w$  signals follow from the linearized plant  $G_{y/\delta_1}(s)$ , which is based on the linearized single-track model. Thus, the resulting signal  $y^f$ , which is the input for the feedforward filter  $F(s)$ , is inexact for the high-fidelity model. A possible solution is to use the single-track model as a state predictor to provide estimated states  $(u_1, v_1, r_1)$  as an input to the reference model, see [21].

Summarizing, these results show that

- the proposed controller can provide significant

improvement in both low- and high-speed performance of the commercial vehicle combinations,

- the uniform controller structure can be used for both type of maneuvers,
- the controller design is robust against unmodeled dynamics.

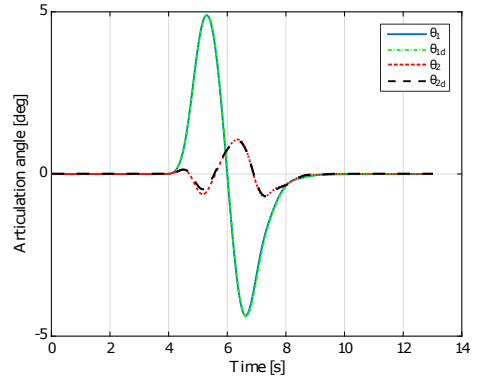


Fig. 18. Reference and actual articulation angles.

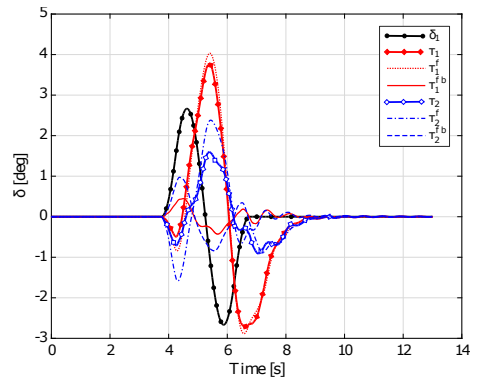


Fig. 19. Driver and controller inputs.

## VI. CONCLUSIONS

In this paper, a generic active trailer steering strategy is developed and applied to truck-dolly-semitrailer combination. The proposed path-following based control method uses gain-scheduling approach to ensure high performance at both low- and high-speeds. The controller improves both the maneuverability at low speeds and improves lateral

stability at high speeds. The swept path width and rearward amplification are considered as assessment criteria for the performance of the vehicle combination. The benefits of the proposed control approach are as follows. Firstly, the method uses single controller structure that can be robustly applied for any velocity in range of 1-90 km/h. Secondly, the usage of the controller leads to significant improvement of the performance, namely at low speed the reduction of swept path reaches 55% and rearward amplification at the high speed is decreased by 33% and 60%, for first and second towed vehicle, respectively. The effectiveness of proposed steer strategy has been tested by extensive simulations with a high-fidelity experimentally validated model, indicating the robustness of the design.

## APPENDIX

### A: VEHICLE MODEL MATRICES

The entries  $M_{ij}$ ,  $i, j \in \{1, 2, \dots, 5\}$ , of the mass matrix  $M$  are given by

$$\begin{aligned}
M_{1,1} &= m_1 + m_2 + m_3 \\
M_{1,2} &= M_{2,1} = 0 \\
M_{1,3} &= M_{3,1} = -m_3 (a_3 \sin(\theta_1 + \theta_2) + l_2^* \sin(\theta_1)) \\
&\quad - a_2 m_2 \sin(\theta_1) \\
M_{1,4} &= M_{4,1} = m_3 (a_3 \sin(\theta_1 + \theta_2) + l_2^* \sin(\theta_1)) \\
&\quad + a_2 m_2 \sin(\theta_1) \\
M_{1,5} &= M_{5,1} = a_3 m_3 \sin(\theta_1 + \theta_2) \\
M_{2,2} &= m_1 + m_2 + m_3 \\
M_{2,3} &= M_{3,2} = -m_3 (h_1 + a_3 \cos(\theta_1 + \theta_2) + l_2^* \cos(\theta_1)) \\
&\quad - m_2 (h_1 + a_2 \cos(\theta_1)) \\
M_{2,4} &= M_{4,2} = m_3 (a_3 \cos(\theta_1 + \theta_2) + l_2^* \cos(\theta_1)) \\
&\quad + a_2 m_2 \cos(\theta_1) \\
M_{2,5} &= M_{5,2} = a_3 m_3 \cos(\theta_1 + \theta_2) \\
M_{3,3} &= (a_2^2 + h_1^2) m_2 + (a_3^2 + h_1^2 + l_2^{*2}) m_3 \\
&\quad + 2a_3 h_1 m_3 \cos(\theta_1 + \theta_2) + 2a_2 h_1 m_2 \cos(\theta_1) \\
&\quad + 2a_3 l_2^* m_3 \cos(\theta_2) + 2h_1 l_2^* m_3 \cos(\theta_1) \\
&\quad + J_1 + J_2 + J_3 \\
M_{3,4} &= M_{4,3} = -J_2 - J_3 - m_2 a_2^2 - h_1 m_2 \cos(\theta_1) a_2 \\
&\quad - 2m_3 \cos(\theta_2) a_3 l_2^* - h_1 m_3 \cos(\theta_1 + \theta_2) a_3 \\
&\quad - h_1 m_3 \cos(\theta_1) l_2^* - m_3 (a_3^2 + l_2^{*2}) \\
M_{3,5} &= M_{5,3} = -J_3 - a_3^2 m_3 - a_3 h_1 m_3 \cos(\theta_1 + \theta_2) \\
&\quad - a_3 l_2^* m_3 \cos(\theta_2) \\
M_{4,4} &= J_2 + J_3 + m_2 a_2^2 + m_3 (a_3^2 + l_2^{*2}) \\
&\quad + 2m_3 \cos(\theta_2) a_3 l_2^* \\
M_{4,5} &= M_{5,4} = m_3 a_3^2 + l_2^* m_3 \cos(\theta_2) a_3 + J_3 \\
M_{5,5} &= J_3 + m_3 a_3^2.
\end{aligned}$$

The entries  $H_i$ ,  $i \in \{1, 2, \dots, 5\}$ , of the column  $H$  read

$$\begin{aligned}
H_1 &= m_1 (-r_1 v_1) + m_2 (h_1 r_1^2 - r_1 v_1 + a_2 r_1^2 \cos(\theta_1)) \\
&\quad + m_2 (a_2 \dot{\theta}_1^2 \cos(\theta_1) - r_1 v_1 - 2a_2 r_1 \dot{\theta}_1 \cos(\theta_1)) \\
&\quad + m_3 (h_1 r_1^2 + a_3 r_1^2 \cos(\theta_1 + \theta_2) + l_2^* \dot{\theta}_1^2 \cos(\theta_1)) \\
&\quad + m_3 (+a_3 \dot{\theta}_2^2 \cos(\theta_1 + \theta_2) + l_2^* r_1^2 \cos(\theta_1)) \\
&\quad + m_3 (2a_3 r_1 \dot{\theta}_1 \cos(\theta_1 + \theta_2) - 2a_3 r_1 \dot{\theta}_2 \cos(\theta_1 + \theta_2)) \\
&\quad + m_3 (-2a_3 \dot{\theta}_1 \dot{\theta}_2 \cos(\theta_1 + \theta_2) - 2l_2^* r_1 \dot{\theta}_1 \cos(\theta_1)) \\
&\quad + m_3 (a_3 \dot{\theta}_1^2 \cos(\theta_1 + \theta_2) + l_2^* \dot{\theta}_1^2 \cos(\theta_1)), \\
H_2 &= m_2 (-a_2 \sin(\theta_1) r_1^2 + 2a_2 \sin(\theta_1) r_1 \dot{\theta}_1 + u_1 r_1) \\
&\quad - m_2 a_2 \sin(\theta_1) \dot{\theta}_1^2 + m_3 (r_1 u_1 - a_3 r_1^2 \sin(\theta_1 + \theta_2)) \\
&\quad + m_3 (-a_3 \dot{\theta}_1^2 \sin(\theta_1 + \theta_2) - a_3 \dot{\theta}_2^2 \sin(\theta_1 + \theta_2)) \\
&\quad + m_3 (-l_2^* r_1^2 \sin(\theta_1) + 2a_3 r_1 \dot{\theta}_1 \sin(\theta_1 + \theta_2)) \\
&\quad + m_3 (2a_3 r_1 \dot{\theta}_2 \sin(\theta_1 + \theta_2) - 2a_3 \dot{\theta}_1 \dot{\theta}_2 \sin(\theta_1 + \theta_2)) \\
&\quad + m_3 (2l_2^* r_1 \dot{\theta}_1 \sin(\theta_1) - l_2^* \dot{\theta}_1^2 \sin(\theta_1)) + m_1 r_1 u_1, \\
H_3 &= m_2 (a_2 h_1 \sin(\theta_1) \dot{\theta}_1^2 - 2a_2 h_1 r_1 \sin(\theta_1) \dot{\theta}_1) \\
&\quad + m_2 (-h_1 r_1 u_1 - a_2 r_1 u_1 \cos(\theta_1) + a_2 r_1 v_1 \sin(\theta_1)) \\
&\quad + m_3 (a_3 r_1 v_1 \sin(\theta_1 + \theta_2) - a_3 r_1 u_1 \cos(\theta_1 + \theta_2)) \\
&\quad + m_3 (-l_2^* r_1 u_1 \cos(\theta_1) + l_2^* r_1 v_1 \sin(\theta_1) - h_1 r_1 u_1) \\
&\quad + m_3 (a_3 h_1 \dot{\theta}_2^2 \sin(\theta_1 + \theta_2) + a_3 l_2^* \dot{\theta}_2^2 \sin(\theta_2)) \\
&\quad + m_3 (h_1 l_2^* \dot{\theta}_1^2 \sin(\theta_1) - 2h_1 l_2^* r_1 \dot{\theta}_1 \sin(\theta_1)) \\
&\quad + m_3 (-2a_3 h_1 r_1 \sin(\theta_1 + \theta_2) (\dot{\theta}_1 + \dot{\theta}_2)) \\
&\quad + m_3 (2a_3 h_1 \dot{\theta}_1 \dot{\theta}_2 \sin(\theta_1 + \theta_2) - 2a_3 l_2^* r_1 \dot{\theta}_2 \sin(\theta_2)) \\
&\quad + m_3 (2a_3 l_2^* \dot{\theta}_1 \dot{\theta}_2 \sin(\theta_2) + a_3 h_1 \dot{\theta}_1^2 \sin(\theta_1 + \theta_2)), \\
H_4 &= m_2 (a_2 h_1 r_1^2 \sin(\theta_1) - a_2 r_1 v_1 \sin(\theta_1)) \\
&\quad + m_3 (a_3 r_1 u_1 \cos(\theta_1 + \theta_2) - a_3 r_1 v_1 \sin(\theta_1 + \theta_2)) \\
&\quad + m_3 (a_3 h_1 r_1^2 \sin(\theta_1 + \theta_2) - a_3 l_2^* \dot{\theta}_2^2 \sin(\theta_2)) \\
&\quad + m_3 (+h_1 l_2^* r_1^2 \sin(\theta_1) + 2a_3 l_2^* r_1 \dot{\theta}_2 \sin(\theta_2)) \\
&\quad + m_3 (-l_2^* r_1 v_1 \sin(\theta_1) + l_2^* r_1 u_1 \cos(\theta_1)) \\
&\quad - m_3 2a_3 l_2^* \dot{\theta}_1 \dot{\theta}_2 \sin(\theta_2) + m_2 a_2 r_1 u_1 \cos(\theta_1) \\
H_5 &= a_3 m_3 (h_1 r_1^2 \sin(\theta_1 + \theta_2) - r_1 v_1 \sin(\theta_1 + \theta_2)) \\
&\quad + a_3 m_3 (l_2^* \dot{\theta}_1^2 \sin(\theta_2) + r_1 u_1 \cos(\theta_1 + \theta_2)) \\
&\quad + a_3 m_3 (l_2^* r_1^2 \sin(\theta_2) - 2l_2^* r_1 \dot{\theta}_1 \sin(\theta_2)).
\end{aligned}$$

The entries  $Q_{v,i}$ ,  $i \in \{1, 2, \dots, 5\}$ , of the column  $Q_v$  read

$$\begin{aligned}
Q_{v,1} &= F_{x,2} + F_{x,3} - F_{y,1} \sin(\delta_1) - F_{y,4} \sin(\delta_4 - \theta_1) \\
&\quad - F_{y,5} \sin(\delta_5 - \theta_1) - F_{y,6} \sin(\delta_6 - \theta_1 - \theta_2) \\
&\quad - F_{y,7} \sin(\delta_7 - \theta_1 - \theta_2) - F_{y,8} \sin(\delta_8 - \theta_1 - \theta_2), \\
Q_{v,2} &= F_{y,1} \cos(\delta_1) + F_{y,2} + F_{y,3} + F_{y,4} \cos(\delta_4 - \theta_1) \\
&\quad + F_{y,5} \cos(\delta_5 - \theta_1) + F_{y,6} \cos(\delta_6 - \theta_1 - \theta_2) \\
&\quad + F_{y,7} \cos(\delta_7 - \theta_1 - \theta_2) + F_{y,8} \cos(\delta_8 - \theta_1 - \theta_2),
\end{aligned}$$

$$\begin{aligned}
Q_{v,3} &= F_{y,1} (a_1 \cos(\delta_1)) + F_{y,2} (-b_1) + F_{y,3} (-b_2) \\
&+ F_{y,4} (-b_3 \cos(\delta_4) - h_1 \cos(\delta_4 - \theta_1)) \\
&+ F_{y,5} (-b_4 \cos(\delta_5) - h_1 \cos(\delta_5 - \theta_1)) \\
&+ F_{y,6} (-b_5 \cos(\delta_6) - h_1 \cos(\delta_6 - \theta_1 - \theta_2)) \\
&+ F_{y,6} (-l_2^* \cos(\delta_6 - \theta_2)) + F_{y,7} (-b_6 \cos(\delta_7)) \\
&+ F_{y,7} (-h_1 \cos(\delta_7 - \theta_1 - \theta_2) - l_2^* \cos(\delta_7 - \theta_2)) \\
&+ F_{y,8} (-b_7 \cos(\delta_8) - h_1 \cos(\delta_8 - \theta_1 - \theta_2)) \\
&+ F_{y,8} (-l_2^* \cos(\delta_8 - \theta_2)), \\
Q_{v,4} &= F_{y,4} (b_3 \cos(\delta_4)) + F_{y,5} (b_4 \cos(\delta_5)) \\
&+ F_{y,6} (b_5 \cos(\delta_6) + l_2^* \cos(\delta_6 - \theta_2)) \\
&+ F_{y,7} (b_6 \cos(\delta_7) + l_2^* \cos(\delta_7 - \theta_2)) \\
&+ F_{y,8} (b_7 \cos(\delta_8) + l_2^* \cos(\delta_8 - \theta_2)), \\
Q_{v,5} &= F_{y,6} (b_5 \cos(\delta_6)) + F_{y,7} (b_6 \cos(\delta_7)) \\
&+ F_{y,8} (b_7 \cos(\delta_8)).
\end{aligned}$$

## REFERENCES

- [1] Eurostat, "Freight transport statistics," 2014. [Online]. Available: <http://ec.europa.eu/eurostat/statistics-explained/index.php>
- [2] European Commission, *EU transport in figures 2012*. Luxembourg: Publications office of the European Union, 2012.
- [3] B. Kraaijenhagen, T. Barth, Karel, J. Pauwelussen, I. Besselink, A. Prati, M. Meijs, and H. Nijmeijer, *Greening and Safety Assurance of Future Modular Road Vehicles: Book of Requirements*, Oct 2014. [Online]. Available: <https://www.han.nl/international/english/about-han/news/greening-and-safety-assur/attachments/htas'ems'bookofrequirements'oct2014.pdf>
- [4] r. A. National Transport Commission, "Performance-based standards scheme – the standards and vehicle assessment rules," 2008.
- [5] W. Henri, "Automatic steering device for swiveling bogies," Patent, Sep. 13, 1932, uS Patent 1,876,684. [Online]. Available: <http://www.google.nl/patents/US1876684>
- [6] J. Wouter, "Bogie vehicle steering mechanism," Jun. 8 1937, uS Patent 2,083,166. [Online]. Available: <http://www.google.com/patents/US2083166>
- [7] P. Bolzern, R. M. DeSantis, and A. Locatelli, "An Input-Output Linearization Approach to the Control of an n-Body Articulated Vehicle," *Journal of Dynamic Systems, Measurement, and Control*, vol. 123, no. 3, p. 309, 2001.
- [8] M. M. Michalek, "A highly scalable path-following controller for n-trailers with off-axle hitching," *Control Engineering Practice*, vol. 29, no. 0, pp. 61 – 73, 2014.
- [9] R. Orosco-Guerrero, E. Aranda-Bricaire, and M. Velasco-Villa, "Global path-tracking for a multi-steered general n-trailer," in *Proceedings of the 15th IFAC World Congress*, vol. 15, no. 1, 2002, pp. 239–239.
- [10] P. Ritzen, E. Roebroek, N. van de Wouw, H. Nijmeijer, and Z.-P. Jiang, "Trailer steering control for a tractor-trailer robot," *IEEE Transactions on Control Systems Technology*, vol. 24, no. 4, pp. 1240–1252, July 2016.
- [11] M. Sampei, T. Tamura, T. Kobayashi, and N. Shibui, "Arbitrary path tracking control of articulated vehicles using nonlinear control theory," *Control Systems Technology, IEEE Transactions on*, vol. 3, no. 1, pp. 125–131, Mar 1995.
- [12] X. Ding, S. Mikaric, and Y. He, "Design of an active trailer-steering system for multi-trailer articulated heavy vehicles using real-time simulations," in *Proceedings of the Institution of Mechanical Engineers, Part D: Journal of automobile engineering*, vol. 227, no. 5. Sage Publications, 2013, pp. 643–655.
- [13] M. M. Islam and Y. He, "An optimal preview controller for active trailer steering systems of articulated heavy vehicles," SAE Technical Paper, Tech. Rep., 2011.
- [14] R. Roebuck, A. Odhams, K. Tagesson, C. Cheng, and D. Cebon, "Implementation of trailer steering control on a multi-unit vehicle at high speeds," *Journal of Dynamic Systems, Measurement, and Control*, vol. 136, no. 2, pp. 021016\_1–021016\_14, 2014.
- [15] S. T. Oreh, R. Kazemi, and S. Azadi, "A new desired articulation angle for directional control of articulated vehicles," in *Proceedings of the Institution of Mechanical Engineers, Part K: Journal of multi-body dynamics*, vol. 226, no. 4. Sage Publications, Dec 2012, pp. 298–314.
- [16] N. Hata, T. Fujishiro, K. van Bremen-Ito, S. Takahashi, and S. Hasegawa, *A Control Method for 4WS Truck to Suppress Excursion of a Body Rear Overhang*. Society of Automotive Engineers, 1989.
- [17] B. A. Jujnovich and D. Cebon, "Path-following steering control for articulated vehicles," *Journal of Dynamic Systems, Measurement, and Control*, vol. 135, no. 3, p. 031006, 2013.
- [18] B. Jujnovich, C. Odhams, R. L. Roebuck, and D. Cebon, "Implementation of active rear steering of a tractor/semi-trailer," in *Proceedings of the 10th international symposium of Heavy Vehicle Transport Technology*, 2008.
- [19] J. Kandathil Jacob, "Improved command steering for a b-double truck combination," Master's thesis, Eindhoven University of Technology, Oct 2012, D&C 2012.051. [Online]. Available: <http://www.mate.tue.nl/mate/pdfs/12050.pdf>
- [20] H. B. Pacejka, *Tyre and Vehicle Dynamics*, 2nd ed., 2006.
- [21] P. Hatzidimitris, "Active trailer steering control for longer heavier vehicles," Master's thesis, Eindhoven University of Technology, 2015, DC 2015.065. [Online]. Available: <http://repository.tue.nl/840236>
- [22] K. Kural, A. Prati, I. Besselink, J. Pauwelussen, and H. Nijmeijer, "Validation of Longer and Heavier Vehicle Combination Simulation Models," *SAE Int. J. Commer. Veh.*, no. 6(2):2013, Sep. 2013.
- [23] I. J. M. Besselink, "Vehicle dynamics analysis using simmechanics and tno delft-tyre," Mathworks International Automotive Conference, Tech. Rep., 2006.
- [24] TASS International, "Delft-tyre," <https://www.tassinternational.com/delft-tyre>.
- [25] P. Ritzen, "Trailer steering control for an off-axle tractor-trailer robot: reducing the swept path width," Master's thesis, Eindhoven University of Technology, Jan 2014, D&C 2013.061.
- [26] S. Skogestad and I. Postlethwaite, *Multivariable Feedback Control: Analysis and Design*. John Wiley & Sons, 2005.
- [27] E. W. Jacobsen, "Multivariable feedback control lecture notes, royal institute of technology (kth)."



**Karel Kural** obtained his M.Sc.-degree at Czech Technical University, Prague, Czech Republic, in 2008. He is a researcher at Automotive Research Group, HAN University of applied Sciences, Netherlands. Moreover he pursuits part time Ph.D.-study at Department of Mechanical Engineering of the Eindhoven University of Technology in the group of Dynamics and Control.

His current research field is vehicle dynamics and control of commercial vehicle combinations, and the driver support systems.



**Igo Besselink** is an associate professor at the Eindhoven University of Technology. He received his M.Sc.-degree (with credits) and Ph.D.-degree in Mechanical Engineering at the Delft University of Technology in 1990 and 2000, respectively. He was with Fokker Aircraft, while responsible for the analysis of landing gear design loads and stability. Later he joined

TNO in Delft where his focus was on development of tyre simulation software and various projects related to vehicle dynamics. Since 2008, Igo became full time employed by the Eindhoven University of Technology. His research interests include tyre modelling, dynamics of commercial vehicles, vehicle control and battery electric vehicles.



**Pavlos Hatzidimitris** received his BSc-degree and MSc-degree in Mechanical Engineering from the Eindhoven University of Technology, in 2013 and 2015 respectively. After the graduation he joined ASML, where he works as mechatronics development engineer.



**Henk Nijmeijer** is a full professor at Eindhoven University of Technology, and chairs the Dynamics & Control Group. He has published a large number of journal and conference papers, and several books, and is or was at the editorial board of numerous journals. He is an editor of Communications in Nonlinear Science and Numerical Simulations. He is a

fellow of the IEEE since 2000 and was awarded in 1990 the IEEE Heaviside premium. He is appointed honorary knight of the "golden feedback loop" (NTNU) in 2011. He is since 2011 an IFAC Council Member. Per January 2015 he is scientific director of the Dutch Institute of Systems and Control (DISC). He is recipient of the 2015 IEEE Control Systems Technology Award.



**Nathan van de Wouw** obtained his M.Sc.-degree (with honours) and Ph.D.-degree in Mechanical Engineering from the Eindhoven University of Technology, Eindhoven, the Netherlands, in 1994 and 1999, respectively. He currently holds a full professor position at the Mechanical Engineering Department of the Eindhoven University of Technology,

the Netherlands. Nathan van de Wouw also holds an adjunct full professor position at the University of Minnesota, U.S.A and a (part-time) full professor position at the Delft University of Technology, the Netherlands. He has published a large number of journal and conference papers and the books. He currently is an Associate Editor for the journals "Automatica" and "IEEE Transactions on Control Systems Technology". In 2015, he received the IEEE Control Systems Technology Award. His current research interests are the modelling analysis and control of nonlinear/hybrid systems, with applications to vehicular platooning, high-tech systems, resource exploration, smart energy systems and networked control systems.



## Chapter 6

# Reversing of Multiple Articulated Vehicles

### 6.1 Introduction

As shown in Chapter 4, an increasing number of articulation points is favourable for low speed manoeuvrability. The swept path is minimized and the vehicle is comparatively easy to control by the driver as the space required to perform the manoeuvre and vehicle combination response do not pose special challenges. This is however not the case for the reversing of a multiple articulated vehicle combination. Hereby the towed vehicle units that were originally pulled by the prime mover will be pushed backwards, which may result in divergent unstable behaviour as the articulation angles tends to increase without actuating the steering wheel of the prime mover. This represents a problematic situation for all vehicle combinations having multiple of articulation points, including introduced Future Vehicle Concepts, as the reversing is always required. An exemplary scenario is when the rear most vehicle unit needs to be parked at the loading dock of the distribution center.

A series of experiments with a number of drivers is presented in this Chapter to derive a framework for a driver support system for reversing. The objective is to understand the fundamental reasons, why reversing of multiple articulated vehicle is a difficult task for the driver.

First a problem definition related to the reversing is given, then the instrumentation and experiments are described. Based on the results, a framework for a driver support is proposed that should result in a reduction of driver errors during reversing. These observations will be subsequently used as an input for Chapter 7.

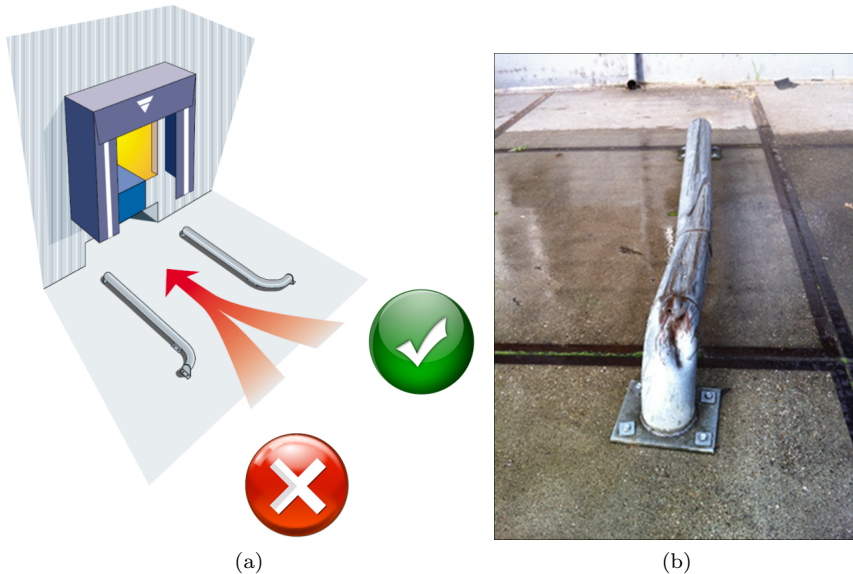


Figure 6.1: (a) Preferred directions of approaching the loading dock by the drivers (b) Frequently damaged navigation rail near the docking gate.

## 6.2 Problem Definition

The reverse manoeuvring with multiple articulated HCVs is recognized as one of the most critical tasks by the majority of professional drivers and fleet operators in the Netherlands as concluded by a query [102]. Because of limited space at the distribution centers majority of vehicle combinations needs to be reversed along the curve, which brings additional complexity to the drivers who are frequently able to complete the manoeuvre with a confidence from one side only as shown in Figure 6.1a. Typically they do not use the rear mirrors, but prefer to open the window on the side of steering wheel for direct observation of the semitrailer orientation.

Therefore parking of vehicle combination towards the loading dock at the distribution centres results frequently in undesirable incidents, with minor damage to the vehicles or property but considerable costs associated with transportation delays. The character of the property damage is shown in Figure 6.1b. It is remarkable that these incidents are exclusively caused by driver errors. Whereas in the majority of all documented accidents with involvement of HCVs the driver is not the originator of the accident [102].

This may be interpreted as follows. The drivers usually have extensive experience in ‘normal forward’ driving on the highway. Additionally, the driving with HCV during such a scenario is very similar to driving a normal single articulated vehicle combination. However, not every driver has sufficient skills for reverse driving with an arbitrary HCV combination. Moreover, the kinematic behaviour of each HCV depends on the main dimensions. In practice, it means the driver needs to apply a

different control strategy depending on the HCV combination while reversing.

In addition, if the vehicle gets beyond the limits, expressed in terms of the maximal road curvature per vehicle unit as described in [88], it will develop into a situation commonly known as low speed jack-knifing. The vehicle combination becomes directionally uncontrollable and needs to be straightened by driving forward in order to bring the articulation angles to a controllable domain again.

Yet, reversing of multiple articulated vehicles by human drivers is not impossible. Drivers are able to learn control patterns in order to maintain the vehicle controllable domain, as shown in practice. These patterns can be different for drivers and may be very difficult to master or understand for some drivers.

While reversing the driver tries to control the vehicle path based on observable signals given by:

- Position and orientation of the prime mover with respect to surrounding environment, as seen by the driver behind the windshield
- Position of the towed vehicles relative to each other and within the surrounding environment as seen by the driver from the rear view mirrors
- A sound or visual signal indicating the distance of the rearmost vehicle combination point to an obstacle.

To control the vehicle combination the driver can actuate the vehicle combination by:

- Forward and reverse driving
- The steering wheel angle.

In the next section a number of experiments will be defined in order to understand the driver control decisions and behavior. Subsequently, possible causes leading to mistakes will be identified which result in losing or complicating the control while reversing.

### 6.3 Tests with novice drivers

A double articulated vehicle combination has been used for conducting the reversing experiments. The vehicle combination consists of a 6x2 tractor, a 2-axle semitrailer and a 2-axle central axle trailer, as shown in Figure 6.2. The tractor is not equipped with any driver support system for reversing and none of the towed vehicles is actively or passively steered. Both towed vehicles are however equipped with deployable outriggers, which are normally used to prevent the vehicle combination from roll-over during dynamic tests. In this case, they can be used as additional reference means for the drivers to better estimate the relative orientation of the vehicle units.

The vehicle is instrumented with a number of sensors to record vehicle states such as position, velocities, and accelerations of each vehicle body in translational and



Figure 6.2: Vehicle combination used in reversing tests.

rotational direction. Furthermore the articulation angles between the vehicles are measured. Several cameras are attached to the vehicle bodies to record the vehicle motion, these views were however not provided to the driver, so they could not be used during the experiment as an aid.

The main focus of the tests is the driver monitoring while reversing. Therefore driver actuation of the vehicle is measured consisting of the steering angle and vehicle velocity induced through the accelerator pedal position. To map the driver view and the gaze direction the eye tracking glasses were used [123]. The eye tracking technique is widely used in psychology research, cognitive linguistics and product design. The glasses can be seen as an ‘eye scanner’. As can be seen in Figure 6.3a, the glasses have an infra red light (IRL) emitter/receiver (red solid arrow) that emits an IRL beam to the pupil. The beam is subsequently reflected back and the gaze vector can be determined based on the directional offset. A second part of the eye tracking glasses is the built-in SVGA camera, indicated by blue dashed arrow in Figure 6.3a. The video signal of the camera is subsequently synchronised with the measurements of the gaze direction from the IRL sensor. Proper synchronization is achieved through the calibration procedure that is executed for each driver separately to acknowledge different shapes of the faces. The calibration is done by prescribed procedure, whereby the driver looks to a predefined grid of external IRL emitters. An example of the resulting video output can be seen in the snapshot shown in Figure 6.3b. The red circles represent the gaze direction and the line in between the circles represents the motion of the gaze. The eye tracking signal together with articulation angles, steer angle, and the velocity are the main sources in the analysis.

Experiments are based on real-life operational scenarios, which involve reverse manoeuvring at low-speeds. They have been executed at the WABCO proving ground near Hannover. The measurements were conducted with seven test drivers of varying age and experience. It should be emphasized that none of the drivers had previous experience with driving and reversing of high productivity vehicles, although one has had some experience with a truck - full trailer combination, which also has two articulation points.



Figure 6.3: (a) Tobii eye-tracking glasses (b) Illustration of the drivers view with the gaze point.

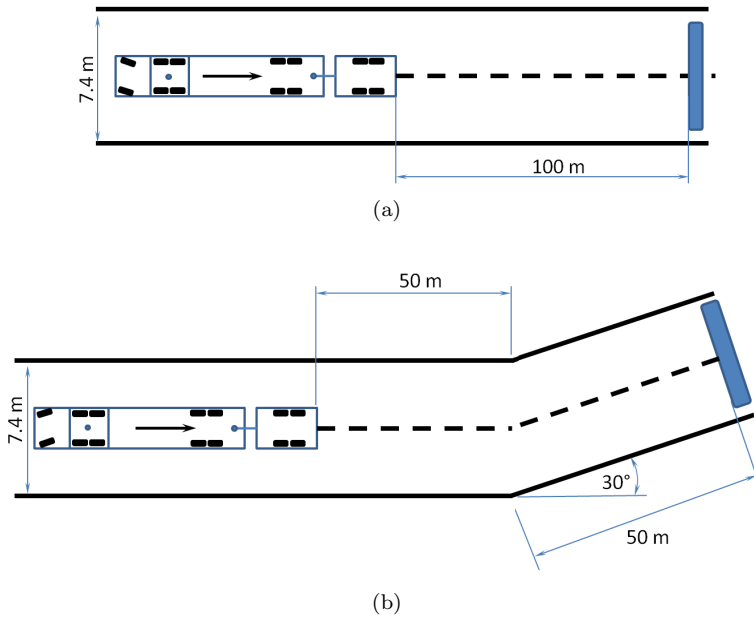


Figure 6.4: Reversing manoeuvres: a)space straight lane b)space curved lane.

Two test scenarios have been considered:

- Firstly, all drivers are asked to perform a reversing manoeuvre in a straight line within a 7.4 m wide lane. The minimal length to complete the manoeuvre was set to one hundred meters, however if the drivers wanted they could proceed further in the corridor. The initial position of the vehicle is precisely in the middle of the lane with zero articulation angles, as depicted in Figure 6.4a. In case of undesired jack-knifing the drivers are allowed to correct the vehicle articulation angles by driving forward. The drivers can freely choose the velocity and strategy to finish the manoeuvre; the only requirement is to stay within the width of the lane with all vehicle units. The test has been performed with three drivers in two configurations, without and with deployed outriggers, while each driver had three attempts for each experiment. The remaining four drivers performed the manoeuvre with deployed outriggers only, due to the time constraints.
- The second reversing manoeuvre, as shown in Figure 6.4b, has an identical initial position but in addition includes cornering. It starts similarly as reversing in a straight line in the previous case, but after fifty meters the direction of the lane is angled by thirty degrees. Herewith the drivers are allowed to cross the outside lane boundaries during manoeuvring, but had to finish between the lines on both sides of the road at the end of the curve. As the manoeuvre is more complicated the outriggers were always deployed. Moreover it has been undertaken only with four test divers that performed best in the previous scenario, with two attempts per driver.

## 6.4 Results form the experiments

Several hours of measurement data were collected and analysed. The results will be discussed separately for each experiment:

- Straight-line reversing, with and without deployed outriggers

An analysis of the results reveals that monitoring the relative orientation of the vehicle units, especially the angle between last two units, is extremely important for the driver to successfully position the vehicle combination. It is very complicated for the drivers to extract this information from the available visual input, as observed from the eye tracking data. They typically try to find visible referencing points on the vehicle units, which are used for estimating positions and angles. Eye tracking measurements furthermore reveal that all involved drivers were using the outriggers, when available, as referencing points. An example of continuous gazing between the outriggers, to estimate the orientation of the last vehicle, is shown in Figure 6.5. When the outriggers were not deployed, the performance of the drivers substantially degraded. Subsequent interviews with the drivers confirmed the hypothesis that outriggers have a positive contribution to the driver's perception of the positioning of vehicle units.



Figure 6.5: Continuous gazing between the outriggers to estimate the orientation of the last vehicle unit, as observed on majority of drivers

An exemplary comparison between the measurements time histories captured with and without deployed outriggers for longitudinal velocity, articulation angles, driver actuated steering angle and distance travelled is shown in Figure 6.6.

Two additional objective measures are used to compare the drivers performances in both scenarios. Firstly, the average speed is considered, which is calculated by averaging of all driver's attempts. It quantifies as a measure for the rate of the progress with the task. In Figure 6.7, it can be observed that the speed is generally higher for all drivers when the outriggers are deployed, which can be translated into increased drivers confidence and awareness about the vehicle state, leading to a higher speed.

As the vehicle combination is unstable during reversing an oscillatory like steering input from the driver is required to stabilize the vehicle combination along a straight path. Hence, the number of zero crossings of the steering angle signal during the manoeuvre was counted and used as second measure, to quantify the steer activity of the driver. The total count is normalized by the achieved distance, as this value vary per driver. This distance normalized steer activity can be correlated to the driver's effort to stabilize the vehicle combination during the reversing manoeuvre.

In Figure 6.8 the results are depicted, which supports the hypothesis that the presence of outriggers improves the driver performance, as the steer activity for all drivers is lower for that condition. In case of drivers #2 and #3 this difference is more visible than for the driver #1. Moreover, none of the drivers was able to completely finalize the task without the outriggers, because the vehicle was either crossing the lane or was brought in a state of articulation angles which prevented any continuation of the reversing manoeuvre.

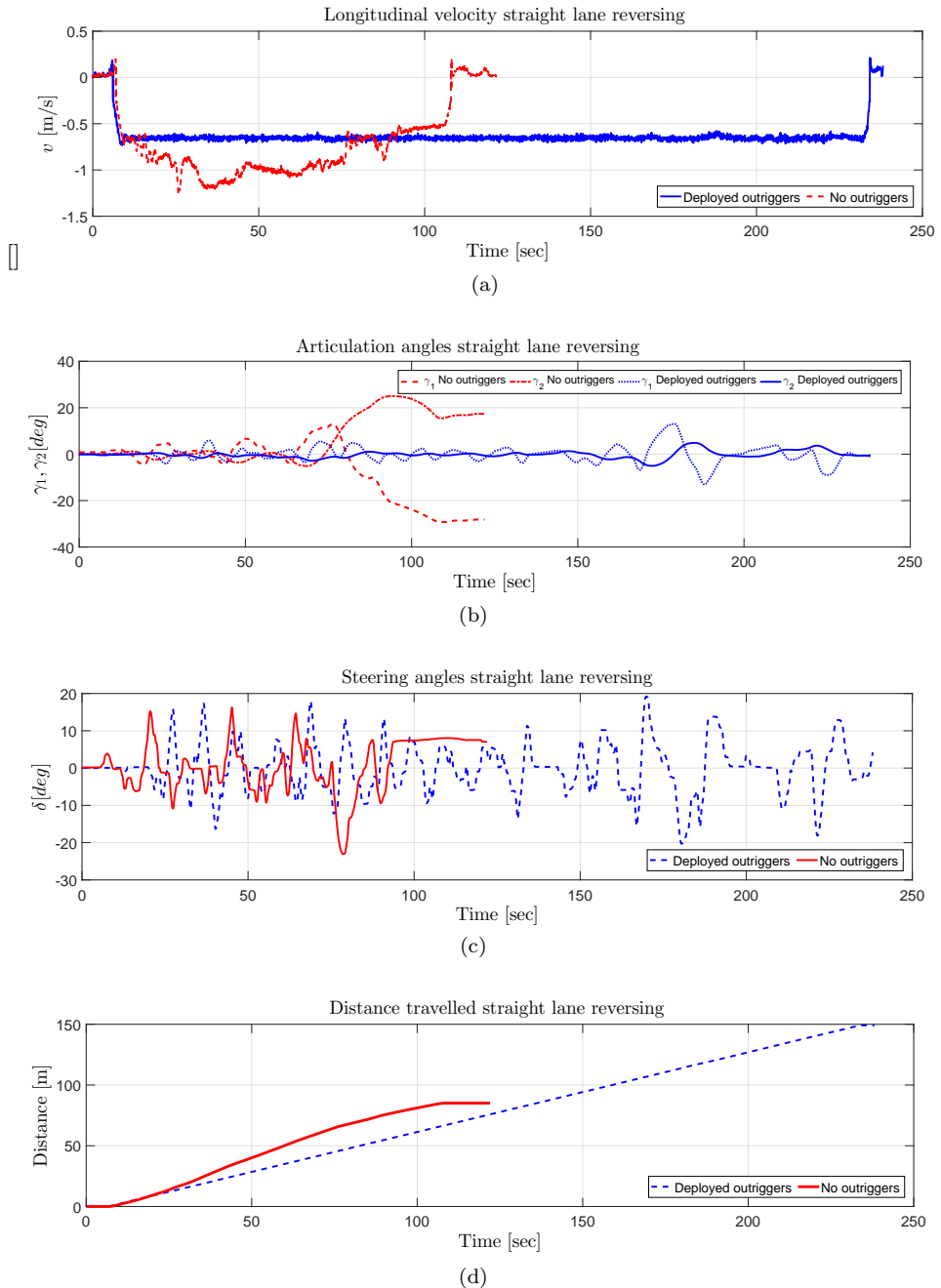


Figure 6.6: Measurement time history of a driver executing the straight lane reversing manoeuvre with and without deployed outriggers providing a) Longitudinal velocity, b) Articulation angles, c) Steering angle, d) Distance travelled.





Figure 6.7: Average speed comparison

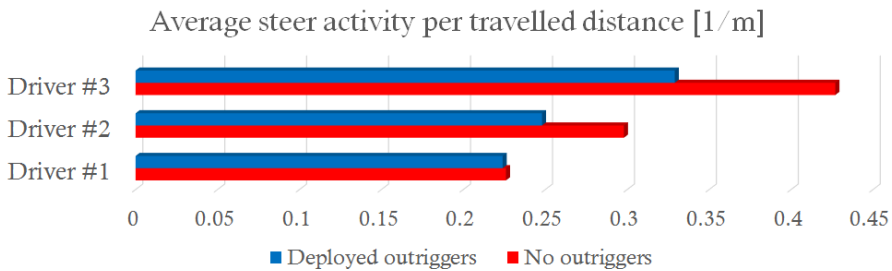


Figure 6.8: Average steer effort per travelled distance comparison

Remaining four test drivers completed the test only with deployed outriggers due to available testing time, so the direct benchmarking is not possible. Nevertheless, reviewing the eye tracking data confirmed that also these drivers used the outriggers as referencing points for estimating the positions and orientations of the vehicle units.

- Reversing a curved lane with outriggers

During the second test the vehicle has to be navigated through a curve with a thirty degree angle, as shown in Figure 6.4b. As cornering is required, bigger articulation angles and new issues related to the reversing in a curve have been observed.

As observed, a critical moment occurs when the orientation of the articulation angles between the interconnected vehicles becomes opposite. In this case the first trailing vehicle conceals the second trailing vehicle unit that needs to be controlled. Thus the driver does not get any visual input on the second vehicle and the control of the whole combination becomes extremely problematic. This is illustrated in Figure 6.9 where the view and the gaze point of the driver during this scenario is shown. As can be seen neither the left rear mirror or the right mirror in Figure 6.9 does provide any information on the second trailing vehicle unit. This visual information is however of a great importance for adequate control.



Figure 6.9: (a) Drivers view and gaze left rear mirror (b) Drivers view and gaze right rear mirror.

A second observation, which was already recognized in the first test scenario, is related to the reachability of the vehicle configuration. A term reachability in this context refers to an ability of the vehicle combination to reach from an initial state, defined by the combination of articulation angles, a state when both articulation angles yields zero, while maintaining the reversing direction and actuating the steering angle within applicable mechanical limits. In practice it means that if the reachability limits are exceeded by incorrect steering actions while reversing the test vehicle is be brought into a state, which is not stabilizeable anymore. The driver has no awareness on this, continues reversing and attempts to control the vehicle. In this situation at least one articulation angle will always continue to increase and the driver eventually decides to stabilize the vehicle combination by a forward drive, being the only way to straighten the vehicle combination again. This move however takes considerable distance and may result in situation that the driver ends-up further away from the destination point, compared to the starting point.

The reachability limits are governed by the maximal applicable steering angle and principal vehicle combination dimensions such as wheel bases and positions of coupling points. In Figure 6.10 the reachability limits are provided for the tested vehicle combination (TR6x2-ST2-CT2), based on the simulations described in [72]. The red crosses indicates the combination of the articulation angles for which the vehicle combination can not be brought into the straight configuration with zero articulation angles while respecting the vehicle combination dimensions and maximal steering angle. The green circles signify combinations of articulation angles, which still can be reduced to zero while reversing.

The situation of exceeding reachability limits as captured during the reversing for a curved lane measurement is shown in Figure 6.11. Hereon, the driver endeavours to reduce the second articulation angle  $\gamma_2$  in order to straighten the vehicle combination by multiple steering actions in the time interval between

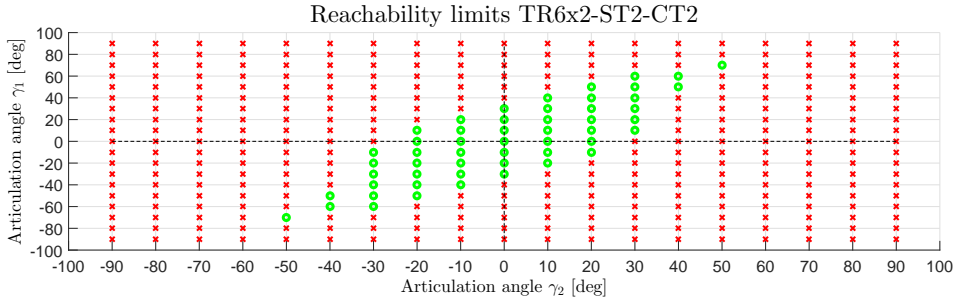


Figure 6.10: Experimental vehicle reachability in dependency of articulation angles, red crosses the vehicle combination can not be straightened, green circles the straightening is possible.

80-120 seconds even though the reachability limits, designated by the dashed and dotted line, were exceeded. As can be observed  $\gamma_2$  remains unchanged even though the first articulation angle  $\gamma_1$  reaches up to forty degrees. Moreover, the driver is suffering with limited view as the first trailing unit is concealing the second one. Hence, the driver eventually decides to straighten the combination by forward driving in a time interval between 130-150 seconds, which was however inevitable already on the time stamp of 80 seconds.

To summarize the results, following reasons can be identified which are making the reversing difficult for the driver :

- Limited view of the driver
- Instability of the vehicle combination
- No driver awareness of the reachability limits

## 6.5 Improving driver performance

In order to improve the driver performance, while reversing multiple articulated vehicles, a general framework for a driver support system will be discussed.

The primary problem for the driver is the limited field of view, which is preventing to observe the absolute position of the vehicle combination with respect to its surroundings and the relative pose of vehicle units with respect to each other. This may be solved by employing a number of cameras that can be placed on the body of vehicle units to monitor vehicle movements and provide additional information to the driver during the reversing manoeuvre. This solution may not be easy to implement in to real life situations however. It is very common that the owner of the hauling unit and the owner of trailing vehicle units are two different entities, therefore one can

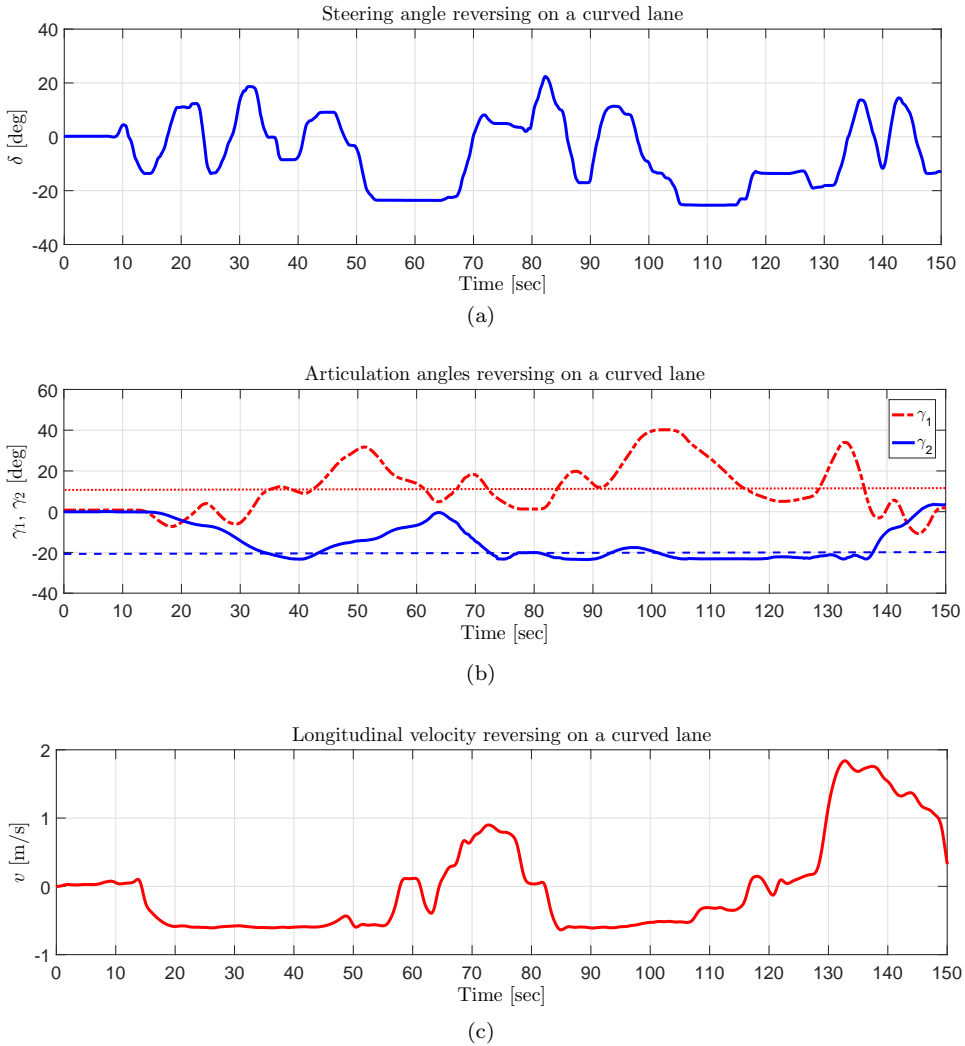


Figure 6.11: Time history of a driver executing the reversing on a curved lane providing a) Steering angle, b) Articulation angles, c) Longitudinal velocity.

not guarantee compatibility of such a camera system. This is one reason why the most of the technology and sensors are typically concentrated in the hauling unit, making it independent of trailing vehicle units. In case that cameras are used, robust and straight-forward interpretation of multiple camera signals to the driver would be required to prevent driver's confusion or misinterpretation. An optimal solution most likely is to combine the camera images and create an artificial bird's eye view of the vehicle combination and its surroundings. This solution would be rather intuitive for the driver and solves the problems with missing referencing points and shading of vehicle units one by another, which has been observed during the experiments.

The remaining two reasons being the instability of the reversing vehicle combination and its reachability limits, are in fact interlinked. They become a problem for the driver if the control of the steering angle is not done correctly. From the observations it appears that a major challenge for the driver is controlling the articulation angles. Essential problem occurs in the directional control of the rear most vehicle unit while reversing, which needs to be exerted through the steering of all preceding vehicle units. This is however fairly difficult as the vehicle combination is unstable and may display non-minimum phase behaviour while reversing. It practically means that if the hauling unit is steered to a certain direction the interconnected loading vehicle unit may turn in the opposite way according to the position of the coupling point. Moreover, every vehicle combination needs to be controlled in a specific manner because of different dimensions, which determine the vehicle kinematics. The issue can be solved by a steering coach system, which instructs the driver how the steering angle should be controlled in order to follow the path connecting destination point and current vehicle position. The form how the information is provided to the driver may be haptic-based through the e.g. steering wheel or vision-based using the elements of augmented reality. The steering coach will in addition ensure that reachability limits will not be exceeded such that the tracking of the reference path is done correctly.



## Chapter 7

# Driver Support for Low-speed Manoeuvring

### 7.1 Introduction

As mentioned in Chapter 6, reversing a multiple articulated vehicle combination proves to be problematic for a driver, because of vehicle directional instability and lack of visibility from the cabin. More importantly, the reversing can not be avoided during daily operation and is demanded anytime the vehicle combination needs to be parked towards loading dock at the distribution centres, where the manoeuvring space is typically very limited. Hence, in this chapter the two main components of driver support for manoeuvring of double articulated High Capacity Vehicle at distribution centres are described, being the path planner and bi-directional path following controller.

This chapter begins with a literature review on path planning techniques and path tracking controllers for reversing articulated vehicle combinations. The next sections cover the derivation of a kinematic model for a double articulated vehicle that will be used as a basis for both the path planning algorithm and path tracking controller, that are described respectively. The chapter is concluded with general principles related to the implementation of the driver support system addressing the vehicle localization and the means the information as provided to the driver.

## 7.2 Literature Review

The proposed driver support for manoeuvring HCVs is based on two sub-systems:

1. Path planning - responsible for the generation of the reference path between an initial and terminal pose of vehicle combination assuming constant forward and reversing speed,
2. Path following controller - responsible to regulate the steering angle and navigating the vehicle combination along the reference path.

Therefore at first a review on different path planning strategies will be given. Subsequently, the research available on controllers intended for reversing articulated vehicles is reviewed.

The path planning problem belongs to the broad field of motion planning. Therefore only the research related to articulated vehicles, and low speed operation is discussed. The general purpose of a path planning algorithm is to generate a path between the pose at initial and the destination node, while considering the kinematic constraints of the vehicle combination and where a certain cost function that is typically related to the length of the path is minimized. Furthermore, jack-knifing should be avoided as well as collisions between coupled vehicle units and stationary objects, such as other parked vehicle combinations.

A method called Rapidly-exploring Random Trees (RRT) is introduced by [81], which is specifically designed to handle systems with non-holonomic constraints in an unknown environment which may include stationary obstacles. RRT is iteratively propagated by applying control inputs, represented in this context by a steering angle, that navigates the system toward randomly selected points, while requiring point-to-point convergence. The RRT method is considered as an effective approach to the computationally difficult motion planning problem, but there are no guarantees on the quality of such solution, in terms of path length or unnecessary curves, as proven in [62]. This approach almost surely converges to a non-optimal solution. This limitation is addressed by an improved algorithm called RRT\*, proposed in [63], which ensures asymptotic optimality through a cost function driven procedure of the path extension towards the new path vertex. Extensive and frequently referred literature related to the motion planning for mobile robots, resembling a tractor-trailer combination, is authored by Laumond et al. [80]. An alternative method of motion planning applied to a n-Trailer system is to use graph based planners like the A\* or D\* path planner [117], [119], which are however not feasible for real time application, due to their complexity and computational demand.

In [106], a collision free path planner for specific double articulated vehicle is proposed where the path properties in terms of the curvature for the rear-most vehicle unit are analysed and an empirical relationship is mapped between the length of the path and the curvature. Subsequently a library of viable path segments is generated and Dijkstra grid search algorithm is applied to connect the segments together in order to generate a path which is collision free.



Zips et al. [140] propose a path planning algorithm applied to the docking scenario, which is using elementary kinematics and makes the approach less computationally demanding. The initial path is planned from the destination pose towards the initial pose using a tree based path planner, and subsequently refined solving an optimal control problem using heuristic rules for direction changes.

As proved by Dubins in [25], the shortest path between two nodes in the two dimensional Euclidean plane, while driving in one direction with a non-articulated vehicle, can be reached by a combination of circular arcs with prescribed maximum curvature and straight lines. The maximal curvature limit of the arc is defined by the vehicle wheel base and maximum applicable steering angle. As an input to generate the Dubins path the initial and destination pose is required.

Since the Dubins curves are computationally very efficient and ensure the optimality in terms of length, their relevance in combination with the initial path generation described in [140], will be explored further.

Next the path following controllers for reversing of articulated vehicles at low-speeds are reviewed, which is a classical nonlinear control problem. Most of existing approaches come from robotics. They typically address the problem for single articulation vehicles only and often through the development of complex, nonlinear controllers. These may prove to be difficult to implement or adjust if the vehicle dimensions and number of articulations differ. Moreover exact model parameters are required which may be difficult to obtain in practice.

Rouchon et al. [109] proved that system of the car with  $n$ -trailers is differentially flat, which can be compared to the controllability characteristics of a linear system. Considering this property, a stabilizing feedback control law is defined by [54], and [101]. Even though the applied control approach is theoretically stable, the multiple derivatives and integration make this method extremely sensitive to noise in the state estimation. Moreover, tuning of the control gains appears to be difficult due to their coupled effect on all the vehicle states, and the absence of any physical meaning.

Welsh et al. [133] propose a control law that is in theory exponentially stable and which can stabilize the tractor-trailer vehicle combination. The approach estimates the gain for the linear control law for each point of the reference trajectory using current position and upcoming shape of the trajectory. The control law is robust with respect to initial condition errors, perturbations introduced along the trajectory and the noise in the sensor data. The robustness with respect to the variation of vehicle parameters, which are accounted to be known exactly, is not however discussed. The pre-computation of the gains involves complicated integral estimations that may be prohibitively long in case the trajectory is longer than a number of meters. Furthermore, the method does not provide any means to prevent the vehicle from the irrecoverable jack-knife situation.

An alternative approach based on ideas of Model Predictive Control (MPC) may be found in [24] and [3]. These schemes use optimization in order to derive a sequence of commands that will navigate the tractor-trailer combination to the reference trajectory or path. Both methods employ a linearised kinematic vehicle model, which is a part of the simulation process to compute the commands that will lead to the best tracking of the reference trajectory. The trajectory can be optimized in accordance

with a selected cost function, which can be minimal time, minimal control effort, or a combination of both. Using this approach, obstacle avoidance can be also implemented by adding position constraints through boundary coordinates such as done by [97].

Additional methods for controlling tractor-n-trailer combinations based on nonlinear control techniques employ feedback linearisation [22],[10], model-based state feedback optimal control [55], backstepping [138], or fuzzy control [121], [104].

A fundamentally different technique for reversing control of articulated vehicles exploits the concept of virtual tractor. Hereby, the rear most trailer is regarded as a virtual tractor, which is controlled along the reference path by propagating virtual set-points through the kinematic chain of the vehicle combination to the steered tractor. A very good overview of research using this principle in different ways is given in [89]. As the theory of a virtual tractor originates from robotics, the tractor is typically modelled without velocity-dependent constraints, and thus the translational and rotational velocities can be actuated independently. The reviewed approaches mainly differ from the perspective of the articulation joint position that may be positioned directly above the axles [86], or having an offset with respect to the axles [20],[137], [108]. The results of these studies show that virtual set-point propagation back to a tractor through identical or heterogeneous off-hitched trailers leads to good performance in trajectory tracking. The errors that may occur in the joint angle measurement, result in deviations from the path, but do not provoke instability [20], which is a beneficial property.

Since the concept of virtual tractor is applicable to arbitrary vehicle combinations defined earlier, it will be used for developing a path following controller, together with the aforementioned Dubins curves for path planning.

### 7.3 Path Planning

As can be seen in Figure 7.1 the vehicle combination is originally positioned in the transfer lane which goes parallel with the distribution center and needs to be parked perpendicularly to the loading dock represented by the the origin of the coordinate system  $\vec{e}^0$ . This manoeuvre is commonly known as a docking, and according to the interviews done with the stakeholders in logistics, and spatial planning of distribution centres, the perpendicular layout is most frequently used. Therefore it will be used as representative scenario for the path planner definition.

The role of the path planner is to establish a set of reference nodes  $R_i$ , in the Euclidean plane  $\mathbf{R}^2$ , where  $i = \{0, n\}, \in \mathbb{Z}_+$ , while minimizing the path length between known initial pose  $R_0$  and terminal pose  $R_n$  of the controlled point  $U$  and considering its operational constraints. Each node is defined as  $R_i = [X_{ref(i)}, Y_{ref(i)}, \theta_{ref(i)}]$  in  $\vec{e}^0$ , where  $X_{ref(i)}, Y_{ref(i)}$  are positions, and  $\theta_{ref(i)}$  represents the orientation. Figure 7.1 depicts the initial and terminal pose of the last vehicle unit  $R_0$  and  $R_n$ , respectively, as well as the location of the controlled vehicle point  $U$ , which is based in the middle of the axle positions of the last vehicle unit. The resulting array of reference nodes  $R_i$  can be used as an input for the path tracking controller to be defined later.

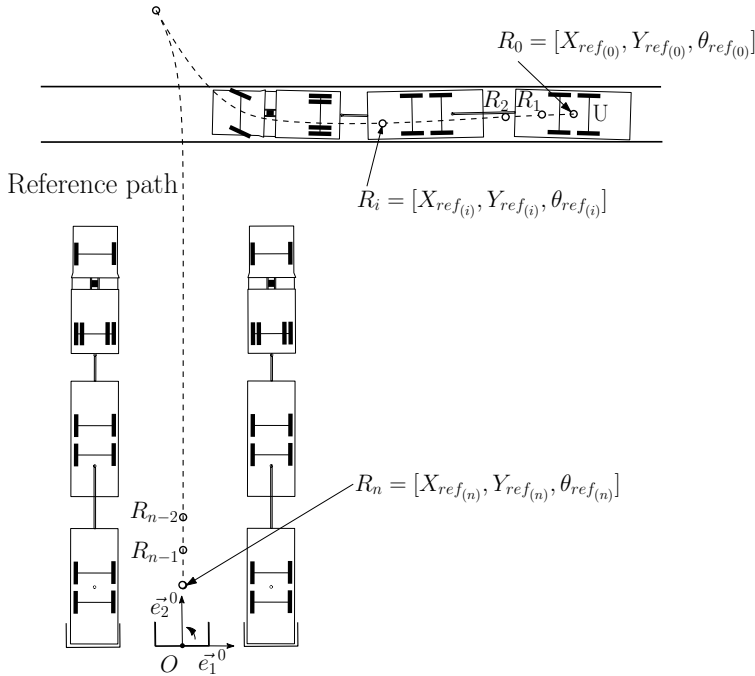


Figure 7.1: Path planner initial and terminal pose.

A number of assumptions and constraints are taken into account considering the perpendicular docking manoeuvre, which is depicted in Figure 7.2. At first, the origin  $O$  of the coordinate system  $\vec{e}^0$ , in which the path is defined, is located at the center of the docking gate. It enables to explicitly define the terminal pose being  $R_n = [0, Q, \pi/2]$  where  $Q$  is the rear overhang defined as the distance between the central turn point and the rear end of the last vehicle unit.

Applying the next constraint in practice means that the driver has to stop the vehicle combination before the loading dock, to receive support from the path planner. Thus, the initial position of a  $X_{ref(0)}$  expressed in  $\vec{e}_1^0$  must satisfy the condition  $|X_{IP}| > |M|$ , where  $M$  is the distance between the controlled point  $U$  and the frontal plane of the hauling unit measured with zero articulation angles in  $\vec{e}_1^0$ . This condition is established to prevent that the initial position of the vehicle front crosses axis  $\vec{e}_2^0$  of coordinate system  $\vec{e}^0$ .

Furthermore, the initial position of all four corners  $H_{(1-4)}$  of the last vehicle unit measured in  $\vec{e}_2^0$  must lie within the upper and lower limits defined by the width of the transfer lane and which are given by  $\max|H_{(1-4)}| < Y_{max}$ , and  $\min|H_{(1-4)}| > Y_{min}$ . The positions of last trailing vehicle unit corner points  $H_{(1-4)}$  are dependent on external dimensions represented by  $N$  and  $Q$ , depicted in Figure 7.2, as well as vehicle initial localisation represented by  $\theta_{ref(0)}$  and  $Y_{ref(0)}$ , which are all assumed to be known.

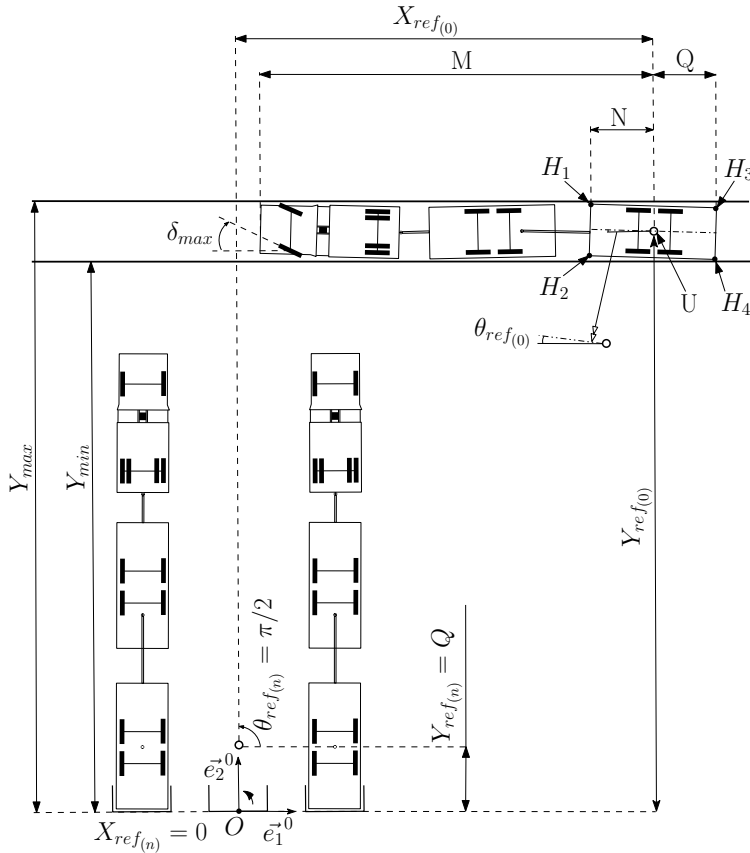


Figure 7.2: Presumptions and constraints of path planner.

No static nor dynamically moving obstacles are considered, except for already parked vehicles, as localization of the moving obstacles is considered to be outside the scope of the current framework. The set of assumptions is completed by known vehicle dimensions, as well as the maximal applicable steering angle  $\delta_{max}$  of the hauling unit.

The principle of the path planner will be explained next. A docking manoeuvre is typically performed in two steps as shown in Figure 7.3. The first step, driving in forward direction along the green-coloured curve  $p$  between the nodes  $R_0$ , and node  $A$ , is exerted to manoeuvre the vehicle combination in a pose that will be favourable for the start of the second step. The second step is the motion driving along the blue-coloured curve  $q$  in reverse direction between the nodes  $A$  and  $R_n$ . The main goal of the path planner is to generate a path that will be optimal with respect to the travelled distance for both steps and which ensures that the transition between the steps will be seamless, i.e. the reversing move starts from the node where the forward move ends. The path needs to be kinematically viable, which implies that rotational movement of all vehicle units is coupled to their translation and can not be actuated independently. No lateral or longitudinal tyre slip is assumed.

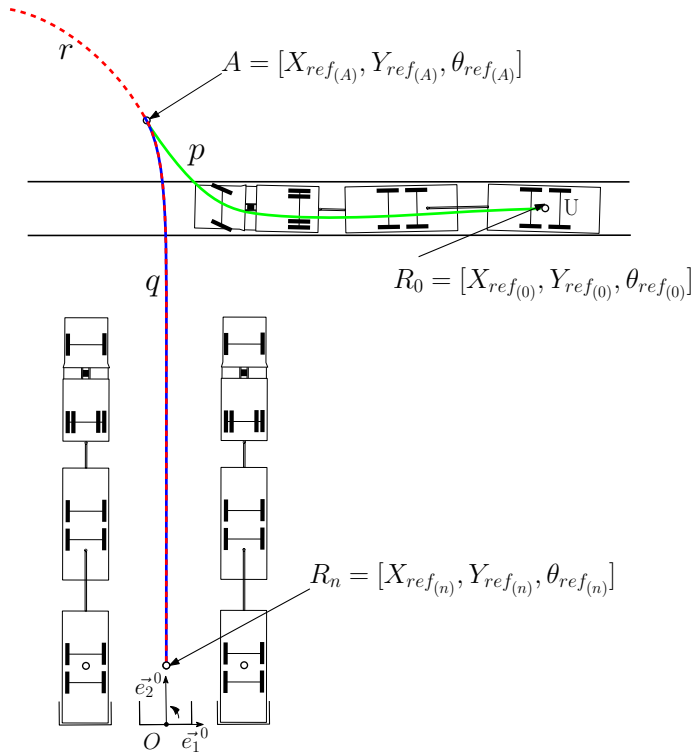


Figure 7.3: Two-step docking manoeuvre along curves  $p$  and  $q$ .

The path planning problem can thus be split in two sub-parts; the forward move, and the reverse move. For clarity, we will start with the determination of the red-coloured dashed curve  $r$  in Figure 7.3, that will subsequently enable the definition of the blue-coloured curve  $q$  for the reverse motion of a double articulated vehicle combination.

The path definition is based on the kinematic behaviour of a double articulated vehicle, which can be described through a model which comprises the nonholonomic constraints as follows:

$$\begin{aligned}
 \dot{y}_0 \cos(\theta_0 + \delta) - \dot{x}_0 \sin(\theta_0 + \delta) &= 0, \\
 \dot{y}_0 \cos \theta_0 - \dot{x}_0 \sin \theta_0 &= 0, \\
 \dot{y}_1 \cos \theta_1 - \dot{x}_1 \sin \theta_1 &= 0, \\
 \dot{y}_2 \cos \theta_2 - \dot{x}_2 \sin \theta_2 &= 0,
 \end{aligned}
 \tag{7.1}$$

while adopting the nomenclature of Figure 7.4.

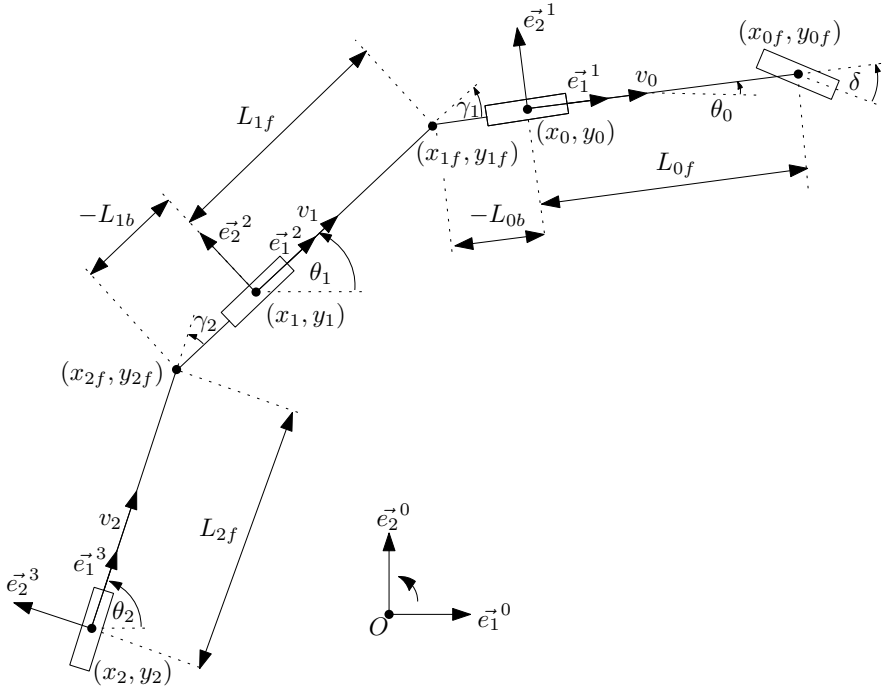


Figure 7.4: Kinematic model of double articulated vehicle combination.

The vehicle kinematic behaviour may be described through a set of differential equations:

$$\dot{\theta}_0 = \frac{v_0}{L_{0f}} \tan \delta, \quad (7.2)$$

$$\dot{\theta}_1 = \frac{v_0}{L_{1f}} \sin \gamma_1 + \frac{L_{0b}}{L_{1f}} \dot{\theta}_0 \cos \gamma_1, \quad (7.3)$$

$$\dot{\theta}_2 = \frac{v_1}{L_{2f}} \sin \gamma_2 + \frac{L_{1b}}{L_{2f}} \dot{\theta}_1 \cos \gamma_2, \quad (7.4)$$

$$v_1 = v_0 \cos \gamma_1 - L_{0b} \dot{\theta}_0 \sin \gamma_1, \quad (7.5)$$

$$v_2 = v_1 \cos \gamma_2 - L_{1b} \dot{\theta}_1 \sin \gamma_2, \quad (7.6)$$

, where  $\gamma_1 = (\theta_0 - \theta_1)$ , and  $\gamma_2 = (\theta_1 - \theta_2)$  are the articulation angles and  $L_{0b}$ , with  $L_{1b}$  are coupling joint positions w.r.t the rear axle. Note that both  $L_{0b}$  and  $L_{1b}$  are measured in  $\vec{e}^1$  and  $\vec{e}^2$ , respectively, implying they are positive for the fifth wheel coupling that is in front of the rear axle, and negative for the draw bar coupling that is behind the rear axle, such as depicted in Figure 7.4 for rigid truck with two central

axle trailers, which will be used hereafter as representation of double articulated vehicle combination. The equations (7.2)-(7.6), can be further used to derive the velocities of the rear most turn point in  $\bar{e}^0$  given by  $\dot{x}_2$  and  $\dot{y}_2$ , respectively:

$$\dot{x}_2 = v_0 \cos \theta_0 - L_{0b} \dot{\theta}_0 \sin \theta_0 + L_{1f} \dot{\theta}_1 \sin \theta_1 - L_{1b} \dot{\theta}_1 \sin \theta_1 + L_{2f} \dot{\theta}_2 \sin \theta_2, \quad (7.7)$$

$$\dot{y}_2 = v_0 \sin \theta_0 + L_{0b} \dot{\theta}_0 \cos \theta_0 - L_{1f} \dot{\theta}_1 \cos \theta_1 + L_{1b} \dot{\theta}_1 \cos \theta_1 - L_{2f} \dot{\theta}_2 \cos \theta_2. \quad (7.8)$$

The curve  $r$ , depicted in Figure 7.3, is constructed by  $x_2(t)$ ,  $y_2(t)$ , and  $\theta_2(t)$ , which can be obtained by solving equations (7.7), (7.8), (7.4) whilst equating the initial conditions to the destination pose  $R_n$ . Thus we will let the kinematic vehicle model drive from the dock in forward direction considering a constant positive velocity  $v_0$ , and providing a steering angle  $\delta t$  according to:

$$[\delta, t]^T = \begin{bmatrix} 0 & 0 & \delta_{max} & \delta_{max} \\ 0 & t_1 & t_1 + dt & t_{max} \end{bmatrix}, \quad (7.9)$$

where  $\delta_{max}$  is the maximal steering angle, which can be applied to the vehicle combination without jack-knifing,  $t_1 = M/v_0$  is the time the vehicle combination needs to leave the docking alley between two already parked vehicle combinations, and  $t_{max} = t_1 + (\pi L_{0b})/(v_0 \tan \delta_{max})$  is the time the prime mover needs to complete the semi-circle that ensure that the curve  $r$  is sufficiently long for the next steps.  $\delta_{max}$  is defined according to principles of maximal curvature limits as published in [87]:

$$\delta_{max} = \arctan \frac{L_{0f}}{\max \left( \sqrt{L_{1f}^2 - L_{0b}^2}, \sqrt{L_{2f}^2 - L_{1b}^2} \right)}. \quad (7.10)$$

This definition of steering angle with respect to time will guarantee that the vehicle combination envelope during the move will not interfere with other stationary vehicles that are assumed to be already parked, yet the potential of the path curvature will be maximally exploited reducing the required manoeuvring space. The full derivation of the kinematic model can be found in Appendix B.

Next, a node  $A = [X_{ref(A)}, Y_{ref(A)}, \theta_{ref(A)}]$  on the curve  $r$ , has to be found which enables a feasible path for controlled point  $U$  from the initial pose  $R_0$  along the curve  $p$ , as depicted in Figure 7.5. The node  $A$  where the vehicle changes from forward to reverse driving has to be chosen such that the length of the curve  $\|p\|$  is minimized. The segment on the path  $r$  that is defined between nodes  $A$  and  $R_n$  is then declared as curve  $q$ , and this specifies a set of reference nodes for the reverse motion as shown in Figure 7.5.

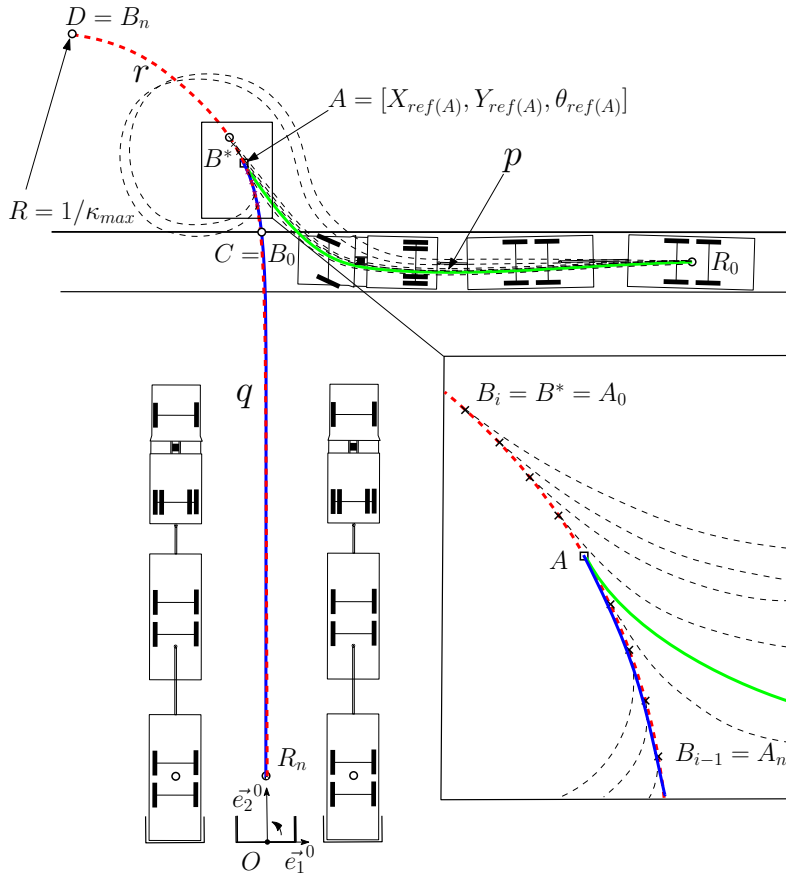


Figure 7.5: Distribution of  $A(i)$  nodes on curve  $r$  in segments between  $C$  and  $D$ .

The node  $A$  is found as follows. First, a number of equally distributed test nodes  $B_{(i)}$  is established on the section of the curve  $r$  limited by nodes  $C$  and  $D$ . The node  $C$  is defined by the intersection of curve  $r$  with boundary of the transport lane, and node  $D$  is given by the last point on curve  $r$  which originates at the terminal pose  $R_n$  in  $\bar{e}^0$ , as depicted in Figure 7.5. For each node  $B_{(i)}$  a path exists towards  $R_0$  applying the principle of the Dubins path [25]. A Dubins path is a curve of minimal length between two nodes in the two-dimensional plane whilst assuming that the vehicle negotiating the path can travel forward only. The curve is a combination of straight line segments and curved segments, which constitute a curve of shortest length that connects a starting pose to a terminal pose, while not exceeding the path curvature limit. Hence, the inputs to generate the Dubins path consist of the prescribed initial and terminal poses,  $R_0$  and  $R_n$ , respectively, and a limit for path curvature  $\kappa_{max}$ .



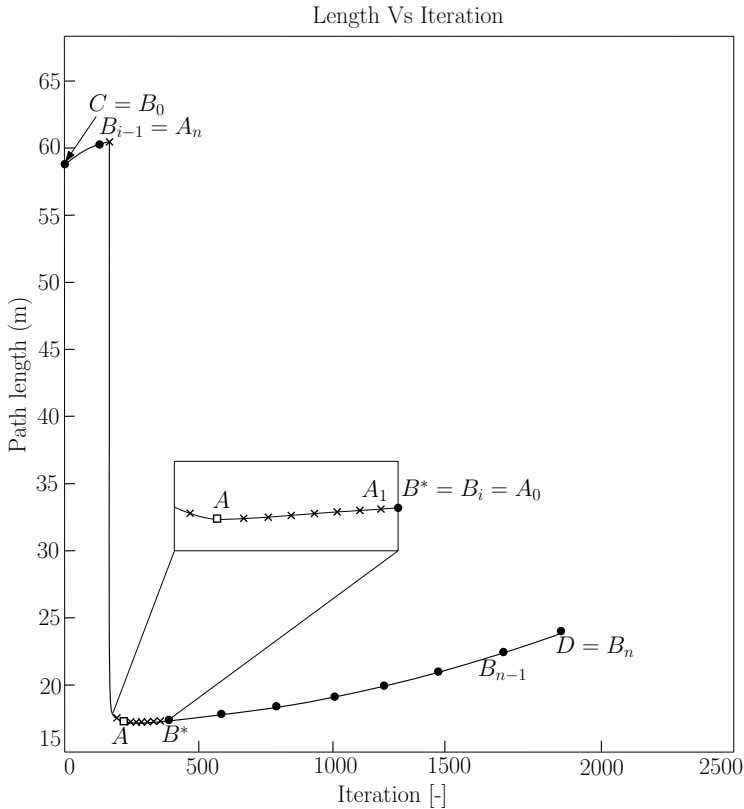


Figure 7.6: Minimization process of finding node  $A$  which delivers shortest reference path length for the forward motion.

Selecting  $\kappa_{max}$  plays an essential role for a properly functioning path planner. In theory, the shortest path is achieved by fixing the maximal curvature limit of the Dubins path as high as possible, implying the radius will be close to zero. Such a path however, would result in extremely tight curve  $p$ , and its tracking by the last vehicle turn point  $U$  would be physically impossible due to the nonholonomic constraints. In contrast, setting the limits of  $\kappa_{max}$  too low would make the path tracking easy, but it leads to an excessive length of curve  $p$ . For establishing the curvature limit  $\kappa_{max}$  the length of the path required to build-up the curvature has to be considered as well as the vehicle dimensions and maximal applicable steering angle. Through numerous simulations of various HCV's it has been observed, that a good balance between the path tracking ability and sharpness of the curve  $p$  is achieved by taking the maximal curvature limit  $\kappa_{max}$  for Dubins path equal to the curvature of the rear most vehicle turn point  $U$  achieved at node  $D$  in Figure 7.5. Herewith, the travelled distance to build up the curvature is comparable and thus can be projected to establish  $\kappa_{max}$ .

All required inputs for construction of Dubins path are now defined, thus a path can be established from known initial pose  $R_0$  to all test nodes  $B_i$ , distributed with constant step size along the segment of  $r$  bounded by the points  $C = B_0$  and  $D = B_n$ .

Subsequently, a test point  $B^*$ , depicted in Figure 7.5, can be found through minimization of the path length  $\min \|p_{B(i)}\|, i = \{0, n\}, \in \mathbb{Z}_+$  among all test points  $B_{(i)}$ . The point  $B^*$  will be afterwards used as a starting point for second round of minimization. In order to seek for a local minimum, the second round of minimization is uses test nodes  $A_{(i)}$  which are finely distributed over the segment of the curve  $r$  bounded by nodes  $B^* = B_{(i)}$  equal to  $B_{(i-1)}$ . The result of the minimization thus delivers the node  $A$  laying on the curve  $r$ , which ensures the shortest path towards  $R_0$  and yet satisfies the constraints of the Dubins path. The minimization process to identify node  $A$  is illustrated in Figure 7.6, where the length of the Dubins path  $|p_{(i)}|$  during the minimization is depicted in dependency of the position on the curve  $r$ . It is noted that between points C and A a step increase of the length occurs. The step change is caused by the development of the Dubins path which turns from a convex to concave shape, such as also illustrated in Figure 7.5. The aforementioned algorithm proved to be fast in calculation and applicable to arbitrary articulated vehicle combination.

## 7.4 Bi-directional path following controller for an articulated vehicle

The main role of the path following controller is to navigate the central turn point  $U$  of the last vehicle unit along the reference path, whilst actuating the steering angle  $\delta$  of the hauling unit. It is required that the controller is bi-directional, thus working for both the forward and reverse motion in the docking manoeuvre, and needs to be modular to be applicable to multiple vehicle combination layouts.

In this section, the control problem will be formulated at first using already described kinematic vehicle model representing an arbitrary vehicle combination. Next, a controller for both forward and reverse driving direction is designed, using the principles of the virtual tractor, which is further enhanced by the improved driver model ensuring the tracking error decreases asymptotically. Subsequently, the controller is subjected to a closed loop stability analysis, which concludes this section.

The control problem is formulated as a path following problem. The vehicle combination is considered with respect to a set of known reference nodes  $R_i$  which constitute the reference path generated by the path planner as shown in Figure 7.7. Each node  $R_i$  is defined by the position represented by  $(X_{ref(i)}, Y_{ref(i)})$  and orientation represented by  $\theta_{ref(i)}$ , all measured in  $\bar{e}^0$ . Although the reference path is characterized by discrete nodes, thanks to their high density no interpolation is considered.

The relevant reference point  $R_{REL}$  is selected based on the actual position of the controlled point  $U$ .  $R_{REL}$  is determined by evaluating which point  $R_i$  of the reference path has the minimal absolute distance towards the controlled point  $U$ . Thus  $R_{REL} = \min_{R_i} d(R_i)$ , where  $d(R_i) = \sqrt{\Delta x_i^2 + \Delta y_i^2}$ , and  $\Delta x_i, \Delta y_i$  are position errors of the point  $U$  with respect to  $R_i$  given by;  $\Delta x_i = x_2 - X_{ref(i)}$ ,  $\Delta y_i = y_2 - Y_{ref(i)}$ , respectively.

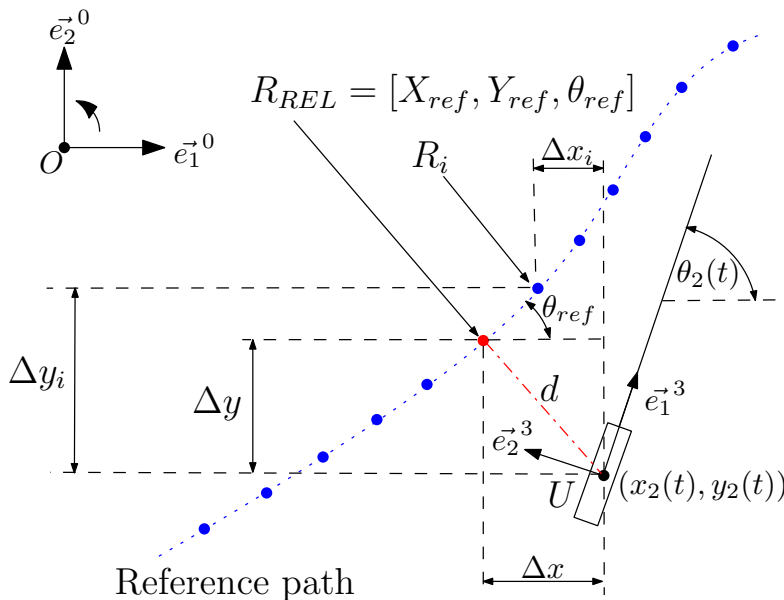


Figure 7.7: Determination of relevant reference path point which is used to determine the tracking errors

Based on the identified reference point  $R_{REL}$ , the lateral error  $e_{y_U}$  can be obtained in the local coordinate system  $\vec{e}^3$  fixed to the controlled turn-point  $U$  of the rear-most vehicle unit. The lateral error reads:

$$e_{y_U} = \Delta y \cos \theta_2 - \Delta x \sin \theta_2. \quad (7.11)$$

Besides the lateral error, an angular error  $e_{\theta_U}$  will be employed too in order to ensure the rear most vehicle has the same orientation as the relevant reference point  $R_{REL}$ . The angular error is defined by:

$$e_{\theta_U} = \begin{cases} \theta_{ref} - \theta_2, & |\theta_{ref} - \theta_2| \leq \pi, \\ \theta_{ref} - \theta_2 - 2\pi \text{sign}(\theta_{ref} - \theta_2), & \text{otherwise.} \end{cases} \quad (7.12)$$

The definition of angular error ensures that it is also correctly interpreted also when  $e_{\theta_U} > \pi$ , which may occur while negotiating circles when  $\theta_2 \rightarrow 2\pi$ .

To formalize the control problem we will employ the model of nonlinear kinematic double articulated vehicle derived earlier in section 7.3 by (7.1-7.6), which can be rewritten as follows:

$$\begin{aligned} \dot{x}(t) &= f(x(t)) + g(x(t), u(t)), \\ y(t) &= \begin{bmatrix} x_2(t) \\ y_2(t) \\ \theta_2(t) \end{bmatrix}, \end{aligned} \quad (7.13)$$

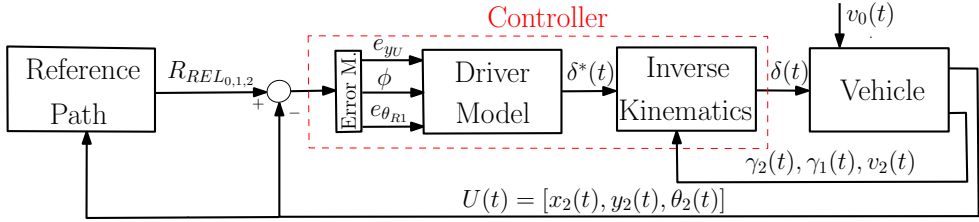


Figure 7.8: Controller structure.

where  $x = [\theta_0, \theta_1, \theta_2, x_0, y_0]^T$  are system states,  $u = [\delta]$  is the control input representing the steering angle of the hauling unit, the velocity of the hauling unit  $v_0$  is known to be constant which can be either positive or negative, and  $y$  is the output which gives the pose of the point  $U$  given by  $x_2$ ,  $y_2$ , and  $\theta_2$ . To solve the control problem the goal is to design the control input  $u$  such that closed-loop stability is guaranteed and the controlled output  $y$  follows the reference path, such that:

$$e(t) := \begin{bmatrix} e_{y_U}(t) \\ e_{\theta_U}(t) \end{bmatrix} = h(y(t), R_i) \rightarrow 0, \quad \text{for } t \rightarrow \infty. \quad (7.14)$$

In Figure 7.8, the control loop structure is depicted. As can be seen, it includes a known set of reference path nodes from which the relevant nodes are selected based on the current pose of point  $U$ , a controller, and kinematic model of the double articulated vehicle represented by (7.13). The controller consists of three blocks being, an error definition, a driver model and the inverse kinematic equations, respectively, which will be described hereafter.

The driver model is similar to models commonly used for forward driving of passenger cars or robots as described by e.g. Amidi [4] or McRuer [85]. In our case the driver model uses two look-ahead points to account for the lateral and orientation error with respect to a predefined reference path. The 'closer' point maintains a central lane position of the reference path and a 'distant' point accounts for the upcoming roadway curvature. This logic proves to be rather consistent with human steering profiles according to research documented in [111].

The driver is assumed to be positioned above the rear-most vehicle turn-point, designated by  $U$ . The controller is intended for the bi-directional operation thus the orientation of the driver's gaze direction is consistent with velocity  $v_2$ , defined in local coordinate system  $\vec{e}_1^3$ , which can be both positive or negative as shown in Figure 7.9.

At first the error models which will be used as inputs for the driver model need to be established. The driver model look-ahead vector is defined by  $\vec{H}_1 = \hat{i}_{v_2} P_{D_1}$ , where the  $P_{D_1}$  is the preview distance, and  $\hat{i}_{v_2}$  is the unit vector oriented according to  $v_2$ , as depicted in Figure 7.9 a), and b). The lateral error  $e_{y_1}$ , measured in  $\vec{e}_2^3$ , is determined via an orthogonal line which is projected from the end of the look-ahead vector  $\vec{H}_1$  to the nearest node of the reference path  $R_{REL_1}$ . On basis of the lateral error  $e_{y_1}$  and the magnitude of look-ahead vector  $\vec{H}_1$  the correction angle  $\phi_1$  can be calculated as  $\phi_1 = atan\left(\frac{e_{y_1}}{|\vec{H}_1|}\right)$ . Similarly the correction angle  $\phi_2$  is obtained through the preview distance  $P_{D_2}$  and look-ahead vector  $\vec{H}_2$ , defined via  $\phi_2 = atan\left(\frac{e_{y_2}}{|\vec{H}_2|}\right)$ , as can be seen in Figure 7.9.  $P_{D_2}$  has been set to be implicitly dependent on  $P_{D_1}$  such that  $P_{D_2} = kP_{D_1}$ , where  $k$  is a scaling parameter to be tuned. The resulting correction angle  $\phi$ , which is responsible for reduction of the lateral error based on profile of the reference path at given preview distance, is given by a weighted summation of  $\phi_1$  and  $\phi_2$ :

$$\phi = w_1\phi_1 + w_2\phi_2. \tag{7.15}$$

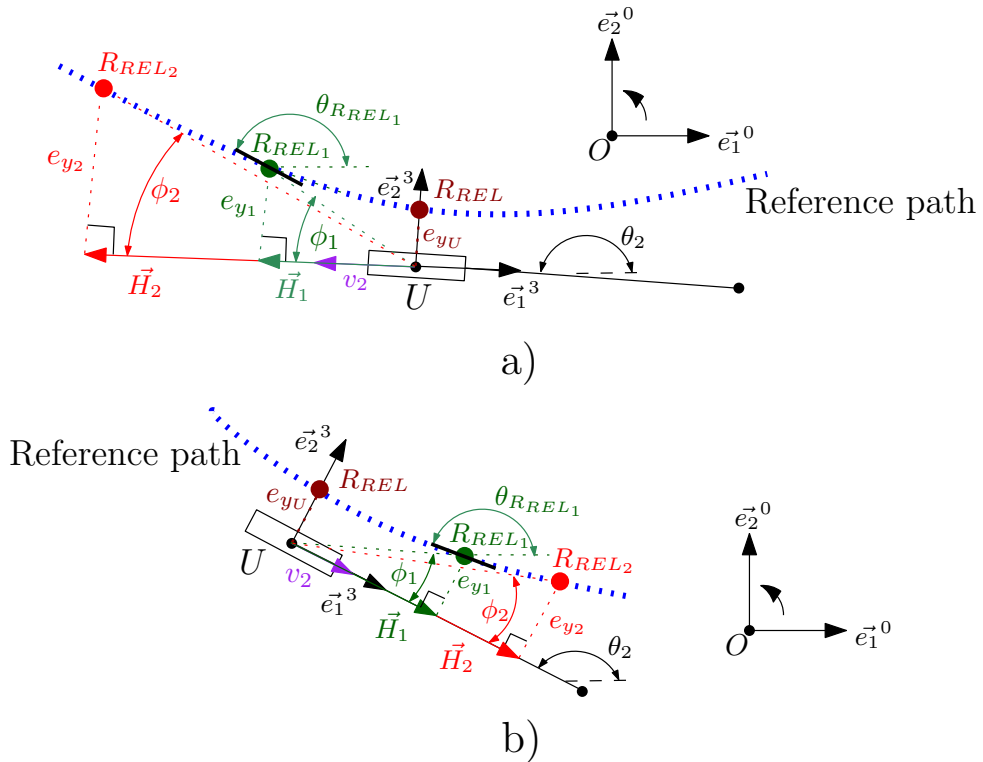


Figure 7.9: Error definitions for bi-directional controller for a) reversing , b) forward driving.

The relative weighting between  $\phi_1$  and  $\phi_2$  through constants  $w_1$  and  $w_2$  enables to prioritize between the precise tracking of the reference path, which is preferable during low-speed manoeuvring, or smoothness of the path that is desirable at high-speeds. Hence in the low-speed case, the weighting is in favour of the closer preview point, determined by  $\vec{H}_1$ . As the intention is to limit the number of scaling parameters to ease up the implementation and avoid unnecessary complexity for subsequent optimization the weighting factors  $w_1$  and  $w_2$  are constrained as follows:

$$\begin{aligned} w_1 &= 1 - w_2, \\ \frac{w_1}{w_2} &= \frac{P_{D_1}}{P_{D_2}}, \end{aligned} \quad (7.16)$$

which considerably simplifies the tuning process of the controller.

Next, the driver model considers the lateral error  $e_{y_U}$  of the point  $U$  to the relevant point of the reference path  $R_{REL}$  in accordance with the definition used for the control problem formulation and given by (7.11).

The last error component used as an input to the driver model is the angular error  $e_{\theta_{R_1}}$ . To compensate for the profile of the reference path at given preview distance the angular error is defined as:

$$e_{\theta_{R_1}} = \theta_2 - \theta_{R_{REL_1}}, \quad (7.17)$$

where  $\theta_2$  is the orientation of point  $U$ , and  $\theta_{R_{REL_1}}$  is the orientation of the reference path at relevant point  $R_{REL_1}$ , which is also employed to calculate  $e_{y_1}$ . Both  $\theta_{R_{REL_1}}$ , and  $\theta_2$  are measured in  $\vec{e}^0$ . Contrary to  $e_{\theta_U}$ , used for the control problem formulation, the angular error  $e_{\theta_{R_1}}$  is determined by the relevant point of the reference path that always lies-ahead of the controlled point  $U$ . Therefore, the driver model has a time to react, which is not the case if the  $e_{\theta}$  is considered.

The driver model functions as a Proportionally-Integral controller, using the various errors as defined previously and determining the virtual steering angle  $\delta^*$  as:

$$\delta^* = K_y \phi + K_I \int e_{y_U} + K_{\theta} e_{\theta_{R_1}}. \quad (7.18)$$

The term  $K_y \phi$  is dominant with its contribution to  $\delta^*$  as it compensates through  $\phi$  for both lateral and angular error, which are defined by (7.11), and (7.12). The integral term  $K_I \int e_{y_U}$  is primarily responsible for the elimination of the lateral steady state error, but due to the non-holonomic constraints of the vehicle model it also eliminates the orientation error  $e_{\theta_U}$ . The last term  $K_{\theta} e_{\theta_{R_1}}$  is contributing to  $\delta^*$  in situations when the curvature of the reference path rapidly changes.

The application of a virtual steering angle  $\delta^*$  to the last vehicle unit would induce a yaw velocity, which minimizes the path following errors  $e_{y_U}$  and  $e_{\theta_U}$  in accordance with the control objective. However none of the axles of the last vehicle unit can be steered. Therefore the required yaw rate  $\dot{\theta}_2$  needs to be propagated through the kinematic chain of vehicle units back to the hauling unit whose front axle can steer

with steering angle  $\delta$ . This approach, mentioned in section 7.2, is commonly known as the virtual tractor and will be described hereafter.

A fundamental part of the virtual tractor approach, is the inverse kinematic model, which can be understood as a feed-forward part of the controller. The model is defined using the same principles as the ordinary kinematic model of double articulated vehicle, used for the path planner in section 7.3, however now the inputs are the virtual steering angle  $\delta^*$ , articulation angles  $\gamma_{1,2}$ , and the velocity of the rear-most trailer  $v_2$ . All signals are assumed to be directly measurable or possible to acquire by recalculations of the measurements.

The inputs can be subsequently entered into a set of equations representing the inverse kinematic model of double articulated vehicle:

$$\dot{\theta}_2 = \frac{|v_2|}{L_{2f}} \tan \delta^*, \quad (7.19)$$

$$\dot{\theta}_1 = \text{sign}(v_0) \cdot \text{sign}(L_{1b}) \left[ -\frac{v_2}{L_{1b}} \sin \gamma_2 + \frac{L_{2f}}{L_{1b}} \dot{\theta}_2 \cos \gamma_2 \right], \quad (7.20)$$

$$\dot{\theta}_0 = \text{sign}(v_0) \cdot \text{sign}(L_{0b}) \left[ -\frac{v_1}{L_{0b}} \sin \gamma_1 + \frac{L_{1f}}{L_{0b}} \dot{\theta}_1 \cos \gamma_1 \right], \quad (7.21)$$

$$v_1 = v_2 \cos \gamma_2 + L_{2f} \dot{\theta}_2 \sin \gamma_2. \quad (7.22)$$

The full derivation of (7.19)-(7.22) can be found in Appendix B.

The yaw rate of the hauling unit  $\dot{\theta}_0$  can be also calculated by (7.2) and substituted into (7.21). In this way, the steering angle  $\delta$  of the hauling unit can be expressed in terms of  $\theta_2$ ,  $\theta_1$ ,  $v_1$ ,  $v_0$ , which are functions of the previously determined inputs  $\delta^*$ ,  $v_2$ ,  $\gamma_{1,2}$ , resulting in:

$$\delta = \arctan \left[ \text{sign}(v_0) \cdot \text{sign}(L_{0b}) \cdot \frac{L_{0f}}{v_0} \left( -\frac{v_1}{L_{0b}} \sin \gamma_1 + \frac{L_{1f}}{L_{0b}} \dot{\theta}_1 \cos \gamma_1 \right) \right]. \quad (7.23)$$

The steering angle  $\delta$ , obtained from (7.23), can now be fed as an input to the model representing the vehicle combination. Although the equation holds for both driving directions, the controller gains depend on the driving direction, and the dimensions of the vehicle combination.

The gains  $K_y$ ,  $K_I$ ,  $K_\theta$  and parameters of preview distance  $P_{D_{1,2}}$  are obtained through a step-wise tuning approach, which in principle aims to minimize the mean squared lateral tracking error  $e_{y_U}$ , defined as:

$$MSE_{e_{y_U}} = \frac{1}{n} \sum_{i=1}^n e_{y_U(i)}^2. \quad (7.24)$$

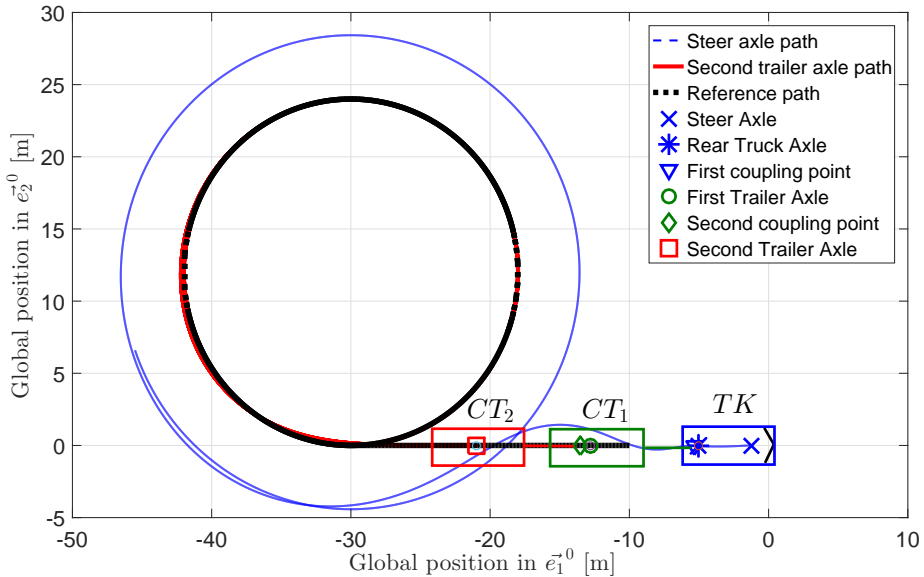


Figure 7.10: Test case reference path used for the controller gain tuning during the reversing. It is represented by a straight line segment which develops into circle with constant radius  $R=12$  m.

A test case reference path consisting of a combination of a straight road segment which develops into a circle with a constant radius has been chosen for both forward and reverse direction to optimize the gains. This path enables to optimize the behaviour when the road curvature changes, moreover it allows to observe the decay of both  $e_{y_U}$  and  $e_{\theta_U}$  with time. The radius is selected to achieve at least the same curvature as the reference paths for the docking manoeuvre. In case of a vehicle combination of a rigid truck with two central axle trailers a radius of 12 m has been selected as depicted in Figure 7.10.

The reason for using this approach is to eliminate the sign changes of lateral  $e_{y_U}$ , which would indicate an oscillatory steering input which is not desirable because of the increased steer effort. Apart from  $MSE_{e_{y_U}}$  also  $e_{\theta_U}$ , and the steering angle  $\delta$  in terms of amplitude and rate limits, are monitored during the tuning process. They are however not considered in the cost function during gain optimization as the minimization of  $MSE_{e_{y_U}}$  is dominant and including additional dependencies in the cost function would increase complexity.

The tuning process consist of four consecutive steps, and to certain extent, is based on logics of the Ziegler-Nichols approach [139] of tuning PID controllers. The steps are as follows:

1. At first, only a single look ahead point is used by setting  $w_1 = 1$ , and  $K_I = K_\theta = w_2 = k = 0$ . Next, the combination of  $K_y$  and  $P_{D_1}$  is tuned, as these two gains have the most significant impact on the poles loci of the closed loop



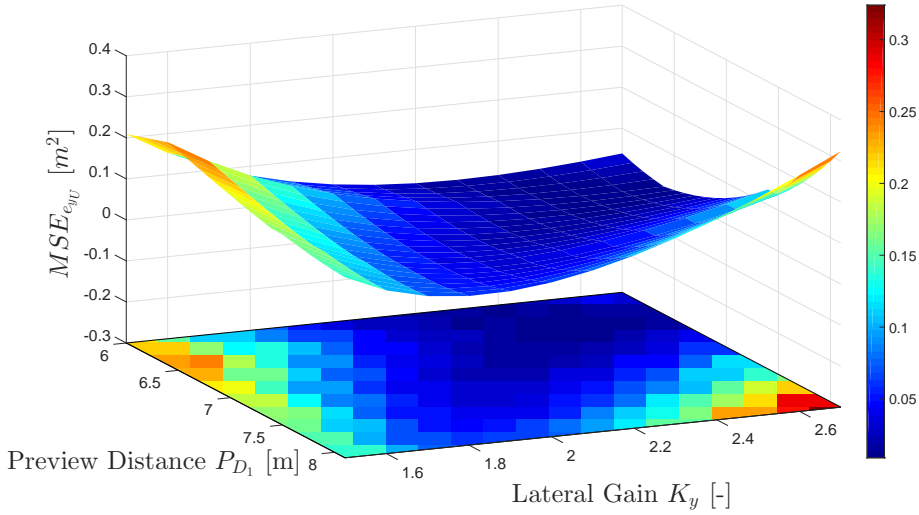


Figure 7.11:  $MSE_{e_{yU}}$  as a function of  $K_y$  and  $P_{D1}$ .

transfer function which will be discussed hereafter (and as shown in Appendix C). Permutations of  $K_y$  and  $P_{D1}$  are tested for a given vehicle combination for the test case reference path. The resulting map of  $MSE_{e_{yU}}$  dependent on  $K_y$  and  $P_{D1}$  is depicted in Figure 7.11, where the colour bar indicates the magnitude of  $MSE_{e_{yU}}$ .

2. In the second step the relation between the first and second preview distance is determined. Hence, a second look ahead distance  $P_{D2}$  is included and  $K_y$ ,  $P_{D1}$  are kept constant as obtained from step 1. The scaling coefficient  $k$ , used to determine  $P_{D2}$ , is varied in interval (1.2, 2), while keeping the remaining gains to zero. Based on the smallest  $MSE_{e_{yU}}$  the value of scaling coefficient  $k$  is chosen.
3. Thirdly the integral part is included.  $P_{D1}$  and  $P_{D2}$  are kept constant at the values obtained in step 2 through the scaling coefficient  $k$ .  $K_y$  and  $K_I$  are tuned again by minimizing  $MSE_{e_{yU}}$ , whilst keeping  $K_\theta$  zero.
4. The last step includes the interaction of all the gains. In this step the  $P_{D1}$ ,  $P_{D2}$  and  $K_I$  are kept constant at the values resulting from all previous steps. The remaining gain  $K_\theta$  can not be tuned individually while disregarding  $K_y$  as both these proportional gain values provide a similar outcome. Hence the final values for  $K_y$  and  $K_\theta$  are obtained by minimizing  $MSE_{e_{yU}}$ .

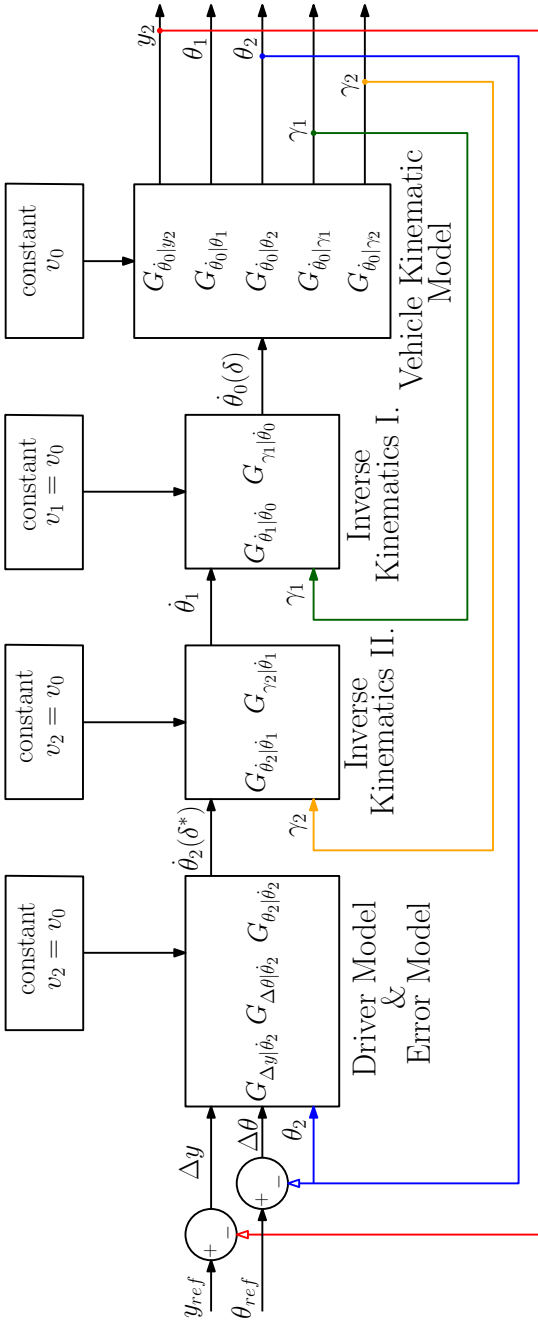
Although the resulting set of controller gains does not guarantee optimal controller performance, as the parameters have not been all tuned simultaneously, the proposed stepwise approach is very efficient in terms of low computational demands, clarity, and applicable for both driving directions. Moreover, it has proven to be functional for different vehicle combinations, while satisfying the control objective. The numerical values of all gains for two selected vehicle combinations, which are used later for the validation, are listed in Appendix D.

Besides the tracking performance, tuning of the gains should result in a stable closed loop system. The error model, the driver model, inverse kinematics and the vehicle represented by the kinematic model, from scheme in Figure 7.8, are linearised for the error stability analysis, whilst considering the vehicle combination driving along a straight reference path.

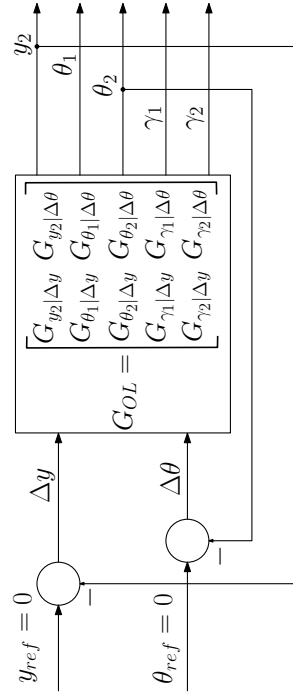
This leads to a number of approximations as:

- All angles are considered sufficiently small such the trigonometric functions can be simplified in following sense;  $\cos \gamma_1 = \cos \gamma_2 = 1$ ,  $\tan \delta = \delta$ ,  $\tan \delta^* = \delta^*$ ,  $\sin \gamma_1 = \gamma_1$ ,  $\sin \gamma_2 = \gamma_2$ ,  $\sin \theta_2 = \theta_2$ ,  $\cos \theta_2 = 1$ .
- Longitudinal velocities of all vehicle units in the combination are equal, i.e.  $v_0 = v_1 = v_2$ .
- The state equation  $\dot{x}_0 = v_0 \cos \theta_0$  of the kinematic model which is used to derive  $x_2$  can be disregarded. Considering the points on the straight reference path, defined as  $R_i = [X_{ref}, 0, 0]$ , the longitudinal component  $\Delta x = x_2 - X_{ref}$  measured in  $\bar{e}^0$ , and used as input to calculate the lateral error  $e_{yU}$  according to (7.11), will always result nil because  $x_2 = X_{ref}$ .

The set of linearised equations can be found in Appendix C. For the error stability analysis hereafter, the linearised differential equations are transformed into the transfer functions, which allow easier manipulation with internal loops in order to convert the original scheme depicted in Figure 7.12a into the equivalent form, shown in Figure C.1b, which is accounted to be more convenient for the stability assessment.



(a) Original closed loop scheme.



(b) Equivalent closed loop scheme used for stability assessment.

Figure 7.12: Linearised closed loop structure.

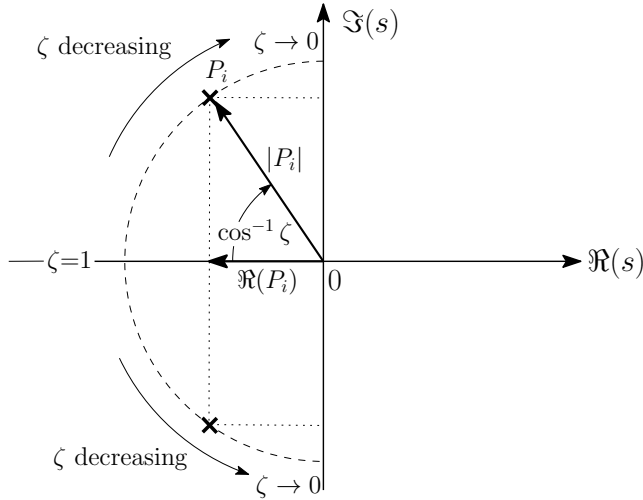
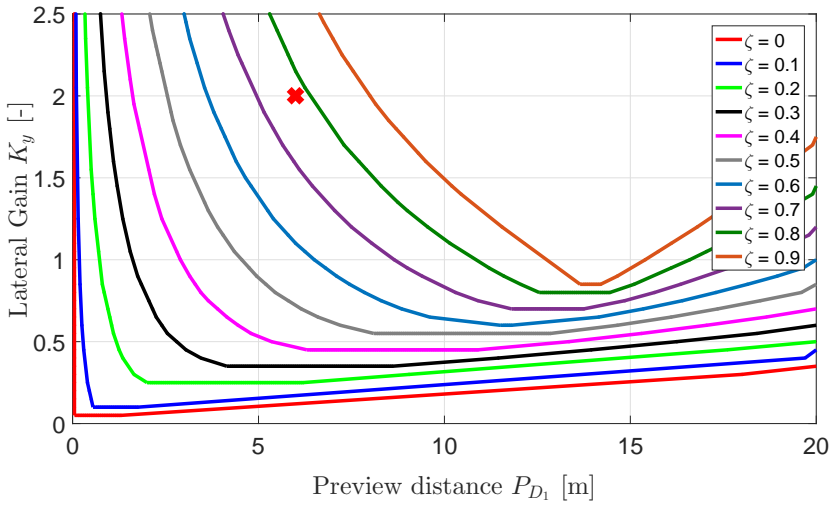


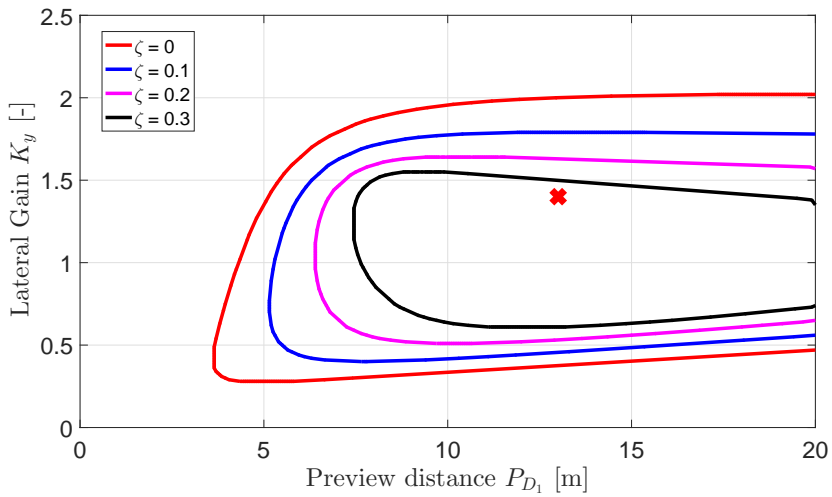
Figure 7.13: Definition of damping ratio  $\zeta$  of the system pole  $P_i$  in s-plane.

The validity and the accuracy of open loop transfer function  $G_{OL}$  against the set of original non-linear equations was examined too whilst providing equal input in terms of  $\Delta y$  and  $\Delta \theta$  and comparing articulation angles  $\gamma_1$  and  $\gamma_2$ . The results listed in Appendix C confirmed that both  $\gamma_1$  and  $\gamma_2$  obtained through  $G_{OL}$ , are in acceptable agreement with the original set of non-linear equations in an intervals  $-25^\circ < \gamma_1 < 25^\circ$ , and  $-20^\circ < \gamma_2 < 20^\circ$ , thus  $G_{OL}$  can be considered representative for the stability analysis. Beyond this interval the accuracy decreases, but the system reachability, as explained in Chapter 6, may be compromised anyway due to maximal applicable steering angle. Moreover, the maximal articulation angles observed during the docking manoeuvre remain within this interval, thus  $G_{OL}$  can be used without a need to additionally linearise the model around the equilibrium in a curved path.

As already stated during the controller tuning, the preview distance  $P_{D_1}$  and the proportional gain  $K_y$  are the two parameters having the biggest influence on the locus of closed loop system poles, and thus also on stability. The combination of  $P_{D_1}$  and  $K_y$  will be studied next with their impact on the damping ratio  $\zeta$ , which will be used as stability criterion. The remaining controller parameters as  $K_I$ ,  $K_\theta$ ,  $k$  are kept at the nominal values obtained from the controller tuning procedure. The dynamics of the system is governed by the poles of  $H(s)$ , which is the closed loop transfer function defined as  $H(s) = G_{OL}(s)(I + G_{OL}(s))^{-1}$ . To fulfil the stability criterion, all poles  $P_i$  of closed-transfer function  $H(s)$  need to satisfy  $\Re\{P_i\} < 0$ . As depicted in Figure 7.13, the least damped poles loci can be furthermore exploited to determine the damping ratio given by  $\zeta = -\frac{\Re\{P_i\}}{|P_i|}$ , which for stable system needs to comply with  $\zeta > 0$ . Considering that the closed loop transfer function has a number of poles, for the calculation of  $\zeta$  the pole  $P_i$  with the lowest damping value is always selected. These poles will have a dominant effect for the system dynamics and stability.



(a) Damping Ratio  $\zeta$  TK-CT-CT reversing



(b) Damping Ratio  $\zeta$  TK-CT-CT driving forward

Figure 7.14: Damping ratios  $\zeta$  of rigid truck with two central axle trailers for reversing and forward driving. Red marker is designating the combination of  $K_y$  and  $P_{D_1}$  obtained by the tuning of the controller.

The plot of constant damping lines of  $H(s)$  for both reverse and forward driving direction of a rigid truck with two central axle trailers (TK-CT-CT) can be seen in Figures 7.14a, and 7.14b, respectively. The red cross marker designates in both Figures the combinations of  $K_y$  and  $P_{D_1}$ , which are found in the tuning procedure to deliver the smallest  $MSE_{e_y}$ . Both the dimensions of the full scale vehicle combination and the controller gains may be found in Appendix D. It can be seen that the shape of constant damping lines for both reverse and forward driving direction differ considerably. In case of reversing the tuned combination of  $K_y$  and  $P_{D_1}$  delivers damping that is approximately two times bigger than for forward driving. The last vehicle in the combination is considerably less responsive when driving forward, which explains lower damping ratio of the loop that is needed to minimize  $MSE_{e_y}$ . Moreover it can be seen that the choice of the lateral gain  $K_y$  is more sensitive to the stability of the system than in the reverse direction. Nevertheless the combinations of  $K_y$  and  $P_{D_1}$  in both cases delivers  $\zeta \gg 0$  confirming the stability during the docking manoeuvre.

## 7.5 Conceptual Functionality of the Driver Support System

Having a path planner for parallel docking scenario with a bi-directional controller defined, in this section a framework of driver support will be outlined for which these two components can be directly adopted.

As confirmed by the measurements, presented in Chapter 6, during the low-speed manoeuvring with articulated vehicle combination the driver primarily suffers from a lack of view from the cabin, which is limited to the frontal outlook and the rear mirrors. Moreover, he is challenged to control the naturally unstable vehicle combination during reversing at the area which is very limited in space. The situation gets further complicated by the fact that typically no sensors on the trailing units are available, which otherwise would ease up the operation for the driver to localize the position and orientation of the vehicle combination with respect to the distribution center. Conventional GPS does not provide sufficient accuracy to determine the vehicle combination pose.

Given these constraints a last mile driver support is proposed, which employs computer vision based localization and smart devices as shown in Figure 7.15.

At first instance a driver is expected to possess any smart device, which can be used as Human Machine Interface (HMI) and where he can download a specially dedicated app, which will enable him to connect to the Warehouse Management System (WMS) while entering a specific distribution center area. The WMS, which assigns the identification number of loading dock, will subsequently navigate the driver with a conventional GPS-basis to the vicinity of the loading dock. Herewith, all vehicle units are accurately localized with respect to the loading dock by a computer vision system using the feeds from the camera cluster that is connected permanently to WMS. The cameras can be based either stationary, attached to the dedicated masts or distribution center, or fixed to the moving platforms such as e.g. Unmanned Aerial Vehicles, which would offer more flexibility but also add considerable complexity. The



Figure 7.15: Concept of Driver Support Functionality using the vision based localisation, smart phone as HMI.

pose of vehicle units obtained through the computer vision localization is provided directly to the app of the smart phone/tablet through the WMS.

The path planner and the bi-directional controller are considered to be a part of the app. Therefore the app can provide a driver with the reference path for both forward and reverse move of the docking manoeuvre, based on the known dimensions and kinematic behaviour of the vehicle combination. The vehicle dimensions can be entered manually by the driver or eventually also delivered by the computer vision system that should be able to localise the positions of the wheels and couplings. Having the reference path defined, the driver will be advised to activate the low-speed cruise control and fully concentrate on the control of the steering wheel. The steering angle, which is subsequently advised to the driver, will be derived by the bi-directional controller, based on the tracking error between the reference path and the actual pose of the vehicle combination, which is obtained through computer vision localization.

In the future it is foreseen that most of the hauling units will be equipped with active elements supporting the steering of the front axle [130]. This will enable actuation of the steering angle without the driver's intervention. Such a option would allow autonomous docking.

## 7.6 Summary

In this chapter a driver support system for manoeuvring of multiple articulated vehicles is proposed using a generic bi-directional path following controller that is applied to a vehicle combination consisting of a rigid truck with two central axle trailers. Furthermore, a novel approach to define the reference vehicle path for a parallel docking scenario of the rear most vehicle is proposed. The path planner considers the vehicle kinematic behaviour in combination with the Dubins curves which are optimized in terms of distance travelled. The bi-directional controller is based on vehicle kinematic behaviour and is a combination of proportionately-integral control actions. It employs 5 parameters in total, of which the tuning approach is outlined too. The closed-loop stability has been verified using linearised system. Finally, the general functionality of the vehicle localization and the driver support framework is outlined.



# Chapter 8

## Implementation and Testing

### 8.1 Introduction

In this chapter a number of steps is described to verify the functionality of the control strategy and the path planner for various scenarios.

First, several simulations are conducted with the high-fidelity multi-body model, as introduced in Chapter 3 combined with the bi-directional controller as designed in Chapter 7. Since the multi-body model is validated with experimental data and is considerably more complex than the set of kinematic equations used in Chapter 7, it can be considered as a more accurate representation of the real vehicle behaviour.

Subsequently, the controller is deployed on a scaled vehicle combination model, and tested in a laboratory environment. With this setup also the robustness of the controller is being examined due to errors, which are present and vehicle localization because of the limited accuracy of the used actuators.

In both cases the aim is to assess the performance of the control strategy. The tracking errors are used as a measure to judge the controller performance in accordance with the control goal. The chapter is concluded with a summary of the results achieved and a discussion.

## 8.2 Testing with Multi-Body Simulation Model

The goal of this phase is to assess the performance of the control strategy using a vehicle model that is closer to the real operational conditions. Therefore, the vehicle block, depicted in Figure 7.8 of the control scheme, will be substituted by a multi-body model that is more advanced than the kinematic model used previously. The kinematic equations (7.13) are in particular replaced by the high-fidelity multi-body dynamic model of rigid truck with two center axle trailers (TK-CT-CT), which was modelled by the library described in Chapter 3. The multi-body model library was validated using the measurements and includes non-linear tyre behaviour, mass distribution and inertial effects, suspension, compliant chassis, and other effects not present in the kinematic model, and for which it can be considered as a more realistic representation. The main dimensions of the model, as well as controller parameters can be found in Appendix D.

The controller performance is tested for the parallel docking manoeuvre, where the vehicle combination is initially aligned with the distribution centre and needs to be parked perpendicularly to the loading dock gate. The reference path is generated by the path planner, described in section 7.3, and is executed along the reference path in two steps: forward driving move designated by a red dashed line in Figure 8.1, and reversing move represented by the dashed magenta line in the same figure. During the simulation the moves are separated with a 5 seconds long transition time when the velocity is zero, which is used to bring the steered axle to the initial straight position. For the rest of the time the velocity for both forward driving and reversing is set constant to 1 m/s.

The simulation results shown in Figure 8.1 display the reference and the accomplished path of the controlled point  $U$  that is placed precisely in between the axles of rear most trailing unit. The results show that the proposed controller is capable to perform well also in combination with a more complex vehicle model. The steering angle and the velocity are given in Figure 8.2a and 8.2b, respectively. Each move starts with a zero steering angle. As depicted, the steering angle stays within the range of  $\pm 30$  deg, with very smooth changes that does not require a high steering rate and thus can be accomplished by the driver.

The tracking errors  $e_{y_U}$  and  $e_{\theta_U}$ , as defined by (7.11) and (7.12), are depicted in Figure 8.2c and 8.2d for the forward and reverse move with blue and red color, respectively. It can be observed, the maximum lateral error  $e_{y_U}$  reaches a value of approximately 0.5 m during the forward move. It is caused by the reference path for the forward move, which is constituted by a Dubins curve. The path consists of a straight segments that are combined with arcs of given maximum curvature  $\kappa_{max}$ . As the directional response of the second trailer is slow and the yaw angle can not be actuated directly, it always needs to travel certain distance to build-up the required curvature. Therefore the lateral error  $e_{y_U}$  is peaking at the transitions between the straight segments and arcs. In general, the lateral error can be minimized by relaxing the curvature limit  $\kappa_{max}$ . This would however lead to an elongation of the reference path, which is not desirable as more space is required. An alternative approach would be to redesign the path planning algorithm and substitute the Dubins curve by a different approach generating the path for the forward move in the same spirit as the reverse motion, and

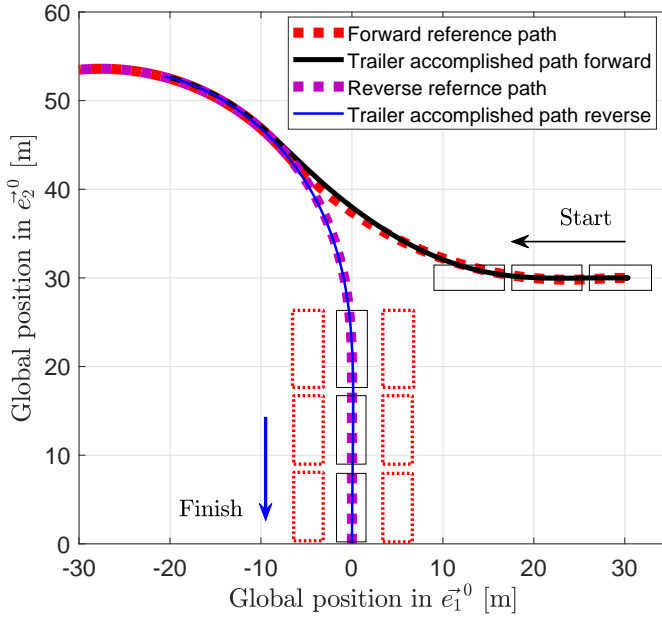


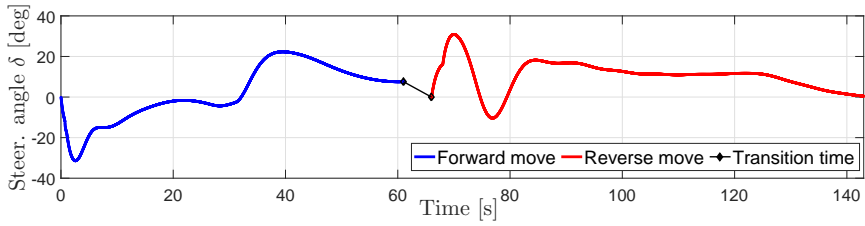
Figure 8.1: Test results of parallel docking with multi-body model.

optimising both in terms of distance travelled. Yet, this approach, and optimization in particular, will be considerably more demanding in terms of processing power and time, compared to the current approach.

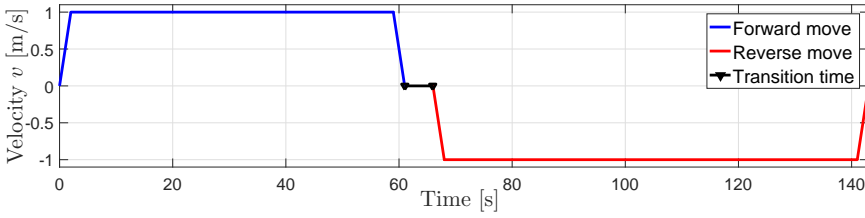
The lateral error during the reversing move is substantially smaller and varies in a range  $\pm 0.1$  m. The final lateral error at the loading dock is smaller than 0.3 cm. The orientation error  $e_\theta$  does not exceed 0.5 deg. The articulation angles  $\gamma_1$  and  $\gamma_2$  are given in Figure 8.2e. Both angles are showing similar trends and are within a range of  $\pm 20$  deg.

### 8.3 Implementation in a Down Scaled Physical Demonstrator

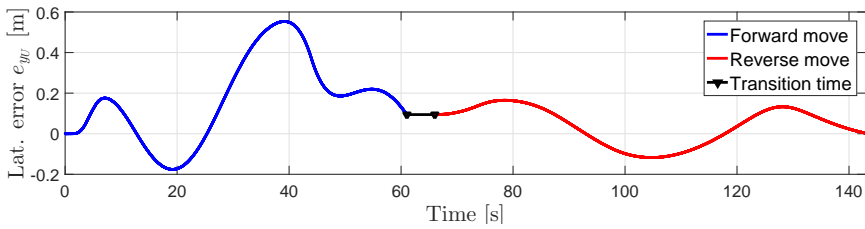
To test the performance of the controller in the physical world, a down scaled test setup is designed. It consists of controller on designated computer, camera based localisation system, scaled vehicle models (1:14), that can be actuated on a remote basis, and a model of a distribution center, as shown in Figure 8.3.



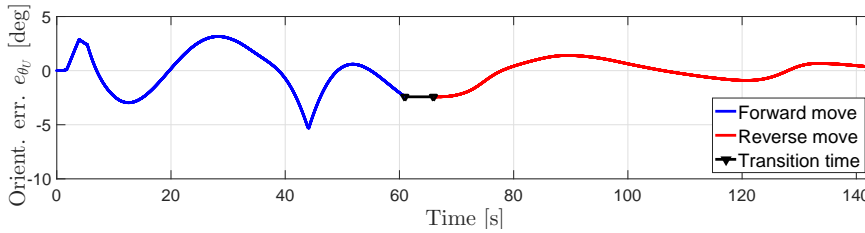
(a) Steering angle



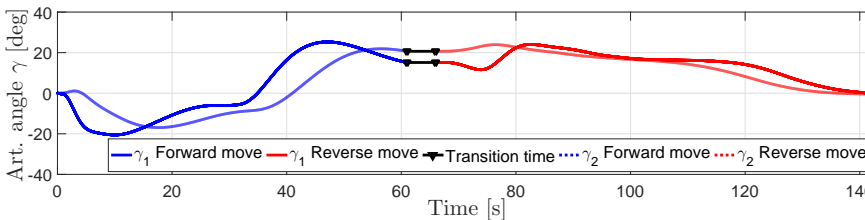
(b) Longitudinal velocity of the Truck



(c) Lateral tracking error



(d) Orientation tracking error



(e) Articulation angles

Figure 8.2: Simulation results of parallel docking with multi-body model.

Each vehicle unit in the combination is equipped with a unique fiducial ArUco marker [49] placed on the top of the vehicle. The markers are used to improve the accuracy and the robustness of vehicle localisation by the camera. Additionally, the origin of the world based coordinate system  $\bar{e}^W$  is represented by a fiducial marker placed in the neighbourhood of the destination point. This ensures the path planning and the vehicle localization are independent of the camera pose, as depicted in Figure 8.4.

In the scaled test environment, the markers are detected with a fixed-base camera which is attached to the ceiling and points downwards. The test area of interest is covering a space of approximately 5 x 5 m. The technical specifications of the camera are listed in Table 8.3.



Figure 8.3: Scaled vehicle combination with distribution center behind.

Specification	Description
Lens	8 mm FL Compact Fixed Focal Length Lens
F-stop	f/1.4
Focal length [mm]	8
Sensor	CMOSIS CMV4000-3E5
Resolution	2048x2048
Frame Rate [Hz]	90 (max)
DR (normal/HDR)	53.19 dB/-

Table 8.1: Grasshopper3 -U3-41C6C technical specifications.



Figure 8.4: Scaled test setup - localization camera topview

As described in section 7.5, the stationary cameras are connected to the system which is responsible for computer vision post-processing and delivering the vehicle combination coordinates. The camera in the scaled test setup is employed in the same fashion. As can be seen in Figure 8.5, the vehicle pose is calculated from captured camera images by detecting the markers and subsequent conversion from the pixels to the domain of length (P2L) units in  $\vec{e}^W$ . For the computer image processing the OpenCV software package is used. Extensive description of camera related aspects of the scaled test setup, which also discusses pose estimate accuracy, camera calibration procedures and conversion of the pixels to the length units domain, can be found in [78]. Next, the coordinates are sent to the Vehicle Control cluster, depicted in Figure 8.5 by a blue dotted line, which is running on the same computer but in a MATLAB environment. The Vehicle Control Cluster contains the path planner and the path following controller which will be in the real life substituted by the driver support app, described in section 7.5.

The parallel docking manoeuvre, representing the test scenario, is defined through a set of reference points  $R_i$  that specify the reference path for forward and reverse move in the coordinate system  $\vec{e}^W$ . Both moves are generated by the path planner as described in Chapter 7, taking into account the dimensions of the scaled vehicle combination, its arbitrary initial and known terminal pose with respect to the  $\vec{e}^W$  origin, and the maximum steering angle of the scaled truck.

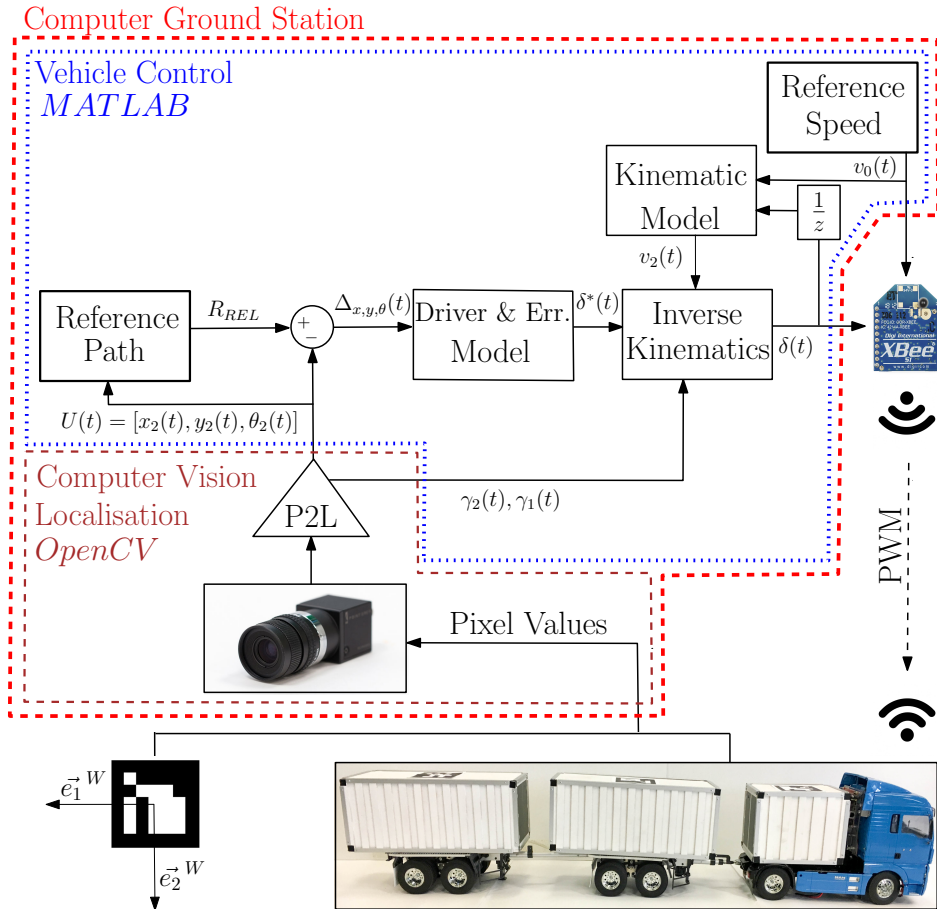


Figure 8.5: Scaled test setup - low-level scheme.

The vehicle combination's pose is acquired by the camera feed determines the positional errors  $\Delta_{x,y,\theta}$ , which are used as an input to the error model to calculate tracking errors  $e_{yU}$ ,  $\phi$ ,  $e_{\theta R_1}$ , as shown in Figure 8.5. The tracking errors, together with articulation angles  $\gamma_1$ , and  $\gamma_2$ , are subsequently used as an input to the controller combining the driver model and the inverse kinematics as described in Chapter 7. The second input to the controller is the velocity of the rear most trailing unit  $v_2$ , which is not obtained through the camera localization system. This is because the camera stream frame rate per second is not constant and acquiring of  $v_2$  would therefore require additional post-processing.  $v_2$  is calculated instead by the kinematic model using known  $v_0$  and  $\delta$  as inputs. In order to avoid an algebraic loop the steering angle signal is delayed with one step as shown in Figure 8.5. The target steering angle  $\delta(t)$  is converted to a pulse-width-modulated (PWM) signal and it is sent through the X-bee wireless module of the scaled tractor. The reference speed of the tractor  $v_0$  is kept constant for each move of the docking manoeuvre. The signal is also transmitted

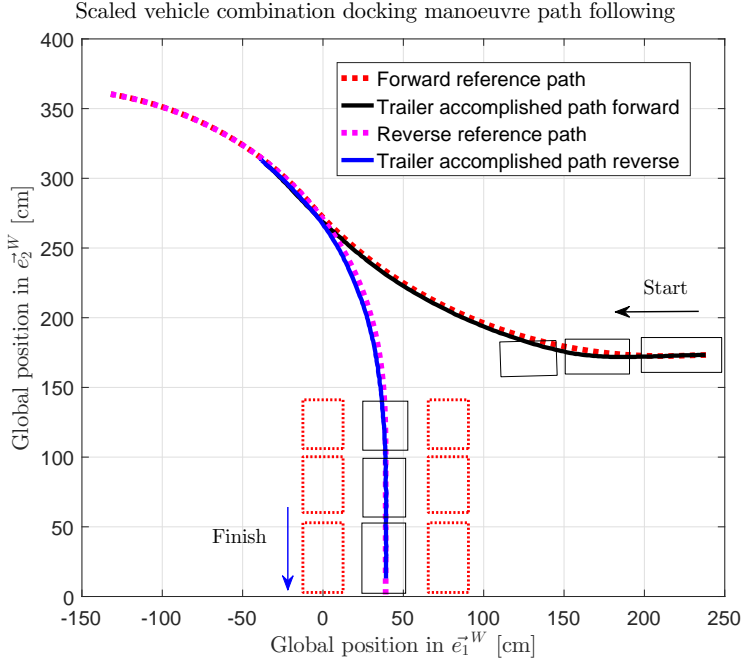


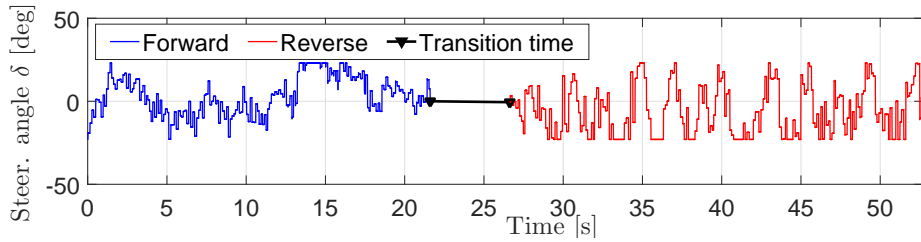
Figure 8.6: Test results of parallel docking with down scaled physical demonstrator.

from the computer ground station through the X-bee as PWM 8-bit integer, as shown in Figure 8.5.

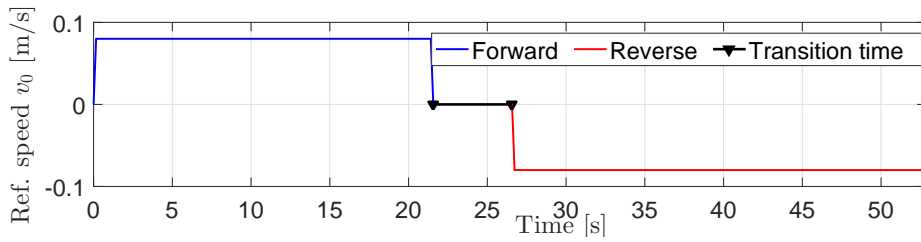
The X-bee on a scaled vehicle is linked to the embedded controller Olimex STM32-E407, which is programmed by the HAN MBD-Toolset [52]. The embedded controller actuates the torque at the driven axle and the steering angle through a speed controller and servo motor, respectively. The drive torque can be both positive and negative enabling bi-directional cruising. To ensure a constant driving speed of the hauling unit under various loading conditions an encoder is placed on the drive shaft whose signal is used for feed-back control of the velocity. The steering angle can be actuated with a resolution of one degree in theory. In practice it appears problematic to achieve this due to considerable play in the steering mechanism ( $\pm 5$  deg). Moreover, the maximum applicable steering angle of the scaled truck ( $\pm 23$  deg) reaches only a half of the value the real vehicle typically has, which limits the manoeuvrability to large extent. As in section 8.2 the test is performed with double articulated vehicle combination consisting of a rigid truck with two central axle trailers (TK-CT-CT). Its dimensions as well as controller parameters can be found in Appendix D.

The results provided in Figure 8.6 display the reference against the accomplished path of the rear most central axle trailer. The tracking errors  $e_{y_U}$  and  $e_{\theta_U}$ , are depicted in Figure 8.7c and 8.7d for forward and reverse movement with blue and red color, respectively. The articulation angles  $\gamma_1$  and  $\gamma_2$  are given in Figure 8.7e. The exact steering angle is not known as there are no sensors placed directly on

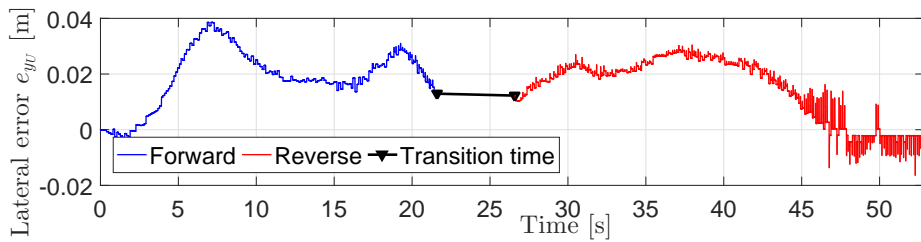




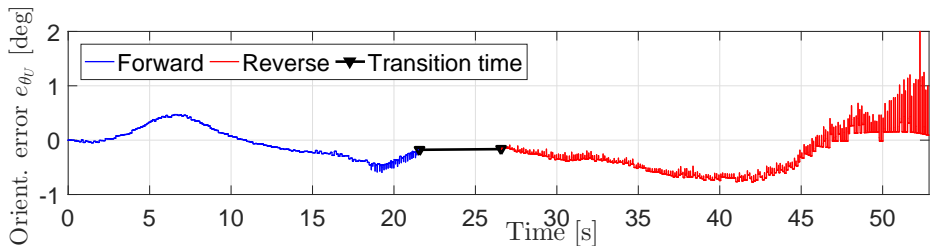
(a) Steering angle



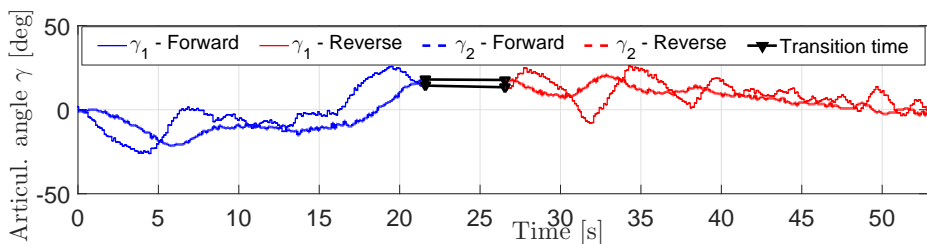
(b) Reference speed



(c) Lateral error



(d) Orientation error



(e) Articulation angles

Figure 8.7: Simulation result of parallel docking scaled demonstrator.

the steering knuckle. Therefore only the requested steering angle by the controller is depicted in Figure 8.7a. As can be seen the steering signal is very noisy and oscillatory because of the poor accuracy in actuation caused mainly by the play in the steering mechanism. The target velocity requested to the actuator for both motions is kept constant and equals 0.08 m/s as shown in Figure 8.7b. The maximal lateral error is kept below 4 cm for the forward motion, and below 3 cm for the reversing motion. The tracking for the forward move appears to be more difficult to negotiate due to slow vehicle response, limitations in maximum applicable steering angle, and reference path shaped by Dubins curve. This results in slow response to the fast curvature changes of the reference path as already observed with the multi-body model. Also here the maximal curvature limit can be relaxed, leading to smaller errors but elongation of the manoeuvre. The orientation error oscillates between  $\pm 0.5$  deg, which is acceptable. While studying the first articulation angle during the reverse motion, designated by the red solid color on Figure 8.7e, an oscillatory behaviour can be noticed. This is primarily caused by the limited accuracy of the steering angle actuator and considerable play in the steer mechanism.

Regarding the error calculation from the camera images, it can be seen in both cases in Figures 8.7c, and 8.7d, that the error at the end of the manoeuvre is rather noisy. This is caused by the camera lens limitations, which does provide decreased accuracy when the object is near the camera's field of view limits. The final error measured by the camera at the dock reaches approximately 2 mm, and 0.2 deg, which is considered to be sufficiently small also if scaled up.

## 8.4 Summary

In this chapter the previously developed path planner and bi-directional path following controller have been tested on a high-fidelity multi-body model and scaled demonstrator test environment. In both cases the results meet the control objectives, and the final pose of the vehicle combination meets the real-world tolerances of the loading dock gate being typically  $\pm 5$  cm, and  $\pm 0.5$  deg for lateral and orientation error, respectively. The observations are as follows:

- The highest lateral errors occur during the forward motion of the docking manoeuvre at the regions where the straight segment of the reference path transforms into an arc. This issue is a result of the nature of the Dubins curve, which combines only the straight segments with the arcs of constant curvature, and thus does not reflect on the transient yaw response of the last vehicle. Although tests did not reveal any direct impact of the path generated by Dubins curve on the ability of the controller to complete the docking manoeuvre within the tolerance limits, it is expected that customizing the reference path for the forward motion closer to the kinematic response of the last vehicle will be beneficial for the overall robustness of the algorithm.
- Detecting the pose of the marker is problematic near the edges of the camera's field of view. Hence for further implementation it is desirable to introduce a safety margin around the camera's field of view.

- Even though the scaled vehicle model experiences significant play in the steer mechanism, the experiments proved to be successful. It is because of the steer actuator speed, which to a certain extent compensates for the inaccuracies in the actuation. Resulting yaw behaviour is however oscillatory, which can be well noticed on the first articulation angle  $\gamma_1$ .



## Chapter 9

# Conclusions and recommendations

The road freight transport demand in EU is expected to increase considerably in the near future. Hence, there exists a need to enhance the road freight transport efficiency to meet the future targets of  $CO_2$  emissions, while operating within the available infrastructure, and maintaining road safety. One of the solutions to face this forthcoming challenge is the application of High Capacity Vehicles. Although HCV's have already proven their benefits in many countries worldwide, their wider implementation in EU has not been accomplished yet. Considering that, the relevance of HCV's for Europe was analysed in this research in two perspectives:

- **Application of Performance Based Standards** as an alternative legislative framework for Europe ensuring safe, infrastructure and environment friendly vehicle performance.
- **Improving the manoeuvrability** of HCV's at low-speeds, which appears to be one of the main limitations due to their increased overall length.

The conclusions and recommendations related to each of the research objectives are addressed in the following sections.

## 9.1 Conclusions

### Application of Performance Based Standards

Even though the current European legislative framework is mainly prescriptive it contains some performance based elements. However, there exists almost no projection of the vehicle performance on the aspect of vehicle operation within the infrastructure network. This restrains more efficient employment of the available infrastructure and may compromise the operational safety and infrastructure deterioration. On the contrary, proposed performance oriented framework ensures a proper match between the vehicle combination and categorized segments of the infrastructure network through explicitly defined performance measures covering the safety, infrastructure impact and societal benefits. The resulting performance of a commercial vehicle can be subsequently used as an access criterion to specific segments of the infrastructure network that is previously assessed and categorized into a number of levels according to design criteria, geographical position, or bearing capacity.

The proposed principles of the performance oriented framework provide more flexibility in the design of vehicle combinations, not being constrained by dimensions, but eliminating dimensional creep which may represent potential danger when the performance criteria are not met. Additionally, it stimulates the development of novel technologies that ensure safety and leads to innovations enhancing the vehicle performance.

Considering the performance legislation being in place, three High Capacity Vehicle combinations are defined that comply with logistic demands for the years 2020+. The future vehicle concepts emits between 8-38% less  $\text{g}/\text{m}^3\text{km}$  of  $\text{CO}_2$  compared to current vehicle combinations. As for the total cost of ownership, the reduction yields between 15-51% of  $\text{€}/\text{m}^3\text{km}$ . Innovations enhancing the performance of the vehicle combinations are:

- Active axle steering of one or more trailing units reduces considerably the swept path and improves the low-speed manoeuvrability.
- A distributed hybrid powertrain enables the vehicle combination to meet uphill performance and at the same moment harvest energy when braking.
- Actively controlled aerodynamic devices such as a trailer boat tail and side skirts, or a prolonged cabin end design will reduce the vehicle combination air drag, and thus improve both environmental and economical performance.
- Increased transport capacity per vehicle combination is beneficial. Future vehicle combinations should use multiples of standardized inter-modal loading units with efficient floor utilization of Euro-pallets. Preferred loading units are 45-foot ISO container, and C745 Swap Body.

### **Improving manoeuvrability of HCV's**

The manoeuvrability of High Capacity Vehicles is compromised with their increased length but can be improved by active axle steering of the trailing units. Herewith, the potential gain for both low- and high-speed performance improvement is considerable. Applying the proposed steering control to all trailing units axles the gain yields in 55% reduction of the low-speed swept path and the rearward amplification is reduced by 33% and 60% for the first and second trailing unit respectively. The gain scheduling control strategy, that is used, enables to maintain one controller structure during entire range of operational speed, which simplifies the implementation.

From measurements it can be concluded that decisive reasons making reversing of articulated vehicles difficult are a limited field of view and the open-loop instability of the vehicle combination. As further confirmed by experiments, the driver performance can be improved by placing suitable referencing markers on the trailing units, which improves their visibility by the driver yet remains very impractical. Therefore a feasible way to support the driver is through the extension of the field of view by cameras placed in a surroundings of a distribution center and a navigation, which consists of reference path planner and the controller providing a steering angle to follow the reference path. Given the fact that none of the vehicle units is equipped with sensors enabling sufficiently accurate localization, the surroundings cameras are to be used for the pose measurement whilst adopting computer vision processing techniques.

The parallel docking manoeuvre towards the distribution center is the most frequently used low-speed operational scenario, which involves reversing of a vehicle combination. Therefore the proposed path planner is aiming at this scenario in particular. The reference path for parallel docking is planned and optimised in two moves using the principles of the vehicle kinematic behaviour and Dubins curves. It can be applied to arbitrary vehicle combinations and does not require high computational demands.

The proposed bi-directional path following controller adopts the principle of a virtual tractor, and is based on the vehicle inverse kinematic behaviour in combination with proportional-integral feedback control actions. The performance and functionality of the controller is verified at two levels. First it is tested with a developed and experimentally validated high-fidelity multi-body model. Herein, the final lateral and orientation error at the loading dock are 0.3 cm and 0.3 deg, respectively, for the combination of rigid truck with two central axle trailers without injecting any disturbances in the loop. Secondly, the controller is tested on a scaled test setup. This is an environment where arbitrary control strategies can be tested on scaled vehicle combinations (1:14), that are actuated on a remote basis. The vehicle units are localized by a computer vision approach, employing the fiducial markers that are placed in the top of vehicle units. The final lateral and orientation error at the loading dock achieved at the scaled test setup reach, 2 mm and 0.2 deg, respectively also for the combination of rigid truck with two central axle trailers. In both cases the final error is within the tolerances given by the spatial layout of the loading dock. Considering the path tracking performance during the entire docking manoeuvre, the maximal lateral error occurred during the forward motion, and equals 0.5 m. The error is primarily caused by sub-optimality of the reference path generated by Dubins curves for the forward motion, which does not guarantee a path that is kinematically

viable for the last vehicle unit. Hence, at the transitions of the reference path between the arcs of the constant radius and the straight segments the lateral error may increase in particular as the last vehicle unit can not instantaneously develop a yaw rotation.

## 9.2 Recommendations

### Application of Performance Based Standards

The criteria for the performance-based framework are identified and the performance of a representative vehicle fleet is simulated. Yet there exists a series of steps that need to be taken to implement this approach.

Primarily, the definition of fail/pass criteria for each measure and specific road class should be determined on EU-jurisdiction level. The main concern are Startability, Gradeability, and Low-speed swept path criteria, which are strongly linked to the infrastructure design criteria that differ per country. The jurisdictions will need to review the methodologies, and adapt them according to local operational conditions.

From the legislative perspective, a regulatory and compliance process needs to be established, in which the PBS scheme can be applied. Subsequently, guidelines that detail the procedures and processes need to be prepared. The definition of legislative arrangements needs to be developed next, so the PBS can operate as an addition to the current prescriptive regulation in the given EU jurisdictions. It is recommended to initiate a pilot project on an international level, which adopts the PBS framework and enables cross-border transport. Furthermore, a mechanism for effective enforcement and monitoring should be explored.

Given the fact that dimensions of preferable inter-modal loading units, as containers and swap-bodies, are known it is not likely that total length of future vehicle combinations will differ considerably. Therefore the approach, known as enveloping, can be exploited furthermore, where the blueprints of certain vehicle combinations are defined with a tolerances over crucial vehicle dimensions, such as for example axle positions. By respecting the tolerances the designer ensures required performance of the vehicle combination, which would simplify the vehicle assessment procedure.



### **Improving manoeuvrability of HCV's**

The proposed active axle steer control is rather demanding on the number of inputs that needs to be provided, and which may be difficult to acquire in sufficient accuracy in real-life operation. Hence, it is recommended to investigate the impact of sensor requirements such as accuracy, noise, and sampling rate on the controller functionality and performance. For the implementation standardisation of communication interfaces between the vehicle units needs to be developed as well. Next, the potential to extend current controller structure by kinematic steering should be investigated, especially for low-speed manoeuvring such that all axles are being steered on individual basis and not as a group. This would result in reduction of the tyre wear.

Given the conclusions related to the path planning, a possibility should be investigated to substitute Dubins curves by an approach that will guarantee kinematic viability of the forward move for an arbitrary vehicle combination, yet can be implemented without excessive computational demands. It is expected that this will result in a reduction of the lateral tracking error. Furthermore, the path planning can be expanded to include features as obstacle avoidance or different parking manoeuvre layouts.

For the path tracking controller it is recommended to investigate whether quantitatively comparable or even improved results may be achieved with alternative driver models, which contain less input parameters than the current one that uses two preview distances. The concept of a virtual tractor with inverse kinematics may be kept, but the tuning process may be simplified in this way. Moreover, the possibility to automate the tuning process through multi-parametric optimization can be examined. Furthermore the impact of disturbances on the performance of the controller should be investigated as well as the possibility to include a feed-forward branch in the loop. Testing the performance of the controller on more test cases is considered to be valuable too.

Considering vehicle localization, new methods are nowadays extensively used in computer vision such as machine learning in combination with plane fitting, which may be employed in order to eliminate the use of fiducial markers.

Finally, it is recommended to continue with the research when including the human subjects in the loop with docking navigation based on the developed path tracking controller. A suitable form of a guidance for the human drivers needs to be developed such that the required steering angle derived by the controller can be translated to the driver and is accepted. Feasible options for this may be the use of a haptic feedback in the steering wheel or utilization of augmented reality. Additionally, emphasis needs to be given to the ergonomics of the system, such the navigation will be effective and intuitive for the driver.



# Appendices



# Appendix A

## A Linear Model of a Double Articulated Vehicle

### A.1 Introduction

The equations of motion for a vehicle combination with two articulations points are derived using the Euler-Lagrange formalism. The resulting single track vehicle combination model does not consider individual axles in an axle group. The tyre cornering characteristics is assumed to be linear.

The modelling assumptions are discussed first and then the equations of motion for a vehicle combination are derived.

### A.2 Modelling assumptions

The following assumptions are made:

- The articulation angles and tyre slip angles are small, so  $\cos x = 1$ , and  $\sin x = x$ .
- The left and right tyres and axle kinematics can be lumped into a single equivalent tyre having constant cornering stiffness.
- Body roll and pitch are not considered i.e. the centers of gravity of all units are on the ground plane.
- Center point steering is assumed for the front axle. No pneumatic or mechanical trail is considered.
- Aerodynamic forces are not included.
- The vehicle combination has constant forward velocity.

### A.3 Derivation of equations of motion

A schematic overview of the modelled vehicle combination is presented in Figure A.1.

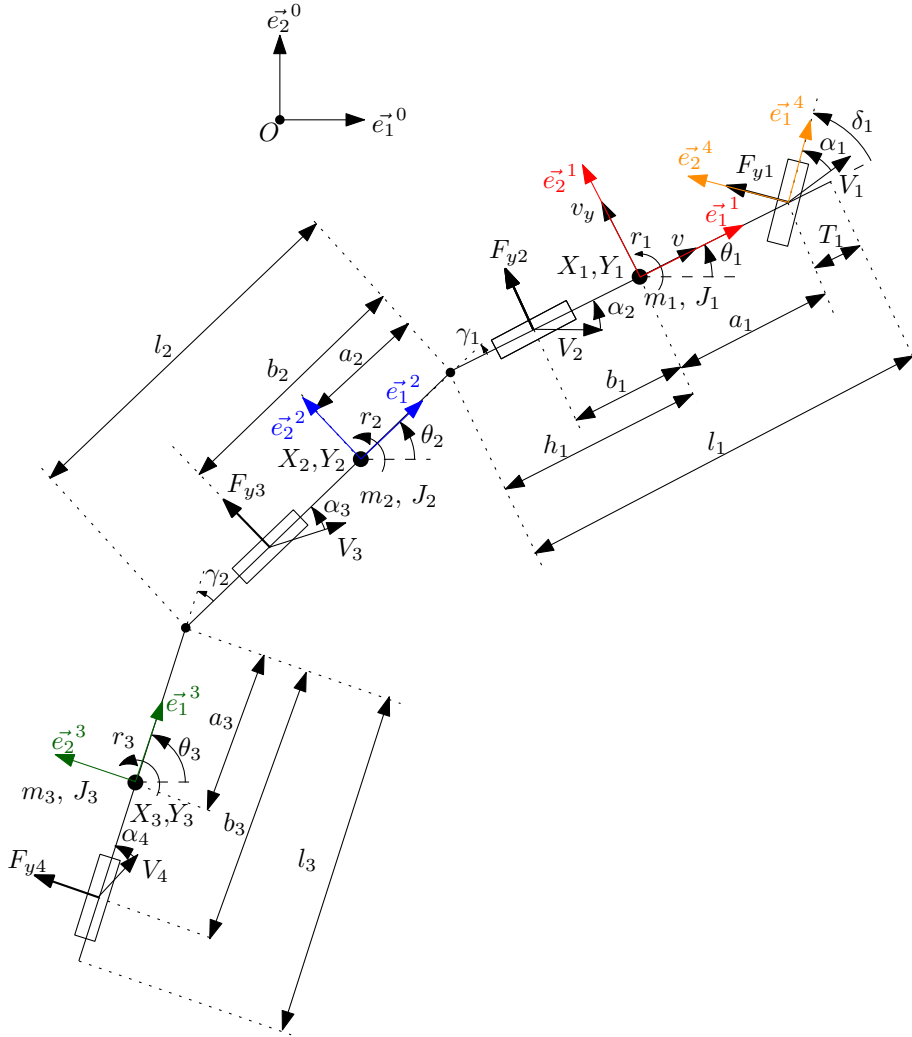


Figure A.1: Double articulated single-track vehicle model

The general form of Euler-Lagrange equations of motion is expressed in equation (A.1):

$$\frac{d}{dt} \frac{\partial T}{\partial \dot{q}_i} - \frac{\partial T}{\partial q_i} + \frac{\partial U}{\partial q_i} = Q_i \quad ; i = 1, \dots, n, \quad (\text{A.1})$$

with  $T$  the kinetic energy,  $U$  the potential energy,  $Q_i$  the generalized force,  $n$  the number of freedom degrees and  $q_i$  the generalized coordinates.

The number of equations is equal to the number of relevant generalized coordinates. The selected generalized coordinates for this vehicle combination model are the global position  $(X_1, Y_1)$  of tractor center of gravity, the yaw angle of the tractor  $\theta_1$ , and the yaw angles of the two trailer bodies  $\theta_2$ , and  $\theta_3$ , respectively. The generalized coordinates thus become:

$$q_i = [X_1, Y_1, \theta_1, \theta_2, \theta_3]^T. \quad (\text{A.2})$$

Since, the motion of the vehicle combination is only considered in the plane of  $\bar{e}^0$ , and as no springs are present the potential energy can be neglected. Therefore, the potential energy term in equation (A.1) is considered zero.

Given the fact the articulation angles and tyre slip angles are assumed to be small and longitudinal velocities of all vehicle units are considered to be constant and equal following the approximations can be justified:

$$\begin{aligned} \dot{X}_1 &= \dot{X}_2 = \dot{X}_3, \\ \dot{Y}_2 &= \dot{Y}_1 - h_1\dot{\theta}_1 - a_2\dot{\theta}_2, \\ \dot{Y}_3 &= \dot{Y}_1 - h_1\dot{\theta}_1 - l_2\dot{\theta}_2 - a_3\dot{\theta}_3. \end{aligned} \quad (\text{A.3})$$

Subsequently, the total kinetic energy of the vehicle combination can be expressed by (A.4), which is the sum of translation and rotational energies of all vehicle units:

$$\begin{aligned} T &= \frac{1}{2}m_1(\dot{X}_1^2 + \dot{Y}_1^2) + \frac{1}{2}m_2(\dot{X}_1^2 + \dot{Y}_2^2) + \frac{1}{2}m_3(\dot{X}_1^2 + \dot{Y}_3^2) \\ &+ \frac{1}{2}J_1\dot{\theta}_1^2 + \frac{1}{2}J_2\dot{\theta}_2^2 + \frac{1}{2}J_3\dot{\theta}_3^2. \end{aligned} \quad (\text{A.4})$$

$\dot{Y}_1$ ,  $\dot{Y}_2$ , and  $\dot{Y}_3$  are the absolute lateral velocities of the centers of gravity of vehicle bodies and  $m_i$  and  $J_i$  are the corresponding masses and moments of inertia.

The five coordinate systems, which are used in the derivation of the equations of motion, are represented in Figure A.1. The first is the global (earth-fixed) coordinate system  $\bar{e}^0$ , whereas,  $\bar{e}^1$  to  $\bar{e}^3$  are the local body-fixed coordinate systems of the tractor and trailer bodies, respectively. The  $\bar{e}^4$  coordinate system is the body-fixed coordinate system of the steer axle tyres. The two most relevant coordinate systems are  $\bar{e}^0$  being the world global coordinate system and  $\bar{e}^1$  being the tractor body-fixed local coordinate system.

Having an expression for the kinetic energy (A.4) the derivatives for each generalized coordinate can be determined:

$$\begin{aligned} \frac{d}{dt} \left( \frac{\partial T}{\partial \dot{Y}_1} \right) &= (m_1 + m_2 + m_3)\dot{Y}_1 - (m_2 + m_3)h_1\ddot{\theta}_1 \\ &- (m_2a_2 + m_3l_2)\ddot{\theta}_2 - m_3a_3\ddot{\theta}_3, \end{aligned} \quad (\text{A.5})$$

$$\begin{aligned} \frac{d}{dt} \left( \frac{\partial T}{\partial \dot{\theta}_1} \right) &= -(m_2 + m_3)h_1\dot{Y}_1 + [(m_2 + m_3)h_1^2 + J_1]\ddot{\theta}_1 \\ &+ (m_2a_2 + m_3l_2)h_1\ddot{\theta}_2 + m_3a_3h_1\ddot{\theta}_3, \end{aligned} \quad (\text{A.6})$$

$$\begin{aligned} \frac{d}{dt} \left( \frac{\partial T}{\partial \dot{\theta}_2} \right) &= -(m_2 a_2 + m_3 l_2) \ddot{Y}_1 + (m_2 a_2 + m_3 l_2) h_1 \ddot{\theta}_1 \\ &+ [J_2 + m_2 a_2^2 + m_3 l_2^2] \ddot{\theta}_2 + m_3 a_3 l_2 \ddot{\theta}_3, \end{aligned} \quad (\text{A.7})$$

$$\frac{d}{dt} \left( \frac{\partial T}{\partial \dot{\theta}_3} \right) = -(m_3 a_3) \ddot{Y}_1 + m_3 a_3 h_1 \ddot{\theta}_1 + m_3 a_3 l_2 \ddot{\theta}_2 + [J_3 + m_3 a_3^2] \ddot{\theta}_3, \quad (\text{A.8})$$

$$\frac{\partial T}{\partial q_i} = 0; \quad i = 1, \dots, n. \quad (\text{A.9})$$

The generalized coordinates can also be written in terms of vehicle local coordinates as follows:

$$\begin{aligned} v &= \dot{X}_1 + v_y \theta_1, \\ v_y &= \dot{Y}_1 - v \theta_1, \\ r_1 &= \dot{\theta}_1, \\ \dot{\gamma}_1 &= r_1 - \dot{\theta}_2, \\ \dot{\gamma}_2 &= \dot{\theta}_2 - \dot{\theta}_3, \end{aligned} \quad (\text{A.10})$$

where  $v$  and  $v_y$  represent the longitudinal and lateral velocity of the hauling unit defined in  $\vec{e}^1$ , respectively.  $\dot{\gamma}_1$  and  $\dot{\gamma}_2$  are the articulation rates representing the differences between yaw rates of vehicle units.

Finally, the equations of motion can be written using local coordinates only by utilizing expressions (A.10). The equation describing the longitudinal dynamics is not considered as the longitudinal velocity  $v$  is assumed to be a constant and known input. Thus, the new local coordinates for the equations of motion used are presented as:

$$q_i = [v_y, r_1, \dot{\gamma}_1, \dot{\gamma}_2]^T. \quad (\text{A.11})$$

The generalized forces can be derived as:

$$Q_i = \sum_{k=1}^4 \vec{F}_k \cdot \left( \frac{\partial \vec{P}_k}{\partial q_i} \right)^T, \quad (\text{A.12})$$

where,  $\vec{F}_k$  are the lateral tyre force vectors,  $\vec{P}_k$  are the absolute position vectors of the tyres in global coordinate system  $\vec{e}^0$ . Thus, the generalized forces consist of the tyre forces and the resulting moments. Therefore, the equation (A.12) can be further expanded for each degree of freedom as presented in equation (A.11). The resulting matrix of the generalized forces (A.13) for each state reads:

$$\underline{Q} = \begin{bmatrix} F_{y1} + F_{y2} + F_{y3} + F_{y4} \\ a_1 F_{y1} - b_1 F_{y2} - F_{y3}(b_2 + h_1) - F_{y4}(b_3 + l_2 + h_1) \\ b_2 F_{y3} + F_{y4}(b_3 + l_2) \\ b_3 F_{y4} \end{bmatrix}. \quad (\text{A.13})$$



The lateral tyre forces are the result of side slip angles. The tyre cornering behaviour is assumed to be linear, so  $F_{y_i} = C_i \alpha_i$ , where  $\alpha_i$  is the slip angle and  $C_i$  is the cornering stiffness. The lateral forces are:

$$F_{y1} = -\frac{1}{v} C_1 (v_y + a_1 r_1) + C_1 \delta_1, \quad (\text{A.14})$$

$$F_{y2} = -\frac{1}{v} C_2 (v_y - b_1 r_1), \quad (\text{A.15})$$

$$F_{y3} = -\frac{1}{v} C_3 (v_y - h_1 r_1 - b_2 (r_1 - \dot{\gamma}_1)) + C_3 \gamma_1, \quad (\text{A.16})$$

$$F_{y4} = -\frac{1}{v} C_4 (v_y - h_1 r_1 - l_2 (r_1 - \dot{\gamma}_1) - b_3 (r_1 - \dot{\gamma}_1 - \dot{\gamma}_2)) + C_4 (\gamma_1 + \gamma_2). \quad (\text{A.17})$$

For the simplification the following abbreviations are introduced:

$$\begin{aligned} C &= C_1 + C_2, \\ C_t &= C_3 + C_4, \\ C_s &= a_1 C_1 - b_1 C_2, \\ C_q &= a_1^2 C_1 + b_1^2 C_2. \end{aligned} \quad (\text{A.18})$$

Finally, the resulting four equations of motion read:

$$\begin{aligned} &\sum_{i=1}^3 m_i (\dot{v}_y + v r_1) - [m_2 (h_1 + a_2) + m_3 (h_1 + l_2 + a_3)] \dot{r}_1 \\ &+ [m_2 a_2 + m_3 (l_2 + a_3)] \dot{\gamma}_1 + [m_3 a_3] \dot{\gamma}_2 = \\ &-\frac{1}{v} [(C + C_t) v_y + (C_s - (h_1 + b_2) C_3 - (h_1 + l_2 + b_3) C_4) r_1] \\ &-\frac{1}{v} [(b_2 C_3 + (l_2 + b_3) C_4) \dot{\gamma}_1 + b_3 C_4 \dot{\gamma}_2] + C_1 \delta_1 + C_t \gamma_1 + C_4 \gamma_2, \end{aligned} \quad (\text{A.19})$$

$$\begin{aligned} &[J_1 + m_2 h_1 (h_1 + a_2) + m_3 h_1 (h_1 + l_2 + a_3)] \dot{r}_1 - m_3 a_3 h_1 \dot{\gamma}_2 \\ &- [m_2 a_2 h_1 + m_3 h_1 (l_2 + a_3)] \dot{\gamma}_1 - (m_2 + m_3) h_1 (\dot{v}_y + v r_1) = \\ &a_1 C_1 \delta_1 - (b_3 + l_2 + h_1) C_4 \gamma_2 - [(b_2 + h_1) C_3 + (b_3 + l_2 + h_1) C_4] \gamma_1 \\ &-\frac{1}{v} [(C_s - (b_2 + h_1) C_3 - (b_3 + l_2 + h_1) C_4) v_y] \\ &-\frac{1}{v} [(C_q + (b_2 + h_1)^2 C_3 + (b_3 + l_2 + h_1)^2 C_4) r_1] \\ &-\frac{1}{v} [-(b_2 (b_2 + h_1) C_3 + (b_3 + l_2) (b_3 + l_2 + h_1) C_4) \dot{\gamma}_1] \\ &-\frac{1}{v} [-b_3 (b_3 + l_2 + h_1) C_4 \dot{\gamma}_2], \end{aligned} \quad (\text{A.20})$$

$$\begin{aligned}
& [J_2 + m_2 a_2 (a_2 + h_1) + m_3 l_2 (h_1 + l_2 + a_3)] \dot{r}_1 - m_3 a_3 l_2 \ddot{\gamma}_2 \\
& - [J_2 + m_2 a_2^2 + m_3 l_2 (l_2 + a_3)] \dot{\gamma}_1 - [m_2 a_2 + m_3 l_2] (\dot{v}_y + v r_1) = \\
& - \frac{1}{v} [(b_2 C_3 + (b_3 + l_2) C_4) v_y + b_3 (b_3 + l_2) C_4 \dot{\gamma}_2] + (b_3 + l_2) C_4 \gamma_2 \\
& - \frac{1}{v} [-((b_2^2 + b_2 h_1) C_3 + (h_1 (b_3 + l_2) + (b_3 + l_2)^2) C_4) r_1] \\
& - \frac{1}{v} [(b_2^2 C_3 + (b_3 + l_2)^2 C_4) \dot{\gamma}_1] + (b_2 C_3 + (b_3 + l_2) C_4) \gamma_1,
\end{aligned} \tag{A.21}$$

$$\begin{aligned}
& - [m_3 a_3] (\dot{v}_y + v r_1) + [J_3 + m_3 a_3 (a_3 + l_2 + h_1)] \dot{r}_1 \\
& - [J_3 + m_3 a_3^2] \dot{\gamma}_2 - [J_3 + m_3 a_3 (a_3 + l_2)] \dot{\gamma}_1 = \\
& - \frac{1}{v} b_3 C_4 (v_y - h_1 r_1 - l_2 (r_1 - \dot{\gamma}_1) - b_3 (r_1 - \dot{\gamma}_1 - \dot{\gamma}_2)) + b_3 C_4 (\gamma_1 + \gamma_2).
\end{aligned} \tag{A.22}$$

# Appendix B

## Normal and Inverse Kinematic Models

### B.1 Introduction

In this appendix the kinematic model of double articulated vehicle is derived. Furthermore, the derivation of an inverse kinematic model used as a part bi-directional path following controller is given.

### B.2 Kinematic model

Firstly the equations for the kinematic model of double articulated vehicle will be derived. The validity of kinematic model for low-speed manoeuvring has been tested against the high fidelity multi-body model described in Chapter 3. The results, documented in [78], provide evidence that the kinematic model can be considered as a sufficiently adequate representation of the real system for these conditions.

The single track model uses the dimensions of the real vehicle combination in terms of wheelbases and the distances to the articulation joints, however each axle group is represented by a single wheel, similarly like in the linearised dynamic model described in Appendix A. Contrary to the dynamic model, the kinematic model does not include a mass distribution between the axles nor tyre slip. Hence, for easier distinguishing between the models and manipulation with equations, a different nomenclature for the vehicle dimensions has been adopted to the kinematic model. Given the vehicle dimensions established in Appendix A the nomenclature for kinematic model is defined as follows:  $L_{0f} = a_1 + b_1$ ,  $L_{1f} = b_2$ ,  $L_{2f} = b_3$ ,  $L_{0b} = b_1 - h_1$ , and  $L_{1b} = b_2 - l_2$ .

As can be seen in Figure B.1  $L_{0f}$ ,  $L_{1f}$ ,  $L_{2f}$  are positive constants representing the wheelbases of the tractor, first trailer and second trailer, respectively.  $L_{0b}$ , and  $L_{1b}$  are coupling point positions w.r.t. the axles which are measured in  $\vec{e}^1$  and  $\vec{e}^2$ , respectively, meaning they are negative if the articulation joint is placed behind the axle, such as

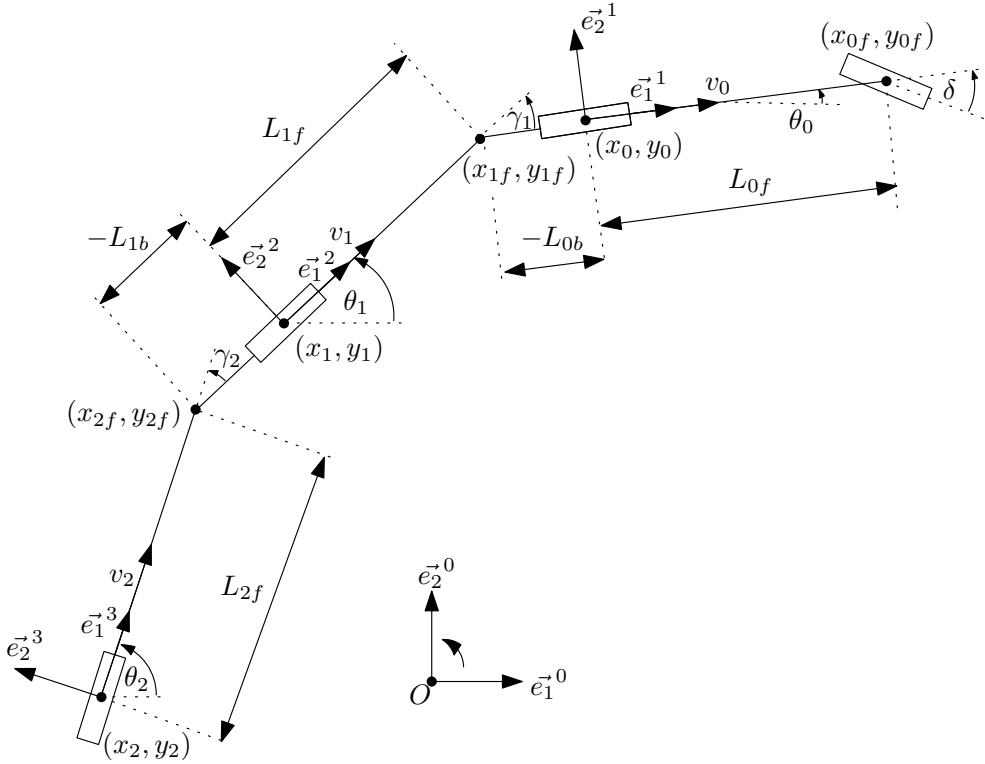


Figure B.1: Kinematic model of double articulated vehicle combination

depicted in Figure B.1. The yaw angle of the tractor, first trailer, and second trailer in the global coordinate system  $\vec{e}^0$  is given by  $\theta_0, \theta_1$ , and  $\theta_2$ , respectively.  $v_1$  represents the longitudinal velocity and the first trailing unit, and  $v_2$  is the longitudinal velocity of the second trailing unit. Since no tyre slip angle is considered the lateral velocities at all wheels must be zero. The positions of the coupling points are given by  $(x_{1f}, y_{1f})$ , and  $(x_{2f}, y_{2f})$ . The inputs are represented by the longitudinal velocity of the tractor drive axle  $v_0$  at  $x_0, y_0$  and the steering angle  $\delta$  applied at the first axle.

Furthermore, we will take the position of the rear axle of the first vehicle  $x_0, y_0$  and its orientation  $\theta_0$  as reference point. Subsequently the positions of the tractor steer axle, trailer axles and the coupling points in  $\vec{e}^0$  can be defined as follows:

$$\begin{aligned} x_{0f} &= x_0 + L_{0f} \cos \theta_0, \\ y_{0f} &= y_0 + L_{0f} \sin \theta_0, \end{aligned} \quad (\text{B.1})$$

$$\begin{aligned} x_{1f} &= x_0 + L_{0b} \cos \theta_0, \\ y_{1f} &= y_0 + L_{0b} \sin \theta_0, \end{aligned} \quad (\text{B.2})$$

$$\begin{aligned}x_1 &= x_{1f} - L_{1f} \cos \theta_1, \\y_1 &= y_{1f} - L_{1f} \sin \theta_1,\end{aligned}\tag{B.3}$$

$$\begin{aligned}x_{2f} &= x_1 + L_{1b} \cos \theta_1, \\y_{2f} &= y_1 + L_{1b} \sin \theta_1,\end{aligned}\tag{B.4}$$

$$\begin{aligned}x_2 &= x_{2f} - L_{2f} \cos \theta_2, \\y_2 &= y_{2f} - L_{2f} \sin \theta_2.\end{aligned}\tag{B.5}$$

The time derivatives of equations (B.1) to (B.5) representing the point velocities in  $\bar{e}^0$  read:

$$\begin{aligned}\dot{x}_0 &= v_0 \cos \theta_0, \\\dot{y}_0 &= v_0 \sin \theta_0,\end{aligned}\tag{B.6}$$

$$\begin{aligned}\dot{x}_{0f} &= \dot{x}_0 - L_{0f} \dot{\theta}_0 \sin \theta_0, \\\dot{y}_{0f} &= \dot{y}_0 + L_{0f} \dot{\theta}_0 \cos \theta_0,\end{aligned}\tag{B.7}$$

$$\begin{aligned}\dot{x}_{1f} &= \dot{x}_0 - L_{0b} \dot{\theta}_0 \sin \theta_0, \\\dot{y}_{1f} &= \dot{y}_0 + L_{0b} \dot{\theta}_0 \cos \theta_0,\end{aligned}\tag{B.8}$$

$$\begin{aligned}\dot{x}_1 &= \dot{x}_{1f} + L_{1f} \dot{\theta}_1 \sin \theta_1, \\\dot{y}_1 &= \dot{y}_{1f} - L_{1f} \dot{\theta}_1 \cos \theta_1,\end{aligned}\tag{B.9}$$

$$\begin{aligned}\dot{x}_{2f} &= \dot{x}_1 - L_{1b} \dot{\theta}_1 \sin \theta_1, \\\dot{y}_{2f} &= \dot{y}_1 + L_{1b} \dot{\theta}_1 \cos \theta_1,\end{aligned}\tag{B.10}$$

$$\begin{aligned}\dot{x}_2 &= \dot{x}_{2f} + L_{2f} \dot{\theta}_2 \sin \theta_2, \\\dot{y}_2 &= \dot{y}_{2f} - L_{2f} \dot{\theta}_2 \cos \theta_2.\end{aligned}\tag{B.11}$$

As the lateral velocities of each wheel must be zero, the non-holonomic constraints for each axle can be defined as:

$$\dot{y}_0 \cos \theta_0 - \dot{x}_0 \sin \theta_0 = 0,\tag{B.12}$$

$$\dot{y}_{0f} \cos(\theta_0 + \delta) - \dot{x}_{0f} \sin(\theta_0 + \delta) = 0,\tag{B.13}$$

$$\dot{y}_1 \cos \theta_1 - \dot{x}_1 \sin \theta_1 = 0,\tag{B.14}$$

$$\dot{y}_2 \cos \theta_2 - \dot{x}_2 \sin \theta_2 = 0.\tag{B.15}$$

The constraints can be hereafter employed to obtain  $\dot{\theta}_0$ ,  $\dot{\theta}_1$ , and  $\dot{\theta}_2$  being the yaw rates of the first, second and third vehicle respectively.

At first, substituting (B.6) and (B.7) into the non-holonomic constraint (B.13) one obtains:

$$[v_0 \sin \theta_0 + L_{0f} \dot{\theta}_0 \cos \theta_0] \cos(\theta_0 + \delta) = [v_0 \cos \theta_0 - L_{0f} \dot{\theta}_0 \sin \theta_0] \sin(\theta_0 + \delta). \quad (\text{B.16})$$

Simplifying (B.16) while using trigonometric identities gives the yaw rate of the tractor as:

$$\dot{\theta}_0 = \frac{v_0}{L_{0f}} \tan \delta. \quad (\text{B.17})$$

Subsequently, the yaw rate of the first trailer  $\dot{\theta}_1$  can be expressed by substitution of equation (B.6), (B.8), and (B.9) in (B.14), which yields in:

$$\begin{aligned} [v_0 \sin \theta_0 + L_{0b} \dot{\theta}_0 \cos \theta_0 - L_{1f} \dot{\theta}_1 \cos \theta_1] \cos \theta_1 = \\ [v_0 \cos \theta_0 - L_{0b} \dot{\theta}_0 \sin \theta_0 + L_{1f} \dot{\theta}_1 \sin \theta_1] \sin \theta_1. \end{aligned} \quad (\text{B.18})$$

By repeated application of trigonometric identities, (B.18) can be simplified into:

$$\dot{\theta}_1 = \frac{v_0}{L_{1f}} \sin \gamma_1 + \frac{L_{0b}}{L_{1f}} \dot{\theta}_0 \cos \gamma_1, \quad (\text{B.19})$$

where  $\gamma_1$  is the articulation angle between the tractor and the first trailer given by  $\gamma_1 = \theta_0 - \theta_1$ .

Similarly the yaw rate of the second trailer  $\dot{\theta}_2$  can be expressed by substitution of equations (B.6), (B.8), (B.9), (B.10), and (B.11) in (B.15), which yields in:

$$\begin{aligned} [v_0 \sin \theta_0 + L_{0b} \dot{\theta}_0 \cos \theta_0 - L_{1f} \dot{\theta}_1 \cos \theta_1 + L_{1b} \dot{\theta}_1 \cos \theta_1 \\ - L_{2f} \dot{\theta}_2 \cos \theta_2] \cos \theta_2 = [v_0 \cos \theta_0 - L_{0b} \dot{\theta}_0 \sin \theta_0 \\ + L_{1f} \dot{\theta}_1 \sin \theta_1 - L_{1b} \dot{\theta}_1 \sin \theta_1 + L_{2f} \dot{\theta}_2 \sin \theta_2] \sin \theta_2. \end{aligned} \quad (\text{B.20})$$

As in case of (B.18) by further simplifications through trigonometric identities one obtains:

$$\dot{\theta}_2 = \frac{v_1}{L_{2f}} \sin \gamma_2 + \frac{L_{1b}}{L_{2f}} \dot{\theta}_1 \cos \gamma_2, \quad (\text{B.21})$$

where  $\gamma_2$  is the articulation angle between the first and the second trailer given by  $\gamma_2 = \theta_1 - \theta_2$ .

The longitudinal velocity of the first trailing unit  $v_1$  given by (B.22) is derived based on projections of  $v_0$  and  $L_{0b} \dot{\theta}_0$  into  $\vec{e}_1^2$  resulting in:

$$v_1 = v_0 \cos \gamma_1 - L_{0b} \dot{\theta}_0 \sin \gamma_1. \quad (\text{B.22})$$

Similarly longitudinal velocity of the second trailing unit  $v_2$  is obtained:

$$v_2 = v_1 \cos \gamma_2 - L_{1b} \dot{\theta}_1 \sin \gamma_2. \quad (\text{B.23})$$

### B.3 Inverse Kinematic model

The role of the inverse kinematic model is to translate desired yaw rate of the rear most vehicle  $\dot{\theta}_2$  (derived on basis of virtual steering angle  $\delta^*$  as explained in Chapter 7) and its longitudinal velocity  $v_2$  defined in  $\vec{e}_1^3$  through the kinematic chain to the first vehicle. Thus, desired yaw rate  $\dot{\theta}_2$  can be generated through a steering angle of the first axle  $\delta$  and longitudinal velocity  $v_0$ .

The inputs for the inverse kinematic model are  $v_2$ , and  $\delta^*$ . To derive the remaining vehicle states we use a similar approach as in Section B.2 starting at the definition of axle and coupling point positions with respect to the pose of the last axle described by  $x_2, y_2, \theta_2$  in accordance with Figure B.2 as follows:

$$\begin{aligned} x_{2f} &= x_2 + L_{2f} \cos \theta_2, \\ y_{2f} &= y_2 + L_{2f} \sin \theta_2, \end{aligned} \quad (\text{B.24})$$

$$\begin{aligned} x_1 &= x_{2f} - L_{1b} \cos \theta_1, \\ y_1 &= y_{2f} - L_{1b} \sin \theta_1, \end{aligned} \quad (\text{B.25})$$

$$\begin{aligned} x_{1f} &= x_1 + L_{1f} \cos \theta_1, \\ y_{1f} &= y_1 + L_{1f} \sin \theta_1, \end{aligned} \quad (\text{B.26})$$

$$\begin{aligned} x_0 &= x_{1f} - L_{0b} \cos \theta_0, \\ y_0 &= y_{1f} - L_{0b} \sin \theta_0, \end{aligned} \quad (\text{B.27})$$

$$\begin{aligned} x_{0f} &= x_0 + L_{0f} \cos \theta_0, \\ y_{0f} &= y_0 + L_{0f} \sin \theta_0. \end{aligned} \quad (\text{B.28})$$

The time derivatives of equations (B.24) to (B.28) representing the point velocities in  $\vec{e}^0$  read:

$$\begin{aligned} \dot{x}_2 &= v_2 \cos \theta_2, \\ \dot{y}_2 &= v_2 \sin \theta_2, \end{aligned} \quad (\text{B.29})$$

$$\begin{aligned} \dot{x}_{2f} &= \dot{x}_2 - L_{2f} \dot{\theta}_2 \sin \theta_2, \\ \dot{y}_{2f} &= \dot{y}_2 + L_{2f} \dot{\theta}_2 \cos \theta_2, \end{aligned} \quad (\text{B.30})$$

$$\begin{aligned} \dot{x}_1 &= \dot{x}_{2f} + L_{1b} \dot{\theta}_1 \sin \theta_1, \\ \dot{y}_1 &= \dot{y}_{2f} - L_{1b} \dot{\theta}_1 \cos \theta_1, \end{aligned} \quad (\text{B.31})$$

$$\begin{aligned} \dot{x}_{1f} &= \dot{x}_1 - L_{1f} \dot{\theta}_1 \sin \theta_1, \\ \dot{y}_{1f} &= \dot{y}_1 + L_{1f} \dot{\theta}_1 \cos \theta_1, \end{aligned} \quad (\text{B.32})$$

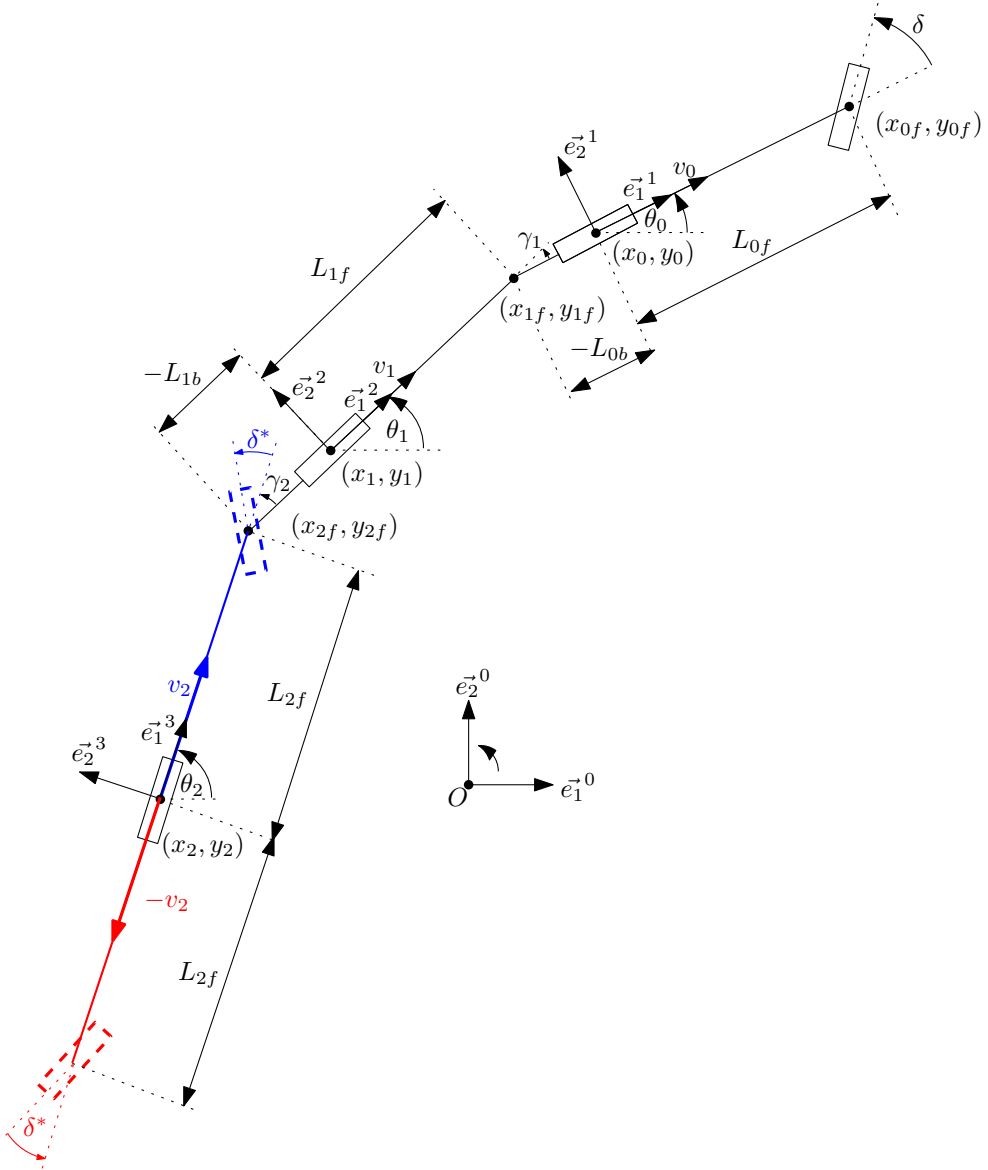


Figure B.2: Inverse kinematic model of double articulated vehicle combination

$$\begin{aligned} \dot{x}_0 &= \dot{x}_{1f} + L_{0b} \dot{\theta}_0 \sin \theta_0, \\ \dot{y}_0 &= \dot{y}_{1f} - L_{0b} \dot{\theta}_0 \cos \theta_0, \end{aligned} \quad (\text{B.33})$$

$$\begin{aligned} \dot{x}_{0f} &= \dot{x}_0 - L_{0f} \dot{\theta}_0 \sin \theta_0, \\ \dot{y}_{0f} &= \dot{y}_0 + L_{0f} \dot{\theta}_0 \cos \theta_0. \end{aligned} \quad (\text{B.34})$$



The set of non-holonomic constraints (B.12)-(B.15) is still applicable. The virtual steering angle  $\delta^*$  (B.35) is depicted in Figure B.2. The constraints for the virtual steering wheel equals:

$$\dot{y}_{2f} \cos(\theta_2 + \delta^*) - \dot{x}_{2f} \sin(\theta_2 + \delta^*) = 0. \quad (\text{B.35})$$

By entering (B.29), and (B.30) into (B.35) we obtain:

$$(v_2 \sin \theta_2 + L_{2f} \dot{\theta}_2 \cos \theta_2) \cos(\theta_2 + \delta^*) = (v_2 \cos \theta_2 - L_{2f} \dot{\theta}_2 \sin \theta_2) \sin(\theta_2 + \delta^*), \quad (\text{B.36})$$

which can be simplified through the trigonometric identities,

$$v_2 \sin(-\delta^*) + L_{2f} \dot{\theta}_2 \cos(-\delta^*) = 0. \quad (\text{B.37})$$

Equation (B.37) finally delivers the yaw rate of the second trailer given by:

$$\dot{\theta}_2 = \frac{v_2}{L_{2f}} \tan \delta^*. \quad (\text{B.38})$$

Subsequently, the yaw rate of the first trailer  $\dot{\theta}_1$  can be expressed by employing (B.14), and substituting (B.29), (B.30), and (B.31), which yields:

$$\begin{aligned} [v_2 \sin \theta_2 + L_{2f} \dot{\theta}_2 \cos \theta_2 - L_{1b} \dot{\theta}_1 \cos \theta_1] \cos \theta_1 = \dots \\ \dots [v_2 \cos \theta_2 - L_{2f} \dot{\theta}_2 \sin \theta_2 + L_{1b} \dot{\theta}_1 \sin \theta_1] \sin \theta_1. \end{aligned} \quad (\text{B.39})$$

By repeated application of trigonometric identities, (B.39) can be simplified into:

$$\dot{\theta}_1 = -\frac{v_2}{L_{1b}} \sin \gamma_2 + \frac{L_{2f}}{L_{1b}} \dot{\theta}_2 \cos \gamma_2, \quad (\text{B.40})$$

where  $\gamma_2$  is the articulation angle between the first and second trailer. Similarly the yaw rate of the prime mover  $\dot{\theta}_0$  can be expressed by substitution of equations (B.29), (B.30), (B.31), (B.32), and (B.33) in (B.12), which yields in:

$$\dot{\theta}_0 = -\frac{v_1}{L_{0b}} \sin \gamma_1 + \frac{L_{1f}}{L_{0b}} \dot{\theta}_1 \cos \gamma_1, \quad (\text{B.41})$$

where  $\gamma_1$  is the articulation angle between the first trailer and the prime mover.  $v_1$  is the longitudinal velocity of the first trailer defined in coordinate system  $\vec{e}_1^2$ , which is expressed now in terms of second trailer longitudinal velocity  $v_2$  as follows:

$$v_1 = v_2 \cos \gamma_2 + L_{2f} \dot{\theta}_2 \sin \gamma_2. \quad (\text{B.42})$$

Equation (B.42) is derived based on projections of  $v_2$  and  $L_{2f} \dot{\theta}_2$  from  $\vec{e}_1^3$  and  $\vec{e}_2^3$ , respectively, into  $\vec{e}_1^2$ . The longitudinal velocity  $v_0$  of the prime mover in  $\vec{e}_1^1$  is derived in identical basis and equates:

$$v_0 = v_1 \cos \gamma_1 + L_{1f} \dot{\theta}_1 \sin \gamma_1. \quad (\text{B.43})$$

All equations mentioned in this section are defined for the case when  $v_0$ ,  $L_{0b}$ , and  $L_{1b}$  are positive, i.e. the vehicle is driving in forward direction and the coupling points are placed in front of the axles. In practice  $L_{0b}$ ,  $L_{1b}$  and  $v_0$  can be both positive and negative, according to the type of HCV, and driving direction, respectively. To make the equations (B.38), (B.40), and (B.41) functional for these permutations two modifications are necessary. Firstly, the sign of  $v_2$  in (B.38) has to be disregarded as it is already taken into account by the driver model. Secondly, the equations (B.40), and (B.41) need to be updated by terms considering sign of  $L_{0b}$ ,  $L_{1b}$  and  $v_0$ . It is because of non-minimum phase (NMP) property of a kinematic vehicle model which occurs for combinations of negative  $L_{0b}$  and  $L_{1b}$  with positive  $v_0$  i.e. for forward driving, and positive  $L_{0b}$  and  $L_{1b}$  with negative  $v_0$  i.e. for reversing. For these NMP kinematic models the zeroes of some input-output transfer functions occur in the right-half plane. By connection of any kinematic model with established inverse kinematic equations, according to the approach shown in Figure 7.12a, the pole-zero cancellation is achieved. In case of NMP models this however leads to the introduction of unstable pole for the transfer functions  $G_{\dot{\theta}_0|\gamma_1}$  and  $G_{\dot{\theta}_0|\gamma_2}$ , shown in Figure 7.12a, that did not have the right-half plane zero, which leads to instability of the loop. Therefore final set of equations is updated as follows:

$$\begin{aligned} \dot{\theta}_2 &= \frac{|v_2|}{L_{2f}} \tan \delta^*, \\ \dot{\theta}_1 &= \text{sign}(v_0) \cdot \text{sign}(L_{1b}) \left[ -\frac{v_2}{L_{1b}} \sin \gamma_2 + \frac{L_{2f}}{L_{1b}} \dot{\theta}_2 \cos \gamma_2 \right], \\ \dot{\theta}_0 &= \text{sign}(v_0) \cdot \text{sign}(L_{0b}) \left[ -\frac{v_1}{L_{0b}} \sin \gamma_1 + \frac{L_{1f}}{L_{0b}} \dot{\theta}_1 \cos \gamma_1 \right]. \end{aligned} \quad (\text{B.44})$$

The equations are employed for close-loop stability analysis of various vehicle combination layouts as documented in [114]. Moreover, it should be denoted that kinematic inversion as described is applicable only for cases  $L_{1b}, L_{0b} \neq 0$ .

# Appendix C

## Closed Loop Stability Analysis at Low Speed with Limited Articulation Angles

### C.1 Introduction

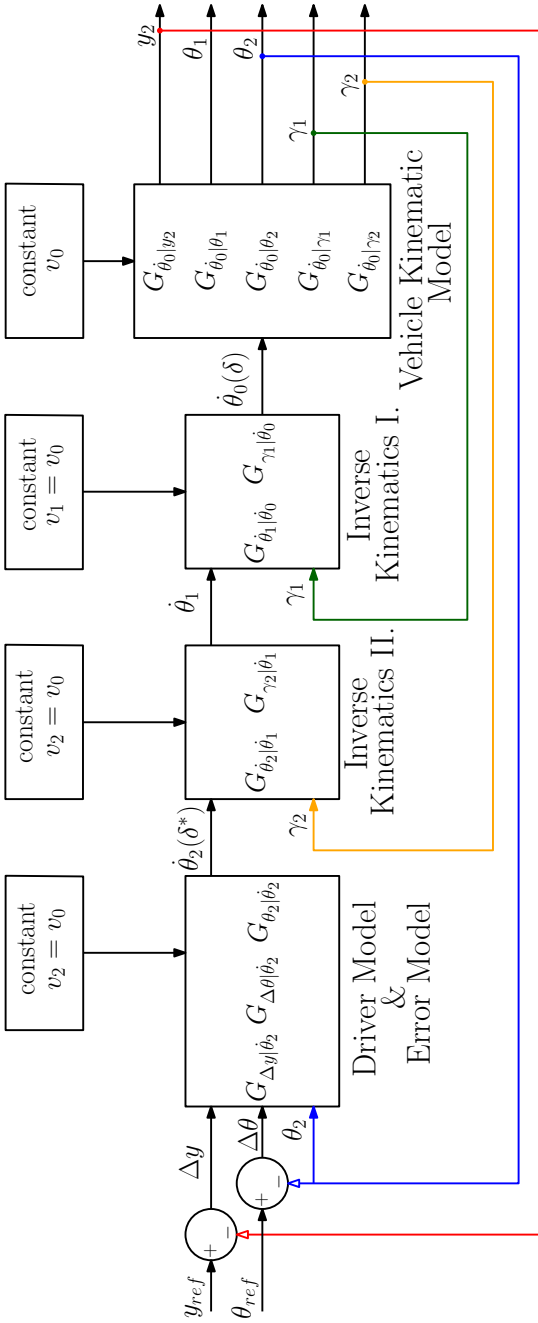
In order to perform a closed-loop system stability analysis the non linear equations of the control scheme described extensively in Chapter 7 are linearised for the driving along a straight curve trajectory. As the complete control scheme is linearised at first. Then the transfer function for open loop and closed loop system is compiled, and used for:

- Accuracy assessment of the linearised model
- Sensitivity study of the driver model parameters
- Assessment of the damping ratio of the closed loop transfer function.

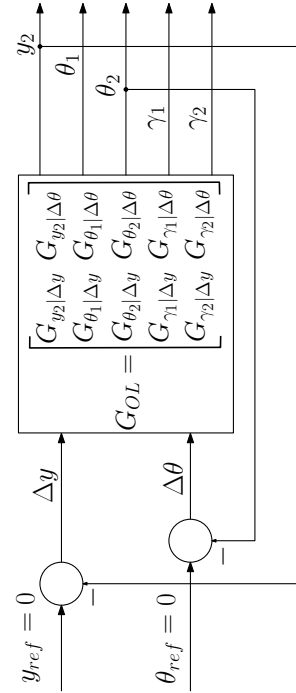
### C.2 Method

The non-linear model of driver, inverse kinematics and vehicle has been linearised for driving along a straight curve trajectory while considering following presumptions:

- All angles are considered sufficiently small such the trigonometric functions can be simplified as  $\cos \gamma_1 = \cos \gamma_2 = 1$ ,  $\tan \delta = \delta$ ,  $\tan \delta^* = \delta^*$ ,  $\sin \gamma_1 = \gamma_1$ ,  $\sin \gamma_2 = \gamma_2$ ,  $\sin \theta_2 = \theta_2$ ,  $\cos \theta_2 = 1$ ,  $\tan \phi_1 = \phi_1$ , and  $\tan \phi_2 = \phi_2$ .



(a) Original closed loop scheme.



(b) Equivalent closed loop scheme used for stability assessment.

Figure C.1: Linearised closed loop structure.

- Longitudinal velocity of all vehicle units in the combination is equal, i.e.  $v_0 = v_1 = v_2$ .
- Considering the straight curve reference path the state equation  $\dot{x}_0 = v_0 \cos \theta_0$  of the kinematic model which responsible to output state  $x_2$  can be disregarded.

This will result in the closed loop scheme depicted on Figure C.1a. The original equations, as described in Chapter 7, are substituted by the transfer functions for more convenient manipulation with internal loops, which can be directly handled by MATLAB. Resulting scheme, depicted in Figure C.1b is to be considered hereafter for analyses explained in Sections C.4, C.5, and C.6.

### C.3 Linearised Equations

The equations used to derive all transfer functions in Figure C.1a are described next.

- Driver Model

The driver model depicted in Figure C.2 combines the principles described in [4], [85], and [111]. It considers two preview distances  $P_{D_1}$ , and  $P_{D_2}$ , which are used to calculate error angles  $\phi_1$  and  $\phi_2$ , respectively. Furthermore, the lateral error  $\Delta y$  and the orientation error  $\Delta \theta$  are employed. These errors are multiplied with the gains  $K_y$ ,  $K_I$ , and  $K_\theta$ . The scheme for the calculation of errors used in the driver model is depicted in Figure C.2 where U is the central turn point of the last trailer to be controlled.

The driver model, as described in Chapter 7, equals:

$$\delta^* = K_y(w_1\phi_1 + w_2\phi_2) + K_I \int e_{yU} + K_\theta e_{\theta_{R_1}}. \quad (C.1)$$

Considering  $\sin \theta_i = \theta_i$ ,  $\cos \theta_i = 1$ , and the error angles  $\phi_i$  sufficiently small such that  $\tan \phi_i = \phi_i$ , then they become:

$$\phi_1 = \frac{y_{ref} - y_2 - P_{D_1}\theta_2}{P_{D_1}}, \quad (C.2)$$

$$\phi_2 = \frac{y_{ref} - y_2 - P_{D_2}\theta_2}{P_{D_2}}, \quad (C.3)$$

where  $P_{D_1}$ , and  $P_{D_2}$  are preview distances of the driver model,  $y_2$  represents the vertical position of the second trailing unit, and  $y_{ref}$  is the vertical position of the reference path. The difference  $y_{ref} - y_2$ , and  $\theta_{ref} - \theta_n$  can be substituted by  $\Delta y$  and  $\Delta \theta$ , respectively.



The lateral error given by  $e_{y_U} = \Delta y \cos \theta_2 - \Delta x \sin \theta_2$  after linearisation becomes  $\Delta y$ , and  $e_{\theta_{R_1}}$  equates to  $\Delta \theta$ , so we obtain:

$$\delta^* = K_y \left( w_1 \frac{\Delta y - PD_1 \theta_2}{PD_1} + w_2 \frac{\Delta y - PD_2 \theta_2}{PD_2} \right) + K_I \int \Delta y + K_\theta \Delta \theta. \quad (C.4)$$

Rearranging (C.4) and transforming it to the s-domain yields:

$$\delta^* = \left[ \left( K_y \left( \frac{w_1}{PD_1} + \frac{w_2}{PD_2} \right) + \frac{K_I}{s} \right) \quad K_\theta \quad -K_y (w_1 + w_2) \right] \begin{bmatrix} \Delta y \\ \Delta \theta \\ \theta_2 \end{bmatrix}. \quad (C.5)$$

The resulting virtual steering angle can be subsequently recalculated for the required yaw rate  $\dot{\theta}_2$  of the second trailing unit. Considering  $\tan \delta^* = \delta^*$ , the linearised equation of  $\dot{\theta}_2$  is defined as:

$$\dot{\theta}_2 = \frac{|v_2|}{L_{2f}} \delta^*. \quad (C.6)$$

The yaw rate of the second trailing unit  $\dot{\theta}_2$  represents an input to inverse kinematics blocks which are described next.

- Inverse Kinematics

The closed loop scheme depicted in Figure C.1a contains two blocks of inverse kinematics named I., and II., respectively. Their role is to transform the target yaw rate for the last vehicle unit  $\dot{\theta}_2$  in series to the required yaw rate of prime mover  $\dot{\theta}_0$ . Each block is able of transforming the yaw rate between two consecutive vehicle units. Thus the internal structure of the blocks is identical, differing only in vehicle dimension parameters. Both models of inverse kinematics were linearised while driving along straight curve trajectory.

Considering articulation angles sufficiently small such that  $\sin \gamma_i = \gamma_i$ , and  $\cos \gamma_i = 1$  the linearised models are described as:

- Inverse Kinematics II.

The model is using two inputs represented by  $\dot{\theta}_2$ ,  $\gamma_2$  to output the yaw rate  $\dot{\theta}_1$ :

$$\dot{\theta}_1 = \left[ \text{sign}(v_2) \text{sign}(L_{1b}) \frac{L_{2f}}{L_{1b}} \quad -\text{sign}(v_2) \text{sign}(L_{1b}) \frac{v_2}{L_{1b}} \right] \begin{bmatrix} \dot{\theta}_2 \\ \gamma_2 \end{bmatrix}. \quad (C.7)$$

- Inverse Kinematics I. The model is using two inputs represented by  $\dot{\theta}_1$ ,  $\gamma_1$  to output the yaw rate  $\dot{\theta}_0$ :

$$\dot{\theta}_0 = \left[ \text{sign}(v_1) \text{sign}(L_{0b}) \frac{L_{1f}}{L_{0b}} \quad -\text{sign}(v_1) \text{sign}(L_{0b}) \frac{v_1}{L_{0b}} \right] \begin{bmatrix} \dot{\theta}_1 \\ \gamma_1 \end{bmatrix}. \quad (C.8)$$

- Kinematic Model of Double Articulated Vehicle Combination

As can be seen in Figure C.1a the linearised kinematic model of the double articulated vehicle has one input represented by the yaw rate of the hauling unit  $\dot{\theta}_0$ , which is a function of steering angle  $\delta$ , and five outputs represented by  $y_2$ ,  $\theta_1$ ,  $\theta_2$ ,  $\gamma_1$ , and  $\gamma_2$ . The lateral position of the last trailing unit  $y_2$  and its yaw angle  $\theta_2$  are used as feedback signals for the calculation of lateral error  $\Delta y$  and orientation error  $\Delta\theta$ , respectively. Articulation angles  $\gamma_1$  and  $\gamma_2$  are used as feedback signals for the inverse kinematics blocks, and yaw angle of the first trailing unit  $\theta_1$  is used only internally to calculate lateral position of the last trailing unit  $y_2$ . For the convenience and further implementation in the control scheme the model is defined by a state space representation:

$$\begin{aligned} \dot{x} &= Ax + Bu, \\ y &= Cx + Du, \end{aligned} \quad (\text{C.9})$$

with the state vector  $x = [y_0, \theta_1, \theta_2, \gamma_1, \gamma_2]^T$ , the output vector  $y = [y_2, \theta_1, \theta_2, \gamma_1, \gamma_2]^T$ , and the input  $u = \dot{\theta}_1$ . The equilibrium point about which the model is linearised corresponds to the driving along the straight trajectory. This allows to assume that all angles are sufficiently small such that  $\cos \gamma_i = \cos \theta_i = 1$ ,  $\sin \gamma_i = \gamma_i$ ,  $\sin \theta_i = \theta_i$  and the velocities of vehicle units equal  $v_0 = v_1 = v_2$ . Resulting matrices of the state equation in (C.9) read:

$$A = \left[ \begin{array}{ccc|cc} 0 & v_0 & 0 & v_0 & 0 \\ 0 & 0 & 0 & \frac{v_0}{L_{1f}} & 0 \\ 0 & 0 & 0 & \frac{v_0}{L_{1f}} \frac{L_{1b}}{L_{2f}} & \frac{v_0}{L_{2f}} \\ \hline 0 & 0 & 0 & -\frac{v_0}{L_{1f}} & 0 \\ 0 & 0 & 0 & \left( \frac{v_0}{L_{1f}} - \frac{v_0}{L_{1f}} \frac{L_{1b}}{L_{2f}} \right) & -\frac{v_0}{L_{2f}} \end{array} \right], \quad (\text{C.10})$$

$$B = \left[ \begin{array}{c} 0 \\ \frac{L_{0b}}{L_{1f}} \\ \frac{L_{0b}}{L_{1f}} \frac{L_{1b}}{L_{2f}} \\ \left( 1 - \frac{L_{0b}}{L_{1f}} \right) \\ \left( \frac{L_{0b}}{L_{1f}} - \frac{L_{0b}}{L_{1f}} \frac{L_{1b}}{L_{2f}} \right) \end{array} \right]. \quad (\text{C.11})$$



The matrices of the output equation in (C.9) read:

$$C = \begin{bmatrix} 1 & (L_{0b} + L_{1b} - L_{1f}) & -L_{2f} & L_{0b} & 0 \\ 0 & 1 & 0 & 0 & 0 \\ 0 & 0 & 1 & 0 & 0 \\ 0 & 0 & 0 & 1 & 0 \\ 0 & 0 & 0 & 0 & 1 \end{bmatrix}, \quad (\text{C.12})$$

$$D = \begin{bmatrix} 0 \\ 0 \\ 0 \\ 0 \\ 0 \end{bmatrix}. \quad (\text{C.13})$$

Given  $\dot{\theta}_1$  as an input, and the fact that velocities of all vehicle units are assumed to be equal and fixed constants, the linearised vehicle model used for the stability analysis has only two states which get involved in the internal dynamics. These are the articulation angles  $\gamma_1$ , and  $\gamma_2$ . Yet, the outlined state space model has five equations which enable to obtain also  $y_0, \theta_1, \theta_2$ . These however, can be calculated directly from  $\gamma_{1,2}$  and  $\dot{\theta}_1$ , for which the first three rows of the matrix  $A$  (C.10) are zeroes, and therefore  $y_0, \theta_1, \theta_2$  do not take a role in the internal dynamics of the linearised vehicle model. This formulation is chosen because of its convenience for further implementation in the linearised closed loop structure depicted in Figure C.1a.

## C.4 Accuracy of the linearised model

To study the impact of the linearisation on the model accuracy we combined the driver model, inverse kinematics I., II., and the vehicle model. The set of original non-linear differential equations has been compared with the transfer function representing the linearised model through a simulations that have been conducted to quantify differences. Both models were provided with identical constant positive velocity, and step input of either  $\Delta_y$  or  $\Delta_\theta$ . Both  $\Delta_y$ , and  $\Delta_\theta$  are varying in magnitude in order to study the its impact on the error of the linear model with respect to non-linear model in terms of articulation angles  $\gamma_1$  and  $\gamma_2$ . For the error calculation the maximal values of the articulation angels are considered. The results for a configuration consisting of a rigid truck with two centre axle trailers (TK-CT-CT) are depicted in Figures C.3a, C.3b, C.3c, and C.3d.

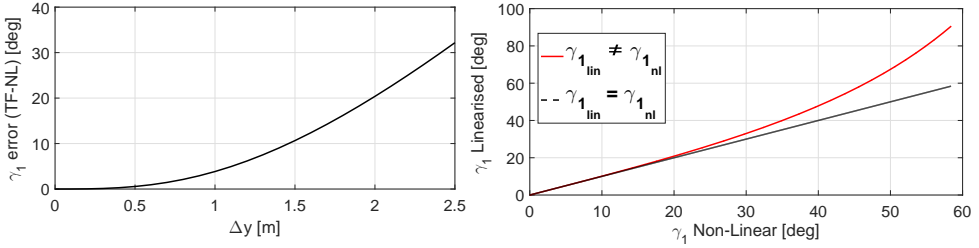
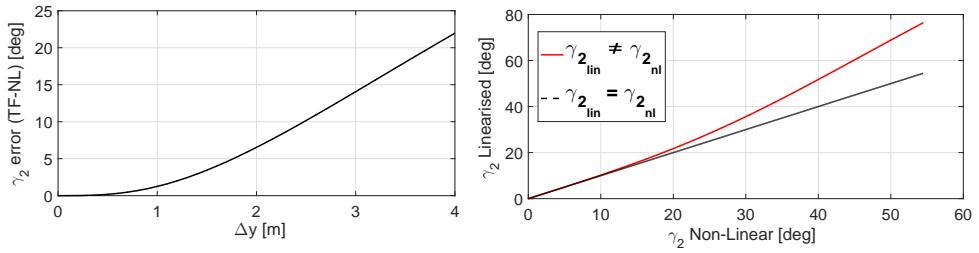
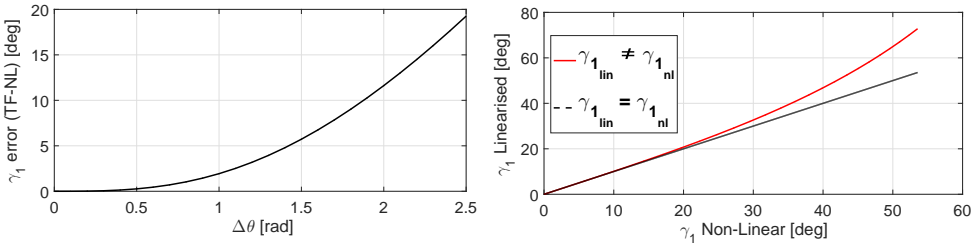
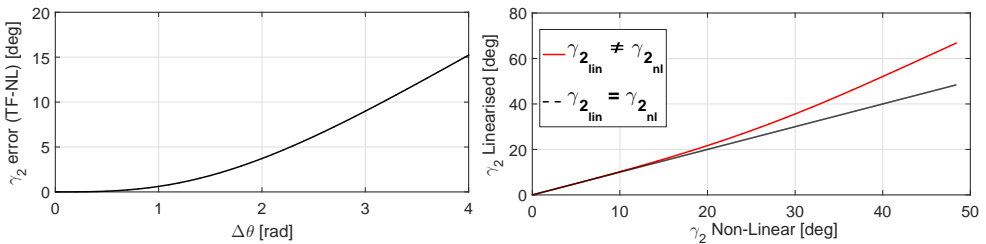
(a) Deviation of  $\gamma_1$  for changing of step input of  $\Delta y$ (b) Deviation of  $\gamma_2$  for changing of step input of  $\Delta y$ (c) Deviation of  $\gamma_1$  for changing of step input of  $\Delta\theta$ (d) Deviation of  $\gamma_2$  for changing of step input of  $\Delta\theta$ 

Figure C.3: Comparison of linearised and non-linear vehicle models.

It can be seen that with increasing magnitude of the inputs  $\Delta_y$ , and  $\Delta_\theta$  the linearised model becomes less accurate, as the effects of goniometric functions for all involved angles are suppressed. The linearised model is sufficiently accurate for  $\gamma_1 \pm 25 \text{ deg}$  and  $\gamma_2 \pm 20 \text{ deg}$ . As shown in Chapter 8, the span of articulation angles during the docking manoeuvre satisfy these limits. Therefore, the closed loop stability analysis with linearised model can be considered as credible for this scenario.

## C.5 Driver Model Parameter Sensitivity Study

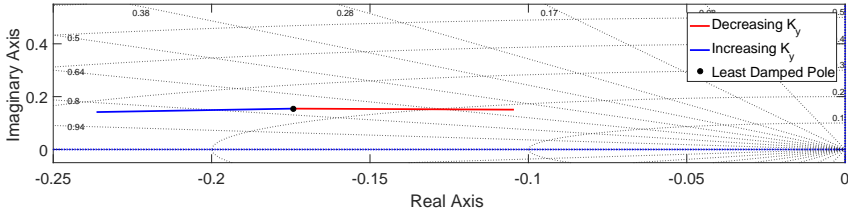
To investigate, which of the driver model parameters, i.e.  $K_y$ ,  $K_I$ ,  $K_\theta$ ,  $P_{D_1}$ ,  $k = \frac{P_{D_2}}{P_{D_1}}$ , has the biggest influence on the on the locus of the linear model poles, which represents the eigenvalues of the system matrix, the following analysis has been done. Each of the gains has been varied in the range  $\pm 30 \%$  and for the sensitivity analysis always the pole with the least damping is chosen. The results are presented in Figure C.4.

As can be seen the gains  $K_y$ , and  $P_{D_1}$  are the most influential for the loci of the less damped poles. A similar trend is observed for forward driving too. Hence it is rational to investigate the influence of  $K_y$  and  $P_{D_1}$  on the closed-loop stability in following steps.

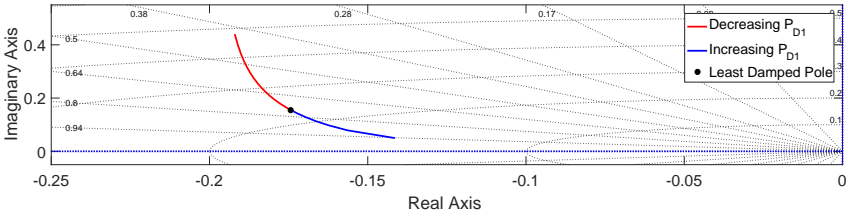
## C.6 Damping Ratio of the Closed Loop Transfer Function

For the stability dependency of the closed-loop system on  $K_y$  and  $P_{D_1}$ , the least damped poles loci in complex plane will be examined. The remaining controller parameters as  $K_I$ ,  $K_\theta$ ,  $k$  are kept on nominal values obtained from the controller tuning procedure, as described in Chapter 7. Stability of the closed loop is ensured if, all poles  $P_i$  of closed-transfer function satisfy  $Re\{P_i\} < 0$ . The less damped poles loci can be furthermore used to determine the damping ratio given by  $\zeta = -\frac{Re\{P_i\}}{|P_i|}$ , which influences the system response and the system is stable only if  $\zeta > 0$ . Considering the fact that closed-loop transfer functions have a number of poles, for the calculation of  $\zeta$  the pole with the lowest damping value is numerically calculated and selected as these poles will have a dominant effect for the system dynamics and stability.

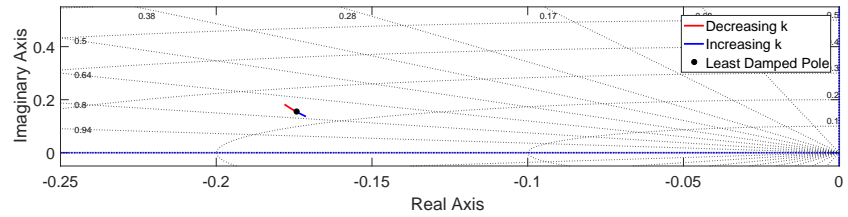
The plot showing constant damping lines for reversing of rigid truck with two central axle trailers (TK-CT-CT) can be seen on Figure C.5a. In the graph, also four markers designated by  $A$ ,  $B$ ,  $C$ , and  $D$  can be seen. Each of the markers represents unique combination of  $K_y$  and  $P_{D_1}$ . Furthermore, the system response for points  $A$ ,  $B$ ,  $C$ , and  $D$  is displayed on Figure C.5b, where the correlation between damping ratio values from Figure C.5a and the system response in time is evident. The red marker designates in Figure C.5a the combinations of  $K_y$  and  $P_{D_1}$ , which were found in tuning procedure to deliver lowest mean square error of  $e_y$ , as described in Chapter 7. Stability boundaries for a controller with different vehicle configurations, as well as validation of the closed loop transfer function against the non-linear model can be found in [114].



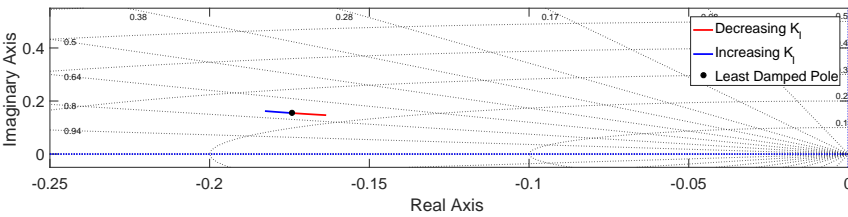
(a) Pole loci for varying  $K_y$



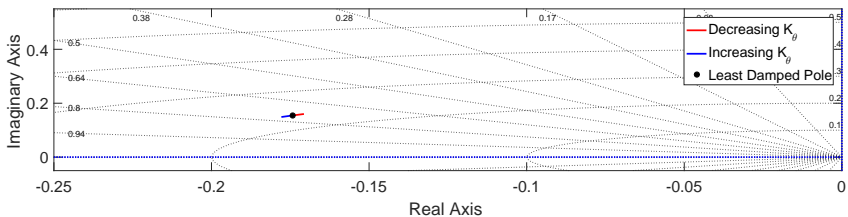
(b) Pole loci for varying  $P_{D1}$



(c) Pole loci for varying  $k$

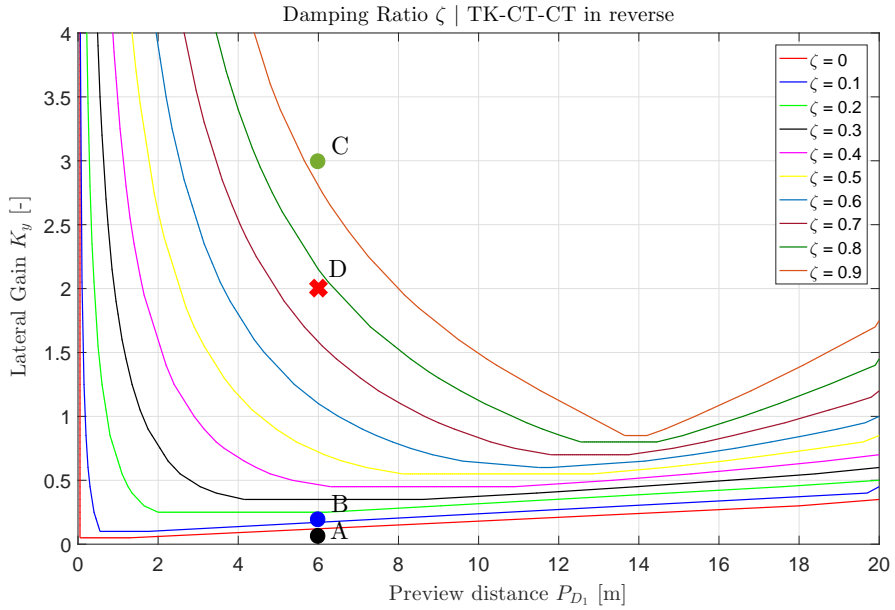


(d) Pole loci for varying  $K_I$

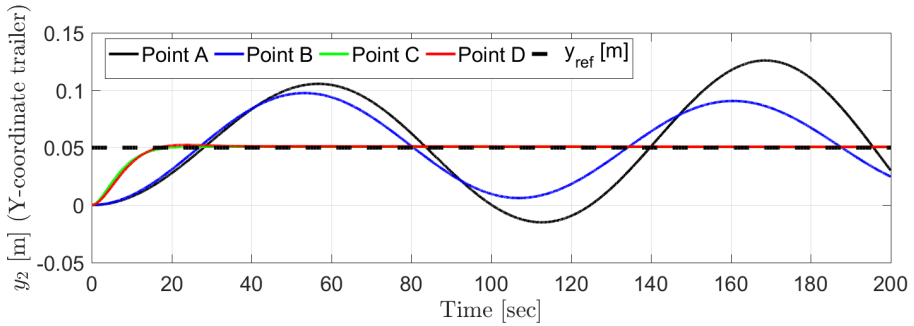


(e) Pole loci for varying  $K_\theta$

Figure C.4: Driver model gains influence on the locus of least damped pole.



(a) Damping ratios as a function of  $K_y$  and  $P_{D_1}$ .



(b) System response for different combinations of  $K_y$  and  $P_{D_1}$ .

Figure C.5: Damping ratios and closed loop system response. Points A, B, C, and D correspond to various combinations of  $K_y$  and  $P_{D_1}$ .



# Appendix D

## Vehicle and Controller Parameters

### D.1 Introduction

This appendix provides the dimensions data of the HCV combinations used for the implementation and verification of the controller functionality documented in Chapter 8. Next the controller gains are provided for both driving directions.

### D.2 Vehicle Parameters

The vehicle combination dimensions as depicted in Figure D.1 are listed in Table D.1:

Vehicle Parameter	Full Size Vehicle	Scaled Vehicle Model
$L_{0f}$	5.475 m	0.27 m
$L_{0b}$	1.875 m	0.08 m
$L_{1f}$	6.585 m	0.295 m
$L_{1b}$	2.005 m	0.09 m
$L_{2f}$	6.585 m	0.425 m

Table D.1: Vehicle Dimensions

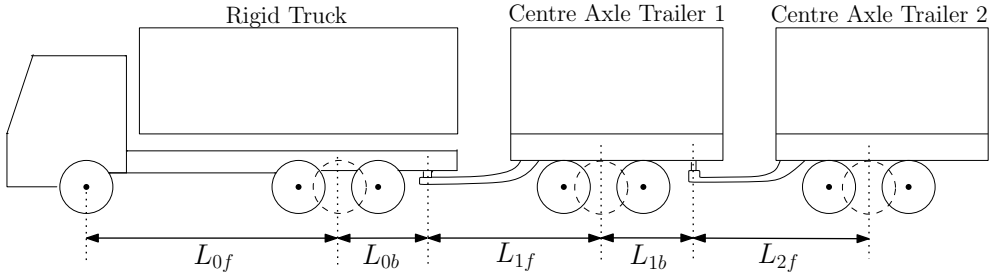


Figure D.1: Rigid Truck with two centre axle trailers.

### D.3 Controller Gains | Full Scale Multi-body Vehicle model

Vehicle Parameter	Forward	Reverse
$K_y$	1.4	2
$P_{D_1}$	13	6
$k$	1.4	1.4
$K_I$	0.001	-0.001
$K_\theta$	0.18	0.15

Table D.2: Controller gains Full Scale vehicle Multi-body model

### D.4 Controller Gains | Scaled Vehicle model

Vehicle Parameter	Forward	Reverse
$K_y$	1.83	1.12
$P_{D_1}$	0.5	1.1
$k$	1.8	1.8
$K_I$	0.001	-0.001
$K_\theta$	0.11	0.08

Table D.3: Controller gains Scaled vehicle model



# Bibliography

- [1] Caricature by Alken H.T., [https://en.wikipedia.org/wiki/History\\_of\\_steam\\_road\\_vehicles#/media/File:1831-View-Whitechapel-Road-steam-carriage-caricature.jpg](https://en.wikipedia.org/wiki/History_of_steam_road_vehicles#/media/File:1831-View-Whitechapel-Road-steam-carriage-caricature.jpg), January, 2016
- [2] Lumsden, K., TRUCK MASSES AND DIMENSIONS, Impact on Transport Efficiency, *ACEA*, 1999
- [3] Altafini, C., Speranzon, A., Wahlberg, B., A feedback control scheme for reversing a truck and trailer vehicle, *IEEE Transactions on Robotics and Automation*, 17(6), pp. 915–922, 2001
- [4] Amidi, O., Integrated mobile robot control, Carnegie Mellon Univ. Robotics Institute, Technical Report CMU-RI-TR-90- 17, 1990.
- [5] Australian Road Transport Suppliers Association, PBS Explained - Performance Based Standards for Road Transport Vehicles, September, 2003
- [6] Aurell, J., Wadman, T., Vehicle Combinations Based on Modular Concept, *Nordiska Vagtekniska Forbundet*, 2007
- [7] Backman, H., Nordstrom, R., Improved Performance of European Long Haulage Transport *Stockholm:TFK* 2002
- [8] Besselink, I.J.M., Vehicle Dynamics Analysis using SimMechanics and TNO Delft-Tyre *Mathworks International Automotive Conference* 2006
- [9] Besselink, I.J.M., Kraaijenhagen, B., Pauwelussen, J., Kural, K., et al., Greening and safety assurance of future modular road vehicles, *proc. HVTT13*, San Luis, Argentina, 2014
- [10] Bolzern, P., DeSantis, R.M., Locatelli, A., Masciocchi, D., Pathtracking for articulated vehicles with off-axle hitching, *IEEE Trans. Control Syst. Technol.*, vol. 6, no. 4, pp. 515–523, 1998
- [11] Byrd, R. H., Mary E. Hribar, and Jorge Nocedal, An Interior Point Algorithm for Large-Scale Nonlinear Programming, *SIAM Journal on Optimization*, Vol 9, No. 4, pp. 877–900, 1999

- [12] Byrd, R. H., J. C. Gilbert, and J. Nocedal, A Trust Region Method Based on Interior Point Techniques for Nonlinear Programming, *Mathematical Programming*, Vol 89, No. 1, pp. 149–185, 2000.
- [13] United States Census Bureau Estimated world population figures, 10,000 BCE–2000 CE <http://www.census.gov/population/international/> Retrieved January, 2016
- [14] CLOSER, High Capacity Transport, <https://closer.lindholmen.se/en/focus-areas/high-capacity-transport-hct> Retrieved March, 2019
- [15] Containerization, <http://portsandshipping.blogspot.nl/>, Retrieved January, 2016
- [16] Commission of the European Communities Intermodality and intermodal freight transport in the European Union pp. I. *Brussels* 1997
- [17] European Commission, Impact Assessment - accompanying document to the White Paper, pp. 137, *Brussels* 2011
- [18] European Commission, Clean Transport, Urban Transport, [http://ec.europa.eu/transport/themes/urban/urban\\_mobility/](http://ec.europa.eu/transport/themes/urban/urban_mobility/), *Brussels* 2013
- [19] European Commission, Infrastructure - TEN-T - Connecting Europe, [http://ec.europa.eu/transport/themes/infrastructure/index\\_en.htm](http://ec.europa.eu/transport/themes/infrastructure/index_en.htm), *Brussels* 2016
- [20] Chung, W., Park, M., Yoo, K., Roh, J., Choi, J., Backward-motion control of a mobile robot with n passive off-hooked trailers, *J. Mech. Sci. Technol.*, vol. 25, no. 11, pp. 2895–2905, 2011
- [21] Davydenko, I.Y., Tavasszy, L., Vrachtauto's zijn toch beter bent? Een eerste kijk naar gewicht, volume en oppervlakte benutting in Nederlands wegvervoer, *Vervoerslogistieke werkdagen*, 2015
- [22] DeSantis, R.M., Bourgeot, J.M., Todeschi, J.N., Hurteau, R., Pathtracking for tractor-trailers with hitching of both the on-axle and the off-axle kind, *Proc. IEEE Int. Symp. Intell. Control*, pp. 206–211, 2002
- [23] de Pont, J., Taramorea, N., Pathtracking for tractor-trailers with hitching of both the on-axle and the Optimisation of heavy vehicle performance, NZ Transport Agency research report 387, *Auckland, New Zealand* 2009
- [24] Divelbiss, A., Wen, J., Trajectory tracking control of a car-trailer system. *IEEE Transactions on Control Systems Technology*, 5(3), pp. 269–278, 1997
- [25] Dubins, L.E., On Curves of Minimal Length with a Constraint on Average Curvature, and with Prescribed Initial and Terminal Positions and Tangents, *American Journal of Mathematics*, 79 (3), pp. 497–516, 1957
- [26] Digital Map of Exemptions, <https://dwo.rdw.nl>, *Netherlands* 2017

- [27] Earl, T., Mathieu, L., Cornelis, S., et.al, Analysis of long haul battery electric trucks in EU Marketplace and technology, economic, environmental, and policy perspectives, *8th Commercial Vehicle Workshop*, Graz, Austria, 2018
- [28] European Council Directive 84/3/EEC, on the weights, dimensions and certain other technical characteristics of certain road vehicles, 1984
- [29] European Council Directive 96/53/EC, laying down for certain road vehicles circulating within the Community the maximum authorized dimensions in national and international traffic and the maximum authorized weights in international traffic, 1996
- [30] European Directive 97/27/EC of the European Parliament and of the Council, relating to the masses and dimensions of certain categories of motor vehicles and their trailers and amending Directive 70/156/EEC, 1997
- [31] European Directive 2002/7/EC of the European parliament and of the council, amending Council Directive 96/53/EC laying down for certain road vehicles circulating within the Community the maximum authorised dimensions in national and international traffic and the maximum authorised weights in international traffic, 2002
- [32] European Regulation (EC) No 661/2009 of the European parliament and of the council, concerning type-approval requirements for the general safety of motor vehicles, their trailers and systems, components and separate technical units intended therefore, 2009
- [33] Euroean Regulation (EC) No 595/2009 of the European parliament and of the council, on type-approval of motor vehicles and engines with respect to emissions from heavy duty vehicles (Euro VI) and on access to vehicle repair and maintenance information and amending Regulation (EC) No 715/2007 and Directive 2007/46/EC and repealing Directives 80/1269/EEC, 2005/55/EC and 2005/78/EC, 2009
- [34] European Commission Regulation (EU) No 582/2011, implementing and amending Regulation (EC) No 595/2009 of the European Parliament and of the Council with respect to emissions from heavy duty vehicles (Euro VI) and amending Annexes I and III to Directive 2007/46/EC of the European Parliament and of the Council, 2011
- [35] European Commission Regulation (EU) No 1230/2012, implementing Regulation (EC) No 661/2009 of the European Parliament and of the Council with regard to type-approval requirements for masses and dimensions of motor vehicles and their trailers and amending Directive 2007/46/EC of the European Parliament and of the Council, 2012
- [36] European Commission Regulation (EU) No 133/2014, amending, for the purposes of adapting to technical progress as regards emission limits, Directive 2007/46/EC of the European Parliament and of the Council, Regulation (EC) No 595/2009 of the European Parliament and of the Council and Commission Regulation (EU) No 582/2011, 2014

- [37] European Regulation (EU) No 540/2014 of the European parliament and of the council, on the sound level of motor vehicles and of replacement silencing systems, and amending Directive 2007/46/EC and repealing Directive 70/157/EEC, 2014
- [38] European Directive (EU) 2015/719 of the European parliament and of the council, amending Council Directive 96/53/EC laying down for certain road vehicles circulating within the Community the maximum authorised dimensions in national and international traffic and the maximum authorised weights in international traffic, 2015
- [39] European Commission, White Paper: Road map to a Single European Transport Area - Toward a competitive and resource efficient transport system, *Brussels*, 2011
- [40] European Energetic Agency, Energy consumption by transport mode in the EU-27, <https://www.eea.europa.eu/data-and-maps/figures/consumption-by-mode-eu-2>, 2012
- [41] Freight Transport Statistics, [http://ec.europa.eu/eurostat/statistics-explained/index.php/Freight\\_transport\\_statistics\\_-\\_modal\\_split](http://ec.europa.eu/eurostat/statistics-explained/index.php/Freight_transport_statistics_-_modal_split), *Publications Office of the European Union, Luxembourg*, April, 2014
- [42] European Environmental Agency, Transport is now Europe's biggest climate problem - EEA data, <https://www.transportenvironment.org/press/transport-now-europe%E2%8%99s-biggest-climate-problem-eea-data>, Retrieved September 30, 2016
- [43] European Committee [https://europa.eu/european-union/law/legal-acts\\_en/](https://europa.eu/european-union/law/legal-acts_en/), October, 2016
- [44] Evers, W.J.E., Besselink, I.J.M., Van der Kanp, A.C.M., Nijmeijer, H., Development and validation of a modular simulation model for commercial vehicles, *Int. J. Heavy vehicle systems*, 2008
- [45] Forbearance of Moving, <http://www.hopewellvalleyhistory.org/Stories-Moving.html>, January, 2016
- [46] Ford Model T 1926, <http://www.oldcarsweekly.com/wp-content/uploads/1926-Ford-TT-main.gif>, January, 2016
- [47] Friedrich, B., Hoffmann, S., Brackelmann, F., Auswertung des niedersächsischen Modellversuchs zum Einsatz von 'Gigalinern' *Liebnitz Universität Hannover*, 2007
- [48] Frost & Sullivan, Delivering to Future Cities - Mega Trends Driving Urban Logistics, <http://www.frost.com/sublib/display-market-insight-top.do?id=272794509>, May, 2016

- [49] Garrido-Jurado, S., Muñoz-Salinas, R., Madrid-Cuevas, F. J., Marín-Jiménez, M.J., Automatic generation and detection of highly reliable fiducial markers under occlusion, *Pattern Recogn.* 47, 6 (June 2014), DOI=10.1016/j.patcog.2014.01.005, pp. 2280-2292, 2014
- [50] Goodwin, F., *The XII Tables, Charleston, USA*, 2010
- [51] Gopfert, I., Froschmayer, A., *Logistik-Stories, Expertenwissen mit Unterhaltungswert, Munchen*, 2005
- [52] HAN Open MBD Toolset <http://openmbd.com>, retrieved March 2018
- [53] Hamilton, E., *The Pictorial Encyclopedia of Rails*, pp. 24-30, *Hamlyn Publishing Group* 1968
- [54] Hermosillo, J., Sekhavat, S., Feedback control of a bi-steerable car using flatness: Application to trajectory tracking, *IEEE:Proceedings of the American Control Conference, Volume 4*, pp. 3567-3572, 2003
- [55] Hoel, C.J., Faclone, P., Low speed maneuvering assistance for long vehicle combinations, *IEEE Intelligent Vehicles Symposium, Proceedings* p. 598-604 art. no 6629532, 2013
- [56] Hils, P., Adler, U., 40t EuroCombi: Ergebnisse der wissenschaftlichen Begleitung des Pilotprojektes in Thüringen., *Fachhochschule Erfurt, Verkehrs und Transportwesen*, 2010
- [57] Hjort, M., Haraldsson, M., Jansen, M., Road Wear from Heavy Vehicles - an overview, *NVF committee Vehicles and Transports*, ISSN 0347-2485, 2008
- [58] Islam, M.M., Fröjd, N., Kharrazi, S., Jacobson, B., How well a single-track linear model captures the lateral dynamics of long combination vehicles, *Vehicle System Dynamics*, pp. 1-23, DOI: 10.1080/00423114.2018.1556796, 2019
- [59] ISO 14791:2000, Road vehicles - Heavy commercial vehicle combinations and articulated buses - Lateral stability test methods, *International Organization for Standardization*, 2000
- [60] Jachner, S., v.d. Boogaart, K.G., Petzoldt, T., Statistical Methods for the Qualitative Assessment of Dynamic Models with Time Delay, *Journal of Statistical Software*, Vol. 22, Issue 8, 2007
- [61] Jacobson, B., Sundström, P., Kharrazi, S., Fröjd, N., Islam, M., An Open Assessment Tool for Performance Based Standards of Long Combination Vehicles, *Research Report*, Department of Mechanical and Maritime sciences, Chalmers University of Technology, Göteborg, Sweden, 2017
- [62] Karaman, S., Frazzoli, E., Incremental Sampling-based Algorithms for Optimal Motion Planning, *Robotics: Science and Systems*, Zaragoza, Spain, 2010
- [63] Karaman, S., Frazzoli, E., Optimal Kinodynamic Motion Planning Using Incremental Sampling-based Methods, *49th IEEE Conference on Decision and Control*, pp. 7681-7687, 2010

- [64] Kharrazi, S., Karlsson, R., Performance based standards for vehicle combinations with weight and/or dimensions exceeding the specified limits in the Directive 96/53/EC, *Linköping, Sweden*, 2015
- [65] Kraaijenhagen, B., Barth, T., Kural, K., Pauwelussen, J.P., & et. all., Greening and Safety Assurance of Future Modular Road Vehicles: Book of Requirements, *Technical University Eindhoven, Netherlands*, 2014
- [66] Kraaijenhagen, B., Kural, K., Pauwelussen, J., Weijers, S. & Besselink, I.J.M., A field research on the need of high capacity vehicles to reduce  $CO_2$  and improve profitability, Proceedings of HVTT 14, *Rotorua, New Zealand*, 2016
- [67] Kati, M.S., On Robust Steering Based Lateral Control of Longer and Heavier Commercial Vehicles , Doctoral Thesis, *Chalmers University of Technology*, 2018
- [68] Kural, K., Besselink, I.J.M., Pauwelussen, J.P. & Nijmeijer, H., Assessment of Dutch longer and heavier vehicles with a performance based approach and its applicability to Europe, Proceedings of HVTT12, *Stockholm, Sweden*, 2012
- [69] Kural, K., Prati, A., Besselink, I.J.M., Pauwelussen, J.P. & Nijmeijer, H., Validation of longer and heavier vehicle combination simulation models, *SAE International Journal of Commercial Vehicles*, 6(2), pp. 340-352, 2013
- [70] Kural, K., Prati, A., Besselink, I.J.M., Pauwelussen, J.P. & Nijmeijer, H., Validation of longer and heavier vehicle combination simulation models, Proceedings SAE ComVeh, *Chicago, USA*, 2013
- [71] Kural, K., Voskuijl, M., Fengnian, T. & Pauwelussen, J.P., Determination of representative loading conditions for effective semitrailer design, *Transport*, 29(4), pp. 363-375, 2014
- [72] Kural, K., Besselink, I.J.M., Pauwelussen, J.P., Nijmeijer, H. & Patel, K., Analysis of driver behaviour during reverse driving of double articulated vehicles, Proceedings HVTT13, *San Luis, Argentina*, 2014
- [73] Kural, K., Besselink, I.J.M., Xu, Y., Nijmeijer, H. & Tomar, A., Driver support system for improved maneuvering of articulated vehicles using unmanned aerial vehicle, Proceedings HVTT14, *Rotorua, New Zealand*, 2016
- [74] Stensson Trigell, A., Rothamel, M., Pauwelussen, J., Kural, K., Advanced vehicle dynamics of heavy trucks with the perspective of road safety, *Vehicle System Dynamics*, Vol. 55, No.10, pp. 1572-1617, 2017
- [75] Kural, K., Hatzidimitris, P., Wouw v.d.,N., Besselink, I., Nijmeijer, H., Active Trailer Steering Control for High Capacity Vehicle Combinations, *IEEE: Transactions on Intelligent Transportation Systems*, Vol. 2, No. 4, pp. 251-265, 2017
- [76] Kural, K., de Saxe, C., Kharrazi, S., Asp, T., Kraaijenhagen, B., Pauwelussen, J., Smart infrastructure access policy: a highway towards more efficient road transport, Proceedings of 7th Transport Research Arena TRA 2018, Vienna, Austria, 2018

- [77] Kural, K., Schmidt, F., Erlingsson, S., Vierth, I., Cebon, D., Lobig, A., Liedtke, G., FALCON Part III. Validation of smart infrastructure access policy, *proc. HVTT15*, Rotterdam, Netherlands, 2018
- [78] Kusumakar, R., Autonomous Parking for Articulated Vehicles, Master Thesis, *HAN University of Applied Sciences* 2017
- [79] Lam, C.P., Comparison of SIMulation and Test Results for Various Truck Combination Configurations, *ISWHD*, 1986
- [80] Laumond, J.P., Sekhavat, S., Lamiroux, F., Robot Motion Planning and Control, *Springer, ISBN 3-540-76219-1*, 1998
- [81] LaValle, S.M., Rapidly-exploring random trees: A new tool for path planning, *Technical Report, Computer Science Department, Iowa State University* (TR 98-11), 1998
- [82] Lehner, M., The Complete Pyramids, *Thames and Hudson, London, UK*, 1997
- [83] Loof, J., Modeling and control of a truck steering-system for active driver support, Eindhoven University of Technology, Doctoral dissertation, 2018
- [84] CROW, LZV's op het onderliggend wegennet 2013, ISBN 978-90-6628-6160 *Ede, Netherlands* 2013
- [85] McRuer, D.T., Allen, R.W., Weir D.H., Klein R.H., New results in driver steering control models, *Human Factors* No.19, pp. 381-397, 1977
- [86] Michalek, M., Geometrically motivated set-point control strategy for the standard n-trailer vehicle, *Proc. IEEE Intelligent Vehicles Symp.*, pp. 138-143, 2011
- [87] Martínez, J.L., Morales, J., Mandow, A., García-Cerezo, A., Steering Limitations for a Vehicle Pulling Passive Trailers, *IEEE Transactions on Control Systems Technology*, vol. 16, nr.4, pp. 809-818, 2008
- [88] Morales, J., Martínez, J.L., Mandow, A., Medina, I.J. Virtual steering limitations for reversing an articulated vehicle with off-axle passive trailers, *IECON Proceedings (Industrial Electronics Conference)*, pp. 2385-2390, Porto, 2009
- [89] Morales, J., Martínez, J.L., Mandow, A., García-Cerezo, A. J., Steering the Last Trailer as a Virtual Tractor for Reversing Vehicles With Passive On- and Off-Axle Hitches *IEEE Transactions on industrial electronics*, Vol 60, no.12, 2013
- [90] Morrison, G., Roebuck, R. L., Cebon, D., Effects of longer and heavy vehicles on traffic congestion *Proc IMechE Part C: J Mechanical Engineering Science*, DOI: 10.1177/0954406213493384, 2013
- [91] NASA, Global Land-Ocean temperature index, <http://climate.nasa.gov/vital-signs/global-temperature/>, 2016
- [92] National Transport Commission, PERFORMANCE BASED STANDARDS SCHEME THE STANDARDS AND VEHICLE ASSESSMENT RULES, *National Transport Commission, Australia*, 2008

- [93] National Climatic Data Center, State of the Climate: Global Analysis for Annual 2012, <http://www.ncdc.noaa.gov/sotc/global/201213>, December, 2012
- [94] Nordengen P., Kienhöfer F., de Saxe, C., Vehicle Safety Performance Improvements Using a Performance-Based Standards Approach: four case studies Proceedings HVTT13, *San Luis, Argentina*, 2014
- [95] Nunn N., Qian N., The Columbian Exchange: A History of Disease, Food, and Ideas, *Journal of Economic Perspectives*, vol. 24(2), pp. 163-188, 2010
- [96] No Megatrucks in EU, <http://www.nomegatrucks.eu/>, December, 2016
- [97] Oliviera, R., Planning and Motion Control in Autonomous Heavy-Duty Vehicles, Master Thesis *KTH Royal Institute of Technology* 2014
- [98] Oreskes, N., The Scientific Consensus on Climate Change, *Science* 3 December 2004: Vol. 306 no. 5702 p. 1686 DOI: 10.1126/science.1103618, 2004
- [99] Pacejka, H., Tyre Vehicle Dynamics, Third Edition, *Butterworth-Heinemann, Oxford, UK*, 2012
- [100] PIRA group, World Oil Demand 1990-2025, <https://seekingalpha.com/article/319166-north-american-oil-production-on-the-rise?page=3>, retrieved October 2018
- [101] Pradalier, C., Hermosillo, J., Koike, C., Braillon, C., Bessiere, P., Laugier, C., The cycab: A car-like robot navigating autonomously and safely among pedestrians, *Robotics and Autonomous Systems*, 50(1), pp. 51-68, 2005
- [102] Rakic B., Stegeman, J., Kind, M., Monitoring Traffic Safety, Longer and Heavier Vehicles, *Rijkswaterstaat*, 2011
- [103] Ramberg K., Fewer trucks improve the environment: Three Short Become Two Long, if the EU Follows the Example Set by Sweden and Finland, *Svensk Näringsliv, Transport and Infrastructure*, 2004
- [104] Riid, A., Ketola, J., Rüstern, E., Fuzzy knowledge-based control for backing multi-trailer systems, Proc. IEEE Intell. Veh. Symp., pp. 498-504, 2007
- [105] Longer and Heavier Vehicles in the Netherlands: Facts, figures and experiences in the period 1995-2010, *Directorate General for Public Works and Water Management, Netherlands*, 2010
- [106] Rimmer, A.J., Cebon, D., Planning Collision-Free Trajectories for Reversing Multiply-Articulated Vehicles, *IEEE Transactions on Intelligent Transportation Systems*, Volume: 17, Issue: 7, pp. 1998-2007, 2016
- [107] Road Freight Transport Vademecum 2010 Report, European Commission DG for Mobility and Transport Unit D.3 – Land transport, September 2010
- [108] Roh, J.I., Chung, W., Reversing control of a car with a trailer using the driver assistance system, *Int. J. Adv. Robot. Syst.*, vol. 8, no. 2, pp. 114-121, 2011



- [109] Rouchon, P., Fliess, M., Levine, J., Martin, P., Flatness and motion planning : the car with n trailers, *Proceedings of European Control Conference*, Groningen, 1993
- [110] Road Transport Association, *Directives for the Design of Urban Roads*, 2006
- [111] Salvucci, D. D., Gray, R., A two-point visual control model of steering. Perception No. 33, pp. 1233–1248, 2004
- [112] de Saxe, C.C., Kural, K., Kharrazi, S., Schmidt, F., van Geem, C., Berman, R., Woodrooffe, J., Cebon, D., FALCON III: Defining a performance-based standards framework for high capacity vehicles in Europe, *Proceedings Heavy Vehicle Transport Technology Symposium*, Rotterdam, 2018
- [113] Setright L. J. K., Drive on! A Societal History of the Motor Car, ISBN 1-86207-698-7 *Granta UK*, 2004
- [114] Saini, M., Autonomous Docking of Articulated Vehicles, Master Thesis, *HAN University of Applied Sciences*, 2018
- [115] Sinn H. W., Das grüne Paradoxon, Plädoyer für eine illusionsfreie Klimapolitik, ISBN 3-43020-062-8 pp. 44-47 *Berlin: Econ-Verlag*, 2008
- [116] EMS, <http://www.scania.es/>, May, 2016
- [117] Stahn, R., Stark, T., Stopp, A., Laser scanner-based navigation and motion planning for truck-trailer combinations, in Proc. IEEE/ASME Int. Conf. on Advanced Intelligent Mechatronics, pp. 1–6, 2007
- [118] TrailerTail, <http://www.stemco.com/product/trailertail/>, May, 2017
- [119] Stentz, A., Optimal and efficient path planning for partially-known environments, in Proc. Int. Conf. on Robotics and Automation, pp. 3310–3317, 1994
- [120] Schwenker B., Raffel T., THOUGHTS Megatrends, Roland Berger School of Strategy and Economics, *Munich*, 2012
- [121] Tanaka, K., Hori, S., Wang, H., Multiobjective control of a vehicle with triple trailers, IEEE/ASME Trans. Mechatronics, vol. 7, no. 3, pp. 357–368, 2002
- [122] Taniguchi E., Thompson G. R., City Logistics: Mapping the Future, Plädoyer für eine illusionsfreie Klimapolitik, ISBN 9-7814-8220-8894 *CRC Press*, 2014
- [123] Eye Tracking Glasses, <http://www.tobii.com>, Retrieved April, 2017
- [124] Transportation in the Middle Ages, <http://www.thefinertimes.com/Middle-Ages/transportation-in-the-middle-ages.html>, January, 2016
- [125] Transportation in the Middle Ages II, [http://www.snipview.com/q/Transport\\_in\\_the\\_Middle\\_Ages](http://www.snipview.com/q/Transport_in_the_Middle_Ages), January, 2016
- [126] Regulation No. 13, Revision 6, uniform provisions concerning the approval of vehicles of categories M, N and O with regard to braking, *Economic Commission for Europe of the United Nations*, 2008

- [127] United Nations Department of Economic and Social Affairs, World Urbanization Prospects, The 2011 Revision [http://www.un.org/en/development/desa/population/publications/pdf/urbanization/WUP2011\\_Report.pdf](http://www.un.org/en/development/desa/population/publications/pdf/urbanization/WUP2011_Report.pdf), pp. 61, *New York* 2012
- [128] United Nations Department of Economic and Social Affairs, UN projects world population to reach 8.5 billion by 2030, driven by growth in developing countries, <http://www.un.org/apps/news/story.asp?NewsID=51526#.Vp-U6013GUk>, Retrieved July, 2015.
- [129] VECTO Tool, [https://ec.europa.eu/clima/policies/transport/vehicles/vecto\\_en](https://ec.europa.eu/clima/policies/transport/vehicles/vecto_en), Retrieved August, 2019
- [130] Volvo Dynamic Steering, <http://www.volvotrucks.nl/nl-nl/trucks/volvo-fm/features/volvo-dynamic-steering.html>, Retrieved June, 2017
- [131] WABCO OptiFlow, <http://www.wabco-optiflow.com/home>, Retrieved May, 2017
- [132] Walmart Advanced Vehicle Experience, <http://corporate.walmart.com/global-responsibility/environment-sustainability/truck-fleet>, May, 2017
- [133] Walsh, G., Tilbury, D., Sastry, S., Murray, R., Laumond, J., Stabilization of trajectories for systems with nonholonomic constraints. *IEEE Transactions on Robotic and Automation*, 39(1), pp. 216–222, 1994
- [134] Waltz, R. A., J. L. Morales, J. Nocedal, and D. Orban, An interior algorithm for nonlinear optimization that combines line search and trust region steps, *Mathematical Programming*, Vol 107, No. 3, pp. 391–408, 2006
- [135] Woodrooffe, J.H., Performance based standards enabling transport decarbonisation, Proceedings of HVTT 2016, *Rotorua, New Zealand*, 2016
- [136] Woodrooffe, J.H., Performance-Based Standards and Indicators for Sustainable Commercial Vehicle Transport, 18th Scientific Advisory group report, ACEA, *Brussels, Belgium*, 2012
- [137] Yoo, K., Chung, W., Pushing motion control of n passive off-hooked trailers by a car-like mobile robot, Proc. IEEE Int. Conf. Robot. Autom., pp. 4928–4933, 2010
- [138] Yuan, J., Huang, Y., Path following control for tractor-trailer mobile robots with two kinds of connection structures, Proc. IEEE Int. Conf. Intell. Robots Syst., pp. 2533–2538, 2006
- [139] Ziegler, J.G., Nichols, N.B., Optimum steerings for automatic controllers, *Transactions of the ASME*, vol: 64 pp. 759-768, 1942
- [140] Zips, P., Bock, M., Kugi, A., An Optimisation-Based Path Planner for Truck-Trailer Systems with Driving Direction Changes, *IEEE International Conference on Robotics and Automation (ICRA)*, 2015

# Acknowledgements

Lastly, I must make here one confession. I adore to cook! Looking back in time, I find plenty of similarities between cooking and doing a part-time PhD research, except one. Contrary to the cooking it is nearly impossible to do a PhD research entirely on your own. On the other side, the list of general elements one needs for both activities appears to be very similar. Therefore, here comes the 'recipe' in terms of what was needed, and who helped me to 'cook' this booklet.

- *Technique & Skills*

To spread a butter over a slice of bread you do not probably need any special technique, but for instance the preparation of proper Egg Benedict will not be the case. The point is, the recipe is not a secret and the ingrediencies are known, but couple of well pointed tips makes the difference between the great meal and epic fail. In this sense I was lucky, and had a privilege, to be guided by a people who I do not hesitate to entitle \*\*\*Michelin chefs in their field of expertise. It is Henk Nijmeijer, Igo Besselink, Joop Pauwelussen, and Nathan van de Wouw who all helped me with many well-aimed advices to improve the quality of my work from so many perspectives. I would like to thank them here, as they navigated me to become a better researcher who should be self-critical, unbiased, and should seek for a clearly defined arguments. I truly enjoyed all the discussions we had at Henk's or Igo's office which were always in a collegial spirit and let me feel to be a part of the team.

- *Fresh and appropriate ingrediencies*

These are always the absolute basis for every meal. Herewith, the ingrediencies are represented by the projects without which the research written in this booklet can not be done. My great thanks and gratitude go again to Joop, Igo, and Henk who originally initiated the HTAS-EMS project, which was in fact the start of my PhD research and a great cooperation between TU/e and HAN. Later it was followed by INTRALOG SIA RAAK-PRO project mainly thanks to my colleagues Bram Veenhuizen, Lejo Buning, and Frans Tillema. And finally, the FALCON project which was subsidized by a Conference of the European Directors of Roads represented by Tomas Asp, and Loes Aarts, and MAN Truck & Bus represented by Ben Kraaijenhagen.

- *Hardware & equipment*

This is in fact the enabler which allows you transform the ingrediencies through various states till the final shape of the dish. As you may realized while reading, some chapters are heavily based on experiments, tests or measurements. All of these were time demanding in terms of preparation, execution, up to the final processing. Although I do not want to compare people listed hereafter to machines or an equipment, the fact is that their effort, skills or expertise allowed me to transform my wishes into the form which could be used for the manuscript. Here my thanks go to students: Mitul, Rakshith, Kapil, Arun, Jeroen, Tom, Mathias, and Ludwig for all their hard work related mainly to the scaled test setup and simulations. Next to my colleagues: Rini van Thiel, Abhishek Tomar, Alberto Prati, Ben Pyman, Roel Boom, Jason van Kolfschoten, and Jan Benders for the help during the tests, setting up the cameras, and providing relevant tools for experiments. And last but not least my thanks go to all the WABCO test drivers for their patience during the reversing experiments.

- *Dosage*

... too much of one or another ingrediency may ruin the dish. Here I was lucky to be a part of IFRTT network work and HVTT community with big bunch of international experts who were always ready to share their opinions if it goes especially about Performance Based Standards. I would like to acknowledge the work we did all together in FALCON project and I would like to especially thank to Chris de Saxe, Sogol Kharrazi, Rob Berman, Carl van Geem, and Franziska Schmidt. Moreover, I would like to acknowledge Pavlos Hatzidimitris for all his hard work related to the active steering of the trailer axles and his MATLAB skills which were for me more than inspiring. Furthermore, I would like to thank Bengt Jacobson for his review which certainly improved the quality of this work with many relevant suggestions which are also of interest for future research.

- *Timing*

Last but probably the most important element. While cooking the time passes always mysteriously and you want to make sure that all the ingrediencies click together at the right time and state and at same moment your guests will not run out of the table to the nearest fast food because of tremendous hunger. Here I can not find words to thank enough to my wife Alena for being a very patient 'guest' that supported me anytime when I was stealing the time from our family while writing. Even though our wonderful kids Kristina and Karel can not read yet, nor speak English, I would like to thank them here as well, they provided a great source relaxing distraction which kept me always enthusiastic and positive minded. Same holds to our friends here in Arnhem, onze lieve buren, but also all the guys from the Milosh's bunch and obviously the old rascal Mr. Sejček. Finally, I would like to thank my beloved parents, grandparents, brother, and my entire family in law for their continuous support and great moments always when we all are together.

# Curriculum Vitae



Karel Kural obtained his M.Sc.-degree in Mechanical Engineering from Czech Technical University, Prague, the Czech Republic, in 2008. He also holds MEng-degree in Automotive Engineering from HAN University of Applied Sciences, Arnhem, the Netherlands, from 2008.

After the graduation, he joined Automotive Research Group at HAN University of Applied Sciences, the Netherlands, as research associate, where he presently holds the position of senior researcher responsible for the knowledge cluster of vehicle dynamics and heavy road transport.

His current research field is dynamics and control of commercial vehicle combinations and the driver support systems. He is a board member of International Forum for Road Transport Technology (IFRTT), where he currently serves as a vice-president for Europe. Karel is a co-author of a number of successful research project proposals on both national and international level.

Mid 2011 he joined Eindhoven University of Technology, Eindhoven, the Netherlands, group Dynamics & Control for part-time PhD on a basis of two consecutive projects. The research conducted in these projects is presented in this dissertation.

